UNIVERSITÀ
DEGLI STUDI
DI PADOVA

Sede amministrativa: Università degli Studi di Padova

Dipartimento di Principi e Impianti di Ingegneria Chimica “I. Sorgato”

SCUOLA DI DOTTORATO DI RICERCA IN INGEGNERIA INDUSTRIALE
INDIRIZZO INGEGNERIA CHIMICA
CICLO XXII

MECHANICS OF DENSE AND MULTIPHASE FLOWS OF GRANULAR MATERIALS

Direttore della Scuola: Ch.mo Prof. Paolo Bariani
Coordinatore d’indirizzo: Ch.mo Prof. Alberto Bertucco
Supervisore: Ch.mo Prof. Paolo Canu

Dottorando: Riccardo Artoni

ER CAFFETTIERE FISOLOFO

L'ommini de sto monno sò l'istesso
Che vaghi de caffè ner macinino:
C'uno prima, uno doppo, e un'antro appresso,
Tutti quanti però vanno a un distino.

Spesso muteno sito, e caccia spesso
Er vago grosso er vago piccinino,
E ss'incarzeno tutti in zu l'ingresso
Der ferro che li sfraggne in porverino.

E l'ommini accusì viveno ar monno
Misticati pe mano de la sorte
Che sse li gira tutti in tonno in tonno;

E movennose oggnuno, o ppiano, o fforte,
Senza capillo mai caleno a fonno
Pe cascà ne la gola de la morte.

G. G. Belli. Roma, 22 gennaio 1833

Summary

Flows of granular materials exist in a wide variety of situations, spanning from industrial plants (silos, hoppers, mixers, fluidised beds) to natural processes (avalanches, rockslides), and even in everyday's life. Being that nearly a half of all goods processed worldwide are in a granular form, it is crucial both for economical and environmental issues to better understand the behavior of these materials. For large scale phenomena, continuum models (i.e. conservation equations equipped with constitutive relations) are the only affordable solution to model the flow of powders and grains.
Being that the type of flow depends on the energy injected into the system, a classification was made in three regimes: 1- the rapid flow regime, for very dilute flows, 2- the quasistatic regime, for very persistent contacts, and 3- the dense flow regime, which is intermediate between the two and which, despite several attempts, lacks of a unifying and satisfying description.
The present work deals with continuum modeling of dense flows of granular materials. The focus is on the development and validation of rheological models; in particular, a model taking into account the dynamics of the fluctuating energy was considered, which gave interesting results, also compared to experimental and numerical data, for both confined and free surface flow. It must be stressed that the model was applied both to simple reference geometries (inclined chute, vertical chute,..) and to industrial scale ones (silo), thus demonstrating the wide range of applicability of the approach.
Then, the problem of realistic boundary conditions was thoroughly discussed, evidencing the importance of correct choices and developing an original treatment considering the effect of the fluctuating force network on slip dynamics. Moreover, due to the possibility of extending the approach to treat processes involving gas-solids flow such as moving bed reactors, an attempt was made to simply characterize coupling between gas and solids flow in vertical pipes below the fluidizatoin threshold, with the focus on gas maldistribution.

At first the reader is introduced to the topic of dense granular flows and to the state of the art (Chapter 1), then a mixing length model of dense granular flows is adopted to assess

its predictions in a vertical chute configuration (Chapter 2). In Chapter 3 a higher-order closure is introduced and a fluctuating energy model developed from conservation laws and phenomenological constitutive relations, and it is tested and extended against Literature correlations and experience in different geometries of flow. Chapter 4 addresses the issue of boundary conditions, which was verified to be crucial: new boundary conditions for the slip velocity at the wall are developed by means of a simple stochastic model and evaluated with the help of dimensional analysis. The problem of countercurrent gas-solid flow below the fluidization threshold and of possible maldistribution deriving from solids motion is discussed in Chapter 5. A procedure for the scale-up of silos for granular-gas flow applications is then discussed (Chapter 6), and experiments obtained in a pilot silo are used to validate the rheological model previously developed, both in the case of solids only and gas-solids flow. Discrete element simulations are the subject of Chapter 7, where insights are derived also from numerical data for both the rheology and the boundary conditions. Before resuming the main results and outlining future perspectives, first results of velocity profiles from experiments of a vertical chute are presented in Chapter 8.

$\sim$

The work was done in the Granular Research Group at the University of Padova, under the supervision of Prof. Paolo Canu and Dr. Eng. Andrea Santomaso, whom I wish to thank for their suggestions and support. I would like to thank also Frédéric Dubois at LMGC in Montpellier and Mathieu Renouf at LaMCoS in Lyon for the precious help given with LMGC90. I then acknowledges partial funding and collaboration from Danieli Research Center.

Padova, January 28th, 2010.

Sommario

I flussi di materiali granulari sono comuni a una grande varietà di situazioni, che vanno dagli impianti industriali (sili, tramogge, mescolatori, letti fluidi,...) ai processi naturali (valanghe, frane), e persino alla vita di tutti i giorni. Dal momento che circa metà dei beni trattati industrialmente si trovano in forma granulare, appare cruciale per ragioni sia economiche che ambientali approfondire la conoscenza del comportamento di questi materiali. Per fenomeni su larga scala, i modelli continui (ossia equazioni di conservazione chiuse da appropriate relazioni costitutive) sono l'unica soluzione possibile per trattare il flusso di polveri e grani.

Dato che il tipo di flusso dipende dall'energia immessa nel sistema, è stata operata una classificazione in tre regimi: 1- il regime di flusso rapido, per flussi molto diluiti, 2- il regime quasistatico, dove i contatti tra le particelle sono assai duraturi, e 3- il regime di flusso denso, che è intermedio tra i due e che manca ancora di una descrizione soddisfacente e unitaria, nonostante i numerosi tentativi teorici.

Il presente lavoro tratta della modellazione continua di flussi densi di materiali granulari. Il principale obiettivo è lo sviuppo e la validazione di modelli reologici; in particolare, si è scelto di sviluppare un modello che descrive la dinamica dell'energia cinetica fluttuante, il quale ha portato a risultati interessanti, anche in confronto a dati sperimentali e numerici, per flussi sia in geometrie confinate che a superficie libera. Si deve sottolineare che il modello è stato applicato sia a semplici geometrie di riferimento (piano inclinato, canale verticale,...) sia a geometrie su scala industriale (sili), dimostrando così l'ampia applicabilità dell'approccio.

Inoltre, è stato discusso a fondo il problema di assumere condizioni al contorno realistiche, evidenziando l'importanza di scelte corrette e sviluppando una trattazione originale che considera l'effetto della rete fluttuante delle force sulla dinamica di scivolamento alla parete. Per di più, vista la possibilità di estendere l'approccio per trattare processi che comportino la coesistenza di flussi di solidi e di gas, come in reattori a letto mobile, si sono gettate le basi per una semplice descrizione dell'accoppiamento tra la reologia del solido e il flusso del gas sotto la soglia di fluidizzazione in canali verticali, con un'attenzione particolare per la maldistribuzione del gas.

Per prima cosa il lettore viene introdotto al tema dei flussi granulari e allo stato dell'arte della reologia (Capitolo 1), in seguito si adotta un modello reologico a lunghezza di mescolamento, per valutarne le predizioni in un canale verticale (Capitolo 2). Nel Capitolo 3 si utilizza una chiusura di ordine superiore per sviluppare un modello reologico basato sull'energia fluttuante a partire dalle equazioni di conservazione e da relazioni costitutitve fenomenologiche; il modello viene quindi comparato con correlazioni di Letteratura e conoscenze sperimentali per differenti geometrie di flusso. Il Capitolo 4 affronta il problema delle condizioni al contorno che si era visto essere cruciale per le predizioni dei modelli: sono sviluppate nuove condizioni al contorno utlizzando un semplice modello stocastico e valutate con concetti di analisi dimensionale. Il problema del flusso controcorrente di gas e solidi sotto la soglia della fluidizzazione è l'argomento del Capitolo 5, considerando il problema dal punto di vista dela maldistribuzione del gas che può derivare dall'accoppiamento con la reologia dei solidi. Nel Capitolo 7 si affrontano invece simulazioni discrete (DEM) di flussi granulari, le quali vengono utilizzate anche per approfondire la reologia e le condizioni al contorno. Prima di riassumere i principali risulltati in relazione anche alle prospettive per future investigazioni, nel Capitolo 8 sono presentati dei risultati preliminari di profili sperimentali di velocità in un canale verticale.

$\sim$

Questo lavoro è stato svolto nel Gruppo di Ricerca sul Granulare nel Dipartimento di Principi e Impianti di Ingegneria Chimica 'I. Sorgato' dell'Università di Padova, sotto la supervisione del Prof. Paolo Canu e dell' Ing. Andrea Santomaso, che ringrazio per gli infiniti suggerimenti e il supporto. Tengo anche a ringraziare Frédéric Dubois del LMGC a Montpellier e Mathieu Renouf del LaMCoS a Lyon per l'aiuto prezioso con il codice LMGC90. Inoltre ringrazio il Centro Ricerche Danieli per la collaborazione ed il finanziamento parziale alla ricerca.

Padova, 28 gennaio 2010.

Contents

Chapter 1

Introduction to the rheology of dense granular flows

Si ne le croyez, je ne m'en soucie,
mais un homme de bien, un homme de bon sens
croit tousjours ce qu'on luy dict
e qu'il trouve par escript.

Rabelais, *La vie treshorrificque du Gargantua pere de Pantagruel.*

1.1 Granular media: general concepts

Granular materials are ubiquitous in everyday's life, as well as this sentence has become ubiquitous in granular materials Literature. In general, granular media can be defined as ensembles of particles with size larger than $1\ \mu m$(de Gennes, 1998). Above this value, thermal agitation is negligible, so Brownian motion does not occur. Therefore a collection of particles results in what is called an *athermal* system. Being that thermodynamic fluctuations do not play an important role, the system cannot explore its phase space without gaining energy from shear, vibration, or external forces such as drag or gravity(Aranson and Tsimring, 2006). Depending on the particle size, granular media can be cohesive or not: typically, above $100\ \mu m$ Van der Waals forces are negligible compared to other forces. The presence and the properties of an interstitial fluid can modify strongly the behavior of the mass, both at the level of interparticle interactions (for example changing interparticle friction properties or cohesion) and on a more higher scale (e.g. pressure gradients in the fluid exert forces on the grains).

Research on granular media, which started from fundamental works of Coulomb (1781) (who studied static friction and defined the angle of repose of heaps), Faraday (1831) (who described a convective instability in vibrated powders which is named after him), Reynolds (1885) (who observed the dilatancy mechanism), Janssen (1895) (who studied the pressure distribution at the wall of a column filled with grains) can be divided mainly in two parts: fundamental and technological. Historically these two branches were respectively held by physicists ad engineers, the relationship between the two areas being few and mostly characterised by two-way distrust. In recent years the attention of the physics community on the subject has grown considerably, probably pushed also by the interest in the topic devoted by important personalities such as the Nobel prize Pierre-Gilles De Gennes. An history and a sociology of research on granular media is not the scope of the present thesis; however, the author wants to underline that more communication between different branches of granular research could be useful in order to proceed with science and technology, together.

1.2 A physical point of view

The athermal nature implies also that granular systems are far from equilibrium, passing from a metastable state to another; therefore classical statistical mechanics fails in these media. However, being that similarities exist between equilibrium thermal systems and driven systems that reach a nonequilibrium steady state(Xu and O'Hern, 2005), many attempts to develop thermodynamic and statistical theories can be found in Literature. Restricting to the case of granular systems, examples of such attempts are the kinetic theory of granular gases(Jenkins and Savage, 1983; Jenkins and Richman, 1985) for the rapid regime of flow, and Edwards' theory of packings in the static limit(Edwards and Oakeshott, 1989; Mehta and Edwards, 1989; Oakeshott and Edwards, 1992). In general, being that energy is in principle not conserved because of the dissipative nature of the interaction between grains (which can be due to friction, inelastic collisions, unrecoverable deformation, breakage, and so on), effective temperatures describing the state of the system cannot be defined from energy conservation principles.

Moreover, looking at the behavior of a granular system (as an example, a flowing one), one can be pushed from analogies with similar behaviors in other physical systems (e.g. liquids) to develop contiuum theories, i.e. theories adopting partial differential equations, thus predicting fields which vary continuously through the system (continuum theories will be largely the subject of the present thesis). Apart from the level of description, the main theoretical problem of continuum theories deals with separation of scales: the

micro-scale (grain level) and the macro-scale can typically differ by a factor $10^3 - 10^4$ (for example, a silo with diameter $\sim 5\ m$ containing material around $1\ mm$ in size), which is not sufficient to strongly affirm the validity of a continuum treatment. Moreover typical phenomena such as shear banding(G. D. R. Midi, 2004) or avalanching in drums(Boateng and Barr, 1997) occur in a limited portion of the system, usually some tenths of diameters wide. Therefore the continuum assumption cannot be used without knowing that it is a stronger approximation than it could be for systems in which a scale separation exists.

1.3 The industrial way of thinking

From the industrial point of view, granular materials are processed in a variety of manners: typical operation are storage, discharge, grinding, milling, granulation, pneumatic conveying, mixing. It is common sense that systems developed for granular materials usually have low efficiency compared with analogous systems processing liquids or gases, without significant improvement of the techniques in the last fifty years(Santomaso and Canu, 2001). Problems coming from the peculiar nature of granular materials tipically occur in industrial applications, such as segregation, comminution, formation of stagnant zones, poor mixing, difficulty in process control,... A detailed understanding of the mechanics of granular materials could therefore help, particularly when also reactive and transport phenomena are intended to take place. As an example, a type of moving bed reactor can be a silo where while the material is continuously discharged and fed, a reactive gas flows co- or countercurrently. In this case attention must be focused on wall stress profiles, residence times of the solid and of the gas, trying to reduce stagnant zones in the solids and maldistribution in the gas.

1.4 Phenomenology

Between the various phenomenologies displayed by granular media, some - though being out from the scope of the present work - can be reminded because they spread a light on general properties of the materials under study.

Compaction. If subjected to tapping, an ensemble of grains experiences a typical ageing dynamics characterized by logarithmic tendence of density towards maximum packing. If the initial state is already near the maximum (random) packing limit, the material needs to expand before compacting again, so density is a little more complex function of

time(Ben-Naim et al., 1996; Herrmann, 1995).

Segregation. When vibrated, a polydisperse ensemble typically segregates, bringing to the surface the biggest grains (this effect is called “Brazil nut effect”); this phenomenon was explained in two ways, one considering excluded volume dynamics (little particle flow due to gravity in the voids generated by the motion of larger particles), the other taking into account convective motion due to vibrations (convective cells bring particles to the top, and only little particles are able to re-enter the bed)(Marques Fernandes et al., 2003). This phenomenon is shown in Fig. 1.1. Segregation may be also driven by the difference in the angle of repose of two materials, as it occurs in rotating drums, and may be driven by boundary conditions(Santomaso et al., 2006).

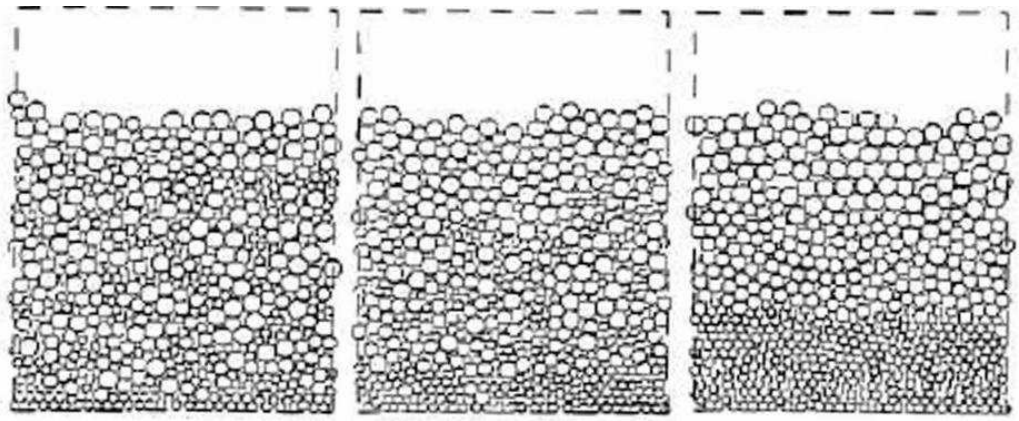

Figure 1.1: *Segregation in a vertically vibrated medium(Oda and Iwashita, 1999).*

Pattern formation. Again, when energy is injected into the system in form of vibrations, tappings, pattern formation at the surface of the medium can occur(Aranson and Tsimring, 2006), as it is shown for example in Figure 1.2, displaying strips, squares, hexagons, spyrals, interfaces, localized oscillons.

Flows. Localization, shear banding, hysteresis are some pheomena which occur when the material flows in confined or free-surface configurations; depending on the nature of dissipation and on the energy injected into the system, various flow regimes appear, which will be the subject of the next section.

1.5 Granular flows

Already in the speculations of Bagnold (1954, 1956) on the flow of particulate materials, three regimes have been identified: 1 - the kinetic, collisional regime which has been

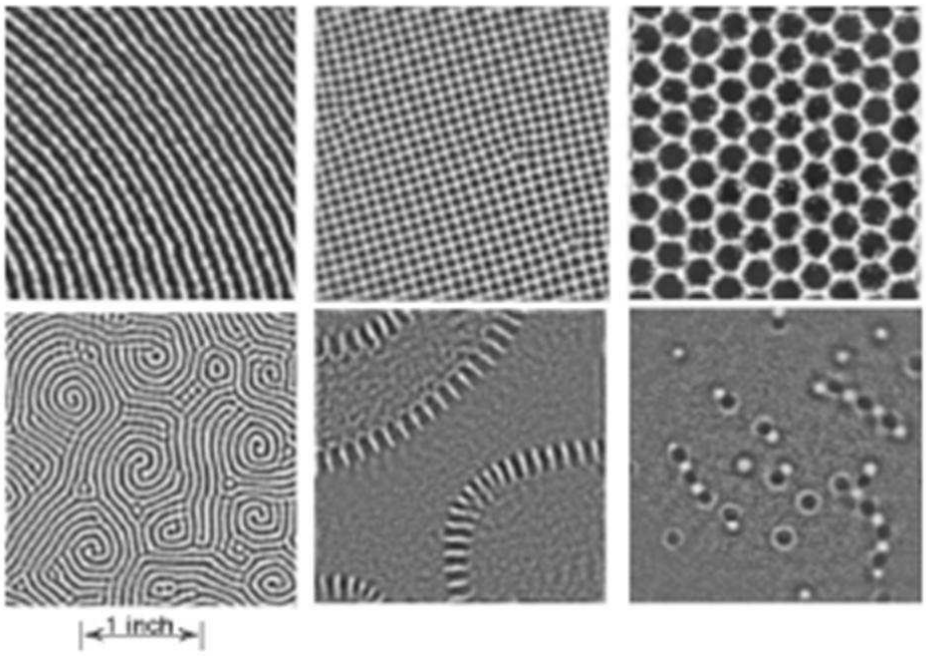

Figure 1.2: *Representative structures in vertically vibrated granular layers(Aranson and Tsimring, 2006).*

succesfully studied by means of corrections of the kinetic theory of gases (Jenkins and Savage, 1983); this regime has the lowest solid fraction, long lasting contacts are negligible and most of the energy is dissipated through inelastic collisions. Analogously to real gases, a temperature can be defined kinematically as the mean square fluctuation of the particle velocities. 2 - the quasistatic case, described by plasticity theories (Schofield and Wroth, 1968); slow deformation can occur with creep phenomena(Komatsu et al., 2001). In this regime particles can be thought in persistent contact: when a large number of particles lose respective contact, the phenomenon is called failure, which is generally localized in shear bands (which are generally different from shear bands appearing in dense flows). 3 - the intermediate, dense flowing regime, in which energy is dissipated by inelastic collisions and interparticle friction (G. D. R. Midi, 2004). Models for this regime, which is the subject of the present work, will be discussed later.

Dense flow of granular materials is a very common occurrence in several industrial chemical and related processes. Applications span from operations expected to be elementary, like transport or discharge from storage silos, to more complex ones like moving beds, rotating ovens, mills, granulators, mixers, etc. Difficulties in predicting the flow of such material surprisingly persist, despite quite a large amount of theoretical and semi-empirical studies. In this perspective, advances in the prediction of stress and flow patterns of the material is preliminary to further design goals. Understanding the stress distribution and the flow behaviour of granular materials in confined geometries has been a research

subject for engineers, both from fundamental (Nedderman, 1992; Savage, 1998) and technological (Böhrnsen et al., 2004; Schulze, 2008) standpoints.
A peculiarity of granular flows which needs to be cited in this introductory chapter is the onset of flow and its hysteretic behavior. Due to the fact that the system is athermal and dissipative, in order to have flow the injected energy must overcome a certain threshold; for this reason rheology for dense flows typically assume a viscoplastic behavior such as, for example, in Bingham fluids. This is common sense and can be exemplified by Dante's verses, when he wrote about a landslide: *"[...] quella ruina che nel fianco/ di qua da Trento l'Adice percosse/ o per tremuoto o per sostegno manco"*[1]. Moreover, it was clearly demonstrated that an hysteresis exists between the starting threshold and the stopping one (for a review, see Forterre and Pouliquen (2008)), such that for example the angle at which avalanche starts on an inclined plane is higher than the angle at which they stop.

1.6 Approaches to model the dense flow of granular materials: state of the art

At the present, two approaches are used in modeling granular flows: discrete and continuum. The first one, known as **DEM (Discrete Element Method)**, models the dynamics of the medium at the particle scale, applying force balances on each particle, possibly accounting for interparticle friction, inelastic collisions, non-spherical and cohesive particles. The attempt dates back to the work of Cundall and Strack (1979). Implementations may use different algorithms (Jean, 1999) and computation strategies, and both commercial and open-source simulation softwares are also available (Renouf et al., 2004). In particular, all DEM techniques start from posing the problem of motion given by Newton-Euler equations, which can be written(Dubois and Renouf, 2009):

$$\begin{cases} \mathbb{M}\dot{\mathbf{v}} & = \mathbb{P}(t) + \mathbf{r} \\ \mathbb{I}\dot{\omega} & = -\omega \wedge (\mathbb{I}\omega) + \mathcal{M}_{\mathbb{P}}(t) + \mathcal{M}_r \end{cases} \tag{1.1}$$

where $\mathbf{v}$ is the velocity of the center of mass, ω the angular velocity, $\mathbb{P}(t)$ and $\mathcal{M}_{\mathbb{P}}(t)$ the resultant and the momentum of external (body) forces, $\mathbf{r}$ and $\mathcal{M}_r$ the resultant and the momentum of contact forces, $\mathbb{M}$ and $\mathbb{I}$ mass and inertia matrices. Typically the resolution strategy is divided into three main steps: contact detection, contact force computation, performing movements, which are continuosly looped (in the sense that after each movement new contacts can be detected, new forces computed, and so on). The difference

[1] Dante, Inf. XII 4-6. Translation:"the rockslide that still marks the flank/ of the Adige, this side of Trent,/ whether by earthquake or erosion at the base" (Princeton Dante Project).

between different techniques lies principally in the way of considering contact forces. A class of methods exists (to which the first model by Cundall and Strack (1979) belongs) which can be called "smooth dynamics methods"(Dubois and Renouf, 2009), which are characterized by (1) explicit time integration and (2) a smooth description of contact laws. Briefly summarizing, these methods represent forces as an explicit function of particle interpenetration, therefore smoothing contacts and allowing to integrate forward in time. Another class of methods exists which is called "non-smooth contact dynamics" (or simply contact dynamics)(Jean, 1999), which is rather different in the sense that forces are calculated implicitly. It is not allowed for particles to deform at the contact interface (also claiming that this may cause unphysical behaviors), but rigid contacts are considered where forces are determined implicitly based on local force balances.
Even if simulation capabilities are growing fast, both because of hardware and software evolution, full size simulations using real particles (and not virtual, much larger ones) are often unachievable. On the other hand, DEM models may provide useful and realistic information on the micromechanics of granular material at a smaller scale.
On the larger, industrial scale, **continuum models** may be an alternative. Also in this case many approaches exist: the relation between strain and stresses, i.e. the constitutive relation has been mimicked by many modeling attempts. A classification can be made extending that proposed by Pouliquen and Chevoir (2002), dividing the main approaches into:

- **Hydrodynamic approaches**. These approaches (to which the model developed in Chapter 3 belongs) use the granular temperature concept derived from the kinetic theory of rapid granular flows, involving together with conservation of momentum, the equation of conservation of fluctuating energy. A 2-D hydrodynamic model was proposed by Savage (1998), using previous results by Hibler (1977). Considering the existence of two scales, characterizing respectively velocity and stress fluctuations, and assuming a stress-strain relation coming from a yield function and an associated flow rule(Nedderman, 1992), and that the distribution of strain rate is a gaussian, he found by averaging momentum balance equations constitutive relations between the average stress tensor and the average strain rate tensor. He showed, with the assumptions summarized above, that the relationship between tensors was viscous-like, with a viscosity depending on solids pressure and granular temperature. To close the system of equations he proposed a constitutive relation for the dissipation rate of fluctuating energy and an Equation of State relating solid fraction, pressure and granular temperature. The main problem with his model seems to be related with the strength of the assumption of large fluctuations of the strain rate

tensor, which would not be valid in the situations described by the author(Mohan et al., 2002). Another similar hydrodynamic model was proposed by Losert et al. (2000); Bocquet et al. (2002b), using constitutive relations coming from kinetic theory, adding a dependence of viscosity on solid fraction via a function diverging near the random close packing. The equation of state used by the authors considered only collisional mechanisms; the main problem with this approach seems to be its too strict relationship with kinetic theory, where different momentum transfer and dissipation mechanisms apply than in dense flow.

- **Cosserat material models**. These models(Mohan et al., 2002) are characterized by the inclusion of the angular momentum balance allowing for the transmission of couple stresses inside the materials. The stress-strain rate relationship is expressed through a yield function and a flow rule(Nedderman, 1992). The model was applied to a Couette cell(Mohan et al., 2002) showing good predictions apart from the solid fraction profiles; also an application to vertical chute flow was made by the authors(Ananda et al., 2008). A problem with these models is related to the assumption that the material trasmits couple stresses, yielding a non symmetric stress tensor. In order to judge whether or not this is feasible, the model should be compared with DEM data. Papers contrasting this assumption can be found in Literature(Goddard., 2008; Pouliquen and Gutfraind, 1996), and the analysis given in Chapter 7 seems to support the idea that even if particle rotate, this does not mean that globally the material transmits couple stresses.

- **Elasto-platic or hypoplastic theories**. These approaches are commonly adopted in the engineering field, usually solved by means of Finite Element Methods.The first are based on elasto-plastic laws (Wu et al., 2007), which describe the stress-rate of strain relationship via a yield surface, a plastic potential and a flow rule, in the spirit described by Nedderman (1992). Extensions are possible: for example, Wu et al. (2007) use a visco-elasto-plastic model, solving only the momentum balance equation in which the stress-rate of strain relationship is given by a viscous (a colinear, constant viscosity term) plus an elastoplastic term derived from Mohr-Coulomb yield criterion via a non-associated flow rule. On the other hand, hypoplastic theories specify constitutitve relations between stress tensor, its Jaumann derivative and the rate of strain, including the effect of void volume and granular skeleton (Kolymbas, 2000). These theories seem promising but neglect the importance of the fluctuating energy dynamics.

- **Self-activated phenomena.** Pouliquen and coworkers(Pouliquen and Gutfraind,

1996; Pouliquen and Forterre, 2009) developed an approach considering the fluctuations in the stress tensor as a source of energy capable to allow flow of the material. Subsequently they translated that phenomenology into a non-local self-activated model; their concepts were used succesfully to model the capillary flow of concentrated colloidal suspensions(Isa et al., 2007).

- **Order parameter description.** An order parameter description was proposed by Aranson and Tsimring (Aranson and Tsimring, 2001, 2002; Volfson et al., 2003), where the material is described as a binary mixture of jammed and flowing grains. The relative concentration of the two phases is given by an order parameter whose dynamics is described by Ginzburg-Landau equation(Ginzburg and Landau, 1950). The stress tensor is given by a liquid-like, viscous contribution plus a solid-like term proportional to the order parameter. The model was shown to be able to predict hysteretical features of dense granular flows, but seemed to fail in predicting the correct rheology(Aranson and Tsimring, 2006; Forterre and Pouliquen, 2008). An important issue which should be observed is that the order parameter introduced by the authors has only an indirect physical meaning, while hydrodynamic and Cosserat theories seem to be based on more reasonable additional variables.

- **Empirical models.** A synthesis of experimental and numerical results regarding simple two dimensional configurations of dense flow (simple shear, inclined chute, vertical chute, flow on a heap, rotating drum), was published by the French group G. D. R. Midi (2004). In that work dimensional analysis was used in order to describe a simple rheology, which was translated in a relationship between the effective coefficient of bulk friction and the inertial number (being a dimensionless number describing the relative importance of shear and pressure). The rheology outlined was tested against Couette cell DEM data(da Cruz et al., 2005) and in inclined plane configurations with good results(Jop et al., 2005). It was also extended in three dimensions simply assuming colinearity of stress and strain rate, and successfully applied to the case of flow on a heap(Jop et al., 2006). Due to its origin in dimensional analysis, the rheology can be interpreted also as a mixing-length model(Ertas and Halsey, 2002). Though the model seems to well behave in the case of free surface flows, it seems to fail when the flow is completely confined(Pouliquen et al., 2006).

Despite several attempts, a fully satisfactory description of granular flows in term of a pseudocontinuum is still lacking. Difficulties arise probably because of the original nature of granular materials, particularly with respect to their mesoscopic and dissipative nature,

but also to the loss of continuity of stress caused by the non-persistence of intergranular contacts. Some issues which have not been fully explained by means of continuum models are hysteresis in inclined chutes, the width of the shear bands in vertical chutes; on more complex geometries, quantitative prediction of both stress and velocity fields has never been properly reached.

In this thesis the work was focused on development and validation of continuum models, where attention is devoted both on simple configurations of gravity driven flow (vertical chute, inclined chute) and on more complex ones (silos, hoppers), and both on qualitative description and prediction of stresses and velocity fields: original contributions were given both regarding the rheology and the interface behavior (boundary conditions to be applied at the walls). Experimental and DEM were used for validation and parameter estimation. Also the problem of gas-solid flow in a channel below the fluidization threshold was addressed theoretically and experimentally.

Chapter 2

Some considerations on mixing length models of dense granular flows

Namque papaveris haustus itemst facilis quod aquarum;
nec retinentur enim inter se glomeramina quaeque
et perculsus item proclive volubilis exstat.

Tito Lucrezio Caro,*De Rerum Natura*, II 453-455

2.1 Introduction

The following chapter contains a work which was mainly published in Europhysics Letters(Artoni et al., 2007a). The main focus is on discussing the advantages and results of using a mixing-length, compressible model to account for shear banding behaviour in granular flow. A general approach was studied based on two functions of the solid fraction to be determined. Studying the vertical chute flow, it is shown that shear band thickness is always independent from flowrate in the quasistatic limit, for Coulomb wall boundary conditions. The effect of bin width is addressed using the functions developed by Pouliquen and coworkers(Jop et al., 2006) predicting a linear dependence of shear band thickness on channel width, while literature reports contrasting data. The influence of wall roughness on shear bands is also discussed. Through a Coulomb wall friction criterion it is shown that the model correctly predicts the effect of increasing wall roughness on the thickness of shear bands. Then a simple mixing-length approach to steady granular flows can be useful and representative of a number of original features of granular flow.

However, it is shown that the choice of boundary conditions has a strong influence on the results of the model, and therefore further analysis on this topic is needed.

2.2 The model

Many of the theoretical approaches appeared in last decade literature neglect the compressibility of granular materials, assuming it as an incompressible fluid with $\rho \approx const$. From a phenomenological point of view, dilatancy is a requirement for shearing a granular material, in other words, the material has to dilate in order to shear. Accordingly, we expect that neglect of dilatancy loses an important part of the granular flow physics.
In this chapter a simple model is formulated explicitly involving the solid fraction influence on the flow properties of granular materials. The model aims at being a generalization of the one developed by the GDR MIDI(G. D. R. Midi, 2004; da Cruz et al., 2005; Jop et al., 2006; Pouliquen et al., 2006) based on the dimensionless parameter I, considered as the ratio between shearing time and rearranging time due to pressure. In the GDR's formulation, the solid fraction is derived from I as being linearly depending on it. Here the formulation is reversed assuming the solid fraction ϕ to be the critical variable, instead of I, to reestablish the physical relevance of the dilation of the medium to determine the flow features. Giving the model an appropriate account of the solid fraction can become important for those geometries (like silos) in which ϕ varies significantly (more than 10%) all over the flow section. In silos flow can be seen to originate from fluidization due to the injection of voids from the exit hole, where solid fraction is quite different from its value in the core.
In this perspective, the ϕ-based model derivation and its application to the vertical chute arrangement are illustrated, to verify the constitutive relations proposed. The model was specifically used to predict the shear bands extension. This issue was considered (Pouliquen et al., 2006) as a weakness of the mixing length approach; predicted shear bands width and its dependence on geometrical and flow parameters apparently do not match some experimental data. In the following it is shown that also a simple mixing-length approach to steady granular flows can appropriatly predict the shear band thickness. The model outlined here is formulated for 2D, steady granular flows. The relevant equations are momentum balance with its two components, and the equation of continuity.
As a fundamental assumption, let's consider the flow structure to be solvable with the steady, compressible Navier-Stokes (N-S) equations, with a solid fraction, pressure and shear-dependent viscosity. In addition, we need a constitutive equation for η, and the de-

gree of freedom introduced by ϕ is saturated with a sort of Equation of State that involves pressure.
Accordingly, equations are:

$$\nabla \cdot \rho\vec{u} = 0 \tag{2.1}$$

$$\nabla \cdot (\rho u\vec{u}) = -\frac{\partial p}{\partial x} + 2\frac{\partial}{\partial x}\eta\left(\frac{\partial u}{\partial x}\right) + \frac{\partial}{\partial y}\eta\left(\frac{\partial u}{\partial y} + \frac{\partial v}{\partial x}\right) + \rho g_x \tag{2.2}$$

$$\nabla \cdot (\rho v\vec{u}) = -\frac{\partial p}{\partial y} + 2\frac{\partial}{\partial y}\eta\left(\frac{\partial v}{\partial y}\right) + \frac{\partial}{\partial x}\eta\left(\frac{\partial u}{\partial y} + \frac{\partial v}{\partial x}\right) + \rho g_y \tag{2.3}$$

where ρ is the local density of the compressible pseudo-homogeneous medium, which is, having neglected the interstitial fluid, and taken ρ_p as material density:

$$\rho = \rho_p\phi \tag{2.4}$$

2.2.1 Constitutive relations

A rheological law is assumed, based on dimensional analysis, like Prandtl's approach to turbulent flows, as discussed by Ertas and Halsey (2002). Because of the eminent precursor, we will call it "mixing length approach".
In this perspective the apparent viscosity of the medium is locally formulated as:

$$\eta = \rho_p\ L^2\ \ |\dot{\gamma}| \tag{2.5}$$

where the unique timescale is $|\dot{\gamma}|^{-1}$; L is a characteristic length, that has to be function of d and ϕ only, with a generic relation of the form:

$$L^2 = d_p^2\ f(\phi) \tag{2.6}$$

The function $f(\phi)$ is not known so far, but some features of it may be prescribed: it should diverge when $\phi \to \phi_{max}$, to limit the material flow (that becomes 'jammed'), i.e. $\eta \to \infty$. To achieve this limit η should diverge faster than $|\dot{\gamma}|^{-1}$, as it can be easily seen from Eq. 2.5. Interestingly, for $f(\phi) = 1$ Eq. 2.6 reduce to Bagnold scaling for shear stress (valid for rapid granular flows), providing a further requirement that $f(\phi \to 0) = 1$. However, the present work addresses dense flow of granular material, and we are not interested, at the moment, in the liquid-gas like transition.
Also, a relation between pressure and solid fraction is needed, which is similar to an Equation of State (EoS). Assuming shear rate plays the role of temperature in a gas, and ϕ acts through a geometrical (excluded volume) function $h(\phi)$ to be specified, dimensional analysis can be used to obtain the following EoS:

$$p = \rho_p\ h(\phi)\ (|\dot{\gamma}|\ \ d_p)^2 \tag{2.7}$$

To keep pressure finite when shear rate vanishes, $h(\phi)$ has to diverge when $\phi \rightarrow \phi_{max}$ (although value and physical meaning of ϕ_{max} is still a matter of debate (Josserand et al., 2006)). When dealing with Eq. 2.7, we must remember that the model is valid only for stationary flows: of course, a static granular packing can be found in a wide range of solid fraction, but we assume that when the system is flowing and is at stationary state, the only state where the material behaves rigidly is when $\phi \approx \phi_{max}$. In the dynamic regime the material explores its phase space to approach a unique solid fraction profile.

Dimensional analysis is broadly used in granular flow modeling attempts, starting from Bagnold's works(Bagnold, 1954, 1956). The formulation of Josserand et al. (2006) uses dimensional analysis with Coulomb friction to develop a constitutive relation for shear stress that is composed by a rate dependent part and a rate independent one, and where the isotropic part of the stress tensor is related to solid fraction by means of entropic considerations. Here, normal and shear stresses are expressed according to Pouliquen (Jop et al., 2006; Pouliquen et al., 2006), with the difference that solid fraction is used explicitly as the key variable, instead of dimensionless shear rate. Note that these laws, are very similar to those developed from hydrodynamic analogies (Bocquet et al., 2002b; Losert et al., 2000), where granular temperature is used to represent the local mobility of the medium. At this moment a simple closure is preferred, based on ϕ and an EoS for it, also because granular temperature is a variable which is difficult to measure and then correctly validate.

Rearranging Eq. 2.5-2.6, it is obtained:

$$\eta = \frac{p}{|\dot{\gamma}|}\frac{f(\phi)}{h(\phi)} = \frac{p}{|\dot{\gamma}|}G(\phi) \tag{2.8}$$

For sake of simplicity, it was replaced the ratio f/h with $G(\phi)$ and introduce:

$$F(\phi) = [h(\phi)]^{-1/2} \tag{2.9}$$

as a simple replacement, provided h always appears in this form in the following developments of N-S eqs. Note that G must vanish if $\eta\dot{\gamma} = \tau \rightarrow 0$.

It is easy to see that the functions F and G correspond, respectively, to the inertial number $I = \frac{|\dot{\gamma}|d_p}{\sqrt{p/\rho_p}}$ and to the effective friction coefficient μ^* as discussed by the GDR MiDi(G. D. R. Midi, 2004)(da Cruz et al., 2005), which was generalized to any configuration and dimensions beyond 1D. In simple, quasi-1D geometries, one can interpret G as the ratio of shear and normal stresses; in this sense μ^* was measured from DEM simulations by da Cruz *et al.*(da Cruz et al., 2005) and possible fittings for its dependence on I were discussed either by da Cruz *et al.* and by Pouliquen *et al.*(Pouliquen et al., 2006). This formulation is a generalization of those results in a 2 or 3-dimensional case, where it is

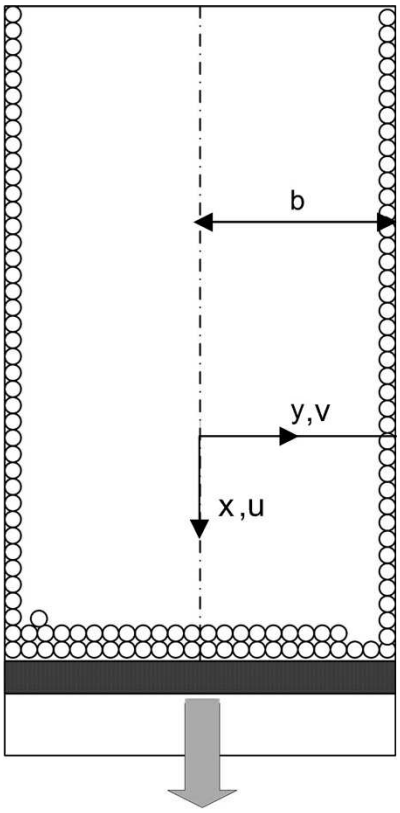

Figure 2.1: *Vertical chute scheme.*

recognized as fundamental the role played by solid fraction.

2.3 Applying the model to the vertical chute

The vertical chute configuration is choosen as a standard benchmark for model evaluation. Original flow structures, principally related to the width of shear zones, can be found in the chute flow, like in Couette cells. Reference for these configurations is the well known paper by GDR MiDi(G. D. R. Midi, 2004). Broadly speaking, the material flows in a plug-like fashion in the central part of the chute, while it is sheared near the wall. The extent of shear bands apparently approaches a typical dimension, of order 10-15 particle diameters. Predicting shear bands' thickness is a benchmark for all models applied to the chute and Couette flow(Pouliquen et al., 2006).

2.3.1 Vertical chute equations

A scheme of the chute is given in Fig. 2.1. For the steady vertical chute 2D flow, N-S equations simplify thanks to:

$$v = 0 \quad \frac{\partial}{\partial x} = \frac{\partial}{\partial t} = 0 \tag{2.10}$$

leading to:

$$\begin{cases} \frac{\partial}{\partial y}\eta\left(\frac{\partial\, u}{\partial y}\right) + \rho_p \phi g = 0 \\ \frac{\partial\, p}{\partial y} = 0 \end{cases} \tag{2.11}$$

It was also included Janssen effect, assuming pressure does not vary in the vertical direction. Eq. 2.11 additionally states that pressure will not vary horizontally either. The other equation can be integrated. With y originating from the center of symmetry and directed to the wall, as shown in Fig. 2.1, it is:

$$|\dot{\gamma}| = -\left(\frac{\partial u}{\partial y}\right) \tag{2.12}$$

to be replaced in the x-momentum balance in combination with Eq. 2.8, to give:

$$\frac{\partial}{\partial y}\eta\left(\frac{\partial\, u}{\partial y}\right) + \rho_p \phi g = -p\frac{\partial}{\partial y}\left[G(\phi)\right] + \rho_p \phi g = 0 \tag{2.13}$$

or

$$G(\phi) = \frac{\rho_p g}{p}\int_0^y \phi dy \tag{2.14}$$

$G(y=0)=0$ follows from Eq. 2.8 and symmetry, which requires the shear stress at the centerline to vanish.

From Eq. 2.14 we expect to identify $\phi(y)$ provided p and an invertible form of G are given. At the same time, $u(y)$ can be obtained from the EoS:

$$|\dot{\gamma}|^2 = \frac{p}{\rho_p\, h(\phi) d_p^2} \Rightarrow \frac{\partial u}{\partial y} = -\frac{\sqrt{p/\rho_p}}{d_p}F(\phi) \tag{2.15}$$

or

$$u(y) = u_{slip} + \frac{\sqrt{p/\rho_p}}{d_p}\int_y^b F(\phi)\, dy \tag{2.16}$$

where b is the half-width of the channel. So far, the unknown functions $\phi(y)$ and $u(y)$ can be formally obtained solving the coupled Eqs. 2.14 and 2.16, but in practice $F(\phi)$ and $G(\phi)$ must be specified, and also the pressure calculated.

The continuity equation can be used in its integral form, correlating local profiles to the total mass flowrate, $\dot{M}$. Experiments are easily performed with constant flowrate, either controlled by a simple hole in the bottom of the silo, or using a moving plate with fixed velocity. Accordingly:

$$2\ \rho_p \int_0^b \phi u\ dy = \dot{M} = \text{const} \tag{2.17}$$

Developing, an expression for the slip velocity can be formulated by using Eq. 2.16:

$$\int_0^b \phi \left(u_{slip} + \frac{\sqrt{p/\rho_p}}{d_p} \int_y^b F(\phi) dy' \right) dy = \frac{\dot{M}}{2\ \rho_p} \tag{2.18}$$

or:

$$u_{slip} = \frac{1}{\int_0^b \phi dy} \left[\frac{\dot{M}}{2\rho_p} - \frac{\sqrt{p/\rho_p}}{d_p} \int_0^b \phi \left(\int_y^b F(\phi) dy' \right) dy \right] \tag{2.19}$$

2.3.2 On boundary conditions

One of the most critical issue in granular flow simulation is identification and application of boundary conditions. For the solid fraction, it will be assumed that in the central zone of the chute material reaches ϕ_{max} (which could be random close packing, or some other critical value of ϕ that leads $h(\phi)$ to diverge(Josserand et al., 2006)). Divergence of h at the center is due to the fact that pressure is constant in the chute, but shear rate has to vanish at $y = 0$.

One constraint on velocity can be formulated as an integral condition, by fixing flowrate as done above. In addition, we must speculate on the interaction between the granular assembly as a continuum and the walls. The simplest view used in literature is assuming a layer of particles glued at the walls, for which a no-slip boundary condition can be used. This assumption is attracting for its simplicity but requires caution in its application. Some doubt can be cast on the fact that the continuum averaged interaction between nearest particles is the same in the bulk and in the layer of particles facing the glued ones. In this perspective, experimental investigation and critical theoretical speculations have to be done. A viable alternative to no-slip assumption is the Coulomb criterion at the wall:

$$\tau_w = \sigma_w tan\delta \tag{2.20}$$

where δ is a characteristic wall friction angle. In case of particle artificially fixed at the wall, this means assuming them as a wall, with a specific roughness measurable by its own δ. Combining Coulomb's law with Eq. 2.8 we obtain a condition on the solid fraction:

$$\tau_w = \eta_w \left|\dot{\gamma}\right|_w = \frac{p}{\left|\dot{\gamma}\right|_w} G(\phi_w) \left|\dot{\gamma}\right|_w = p\ G(\phi_w) \tag{2.21}$$

which leads to

$$G(\phi_w) = tan\delta \tag{2.22}$$

given that $\sigma_w = p$. Very important, with Coulomb's criterion the slip velocity is not zero, and has to be determined from Eq. 2.19 using flowrate. In addition Eq. 2.22 allows to calculate the pressure (normal stress), provided that:

$$G_w = G(y=b) = \frac{\rho_p g}{p} \int_0^b \phi \, dy \tag{2.23}$$

which gives:

$$p = \frac{\rho_p g \int_0^b \phi \, dy}{tan\delta} = \frac{\rho_p \phi_{ave} \, g \, b}{tan\delta} \tag{2.24}$$

where the average solid fraction, defined by $\int_0^b \phi dy = b\phi_{ave}$, has been introduced.

Combining Eqs. 2.24, 2.19, and 2.16, the velocity profile can be explicitly written as:

$$\begin{aligned} u(y) &= \frac{1}{\phi_{ave} b} \left[-\frac{\sqrt{\phi_{ave} g b}}{d_p \sqrt{tan\delta}} \int_0^b \phi dy \left(\int_y^b F(\phi) dy' \right) \right. \\ &\quad \left. + \frac{\dot{M}}{2\rho_p} \right] + \frac{\sqrt{\phi_{ave} g b}}{d_p \sqrt{tan\delta}} \int_y^b F(\phi) dy \end{aligned} \tag{2.25}$$

The result of Eq. 2.24 together with Eq. 2.14 leads to:

$$G(\phi) = \frac{tan\delta}{b \, \phi_{ave}} \int_0^y \phi \, dy \tag{2.26}$$

stating that in the approximation of $\phi \approx \phi_{ave}$

$$G(\phi) \approx \frac{y}{b} \, tan\delta \tag{2.27}$$

or G is a linear function of y, which provides a consistence criterion for the identification of the unknown function G.

Interestingly, the model, based also on Coulomb wall criterion, predicts the invariance of the velocity profiles with flowrate in the quasistatic limit (where $\phi \approx \phi_{ave}$ is valid). In other words, the scaled velocity profile:

$$\tilde{u} = \frac{u(y) - u_{slip}}{u_{max} - u_{slip}} = \frac{\int_y^b F(\phi(y)) dy}{\int_0^b F(\phi(y)) dy} \tag{2.28}$$

does not depend on flowrate, that influences only the slip tangential velocity. In this limit, the solid fraction profile also does not depend on flowrate, as predicted by Eq. 2.27, but only on bin width and wall friction angle. It has to be underlined that the result is independent of the particular formulation of the functions F and G. Also with Pouliquen's formulation for the effective friction coefficient (which can be seen as a particular choice for F and G), but with a Coulomb slip criterion, the independency of shear bands from flowrate is obtained. This is indeed a result supporting the mixing length approach. We think that shear bands independence on flowrate could be related to the stress structure

of granular matter, which develops internal stresses, supported by walls, to sustain itself; in this perspective, taking into account stresses in the formulation of boundary conditions would be necessary. However, far from the quasistatic limit, or in conditions where $\phi \approx \phi_{ave}$ is no more acceptable, flowrate can significantly affect $\phi(y)$ and $u(y)$ because of the close coupling of the two equations.

2.3.3 Deriving expressions for $F(\phi)$ and $G(\phi)$

Following the work of Pouliquen and coworkers, the functions would take the form:

$$\begin{cases} G(\phi) &= \mu_s + \frac{\mu_2 - \mu_s}{I_0/\tilde{\phi}+1} \\ F(\phi) &= \tilde{\phi} \end{cases} \tag{2.29}$$

where $\tilde{\phi}$ is the scaled solid fraction given by:

$$\tilde{\phi} = \frac{\phi_{max} - \phi}{\phi_{max} - \phi_{min}} \tag{2.30}$$

The authors (Pouliquen et al., 2006) acknowledged a major difficulty in the application to the vertical chute with no-slip at the walls; shear bands are not finite and of constant width in the quasistatic limit. It was have already demonstrated that a Coulomb wall slip criterion can correct this. In the following the results from the mixing length model including Coulomb wall slip criterion and F and G functions as in Eq. 2.29 will be illustrated for different chute width and wall roughness.

Before that, note the analytical solution achievable in the quasistatic limit, obtained combining Eq. 2.27 and 2.29:

$$\tilde{\phi} = \begin{cases} I_0 \frac{y - \mu'_s}{\mu'_2 - y} & for \;\; y > \mu'_s \\ 0 & for \;\; y \leq \mu'_s \end{cases} \tag{2.31}$$

where $\mu'_s = \mu_s b/tan\delta$ and $\mu'_2 = \mu_2 b/tan\delta$. The scaled velocity profile, obtained combining Eq. 2.28,2.29 and 2.31, is indeed a simple function of y:

$$\tilde{u} = \begin{cases} A(y-b) + B\ ln(C - Dy) & for \;\; y > \mu'_s \\ 1 & for \;\; y \leq \mu'_s \end{cases} \tag{2.32}$$

where A,B,C,D are known constants, depending on model parameters, wall friction angle and channel width.

In the following an analysis is performed, based on these analytical results; far from the quasistatic limit, one can repeat the calculations using Eq. 2.26 instead of Eq. 2.27, in a numerical fashion.

2.3.4 Shear bands thickness and chute width

It was already demonstrated that the model predicts that the shear band is independent on flowrate. Here the effect of bin width is explored.
Let's choose, as a measure of shear band width, the Δy from the wall to the point where $\tilde{u} \approx .99$. Using the quasistatic assumption, we calculate $\tilde{u}$ from Eq. 2.32, for different widths, b. Other model parameters must be given and they depend on the specific material choosen. for the purpose of illustrating the model, we used values determined by Jop *et al.*(Jop et al., 2006), collected in table 2.1, were used.

Table 2.1: *Parameters of the model(Jop et al., 2006).*

I_0	0.279	(adim)
μ_s	$tan(20.9)$	(adim)
μ_2	$tan(32.76)$	(adim)
ϕ_{max}	0.83	(adim)
ϕ_{min}	0.75	(adim)

Fig. 2.2 shows that the model predicts a linear correlation between shear band width and channel width. The slope of the linear dependency may change with different materials, but remains linear. It is frequently stated that the thickness of shear bands is expected to be independent from channel extension. However, literature reports data supporting (e.g. (Pouliquen and Gutfraind, 1996)) and contrasting (Nedderman and Laohakul, 1980) this statement. Our results agree with the experimental results by Nedderman and Lahoakul, but the issue requires further investigation of the vertical chute, in order to discriminate the applicability of a mixing-length model to this configuration. From the solid fraction profiles, it can be argued that $F(\phi) < 0.125$, that is, we are in the dense regime. Even if we are not in the quasistatic limit, the approximation $\phi \approx \phi_{ave}$ is still valid because the body force varies less than 2%, and so profiles can be calculated by means of Eq. 2.31 and 2.32. In fact, it is useful to see how the condition $\phi \approx \phi_{ave}$ can be valid beyond the quasistatic limit, and so the equations cited above can be used also in the dense regime.

2.3.5 Shear bands thickness and wall roughness

Wall roughness can influence the extension of the shear bands, according to the model. Adopting Coulomb criterion at the wall yields a simple expression of wall roughness, related to the wall friction angle δ, while using a no-slip condition makes impossible to

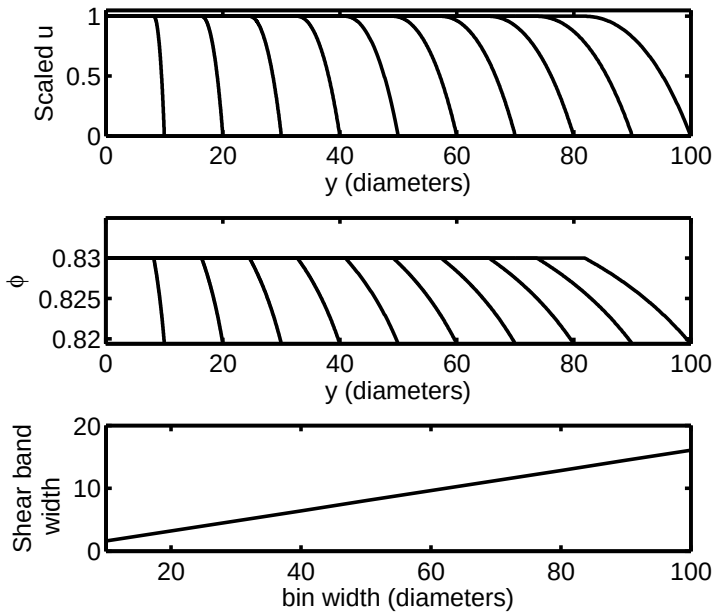

Figure 2.2: *First two figures: Non-dimensional axial velocity $\tilde{u}$, solid fraction* vs *non-dimensional channel width, in chutes with different extension (wall friction angle $\delta = 25\,\mathrm{deg}$). Third figure: shear bands thickness* vs *chute extension.*

account for roughness within a continuum approach. Also in view of real scale application of a mixing-length model, wall friction must be correctly accounted for, and the wall friction angle is a wide-spread approach. Furthermore, real world applications aim at perfect wall slip, but are often in an intermediate situation, where wall roughness plays a role.

Kishida and Uesugi (1987) performed experiments in shear cells probing that a correlation exists between a normalized wall roughness and the wall friction coefficient μ_w, that in their case was linear; in the case when wall roughness is built by gluing particles at the wall of the same material of the bulk, we would have:

$$\mu_w = m\,\chi + \mu_p \tag{2.33}$$

where χ is the ratio between wall and bulk particle diameters, μ_p the microscopic coefficient of friction, m a coefficient of order 1. However, their experiments showed that μ_w is upper-limited, and according to the paper, our values of χ would belong to a region of constant μ_w. A more recent work by Goujon *et al.*(Goujon et al., 2003) on the role of roughness in flows down inclined planes showed that friction reaches a maximum for a certain value of the ratio χ, and they related the behaviour at higher roughness to the fact that holes are filled by bulk particles, thus reducing friction. For the 2-D case, using the simple model by Goujon, it turns out from geometrical considerations that the value of

the ratio χ at which friction reaches a maximum is 4. Thus in the range $0-4$ friction is an increasing function of the relative roughness χ.

Results according to Eq. 2.32 are given in Fig. 2.3, showing that the model predicts a de-

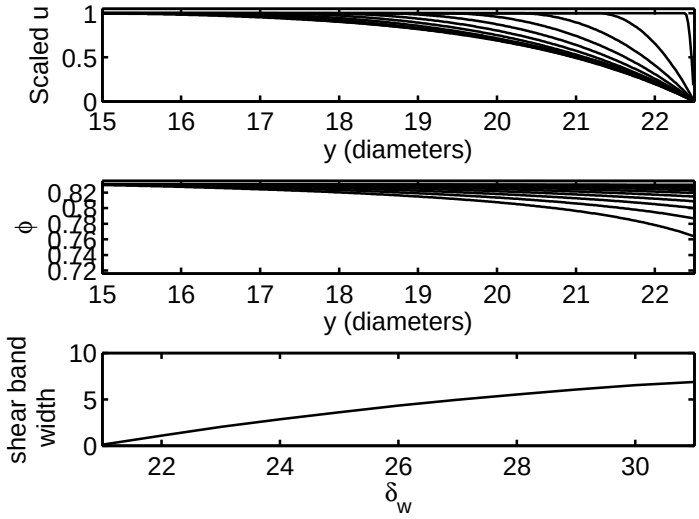

Figure 2.3: *First two figures: Non-dimensional axial velocity $\tilde{u}$, solid fraction* vs *non-dimensional channel width, in chutes with different wall friction (channel width = 50 particle diameters).Third figure: shear bands thickness* vs *wall friction angle.*

pendence of shearing regions on wall roughness. However, the effect of δ is approaching an asymptote. At small values slip occurs, whereas larger friction reduces its influence on the shearing bands. From the solid fraction profiles, the assumption $\phi \approx \phi_{ave}$ can be considered again as valid, because ϕ varies less than 10%. The enlargement of shear zones with increasing wall roughness is supported also by DEM results of Prochnow (Prochnow, 2002) (where χ is respectively 0.5, 1 and 4). Figure 2.4 illustrates qualitatively the comparison between DEM and our mixing-length, continuous model. The mixing length approach can capture the effect of increasing wall roughness predicted by DEM calculations by means of different sizes of particles fixed at the wall.

2.4 Is the mixing length model an answer to all of our questions?

The analysis developed in these pages seems to suggest that a mixing length model, when equipped with proper boundary conditions, can represent the physics of vertical chute flow predicting correct velocity profiles. This is true, but some considerations have to be introduced regarding both boundary conditions and the amount of physics embedded

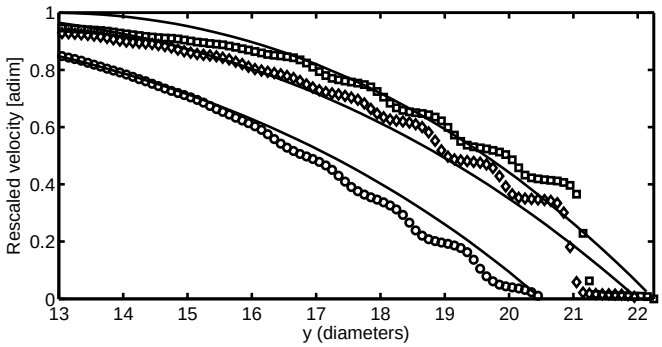

Figure 2.4: *Rescaled velocity profiles from DEM simulations by Prochnow (Prochnow, 2002) and continuous, mixing-length model. (circles: $D = 4\ d$, diamonds: $D = d$, squares: $D = 0.5\ d$), while continuous model calculations use different δ values.*

in the model. First, it is true that Coulomb boundary condition is more realistic than no-slip, even in the case where some particles are glued at the wall. However, Coulomb friction is valid in principle only if the material at the wall undergoes steady sliding; if the grains exhibit stick-slip behavior, it is reasonable to expect that Coulomb friction is no more a correct boundary condition. Moreover, it can be verified that in the quasistatic limit assuming a Coulomb boundary condition can yield negative slip velocitites (which is evidently not physical), once flowrate is controlled independently. Therefore, for a last word on the subject of the effectiveness of the mixing length model as well as of other models in general, correct boundary conditions must be developed and implemented. This will be the subject of Chapter 4. As regards the other problem, related to the ability of the zero-order closure mixing length model to represent important aspects of the physics of granular flows, it seems that some extension to the simple theory of G. D. R. Midi (2004) should be developed, in order to include dynamical features, such as hysteresis, and also to assess if the strong dependence of the results on the boundary conditions adopted is a property of the specific model or of granular rheology in general. This will be studied in Chapter 3.

Chapter 3

A fluctuating energy model for dense granular flows

La arena de los ciclos es la misma
E infinita es la historia de la arena;
Asì, bajo tus dichas o tu pena,
La invulnerable eternidad se abisma.

No se detiene nunca la caìda
Yo me desangro, no el cristal. El rito
De decantar la arena es infinito
Y con la arena se nos va la vida.

Jorge Luis Borges, *El reloj de arena*

3.1 Introduction

In this chapter the development of a new rheological model will be presented, whose results was published in Chemical Engineering Science(Artoni et al., 2009c) as well as at some conferences(Artoni et al., 2009a, 2007b, 2008). A model to simulate the dense flow of granular materials is presented. It is based on continuum, pseudo-fluid approximation. Balance equations and constitutive relations account for fluctuations in the velocity field, through the 'granular temperature' concept.
Here, it is choosen to derive the constitutive relations from analogies with the behavior of complex fluids, with the hypothesis that the granular material, intrinsically multiphasic, can be treated as a pseudo-fluid with a suitable reological behavior. Then, flow and stress

distribution might be simulated like other fluids in suitably modified computational fluid dynamics codes, for arbitrary geometries and constitutive models. Among the various rheologies proposed, the so-called hydrodynamic models (Savage, 1998; Bocquet et al., 2002b), developed from analogies with the kinetic theory of gases, introduce a second-order closure, taking into account the fluctuating part of the velocity field and its effects on the viscosity.

In this chapter, a phenomenological hydrodynamic model is presented, derived from considerations which are peculiar to the dense (and not gas-like) flow of granular materials, first of all the dissipation of mechanical energy due to friction. The model is formulated for cohesionless, dry granular materials, very common in many industrial scale flows. Fine powders and polymeric materials likely to accumulate charges and develop significant electrostatics effects, including tribocharging, are beyond the present scope. Because the model treats the granular material as a pseudo fluid, it can account for mixtures of granules of different nature or size, as long as the phenomenological parameter that describe the materials are determined, the composition and particle size do not vary (in time and space), additional mechanism not accounted in the model development become relevant (like drag of interstitial fluid or electrostatic interactions).

The derivations of the equations, together with the constitutive choices, are illustrated. The model is first applied to an industrial silo geometry, though not limited in its formulation to any geometry or flow configuration. It is shown that the model predicts realistic flow patterns, requiring quantitative validation with detailed measurements. Regarding the prediction of the normal stress at the wall during discharge, profiles closely match available correlations by Jannsen and Walker, including prediction of peak pressure where section changes. The prediction of both stress and velocity profiles is a non-trivial task for the continuum approaches(Böhrnsen et al., 2004). Also, the non-obvious issue of wall boundary conditions is also addressed and a partial slip model illustrated and applied. Connections with literature correlations together with a sensitivity analysis provide clues to link model parameters to intrinsic material properties. Moreover, also stress and flow patterns in a flat bottom geometry are presented. Finally, it is shown for a slightly modified version of the model that hysteretical behavior of free surface avalanches can be predicted together with the typical shape of the velocity field and dependence of the starting and stopping angles on the flow depth.

3.2 Model outline

Velocity fluctuations are a fundamental concept used in models for the collisional, gas-like regime of granular flows, based on analogies with dense gases (Chapman and Cowling, 1960). The notion of *granular temperature* was introduced to summarize and quantify such fluctuations (Jenkins and Savage, 1983), i.e. $\theta =< \tilde{v}^2 > /3$, where $\tilde{\mathbf{v}}$ is the fluctuating component of the velocity vector.
In dense, slow flow of granular materials, even if the mechanisms of dissipation of energy are different from the collisional flow, yet velocity fluctuations are not negligible. The granular temperature can be assumed as a local measure of the *dynamic* flowability of the pseudo-fluid, or a local mobility.
Experiments have been done (Natarajan et al., 1995) to measure granular temperature in vertical chute flows and to include θ in models of dense granular flow (Savage, 1998; Losert et al., 2000; Bocquet et al., 2002b; Strumendo and Canu, 2002). The model presented here is based on conservation laws for the key quantities (mass, momentum and fluctuating energy) and the fundamental mechanisms are described by constitutive laws relating the unknowns variables $\mathbf{v}$ and θ.

3.2.1 Conservation laws

In order to derive the general balance equations for mass, linear momentum and translational kinetic energy for granular materials, the macroscopic space-time weighted balance equations have been written as follows:

$$\partial_t (\rho) + \nabla \cdot (\rho \bar{\mathbf{v}}) = 0 \tag{3.1}$$

$$\partial_t (\rho \bar{\mathbf{v}}) + \nabla \cdot (\rho \bar{\mathbf{v}} \bar{\mathbf{v}}) = -\nabla \cdot \underline{\underline{\sigma}} + \rho \mathbf{g} + \mathbf{t}^F \tag{3.2}$$

$$\partial_t \left[\rho \left(\epsilon^T + E^T\right)\right] + \nabla \cdot \left[\rho \left(\epsilon^T + E^T\right) \bar{\mathbf{v}}\right] = \\ -\nabla \cdot \left(\underline{\underline{\sigma}} \cdot \bar{\mathbf{v}} + \mathbf{q}^T\right) + \rho \mathbf{g} \cdot \bar{\mathbf{v}} - z^T + \mathbf{t}^F \cdot \bar{\mathbf{v}} + D^{TF} \tag{3.3}$$

Equations are based on Babić (1997) formulation, but the sign convention for the stress tensor and the energy flux has been changed.
The balance equation for the angular momentum has been neglected, based on the assumption that Cosserat effects are negligible in the absence of external couples, even if particles are known to roll somehow at their scale, as demonstrated by (Goddard., 2008). Moreover, in most dense, slow flow configurations the momentum transport arising from the coupling with the interstitial fluid, *i.e.* $\mathbf{t}^F$ and D^{TF}, can be neglected. Taking the product of $\bar{\mathbf{v}}$ with Eq. (3.2), and considering the tensorial relation:

$$\nabla \cdot \left(\underline{\underline{\sigma}} \cdot \bar{\mathbf{v}}\right) - \bar{\mathbf{v}} \cdot \nabla \cdot \underline{\underline{\sigma}} = \underline{\underline{\sigma}}^{\dagger} \colon \nabla \bar{\mathbf{v}} \tag{3.4}$$

for the stress tensor $\underline{\underline{\sigma}}$, the following equation can be obtained:

$$\partial_t \left(\rho\epsilon^T\right) + \nabla \cdot \left(\rho\epsilon^T \bar{\mathbf{v}}\right) = -\underline{\underline{\sigma}}^{\dagger} \colon \nabla\bar{\mathbf{v}} - \nabla \cdot \mathbf{q}^{\mathbf{T}} - z^T \tag{3.5}$$

where the two most significant terms for this study, $\mathbf{q}^{\mathbf{T}}$ and z^T are evident, i.e. the flux of energy and the its dissipation rate, respectively.
By means of the mentioned definition of granular temperature, θ, the last equation rearranges to:

$$\frac{3}{2}\partial_t \left(\rho\theta\right) + \frac{3}{2}\nabla \cdot \left(\rho\theta\bar{\mathbf{v}}\right) = -\underline{\underline{\sigma}}^{\dagger} \colon \nabla\bar{\mathbf{v}} - \nabla \cdot \mathbf{q}^{\mathbf{T}} - z^T \tag{3.6}$$

Splitting the stress tensor $\underline{\underline{\sigma}}$ into its spherical ($p\mathbf{I}$) and deviatoric ($\underline{\underline{\tau}}$) part, the linear momentum Eq. (3.2) simplifies to:

$$\partial_t \left(\rho\bar{\mathbf{v}}\right) + \nabla \cdot \left(\rho\bar{\mathbf{v}}\bar{\mathbf{v}}\right) = -\nabla p - \nabla \cdot \underline{\underline{\tau}} + \rho\mathbf{g} \tag{3.7}$$

Assuming the stress tensor to be symmetric, as a consequence of the absence of couple stresses and using the splitting of $\underline{\underline{\sigma}}$, Eq. 3.6 can be rewritten as:

$$\frac{3}{2}\partial_t \left(\rho\theta\right) + \frac{3}{2}\nabla \cdot \left(\rho\theta\bar{\mathbf{v}}\right) = -p\nabla \cdot \bar{\mathbf{v}} - \underline{\underline{\tau}} \colon \nabla\bar{\mathbf{v}} - \nabla \cdot \mathbf{q}^{\mathbf{T}} - z^T \tag{3.8}$$

Finally, it is assumed assume that the flow is nearly incompressible, i.e. $\rho \approx$ const. This is perceived as a crucial issue. As argued in Chapter 2, allowing for dilatancy effects by assuming a compressible pseudo-fluid would be a major advancement both for physical consistency of the model and its practical application. As a matter of fact, in several dense flow configurations the solid fraction ϕ varies more than 10%, like in the discharge region of a silo. The issue is relevant also in those cases where a gas is forced to flow across the granular material, to predict preferred paths and residence time distibutions of the gas. So far, whenever ϕ is known to vary less than 10%, equations have been derived using the incompressibility assumption. Accordingly, the continuity equation reduces to $\nabla \cdot \bar{\mathbf{v}} = 0$ allowing for simplifications in the linear momentum and energy balances, Eq. 3.7 and Eq. 3.8, leading to their final form used for calculations:

$$\frac{3}{2}\rho\partial_t \left(\theta\right) + \frac{3}{2}\rho\bar{\mathbf{v}} \cdot \nabla\theta = -\underline{\underline{\tau}} \colon \nabla\bar{\mathbf{v}} - \nabla \cdot \mathbf{q}^{\mathbf{T}} - z^T \tag{3.9}$$

$$\rho\partial_t \left(\bar{\mathbf{v}}\right) + \rho\bar{\mathbf{v}} \cdot \nabla\bar{\mathbf{v}} = -\nabla p - \nabla \cdot \underline{\underline{\tau}} + \rho\mathbf{g} \tag{3.10}$$

On the other hand, when the ϕ variation is significant, the more general Eqs. 3.7 and 3.8 should be used, together with some "Equation of State"-like relationship to close the system of equations. However, the development of some approximation like Boussinesq's one (i.e. retaining the effect on the density variations only for the body forces) would be helpful to limit mathematical complexity and improve numerical stability.

3.2.2 Constitutive relations

The equations listed above are based only on conservational principles, thus they are always valid under the assumptions made. However, as it is often the case, they do not provide insights into the physics of the problem, which must be expressed in form of constitutive relations for the unknowns in the system of equations. These unknowns are the stress tensor $\underline{\underline{\sigma}}$, the energy flux vector $\mathbf{q^T}$ and the energy dissipation rate z^T.
In order to solve our system of equations, we need now to express some constitutive hypothesis for these variables.

Energy flux and stress tensor

With the assumption that fluctuating energy can propagate by a diffusion-like mechanism, then proportional to its gradient (Savage, 1998),

$$\mathbf{q^T} = -\underline{\underline{K}} \cdot \nabla\theta \tag{3.11}$$

Hereafter it will be assumed isotropic diffusion, so that the diffusivity tensor $\underline{\underline{K}} = k\underline{\underline{I}}$, simplifying to:

$$\mathbf{q^T} = -k\nabla\theta \tag{3.12}$$

Regarding the stress tensor, dense granular flows appear to exhibit a viscous-like character, whose origin is a matter of debate. Savage (1998) used previous results by Hibler to demonstrate that if a plasticity framework was applied to the instantaneous stress field, with the hypothesis that the fluctuations were gaussian, the average stress tensor had a viscous-like dependence on the average strain rate tensor. In this case, we can assume that the deviatoric part of the stress tensor can be expressed as:

$$\tau_{ij} = -\eta\left(\frac{\partial v_i}{\partial x_j} + \frac{\partial v_j}{\partial x_i}\right) \tag{3.13}$$

meaning that the granular material can be treated as a generalized Newtonian fluid (Bird et al., 2002). Note that only one viscosity appears due to the usual approximations involving the incompressibility condition, which permit to neglect the bulk viscosity coefficient (Aris, 1962; Bird et al., 2002). The generalized Newtonian fluid is a non-newtonian fluid whose viscosity can depend on all the variables, particularly on the invariants of the deformation rate tensor. In our case, we aim at highlighting dependencies on the fluctuating energy summarized by the granular temperature.
It is worth underlining that this formulation implies that in a vertical chute (for example in the cylindrical section of a silo) the ratio of the stress tensor components σ_{rr} and σ_{zz} is 1, because the deviator components vanish along those directions. This results was

already stated by (Savage, 1998), and is common to all the generalized newtonian models such as Jop's one (Jop et al., 2006). Such an implication might be questionable; however there is not a clear proof of the contrary, particularly when dealing with *flowing* granular materials. This is an often neglected issue which at least needs to be recognized, in order to better understand the subtle implications of many modeling choices. This topic will be further discussed in chapter 7, in analysing DEM data.

The next step in the development of constitutive relations is thus the determination of the constitutive coefficients k and η, which will be in general functions of all the dependent and independent variables and their derivatives. To recover scaling of the flow profiles with particle diameter and bulk density, k and η must depend on ρ and d_p as follows:

$$k = \rho d_p^2 k' \qquad \eta = \rho d_p^2 \eta' \tag{3.14}$$

where primes indicate that are functions of the remaining variables. For k', it is choosen not to follow Savage (1998) who suggested $k/\eta \approx$ const, extrapolating a result of Jenkins' kinetic theory, which is not valid in the dense regime under study. So far k' will be considered as a constant.

Granular materials are often considered to belong to the family of glassy systems (Tarzia et al., 2004; Grebenkov et al., 2008), in which a transition between flowing and non-flowing behaviour is characterized by a sharp increase in viscosity, also typical of yield-stress fluids. The liquid-glass transition has been extensively studied, both experimentally and theoretically. The empirical equation proposed long ago by Doolittle (1951) for the fluidity (*i.e.* the reciprocal of viscosity, η^{-1}) of a glass is

$$\psi = \psi_0 exp\left(-\gamma \frac{v_m}{v_f}\right) \tag{3.15}$$

where v_m and v_f are the volume of the molecule and the free volume respectively. This relation has been justified theoretically within a free volume approach (Cohen and Grest, 1979). Analogous expression containing free volume was derived for the viscosity of simple liquids by Eyring and coworkers (Glasston et al., 1941) within the theory of rate processes, where the deformation of the medium was described as a thermally activated process in a system characterized by energy barriers imposed by caging effects (considering that in dense media the passage of a molecule of fluid from a position to another requires that a suitable hole is provided).

It is possible to take advantage of these results to formulate a semi-theoretical approximation, considering Doolittle equation to apply to η and identifying an analog of the free volume in the granular material. As a candidate, the simplest choice would be the porosity which is the quantity with the closest physical meaning. Defined as the complement

of the solid fraction, $1-\phi$, the porosity measures the amount of *void* volume. However, this analogy does not explain several aspects. Porosity is rather a static than a dynamic measure of the free volume. The free volume does not necessarily coincide with the volume being effectively void, but is rather an expression of the local 'mobility' of the fluid. The role of mobility could be better described by the granular temperature, that, being a measure of the amplitude of velocity fluctuations, is indeed related to the local ability to move, and thus to the concept of free volume. Also the compactivity X introduced by Edwards and Oakeshott (1989) to describe the packing ability of granular materials through cooperative spatial rearrangements (and therefore related to free volume fluctuations), has not been directly correlated with the fluctuations of velocity.
Intuition suggests that both free volume and velocity fluctuations are stricly related and play a major role in the dynamics of flowing granular assemblies. A detailed and reliable microstuctural theory proving the connection between these variables has to be developed. Here the rheological properties of the granular medium have been semi-theoretically assumed to depend on the velocity fluctuations. Accordingly, the viscosity has been tentatively formulated to mimick Eyring's equation for simple liquids, $\eta = Aexp\left(\frac{E}{T}\right)$ by replacing the thermodynamic temperature, T, with granular temperature, as follows:

$$\eta' = \eta_0 exp\left(\frac{\theta^*}{\theta}\right) \tag{3.16}$$

where θ^* has granular temperature dimensions, and is a sort of *temperature scale*. It is worth noticing that recent numerical results for Newtonian liquids with a highly temperature-dependent viscosity, like magma flows (Costa and Macedonio, 2003, 2005) show velocity and (thermodynamic) temperature profiles which are very similar to those reported for granular chute flows.
In the expression for η' it was neglected a direct dependence on the history of deformation (though it acts indirectly through θ): while this hypothesis is useful to work with simple equations, it could be an over-simplification restricting the validity of the approach to time-invariant processes (Goddard, 2006).

Energy dissipation rate

In this paragraph a model for the energy dissipation rate z^T is formulated. Consider an undeformable solid block moving at constant velocity on a flat surface. It is well known that in order to have a positive velocity, friction requires that a force $\mathbf{F}$ is supplied higher the frictional force $\mathbf{F}_f$. The energy dissipated by friction, in this simple situation, is the work done by the frictional force $\mathbf{F}_f$. It is straightforward to derive the rate of dissipation of energy by friction, which will be $dE_{diss}/dt = \mathbf{F}_f \cdot \mathbf{dx}/dt = \mathbf{F}_f \cdot \mathbf{v}$.

Moving forward, the above definition is applied to a stack of infinitesimal sheets sliding one above the other in the absence of gravity, suffering a vertical constant pressure as shown in Figure 3.1. From the friction law, the force is proportional to the pressure and

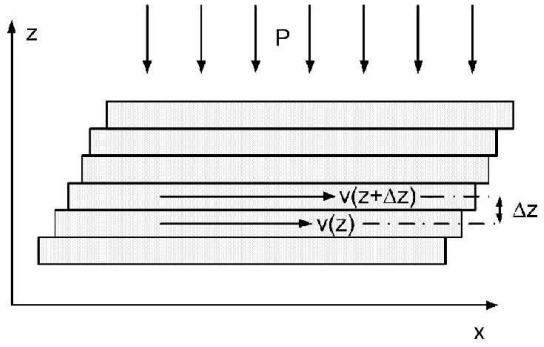

Figure 3.1: *Illustration of the frictional energy dissipation mechanism.*

the extent of contact between two layers, S, i.e. $F_f = \mu PS$. Friction between the layers at z and $z+\Delta z$ dissipates energy at a rate $\dot{E}_{diss} = \mu PSv'$, where v' is the relative velocity of the two layers, $v(z+\Delta z) - v(z)$. The rate of energy per unit volume dissipated by friction in this configuration, which corresponds to the term z^T of the rheological model, can thus be obtained by:

$$\dot{E}_{diss} = \frac{d\dot{E}_{diss}}{dV} = \mu P \frac{dv}{dz} \tag{3.17}$$

Compared to a real granular flow, the representation of Figure 3.1, which yields Eq. 3.17, is quite simplistic. The original network of forces of granular materials under shear together with the bi- and tri-dimensional arrangement of the particles and the threshold behaviour of microscopic friction define a more complex scenario. However, there is still a chance to take advantage phenomenologically of the meaning of the simple expression provided by Eq. 3.17. Equation 3.17 states that the rate of dissipation of the specific energy related to friction in a continuum of contacts is proportional to normal stresses and to the spatial gradients of the velocity, via a friction coefficient. The result can be extended to higher-dimensional cases, recalling that a measure of the spatial velocity gradients is the shear rate $|\dot{\gamma}|$, (the reciprocal of which is a fundamental time scale of the system) , and taking the isotropic part of the stress tensor p as a measure of normal stresses. Shortly, the following formulation is proposed:

$$z^T = \mu p \, |\dot{\gamma}| \tag{3.18}$$

where μ is now an effective friction coefficient, which will be in principle different from the microscopic one. Shear rate can be defined as:

$$|\dot{\gamma}| = \sqrt{\frac{1}{2} \sum_i \sum_j (\epsilon_{ij} \epsilon_{ij})} \tag{3.19}$$

where

$$\epsilon_{ij} = \frac{\partial v_i}{\partial x_j} + \frac{\partial v_j}{\partial x_i} \tag{3.20}$$

In the following the effective friction coefficient μ will be considered as a constant. However, it is likely that, being μ an effective coefficient and not a material property, it can be a function of shear rate, pressure, granular temperature.

With the help of the constitutive relations above, the fluctuating energy balance can be further simplified to:

$$\frac{3}{2}\rho\partial_t(\theta) + \frac{3}{2}\rho\bar{\mathbf{v}}\cdot\nabla\theta = k\Delta\theta + \dot{Q} \tag{3.21}$$

where $\dot{Q}$ collects the production ('heating'), due to shear, and the dissipation ('cooling') because of friction, of the fluctuating energy:

$$\dot{Q} = -\underline{\underline{\tau}}\colon \nabla\bar{\mathbf{v}} - z^T \tag{3.22}$$

The viscous 'heating' term can be represented in Cartesian notation as:

$$\eta\left(\frac{\partial v_i}{\partial x_j} + \frac{\partial v_j}{\partial x_i}\right)\frac{\partial v_i}{\partial x_j} = \eta\left|\dot{\gamma}\right|^2 \tag{3.23}$$

where summation over repeated indices is implied. Thus, the heating and cooling terms can be written as:

$$\dot{Q} = \left|\dot{\gamma}\right|\left(\eta\left|\dot{\gamma}\right| - \mu p\right) = \left|\dot{\gamma}\right|\left(\left|\tau\right| - \mu p\right) \tag{3.24}$$

to be included in Eq. 3.21, resulting in the form actually used for calculations. This energy balance determines whether yielding leads to dilatancy or to contractancy (compression) of the material. In this sense the model bears some analogy with the critical state theory developed in soil mechanics. If the material is not sheared, nothing changes its potential mobility (the material does not acquire nor lose flowability) because $|\dot{\gamma}| = 0 \Rightarrow \dot{Q} = 0$, and θ remains at its initial distribution. Under shear, the condition when $|\tau| = \mu p$ is analogous to the critical state condition of granular flow without volume variations. However material can both increase its fluidity when $|\tau| > \mu p$ or lose it ($|\tau| < \mu p$). Accordingly, the total net production (or consumption) of fluctuating energy is formulated to involve the timescale $|\dot{\gamma}|^{-1}$ and the distance from the critical state condition. Using chemical terms, the shear rate plays the role of a kinetic constant, while the distance from the critical state is like a $C - C^{eq}$ term. In addition, it is possible to see that in case of plane shear (constant shear stress, τ_0), the shear rate acts as a kinetic constant with an Arrhenius dependence on granular temperature:

$$\left|\dot{\gamma}\right| = \frac{\tau_0}{\eta} \sim \exp\left(-\frac{\theta^*}{\theta}\right) \tag{3.25}$$

somehow confirming the role of θ in activating the flow process.

3.3 Wall boundary conditions

The issue of boundary conditions is of major importance in dense granular flows. Close to the walls, partial slip, rather than no-slip at all, is the most common behaviour.
Traditionally, slip is characterised via a Coulomb yield criterion, relating tangential and normal stresses at the walls through a constant friction coefficient. Though appearing a physically sound choice it has been shown that wall friction coefficient may vary, resulting in an apparent coefficient, not corresponding to the microscopic, wall-particle friction coefficient. In fact, an investigation of the dependence of such effective coefficient on relevant variables is still lacking and we can speculate that its value will strongly depend on the flow properties, in addition to the local stress. Reflections on this topic were the nucleus of the development of new boundary conditions, which are described in Chapter 4.
In this chpater a different approach based on the so-called Navier slip condition has been used, relating the tangential velocity at the boundary to its gradient in the normal direction through a constant parameter, λ, called "slip length":

$$u_t = \lambda \left| \frac{\partial u_t}{\partial n} \right| \tag{3.26}$$

This condition allows for a certain amount of slip, which is expressed by means of a simple and measurable quantity. The approach is general and not restricted to uniformly flat walls; ,it can be used also for bumpy surfaces which are expected to reduce particle slip, due to a much larger roughness, resulting in a lower coefficient λ. Experimental and numerical work is needed calibrate λ on material and flow properties, and we are working on it. Nevertheless, the Navier approach is interesting because (1) it contains both no-slip and perfect slip situations (in the two limits $\lambda \to 0$ and $\lambda \to \infty$) and (2) because it respects the physics: in the limit of high normal stress no-slip behaviour is approached. Interestingly, its implementation improves convergence with respect to Coulomb's condition.
In the following the value of the slip length will be quantified in terms of particle diameters, provided that d_p is the characteristic inner length scale of the flowing material. Accordingly, slip will be characterised by a dimensionless number λ/d_p. Details about the non-obvious implementation of conditions given by Eq. (3.26) are reported in the next section.

3.4 3D Navier slip boundary condition

It can be useful to represent the generic 3-D formulation of this condition, which is often used in microfluidic problems; at first, the condition asks that the normal velocity vanishes at the boundary:

$$\mathbf{v} \cdot \mathbf{n} = 0 \tag{3.27}$$

which, together with Eq.3.26, which can be rewritten as:

$$\begin{aligned} \mathbf{u_1} &= \lambda \frac{\tau_\mathbf{1}'}{\eta} \\ \mathbf{u_2} &= \lambda \frac{\tau_\mathbf{2}'}{\eta} \end{aligned} \tag{3.28}$$

where the $\tau_\mathbf{i}'$ are the deviatoric components of the stress tensor, form an appropriate set of boundary condition for the 3-D case. After having defined an orthonormal basis $[\mathbf{n}\ \theta_\mathbf{1}\ \theta_\mathbf{2}]$ where the first component is the normal to the surface, while the other two components represent two *tangents* identifying the surface. The normal stress is given by:

$$\sigma = t_x n_x + t_y n_y + t_z n_z \tag{3.29}$$

and the tangential stress is identifyied by two vectors:

$$\begin{aligned} \tau_\mathbf{1} &= \mathbf{t} \cdot \theta_\mathbf{1} \\ \tau_\mathbf{2} &= \mathbf{t} \cdot \theta_\mathbf{2} \end{aligned} \tag{3.30}$$

The deviatoric components of the stress tensor with respect to the surface are calculated in analog way, taking into account the fact that in the present model the deviatoric cmponents of the force per unit area at the boundary are given by:

$$t_i' = \sum_j n_j \eta \left(\frac{\partial u_i}{\partial x_j} + \frac{\partial u_j}{\partial x_i} \right) \tag{3.31}$$

From this it can be derived, for the i-th component of the projection of $\mathbf{u}$ on k ($k = 1, 2$), i.e. the i-th component of $\mathbf{u_1}$ or $\mathbf{u_2}$, the relation (where summation over j is implicit (Einzel et al., 1990)):

$$u_{ki} = u\theta_{ki} = \lambda n_j \left(\frac{\partial u_i}{\partial x_j} + \frac{\partial u_j}{\partial x_i} \right) \theta_{ki} = \lambda n_j \epsilon_{ij} \theta_{ki} \tag{3.32}$$

Two BCs will be defined, formally given by (f_{ki} is the right member of Eq.3.32, and $k = 1, 2$):

$$u_k - \sum_i f_{ki} = 0 \tag{3.33}$$

that becomes, with implicit summation over i and j:

$$u_k - \lambda n_j \epsilon_{ij} \theta_{ki} = 0 \tag{3.34}$$

or, in a more plain form:

$$u_k - \sum_i \left\{ \lambda \sum_j \left[n_j \left(\frac{\partial u_i}{\partial x_j} + \frac{\partial u_j}{\partial x_i} \right) \right] \theta_{ki} \right\} = 0 \tag{3.35}$$

3.5 Silo with converging hopper

Storage silos and hoppers are considered a reference for the dense regime of granular flow, although many different configurations have been studied, as nicely catalogued in the report of G. D. R. Midi (2004). Prediction of the flow patterns in a silo is required to guarantee an effective use of the silo volume, preventing the formation of stagnant zones of material (due to core flow and piping regimes) that affect the residence time distribution of the stored material. The issue is relevant when the material can undergo physical of chemical tranformations, changing its nature or applicative properties (Santomaso et al., 2006). In addition, predicting the stress distribution in the flowing material is important to prevent 1) arching and flow stoppage, 2) failure of the wall structure, and 3) breakage and comminution of particles due to stress in the bulk.

Real scale silos show a complex dynamic behaviour (Nielsen, 1998; Schwedes and Feise, 1995). The onset of flow is characterised by a pressure wave (see Figure 3.2) that changes the stress distribution in the converging section. The hopper is said to be in an active stress state (with the major principal stesses vertically oriented) after filling and in a passive state (with the major principal stesses horizzontally oriented) when discharging (Nedderman, 1992). The cylindrical part is frequently assumed to be permanently in an active stress state. The change in stress orientation is called the *switch*. The switch is characterized by a marked stress peak at the wall which moves progressively from the outlet (at the onset of the flow) up to the transition between the cylindrical and the converging part, where it remains, at steady state. The steady state stress profile is however only an approximation, because the stress field (and the velocity field as well) can be unsteady during discharge, with oscillations and symmetry-breaking effects (Nielsen, 1998; Böhrnsen et al., 2004). Moreover the assessment of the true stress profile is not obvious because experimental measurements can be affected by local autoinduced phenomena created by load cells. Nevertheless, in axysimmetric silos, where the loss of symmetry is unlikely (Nedderman,

1992), regular flow can be observed and Janssen and Walker solutions can be taken as a reference for wall stress profiles at steady state.

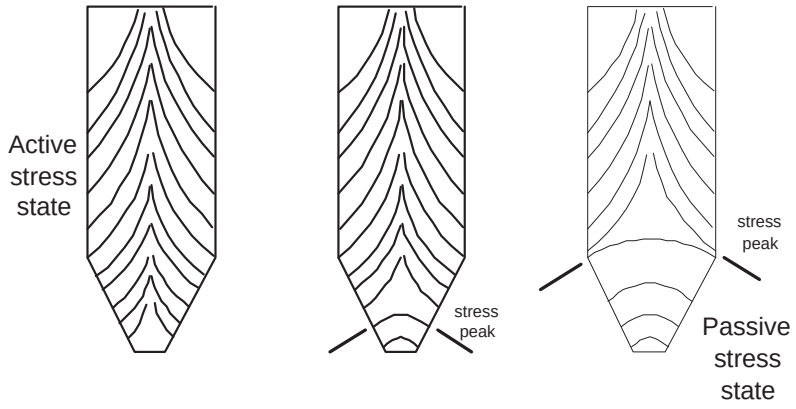

Figure 3.2: *Development of active and passive states in silos. Switch mechanism. Lines represent principal stress directions. Modified after Böhrnsen et al. (2004)*

3.5.1 Numerical calculations

Eqs. 3.9 and 3.10 are four PDEs in a 3D geometry. They are coupled because granular temperature affects the viscosity in the momentum equations, which determine velocities that modify the granular temperature distribution. Mathematically, Eqs 3.9 and 3.10 are very similar to advection and diffusion eqs. whose solution is implemented in many commercial and open source codes, using state-of-the-art numerical methods and graphical pre- and postprocessors to address complex geometries. It was found more efficient, general and verifiable to implement our model equations in a wide spread FEM code, COMSOL Multiphysics(COMSOL, 2005). An axysimmetric silo made of a cylindrical section and a steep hopper was chosen for reference and its dynamic behaviour during discharge up to steady state was simulated. A small hopper angle was chosen to ensure mass flow in the geometry. This condition was required to compare the numerical solutions with the analytical models, only available for mass flow regimes. The geometry is outlined in figure 3.3.

The model parameters for standard simulation, assumed heuristically as typical values for dense flows, are given in Table 3.1. A sensitivity analysis is presented later, and modified values will be mentioned in the text. The momentum balance equations have been closed with Navier BCs (Eq. 3.26) at the wall, as previously stated, and by a tangential stress free upper boundary. The flowrate was fixed, as common in industrial practice where rotary, screw or belt feeders are used and designed to withdraw material at a

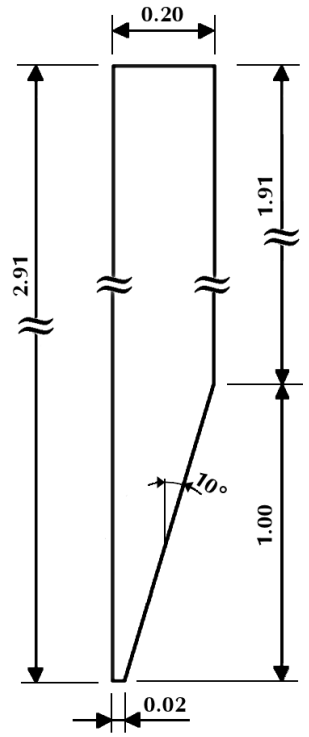

Figure 3.3: *Geometry of the silo studied in the present work. For better visualization, the coordinates do not scale with each other. Units are expressed in* m.

constant mass flow. This simply translates in a constant, plug flow outlet velocity v_{out}. Boundary conditions for the energy equations are "insulation"-type at the walls, constant temperature on the upper, free surface set to the average value of the temperature in the cylindrical section of the silo.

Calculations assumed that the height of the material in the silo was constant (the no tangential stress upper condition mimicks a free surface) as if the material was constantly replaced; a steady solution was obtained after all transient effects had finished.

Table 3.1: *Basic model parameters.*

μ	0.3	-
θ^*	10	s^2m^{-2}
η_0	1	s^{-1}
k'	1	s^{-1}
ρ	1000	kg/m^3
d_p	3	mm
λ/d_p	1	-
v_{out}	5	cm/s

Simulations provide local, instantaneous values of unknown variables (velocity and temperature), together with their fluxes, among which stresses are particularly interesting.

Stress distribution under flowing conditions is indeed rarely investigated with hydrodynamic models.

3.5.2 Flow distribution

The model predicts a distribution of velocity in good qualitative agreement with available experimental results (e.g. Natarajan et al. (1995)). Pointwise, detailed validation requires accurate measurements, that it was not possible to collect in the open literature, notwithstanding the relevance of these data. Within the context of an industrial research program, pressure and velocity data were collected, that will be the subject of Chapter 6. In this chapter, following the paper published in *Chem. Eng. Sci.*, results from the model will be compared mainly with literature correlations. Figure 3.4 shows that the model correctly predicts the typical shape of the velocity profile in the cylindrical section, with an inner plug-flow region and a shear band near the wall. Calculation shown in Figure 3.4 assumed $\lambda/d_p = 0.1$ to reduce slip and make the profile structure clearer. The calculated width of the shear band always approaches the typical value of $10 - 15$ particle diameters, and is quite independent of the ratio λ/d_p. The width of the shear bands was observed to depend linearly on the parameter θ^* of the model, that rules the sensitivity of the apparent viscosity to the local granular temperature, according to eq. (3.16). It suggests that θ^* might depend on particle diameter since experiments have shown that the width of shear bands strongly and linearly depends on particle diameter (G. D. R. Midi, 2004). As a final comment, it is important to highlight that the slip-length approach is particularly appropriate and effective to predict the experimentally observed wall slip in granular flows.
An important feature of velocity profiles in dense granular flows is that shear is tipically localized in rather narrow bands: in cylindrical bins, this structure is best observed far from the orifice, where the flow shows a shear zone close to the boundary and a region of plug flow in the center. In flat-bottomed silos, stagnant zones develop in the corners. In the geometry studied here, like many industrial applications, stagnant zones are prevente using steep hoppers. The discontinuity in shear is predicted in the cylindrical part, where the model describes the formation of shear band. This behavior is possible in the model because of the balance between generation of fluctuating energy due to shear and dissipation due to compression, which defines zones with a different granular temperature, i.e. local mobility, and thus with a different viscosity (thus difference in shear).

3.5.3 Stress distribution

Fig. 3.5 shows the normal stress profile along the walls, obtained through the model with reference parameters of Table 3.1 It can be observed that the wall normal stress has the

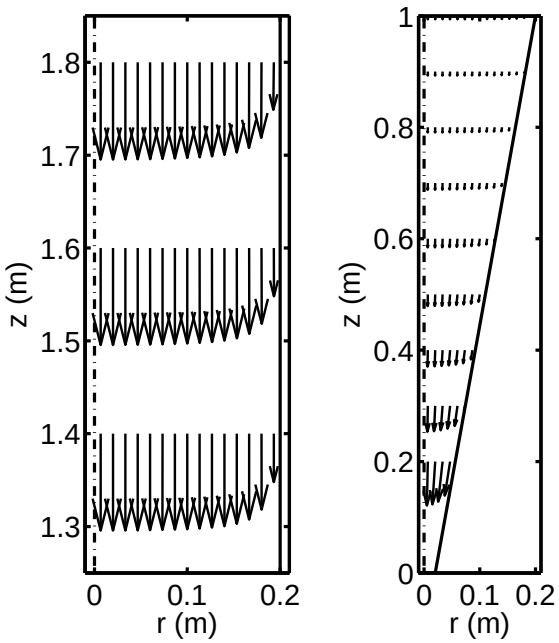

Figure 3.4: *Velocity vectors ($\lambda/d_p = 0.1$, other parameters as in Table 1).*

typical features expected for a discharging granular material. In the cylindrical upper section, the stress does not increase linearly with the depth (constant vertical gradient), like pressure in a fluid, but the increase with depth is smaller and smaller, approaching asymptotically a maximum (the Janssen asymptote). At the transition from the vertical section to the hopper, a local switch stress peak occurs. Below, stress decreases, again asympotically, toward zero at the hopper's end. This behavior is usually associated with a passive stress state in the convergent hopper. The consistency of the simulation results both in the upper and lover sections of the silo is quite surprising and to author's knowledge never obtained before by hydrodynamic models simulating discharging silos. Although simulations are essentially based on a model of flow, they also predict the stress distribution with the expected features. This approach is somehow complementary to the plasticity theories which determine the flow field after complete description of the stress distribution, through a flow rule (Nedderman, 1992).
Simulation results can be approximated using the classical model of Janssen for the upper cylindrical section, and Walker's approach for the lower, conical one (Nedderman, 1992). The best fit yielded $\delta = 16.1^o$ and δ_w equal to 11.4^o and 13.3^o in the upper and lower parts, respectively. In the upper section the stress ratio (Janssen constant) is expected to be $K = 1$ since the model assumes a viscouslike stress tensor with zero normal stress difference. This value was verified in all the numerical simulations.

To better understand the prediction of the model, its capability and the influence of its

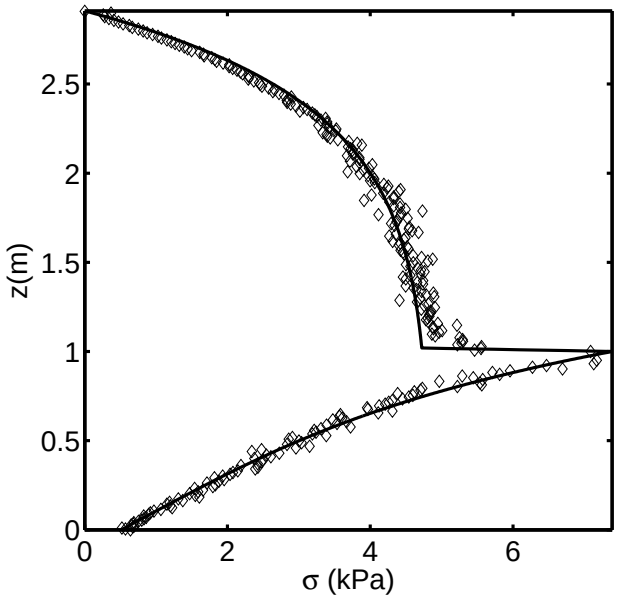

Figure 3.5: *Wall normal stresses calculated with the parameters of Table 3.1 (symbols). Line is the best fit approximation with Walker's equations, adjusting δ_w and δ.*

parameters, a sensitivity analysis on the most critical ones was carried out.

Figure 3.6 displays the results obtained by varying the parameter μ, tuning the ability of the pseudo-fluid to dissipate mechanical energy. This parameter is also expected to be closely related to the internal friction angle of the material, δ. Results indicate that decreasing μ, wall normal stresses grow in the whole geometry. In the cylindrical section the saturation value is approached earlier, nicely reproducing the well known pressure distribution in a confined bulk of granular material.

Experience and static calculations (Nedderman, 1992) report that the angle of internal friction affects how rapidly the stress curve saturates, but not the saturation value, which depends only on bulk density, bin diameter and wall friction coefficient, μ_w. However, because of the slip boundary conditions that was used, the value of the effective *wall* friction coefficient will depend on the rheological model assumed for the bulk. This is a consequence of assuming a Navier slip condition at the wall, which is not a model-independent relation, as Coulomb's one; this is indeed due to the fact that Coulomb's law directly relates stresses, and so it does not depend on the rheological behavior of the medium, while Navier's condition involves shear rate, that means that it needs information from stresses and rheology ($|\dot{\gamma}| \sim \frac{\tau}{\eta}$). Therefore the effective friction coefficient at the wall is expected to be primarily a function $\mu_w(\mu, \lambda, V_{slip}, d_p)$, while other dependencies are minor. The overall effect of bulk μ on wall stress profiles is therefore a consequence

of how it influences the effective angle of wall friction. Recalling Janssen's equation:

$$\sigma_w = \frac{\rho g D}{4\mu_w}\left[1 - exp\left(-4\frac{\mu_w K z}{D}\right)\right] \tag{3.36}$$

it can be observed that decreasing μ_w has the double effect of increasing the stresses in the whole geometry and of slowing down the approach to the saturation stress: a change in the parameter μ of the model modifies the wall stress profile in the way represented in Figure 3.6, because it indirectly changes the effective wall friction coefficient μ_w.
The μ_w effect is even clearer when comparing δ and δ_w values that fit modeling results, obtained at different μ_w, Figure 3.7. Both increase monotonically with μ; δ_w in the upper and lower sections of the silo do not differ significantly. Remarkably, for low values of δ, typical of cohesionless particles, δ correlates to parameter μ according to

$$\mu = \tan\delta \tag{3.37}$$

implying that the effective coefficient μ in the model quantitatively approaches the coefficient of internal friction, $\tan\delta$. Interestingly, beside providing a physical grounding to the effective parameter μ by relating it to a characteristic property of the granular material, eq. (3.37) allows to estimate the value of μ to be used in simulating the flow of a specific material.

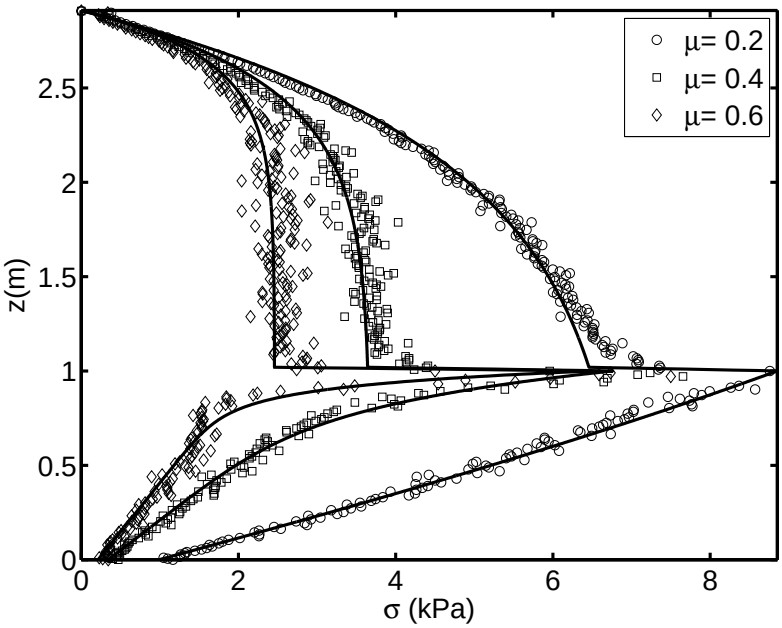

Figure 3.6: *Wall normal stresses varying the parameter μ, other parameters as in Table 3.1.*

In Figure 3.8 the effect of varying the slip length to particle diameter ratio λ/d_p, which determines the amount of slip at the walls, is investigated. It was expected that a higher

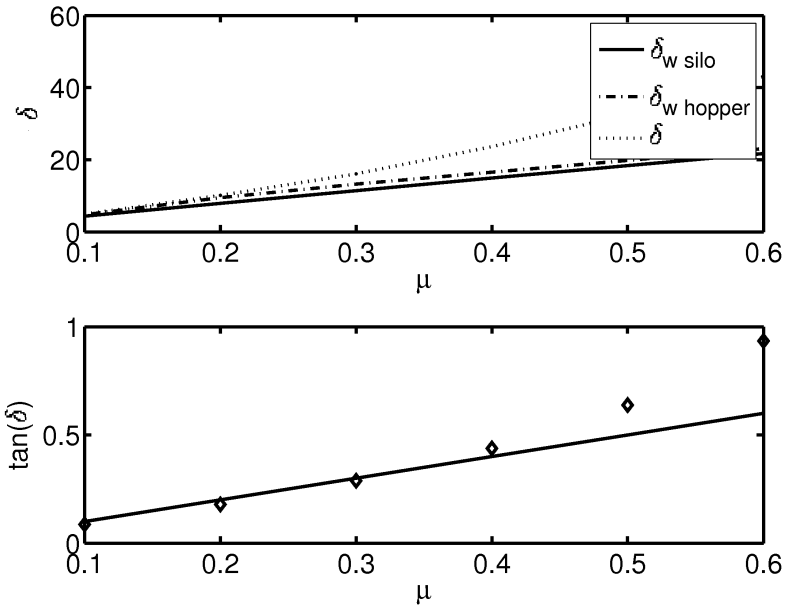

Figure 3.7: *Calculated δ and δ_w vs. coefficient μ, above. Coefficient of internal friction, $\tan\delta$, (symbols) vs. coefficient μ, and linear extrapolation of the low-values behavior(line), below.*

slip length corresponded to a lower value of the wall friction coefficient, thus higher normal stress at the wall. The results confirm the expectations, both in the upper and lower part of the silo. A larger slip at the walls determines high wall normal stresses because the wall looses its ability to sustain the material. Results are clearer if δ_w is determined and compared for each value of λ/d_p, as shown in Figure 3.9. It can be realized that $\delta_w \to 0$, monotonically when slip length increases. Again, no significant difference between the upper and the lower part of the silo are observed. In addition, in a wide range of λ/d_p values, the calculated internal friction coefficient $\tan\delta$ stick to the μ value used to obtained the data, and is nearly independent on the slip length. Note that $1 < \lambda/d_p < 30$ is quite a broad range, that encompass most practical applications, from extremely rough to perfectly smooth walls. In the no-slip limit, $\lambda/d_p < 1$, the calculated values of δ and δ_w appear to diverge. However, this is likely due to difficulties in the fitting equations that yield δ and δ_w values. The no-slip limit requires $\delta_w \sim \delta$, which causes numeric instabilities in static calculations that are the basis of the fitting. Moreover, in this limit particles near the wall will likely approach a typical stick-slip behavior, which cannot be captured by the Coulomb slip boundary condition (as assumed in Janssen and Walker stress analysis), but can be treated within a Navier slip-length approach, as described in Chapter 4, through a proper average.

Figure 3.10 shows the predicted effect on wall normal stresses of the discharge velocity. According to the model, the stresses during discharge increase with flowrate. Figure

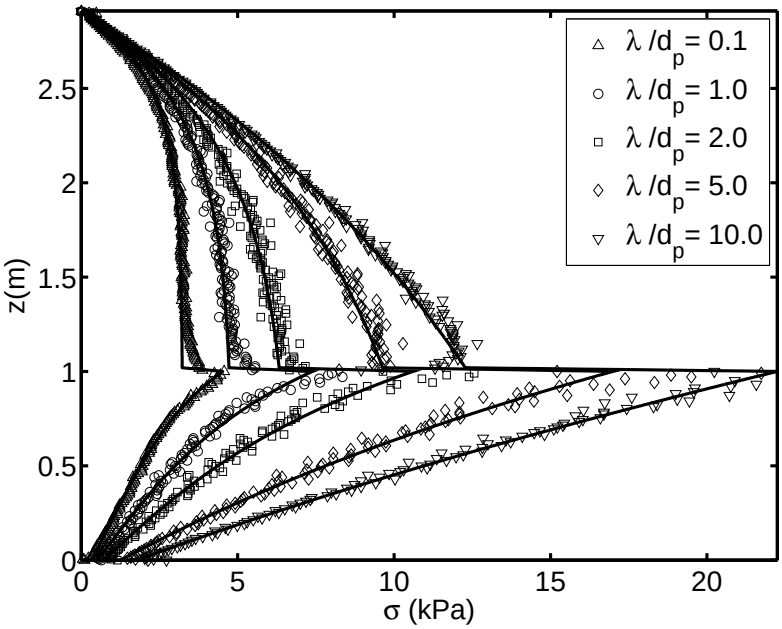

Figure 3.8: *Wall normal stresses varying the parameter λ, other parameters as in Table 3.1.*

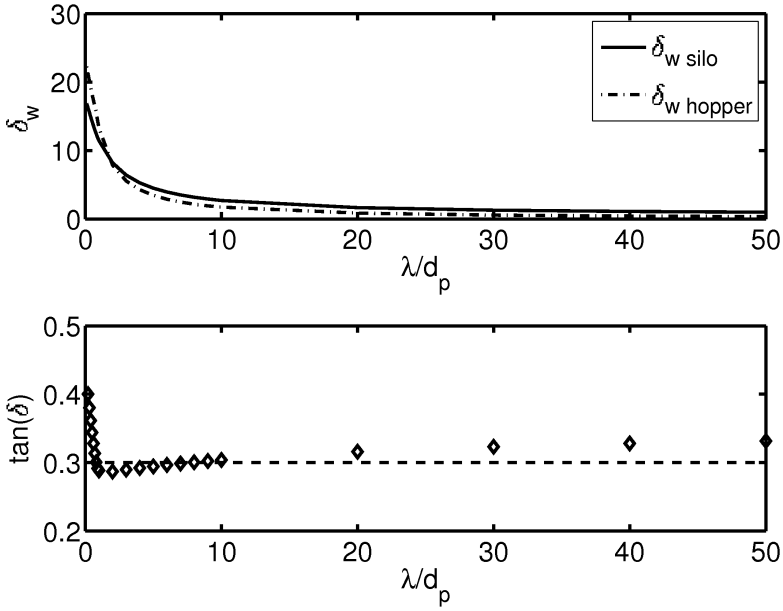

Figure 3.9: *Calculated values of δ_w vs slip length λ/d_p (above). Coefficient of internal friction,$\tan\delta$, (symbols) vs. model pameter μ (dotted line) vs slip length λ/d_p (below).*

3.11 systhematically collects the results, showing that flowrate has a major effect on wall slip, decreasing the corresponding angle of wall friction. In contrast, the outlet velocity (non-material parameter) very weakly affects the calculated angle of internal friction, further proving that the model parameter μ can be considered as a material property, which can be estimated from the angle of internal friction by means of Eq. 3.37, within the range of parameters considered.

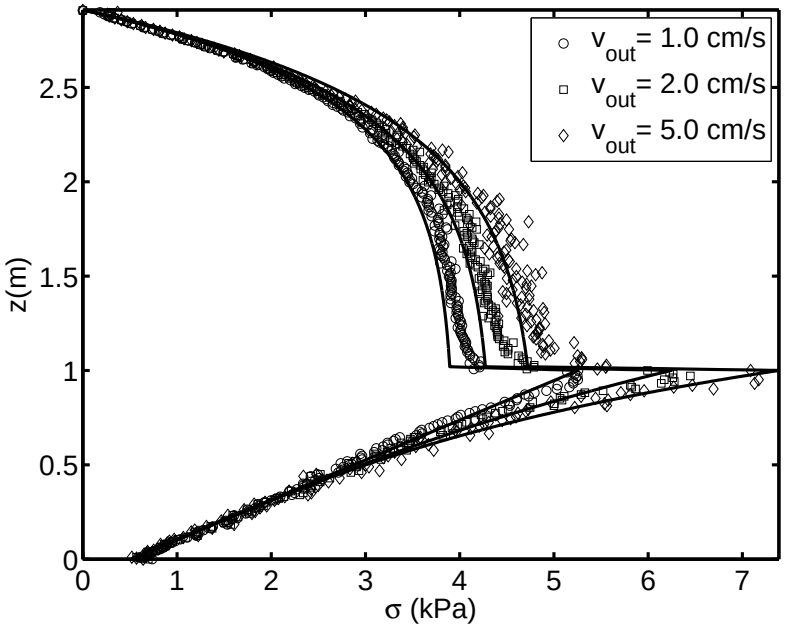

Figure 3.10: *Wall normal stresses varying the outlet velocity, other parameters as in Table 3.1.*

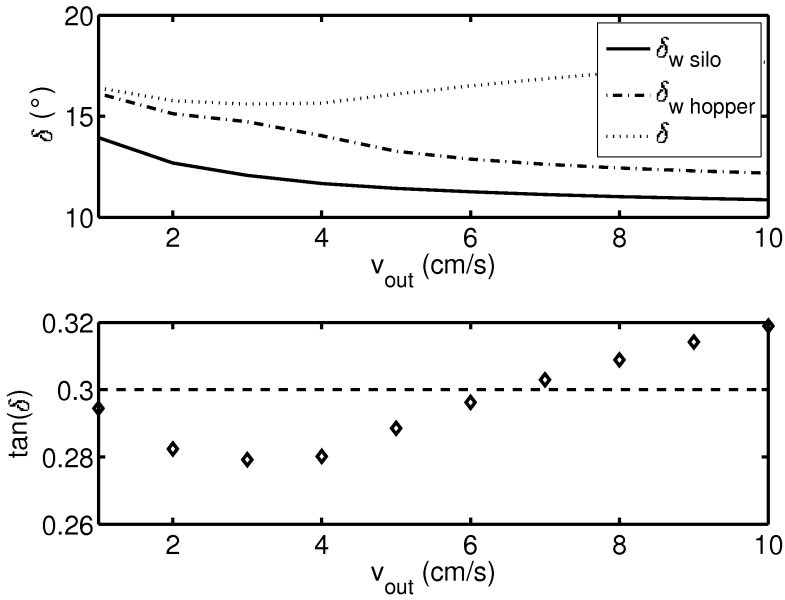

Figure 3.11: *Calculated δ and δ_w vs. discharge velocity (above). Coefficient of internal friction, $\tan\delta$, (symbols) and model parameter μ (dotted line) as a function of discharge velocity (below).*

Fig. 3.12 illustrates the evolution of wall normal stress distribution at the beginning of the discharge. It has been obtained by gradually increasing the outlet velocity from 0 to 1 cm/s, in a time span of 20 seconds. A travelling wave, with a stress peak moving from the outlet to the hopper corner can be clearly observed. Such effect is indeed expected in real hoppers, reflecting the switch from the active to the passive stress state (see Figure 3.2). Notwithstanding that, the model predicts a substantially different mechanism. Instead of a switch between active and passive state, the model describes a transition from static

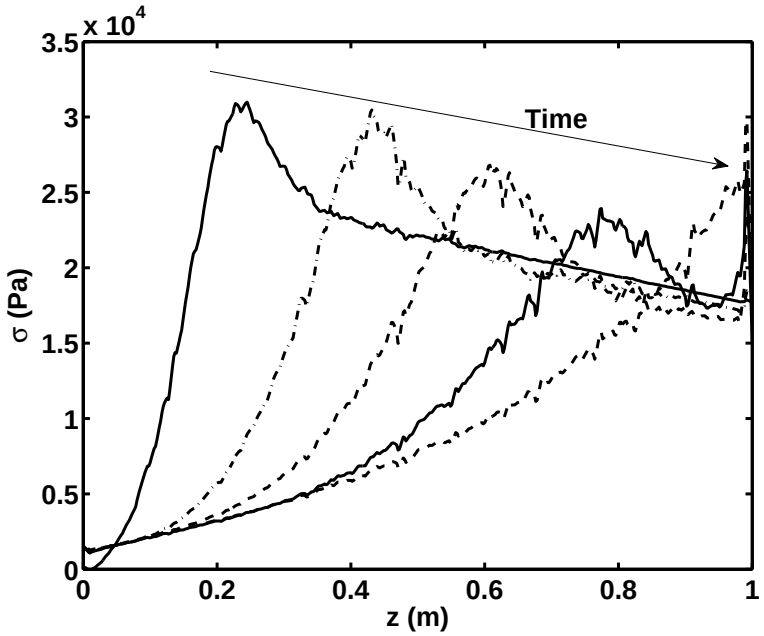

Figure 3.12: *Pressure wave in the hopper at the beginning of discharge (times: 10s, 20s, 40s, 80s, 400s).*

to dynamic conditions, and the switch is between a true hydrostatic initial solution (at zero velocity), with linearly increasing pressure, to the passive state of discharge. This is a consequence of considering the granular material as a non-Newtonian fluid, with zero shear stress at rest. Future improvement of the model will consider allowance for a threshold stess, able to determine the onset of flow, as in Bingham plastic fluids; this will be partly addressed in next sections dealing with hysteresis in inclined chute flows.

3.5.4 Experimental determination of model parameters

In the preceding subsection the model predictions of vertical profiles of wall stress were illustrated, when model parameters are varied. Results follow the expectations, considering the physical meaning of each parameter. Here, the issue of parameter estimation is briefly discussed. The model contains five parameters, one of which (λ) is not a property of the material itself but of the particle-wall couple. Among these, the temperature scale, θ^* , and the parameters η_0 and k', mostly affect the velocity and temperature fields. Their experimental determination is based on measurements of velocity profiles in simplified flow arrangements. For the present, it can be assumed that θ^* scales with the particle diameter. The parameter μ was shown in the preceding section to correspond to the internal angle of friction of the material, which can be easily measured with shear cells. Parameter λ determines the particle-wall interaction. According to an original approach that was developed, here it is allowed for the possibility of the material to slide on the wall, to a degree determined by the "slip length" coefficient, λ. Calibration of λ requires dedicated,

simple experiments where solids velocity profiles close to the boundary are measured, using the same type of particles and surfaces. Then λ can be calculated from its definition, Eq. 3.26, which implies that $\lambda = \frac{u_t}{|\frac{\partial u_t}{\partial n}|}$.

3.6 Silo with flat bottom

In this section results from the model described previously are presented for an axisymmetric silo with flat bottom, 800 particle diameters high and with a radius of 50 particle diameters. A simple first choice for the parameters invoked by the model is resumed in table 3.2. Flowrate is fixed at the orifice, no slip is assumed at the walls, together with

Table 3.2: *Parameters of the model*

μ	.3	$adim$
θ^*	10	s^2m^{-2}
η_0	1	s^{-1}
k_0	1	s^{-1}
ρ	$1e3$	kg/m^3

insulation for θ (*i.e.* $k\frac{\partial\theta}{\partial n} = 0$). Figure 3.13 summarizes the development of the velocity profiles along the silo, from Bessel-like profiles near the orifice to a plug flow with shear bands at the walls higher up the bin. In the higher part of the silo shear bands are of order 10 diameters thick. The temperature profile is qualitatively approaching data, with a peak at the wall, where material is sheared. Imposing a low temperature at the wall, it was able to reproduce the fast decaying of θ close to the wall as observed in DEM simulations (G. D. R. Midi, 2004). Looking at velocity maps and profiles near the orifice, it is possible to see that our model predicts well-defined static zones in the corners; this behavior can be explained by analysing temperature maps. A narrow zone at higher θ develops from the orifice to high up in the silo, finally positioning itself close to the wall. In the framework of this model, this layer has a lower viscosity that allows the two zones that it delimits to move independently one from another, thus insulating the corner, which 'cools' due to pressure rearranging action. Moreover, the map of granular temperature reveals that the flow pattern is very similar to that proposed by Brown and HawksleyBrown and Hawksley (1947)

As a next step, wall normal stresses as predicted by the model are shown in figure 3.13d. Again, perhaps surprisingly, profiles follow qualitatively Janssen's behaviour.

Finally, recent numerical simulations developed for non-stationary flow in the silo, discharging freely, show that the model predicts a constant flowrate, another original feature

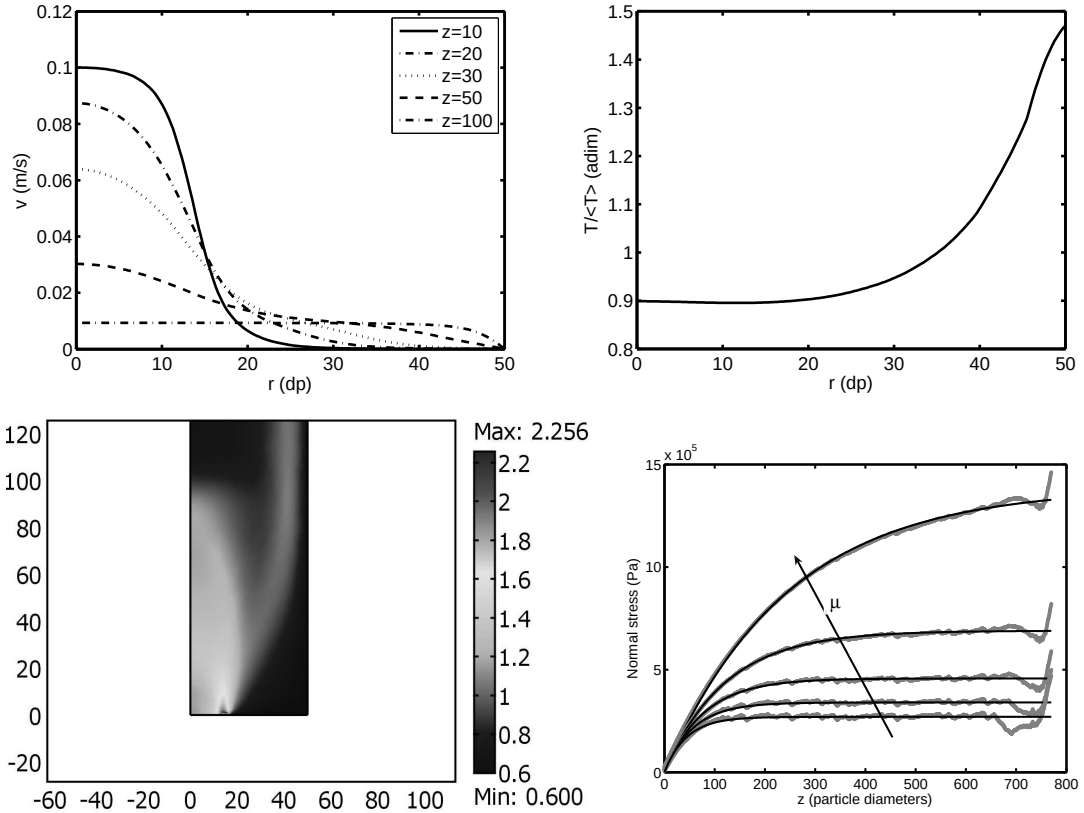

Figure 3.13: *Silo with flat bottom (all lengths are in d_p units): (a) Velocity profiles at different heights (b) Temperature profile far from the orifice (rescaled with the average value) (c) (Rescaled) temperature map (d) Normal stresses (grey lines) and Janssen equation (black lines) ($\sigma_w = A\,[1 - \exp(-B\ z)]$).*

of dense granular flows.

3.7 Hysteresis in inclined chute flows

Recent advances in the comprehension of granular free surface flows have been pushed by research on simple geometries of flow; among these, a very important one is the inclined chute. This geometrical configuration is common to many natural flows (such as avalanches, debris flows,...) but also industrial flows related to the conveying of granular materials. Regarding this set-up, many experimental results have been collected concerning velocity profiles or more averaged variables such as flowrate, showing typical scalings, and a strong effect of the lateral walls separation, as well as of the depth of the layer of grains(Pouliquen, 1999; Jop et al., 2005; Santomaso and Canu, 2001; G. D. R. Midi, 2004). From the modeling point of view, many rheologies(Jop et al., 2006; Bocquet et al., 2002a; Aranson and Tsimring, 2002) have been proposed in order to provide a unifying view of all types of flow. Unfortunately, at present a ultimate description of dense granular flows is still lacking. In this section the previously developed hydrodynamic model

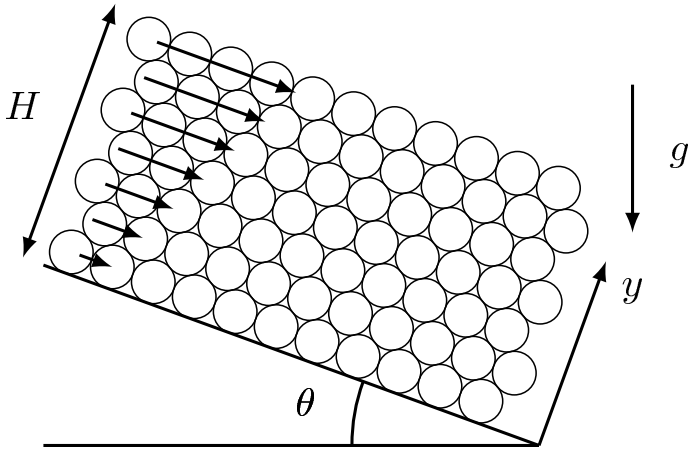

Figure 3.14: *Sketch of the inclined chute geometry.*

for granular flows is extended to study the free surface flow down an incline. The model, whose constitutive relations were developed in order to represent the dense, frictional regime of flow, can be intended as a possible extension of the phenomenology described *e.g.* by the French group G. D. R. Midi (2004) with the inclusion of the fluctuating energy dynamics; here it is applied to a free surface inclined chute flow, where velocity scaling and the hysteresis between starting and stopping angles(Daerr and Douady, 1999; Pouliquen O, 2002) is reproduced, together with the qualitative behavior of these angles when varying flow depth.

Note: in the present section, differently from what was previously defined, granular temperature will be referred as T, while the symbol θ will be used for the tilting angle. Such a notation was preferred for coherence with literature on starting and stopping avalanche angles.

3.7.1 Conservation equations & model

In the inclined chute geometry, the equations of conservation of momentum yield, in steady state:

$$\tau = \tau_0 + \rho g \sin\theta (H - y) \tag{3.38}$$

$$p = p_0 + \rho g \cos\theta (H - y) \tag{3.39}$$

where H is the thickness of material, y the direction orthogonal to the flow, θ the tilting angle, ρ the density of the medium, which was verified to be approximately uniform in y in many experiments(G. D. R. Midi, 2004). A sketch of the geometry is presented in figure 3.14.

Previous models for the dense flow have considerably improved the understanding of the behavior of this geometry, but they can't manage to represent complex phenomena like the

presence of an avalanche starting angle, θ_{start}, higher than the stopping one, θ_{stop}(Forterre and Pouliquen, 2008). This hysteretic phenomenon, common to other free surface (like flow in a rotating drum) and confined (annular Couette) flows, is a very peculiar feature of the dense flow of granular materials. Thus it would be tempting to improve rheological models to account for this feature. The presence of a stopping angle below which no flow is possible was predicted by Bocquet et al.(Bocquet et al., 2002a) who demonstrated in their approach the existence of a curve $\theta_{stop}(H)$ explaining the observed dependence of the angle on the flow depth. Notably, they proposed that a special boundary condition exists for the pressure p_0 at the free surface, such as the hydrodynamic boundary was shifted downwards of a quantity comparable with the particle diameter. With this boundary condition, when the thickness of the material is sufficiently low, θ_{stop} strongly depends on the thickness itself.

Such an assumption seems reasonable, and it will be adopted also in the following as a physical translation of the fact that clustering phenomena induce correlations in the flow that become increasingly more important when the moving layer becomes shallower. Beside the possibility to predict variation of the angle θ_{stop} with the thickness of the flow, a modeling framework should also indicate the presence of a second angle, higher than the first, which is the angle needed to trigger flow, and will be called θ_{start}. Due to the dynamical nature of the hysteresis, it seems reasonable that, in order to reproduce this typical behavior of avalanches, some "order parameter" dynamics has to be added to the system, in form of a differential equation. An order parameter approach was applied by (Aranson and Tsimring, 2002) to this topic, which however seems to fail in predicting the correct rheology(Forterre and Pouliquen, 2008). In the model, as an order parameter, that should describe the variations in the mobility of the system, as well as reduced free volume characteristics, it was choosen to use a well known quantity which characterises fluctuations of mechanical energy in granular materials under flow: granular temperaure. To extend the results of the GDR Midi(G. D. R. Midi, 2004), where closure was given in a first-order scheme, simply forcing a dependency of viscosity on shear rate (and pressure), a second order closure is used instead, considering the fluctuating energy balance. Defined as $T =< v'^2 > /3$, where v' is the fluctuating part of the velocity field, granular temperature measures the capability of a particle to move, in the cage defined by its nearest neighbours.

The notion of fluctuating energy is very important in the kinetic theory of granular gases, due to the analogy with the kinetic theory of gases, where the correlation of fluctuations at the molecular scale define the macroscopic thermodynamic temperature; however, it is not obvious that the considerations drawn, e.g., by Bocquet et al.(Bocquet et al., 2002a)

and Jenkins(Jenkins, 2007), who used directly the equations for the rapid collisional flow of grains (with corrections for the singularities near random packing and formation of clusters), apply to dense granular flows, where some fundamental assumptions of kinetic theories (such as that particle do not undergo long-lasting contacts) fail; such theories cannot avoid the risk of not truly accounting for the basic physics of the problem, because in quasistatic and dense regimes frictional dissipation should be accounted for in a clear way.

Thus, in this section the previous development will be extended, which involves as collisional theories the equation of conservation of fluctuating energy, but where a different energy dissipation rate, inspired by the preponderant, frictional mechanism, is specified. At steady state, in this geometry the fluctuating energy equation reduces to:

$$\frac{\partial}{\partial y}\left(k\frac{\partial T}{\partial y}\right) + |\dot{\gamma}|\,(\tau - \mu p) = 0 \tag{3.40}$$

where k is a coefficient of "diffusion" of fluctuating energy, $|\dot{\gamma}|$ is the shear rate, τ and p are stresses defined by Eqs. 3.38 and 3.39, and μ is an effective friction coefficient, whose physical meaning will be clarified from the following.

Extending previous work, where only the rate dependent term was considered, the shear stress component is expressed as a rate-independent Coulomb term plus a rate-dependent Bagnold like term of the form:

$$\tau = \mu_Y p + \rho d_p^2 \left|\dot{\gamma}\right|^2 \eta_0 f(T) \tag{3.41}$$

where η_0 is a dimensionless constant, ρ the bulk density, d_p particle diameter, and $f(T)$ is a function diverging for $T \to 0$ and tending to 1 when $T \to \infty$ to account for Bagnold scaling for rapid granular flows.

This could be extended in 3-D in Jop's(Jop et al., 2006) way by simply assuming colinearity of the stress and the strain rate tensors:

$$\tau_{ij} = \frac{\tau}{|\dot{\gamma}|}\dot{\gamma}_{ij} \tag{3.42}$$

where τ is taken from Eq. 3.41. This assumption, sometimes known as the *principle of coaxiality*, is commonly advocated in the mechanics of granular materials and is equivalent to saying that there can be no shear strain on planes along which no shear stress acts(Nedderman, 1992). From dimensional analysis the coefficient of diffusion of fluctuating energy scales as:

$$k = k_0 \rho d_p^2 \left|\dot{\gamma}\right| \tag{3.43}$$

where k_0 is a dimensionless constant. The coefficient of energy dissipation μ could be, in principle, a function of all the state variables of the system; it could be tempting to express

it as a function of the inertial number $I = |\dot{\gamma}|\, d_p/\sqrt{p/\rho}$ for example with an expression like(da Cruz et al., 2005):

$$\mu(I) = \mu_0 + b\, I \tag{3.44}$$

where μ_0 and b were material parameters. In the following it will be taken as a constant, for the sake of simplicity. From the definition of τ, the rheology can be reformulated in an expression for the effective friction coefficient, which is defined as $\mu^* = \tau/p$, an expression which is independent on the geometry:

$$\mu^* = \mu_Y + I^2 \eta_0 f(T) \tag{3.45}$$

3.7.2 Results

With the boundary conditions (Bocquet et al., 2002a) $\tau_0 = 0$ and $p_0 = \rho g z_0 \cos\theta$ at $y = H$, the latter coming from the already stated assumption that the effective hydrodynamic boundary is located slightly inside the material (at a depth z_0), in the present geometry μ^* corresponds to:

$$\mu^* = \frac{\tan\theta(H-y)}{H-y+z_0} \tag{3.46}$$

from which the effect of the hydrodynamic boundary condition can be appreciated, which states that μ^* is not a constant but ranges from 0 (near the surface) to $H/(H+z_0)\tan\theta$ (at the bottom), but this is significant only when the ratio z_0/H takes large values (in shallow beds). An example of the behavior of μ^* is depicted in Fig.3.15.

From Eqs. 3.45 and 3.46, an expression for the shear rate can be derived:

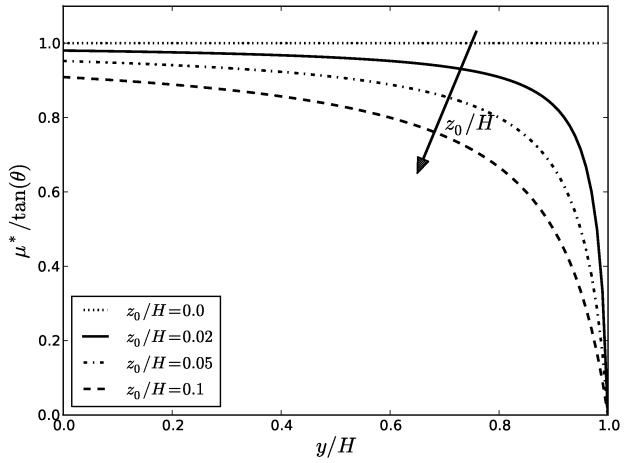

Figure 3.15: *Profile of effective friction coefficient μ^* depending on the ratio z_0/H.*

$$|\dot{\gamma}|^2 = \left[\tan\theta \frac{(H-y)}{H-y+z_0} - \mu_Y\right] \frac{g\cos\theta(H-y+z_0)}{\eta_0 d_p^2 f(T)}$$
$$\text{for } \frac{\tan\theta(H-y)}{H-y+z_0} \geq \mu_Y \tag{3.47}$$

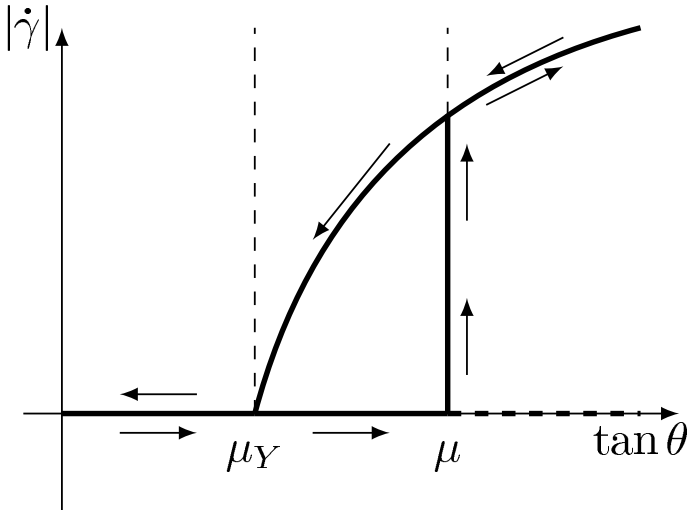

Figure 3.16: *Schematic bifurcation/hysteresis diagram for the simplified system (Eqs. 3.49 and 3.50). Note: the real sheared solution of the system has not a unique value of $|\dot{\gamma}|$, as it may seem from this graphic: this scheme is only for exemplification of the hysteresis.*

and zero otherwise. Rewriting Eq. 3.40, with the help of momentum balances, Eqs. 3.38,3.39, and of boundary conditions:

$$\begin{array}{l} \frac{\partial}{\partial y}\left(|\dot{\gamma}|\,\frac{\partial T}{\partial y}\right) + \frac{g\cos\theta}{d_p^2 k_0}\,(H+z_0-y)\,|\dot{\gamma}|\,\cdot \\ \cdot\left(\tan\theta\frac{H-y}{z_0+H-y} - \mu\right) = 0 \end{array} \tag{3.48}$$

From a simple analysis on the system of equations 3.47 and 3.48, it can be said that, depending on the inclination angle, there may be one or two simple solutions. We are in presence of a simple bifurcational behavior: a scheme of the behavior is given in Fig.3.16, and its derivation is detailed in the following discussion. In order to describe the hysteresis, let's restrict to the hypothesis of large height of material, which implies that $z_0 << H - y$ in the most part of the geometry. In this case Eq. 3.48 reduces to

$$\frac{\partial}{\partial y}\left(|\dot{\gamma}|\,\frac{\partial T}{\partial y}\right) + \frac{g\cos\theta}{d_p^2 k_0}\,(H-y)\,|\dot{\gamma}|\,(\tan\theta-\mu) = 0 \tag{3.49}$$

Moreover, the effective friction coefficient can be approximated as a constant $\mu^* \approx \tan\theta$, and the shear rate is given by:

$$|\dot{\gamma}|^2 = [\tan\theta - \mu_Y]\,\frac{g\cos\theta(H-y)}{\eta_0 d_p^2 f(T)} \quad \text{for } \tan\theta > \mu_Y \tag{3.50}$$

First, for angles lower than $\tan^{-1}\mu_Y$, the shear stress in the material does not overcome the yield stress, so only one unsheared solution is possible, $|\dot{\gamma}| = 0$. For inclinations higher than $\tan^{-1}\mu_Y$, $|\dot{\gamma}| = 0$ is again a solution of the system (with Eq. 3.50 implying $T = 0$), but, being that the shear stress is higher than the yield stress, also a sheared, flowing solution is possible. To understand which solution is choosen by the system,

the stability of the unsheared solution must be assessed. It is easy to see that the balance between fluctuating energy production and dissipation can be positive or negative depending on the inclination angle. If $\theta < \tan^{-1}\mu$, dissipation overcomes production, so, when perturbing an initially unsheared solution, the perturbation is cooled down to the jammed state, while if $\theta > \tan^{-1}\mu$ production overcomes dissipation, thus a perturbation is amplified leading the material to flow. It can be said that $|\dot{\gamma}| = 0, T = 0$ is stable for $\theta < \tan^{-1}\mu$ and unstable elsewhere.

The system shows an hysteretical behavior: gradually increasing the angle θ from 0, for $\theta < \tan^{-1}\mu$ the system remains jammed, while for $\theta > \tan^{-1}\mu$ material suddenly yields and starts flowing. If then θ is decreased, the system does not follow the previous path, but it follows the upper curve of Fig. 3.16 until $\theta > \tan^{-1}\mu_Y$, below which all flow is forced to stop. Therefore, $\tan^{-1}\mu$ can be interpreted as a "starting angle", while $\tan^{-1}\mu_Y$ is a "stopping angle".

Before relaxing the hypothesis of large bed depths, some ideas can be collected, in order to clarify the following. First, the sheared solution $|\dot{\gamma}| \neq 0$ is compatible with a uniform granular temperature profile, $\frac{\partial T}{\partial y} = 0$, which was observed in many experiments (with deviations at the bottom and at the top), and seems to be related also to a uniform solid fraction profile. This means that the material explores its phase space finally reaching a critical state(Nedderman, 1992; Schulze, 2008) where "heating" (increase in fluctuating energy due to shear stress) ad "cooling" (due to pressure's rearranging action) balance one each other. In our model temperature uniformity requires $\tan\theta = \mu$, which means that μ is a sort of critical state coefficient, supporting the ideas described in the development of the model.

From Eq.3.50 it can be easily seen that if $T \approx$ const. or T is sufficiently high in all the layer (due to the fact that $f(T)^{-1}$ is limited between 0 and 1, and tends to 1 as $T \to +\infty$),$|\dot{\gamma}|$ scales as $\sqrt{H-y}$, which means that $u(y)$ will scale as $(H-y)^{\frac{3}{2}}$, the typical velocity scaling commonly observed in inclined chute flows(Bagnold, 1954). Thus the simplified model correctly reproduces the typical velocity profile of dense flows down inclines: when relaxing the hypothesis $H - y >> z_0$, this means that the full model also predicts the typical simple scaling far from the bed surface, and a slightly more complex behavior near the top.

Based on the analysis developed for large depths of material, relaxing the hypothesis $H - y >> z_0$, it is possible to define analytically a *stopping angle* θ_{stop}, as the angle below which only one solution is possible, *i.e.* the jammed one. The minimum angle which is required in order to have some shear (at the bottom) is:

$$\theta_{stop} = \tan^{-1}\left(\mu_Y \frac{z_0 + H}{H}\right) \tag{3.51}$$

No flow is possible below this angle because the shear stress does not overcome the Coulomb yield stress required for the material to flow. As represented in Fig. 3.17, where z_0 was assumed to be of order of the particle diameter, the stopping angle determined here is then a function of the flow depth which diverges as $H \to 0$ and tends to a constant finite value for large depths. This behavior qualitatively corresponds to the stopping angle which was observed in experiments on inclines(Forterre and Pouliquen, 2008). The existence of a stopping angle for a hydrodynamic model of dense granular flows has already been shown by Bocquet et al. (2002a); it can be seen that the model, which belongs to the class of hydrodynamic models too, but is different in the specification of constitutive relations, predicts the same qualitative behavior. In fact, the model by Bocquet *et al.* seems to stop here, not giving insights on the existence of a starting angle, and so of the hysteretical nature of free surface flows, which is a peculiar character of granular matter. As it was already shown, the existence of a *starting angle* is related to the stability of the solution $|\dot{\gamma}| = 0,\ T = 0$. The value $\theta = \tan^{-1}\left(\mu\frac{H+z_0}{H}\right)$ indicates the minimum value of the inclination above which a fluctuation can be ampified, and below which all fluctuations are suppressed. Thus the curve

$$\theta_{start} = \tan^{-1}\left(\mu\frac{z_0 + H}{H}\right) \tag{3.52}$$

can be interpreted as the minimum angle required for the material to flow starting from an initial stopped configuration. Its behavior, depicted in Fig. 3.17, is similar to the previous found θ_{stop} function, as indeed it was observed in lab experiments(Forterre and Pouliquen, 2008). It will be obviously that $\mu_Y < \mu$. Therefore the simple model described here is able to qualitatively reproduce the hysteresis between starting and stopping of avalanches in dense granular flows down inclines. This will in all likelihood apply also to the hysteresis in rotaing drums (the slumping regime) and annular Couette cells. While the existence of an hysteresis is a robust result of our model, the existence of a dependence on H of the angles as $H \to 0$ depends on the boundary condition assumed for the pressure, which implies an additional length scale which is important when compared with H; it is phenomenologically correct that the surface influences the behavior at the boundaries the less the distance between them. This boundary condition is however slightly problematic for the model because near the top, where $y > H - \frac{\mu_Y z_0}{\tan\theta - \mu_Y}$, it implies that the material is not sheared ($|\dot{\gamma}| = 0$) because the shear stress is lower than the threshold, $\tau < \mu_Y p$. While experiments(G. D. R. Midi, 2004) support the fact that the derivative of the velocity profile is typically zero at the surface, the existence of a finite zone with zero derivative can be questionable, and needs further investigation. However, if $z_0 \sim d_p$ this may not be a problem, being this zone thus limited to a small portion of the flow depth.

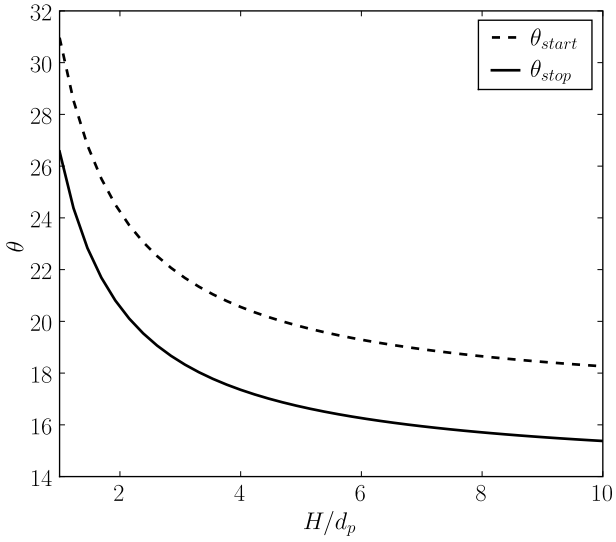

Figure 3.17: *Curves of h_{stop} and h_{start} from Eqs. 3.51 and 3.52, for $\mu_Y = 0.25$, $\mu = 0.3$, $z_0 \sim d_p$.*

3.8 Conclusions and Perspectives

In this chapter a novel continuum model to simulate the dense granular flow has been formulated and applied. It is based on conservation equations for mass, momentum and fluctuating kinetic energy and the rheology is described through a generalized newtonian model whose viscosity depends on granular temperature. The phenomenology contained in the fluctuating energy balance implies a dynamic interplay between mobility induced by shearing and jamming (frictional dissipation) induced by compression.

The model has been first applied to a mass flow silo with a converging hopper. This is a reference in the field, but the model is not limited to any geometry or flow configuration. The model predicts a distribution of flow in the two silo's sections in agreement with the expected behavior. In this work, we focused on the stress distribution prediction, which is of great theoretical and practical interest. The flow model predicts the development of the typical wall normal stress profiles characterised by a peak at the transition between the cylindrical and the conical sections of the structure. Comparison were made between the results and the static-like solutions of Janssen and Walker, showing a good agreement and verifying the expected dependence on the amount of slip and flowrate. To authors' knowledge, it is definitely unusual for a hydrodynamic continuum model to predict the peculiar stress distribution of granular materials in confined geometries, in addition to the flow patterns.

An important feature of the model is the allowance of partial wall slip, by means of a Navier slip length approach, replacing the two unrealistically extreme boundary conditions of no-slip and perfect slip. It is well known that granular material tend to slip, at

least partially, on surfaces, and a proper quantification is definitely needed; we suggested a viable and promising approach.

The success of the model relies upon the possibility of using it for design purposes and this still needs work in order to set the model on a more quantitative ground. This can be achieved with comparison with experimental results and discrete element models, in order to evaluate the parameters of the model and characterize slip. So far, a sensitivity analysis gave important informations on the correlations between model parameters and material properties, such as the angle of internal friction, limiting the arbitrarity in the model. It is believed that an original contribution was given regarding these issues $1)$ develop a flow model: most of the models of granular flow used industrially are actually static. They do not predict flow rates but focus on stresses, assuming the velocity distribution; $2)$ a simple, intuitive rehological model based on analogies with liquids and glasses, was introduced; $3)$ it is accounted for particle slip of the walls based on a Navier boundary condition, physically sound; $4)$ results were transferred from Physics literature to the industrial scale (silos) and $5)$ comparison with well-established correlations. The possibility of the model are huge in principle, not being limited by geometry of flow arrangements. Results obtained so far are encouraging. However, non-trivial efforts are required to validate and extend it to account for more complex effects such as the formation of stagnant zones (i.e. funnel flow).

On the other hand, regarding free surface flows, results were presented in this chapter for the case of free surface flow down an incline, with a particular focus on the hysteretical properties fo the flow. It is shown that the model can capture important features of granular flows, such the existence of an avalanche starting angle θ_{start} above which an initially jammed configuration begins to flow, and an avalanche stopping angle θ_{stop} below which no flow is possible, in agreement with experience. The known dependence of these angles on the flow depth is found and the two curves $\theta_{start}(H)$ and $\theta_{stop}(H)$ are determined analitically. The existence of this two angles is a strong result in favour of the model, because it is the sign of hysteresis in dense granular flows. Besides, it was shown that the model correctly predicts the scaling of the velocity profile. On the basis of the analysis performed, it is possible to conclude also that, in order to extend the phenomenology proposed by the GDR MiDi(G. D. R. Midi, 2004) to more complex flow dynamics, a hydrodynamic approach can be useful because it can bring into the description some non-trivial behaviors which are peculiar to dense granular flows.

Chapter 4

Effective boundary conditions for dense granular flows

Et sur leur sang ineffaçable
verse ton sable intarissable.

Alfred Jarry, *Les minutes de sable memorial*, 1894

4.1 Introduction

This chapter is centered on the topic of boundary conditions for dense granular flows. The need for reliable expressions for the BCs at the walls was raised in Chapter 2, and this part of my research was devoted to the development of an effective boundary condition by means of a simple stochastic model of the behavior of a particle at the wall, considering the presence of a force network and the randomness of force variation during flow. Part of the work presented here was published on Physical Review E(Artoni et al., 2009b).
In Chapter 2 the mixing-length model proposed by the GDR MiDi was used and it was shown that using a slip boundary condition instead of a no-slip one considerably improved the predictions of the model in the vertical chute configuration; there a Coulomb friction condition was, which could be a valid alternative to the no-slip condition. In this chapter astep is made further, deriving effective boundary conditions for granular flow taking into account the effect of the heterogeneity of the force network on sliding friction dynamics. This yields an intermediate boundary condition which lies in the limit between no-slip and Coulomb friction; two simple functions relating wall stress, velocity, and velocity variance are found from numerical simulations. Moreover, it is shown that this effective boundary condition corresponds to Navier slip condition when GDR MiDi's model is as-

sumed to be valid, and that the slip length depends on the length scale that characterises the system, *viz* the particle diameter. Finally, based on the hints obtained from the previous analysis, an attempt is made to generalize the approach by means of dimensional analysis. Possible functional forms for the generalized boundary condition on the slip velocity require experimental or numerical data; therefore a full discussion on the validity of the approach will be given in Chapter 7.

4.2 Outline of the problem

As it was already noticed in previous chapters, in dense granular flows the physics at a boundary is rather complex: force chains are breaking and forming, contacts are long lasting but not eternal, the number of contacts may change along time, et cetera. When dealing with non-Coulomb friction things may be even more complex because of the variation of microscopic contact area with load(Tüzün et al., 1988). From the modeling point of view, rheological models need specification for stresses or velocities at the boundary which should represent at least in an average sense this complex behavior. Despite the great attention towards continuum models and rheologies, little effort has been devoted to develop realistic boundary conditions for the velocity field at smooth or rough walls, even if the crucial role of side walls was recognized, for example, for inclined chute flows (Jop et al., 2005).

For the rapid flow of dense granular materials, boundary conditions were developed (both in the case of bumpy(Richman and Chou, 1988) and flat, frictional walls(Jenkins and Louge, 1997)); in that case some regime-specific hypotheses were employed in the development, such as the existence of binary collisions, or of instantaneous contacts. The resulting boundary conditions are rigorous and contain almost all the physics involved in the process. In dense flows, being that the assembly physics is more complex, involving the dynamics of several bodies experiencing multiple enduring frictional contacts, specifying rigorous boundary conditions is more difficult. The same holds for the bulk, where the complexity of interactions and the presence of mesoscale phenomena (clusters, shear bands,...) has up to now prevented from developing a precise and satisfying continuum description (as the Granular Kinetic Theory is for rapid collisional flows).

Practically, in the flow of granular materials in confined geometries such as silos, hoppers, etc., the behavior at a boundary is described by means of the (effective) wall friction coefficient, that is $\mu_w = \frac{\sigma_{xy}}{\sigma_{xx}}$, where σ_{xy} is the shear stress and σ_{xx} is the normal stress in the direction orthogonal to the wall. Such a coefficient is not a constant but can depend (1) on the normal load, (2) on the assembly flow behavior (presence of shear). The work by Tüzün et al. (1988) showed, for flow in a vertical channel, that in absence of

shear in the material (full plug flow), the effective wall friction coefficient depends on the normal load only if the particle-wall friction coefficient is load dependent (i.e. non-Coulomb behavior), otherwise $\mu_w = \mu_{pw}$ where μ_{pw} is the (particle-scale) particle-wall friction coefficient. In this chapter the effect of fluctuations of the force network (which can be driven by shear) on boundary conditions (and incidentally on the wall friction coefficient) is studied, starting from the idea that the stronger the phenomenon of force chains breaking and forming in the material, will result for the particles at a boundary that the condition of steady sliding is not correct, implying generally that $\mu_w < \mu_{pw}$.
In the physics community, a common experimental approach developed to overcome the issue of unknown boundary condition is the practice of gluing particles to the walls, in order to assume a no-slip boundary condition in the interpretation of the results. This choice can be of fundamental importance but possesses two major drawbacks: at first, it is known(G. D. R. Midi, 2004) that for high shear rates particles undergo strong slip at the glued particles - bulk particles interface, a slip that adds some difficulty in holding the continuum hypothesis; thus it is not clear whether the glued particles are part of the bulk or of a bumpy wall, so that boundary conditions must be expressed on the first moving layer in contact with the glued one. The second drawback of this experimental practice is the partial applicability to real situations: the flow on smooth surfaces such as in hopper discharge usually shows particles slipping at the solid interface. Slip can be promoted or can be an undesired phenomenon, often we are concerned with stick-slip phenomena(Nasuno et al., 1998; Baldassarri et al., 2006), which are common in dry-friction dynamics(Heslot et al., 1994) ; in all of these cases, a deeper understanding of the behaviour of granular materials flowing near a boundary is needed, and the no-slip boundary condition is not the most valid approach.

4.3 A simple model

Consider a single particle of mass m and diameter d lying on a plane, moving with instantaneous velocity V; the particle is subjected to a normal force P and to a tangential force T. It will be neglected, for simplicity, the effect of couples acting on the particle considering only traslational, sliding movements. The next assumption is that due to the heterogeneous nature of the medium the normal force P is a random function of time with a given distribution function. Alternatively, even T could fluctuate, but it can be assumed for the sake of simplicity that only the normal force does; qualitative results are not affected by the choice of the fluctuating force. Let F be the friction force; considering the simplest model of solid friction, e.g Amontons law, with only one friction coefficient μ,

it can be written as:

$$F = \begin{cases} T \; if \;\; V = 0 \; and \; T < \mu P \\ \mu P \; else \end{cases} \tag{4.1}$$

The motion of the particle is calculated from Newton's law:

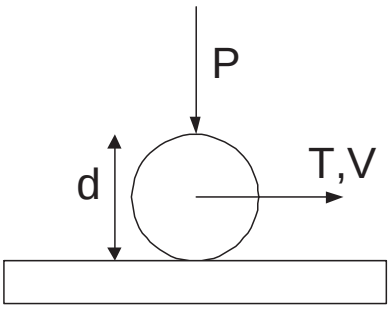

Figure 4.1: *Schematism of the variables considered in this section.*

$$m\frac{dV}{dt} = T - F \tag{4.2}$$

If the normal force was constant, only two situations would be possible, corresponding respectively to no-slip and Coulomb conditions. But if the force fluctuated, the particle would undergo slip and no-slip events, which globally represent a non-Coulomb slip phenomenon; our aim is to derive an average expression for the slip velocity as a function of the forcings. Let's consider a typical distribution of normal forces of the form:

$$p(f) = a(1 - be^{-f^2})e^{-\beta f}. \tag{4.3}$$

as suggested in (Mueth et al., 2000), where $f = P/P_{ave}$ and a is a normalization coefficient. This distribution of forces holds for normal forces in uniaxial compression, in a spatial sense; the key assumption will be made that, in dense granular flows, this distribution acts also between successive rearrangements of tangential forces in time. This choice is supported by the fact that results do not depend on the particular choice of the distribution, apart from one point (the existence of a cutoff value in the force) which will be discussed later, and whose influence is limited. It is further supposed that the force is a piecewise linear function whose nodes are extracted from this distribution. Let P_{ave} be the average value of the normal force. The time step between successive force rearrangements can be choosen to be equal to the relaxation time $\tau = \sqrt{\frac{m\,d}{P_{ave}}}$(G. D. R. Midi, 2004); it follows directly that rescaling t by τ the time step over which the force rearranges is 1. Further rescaling leads to the dimensionless variables: $V' = V\sqrt{\frac{m}{P_{ave}\,d}}$ and $T' = T/\mu P_{ave}$, $P' = P/P_{ave}$. If a variable $\alpha(t)$ is defined as:

$$\alpha = \begin{cases} 0 \; if \;\; V = 0 \; and \; T < \mu P \\ 1 \; else \end{cases} \tag{4.4}$$

the equation of motion becomes:

$$\frac{dV'}{dt'} = \alpha\mu\,(T' - P') \tag{4.5}$$

from which the average rescaled slip velocity can be computed, which is defined as:

$$V'_{ave} = \mu \lim_{\tau\to+\infty} \frac{1}{\tau} \int_0^{\tau} dt' \left[\int_0^{t'} \alpha\,(T' - P')\,dt \right] \tag{4.6}$$

We solve numerically the equation of motion; an example of the stick-slip behavior of the system is given in figure 4.2. An initially motionless particle can start to move only if the instantaneous normal force is below the yield threshold. A moving particle can decelerate only if the normal force is higher than the threshold. Moreover, it is clear from Fig. 4.2 that the area in which normal forces oppose motion is larger than the area in which they promote motion; it is the dynamical nature of the system that causes the body to have a non null average velocity. It would be desirable to find a relationship between the average slip velocity computed by means of Eq. 4.6 and the rescaled average tangential force (which corresponds to a rescaled effective friction coefficient, being $\mu_{eff}/\mu = T/\mu P_{ave}$). After solving Eq. 4.5 it is possible to look at the dependence of the statistics of the particle motion on the average value of the force in Fig. 4.3.

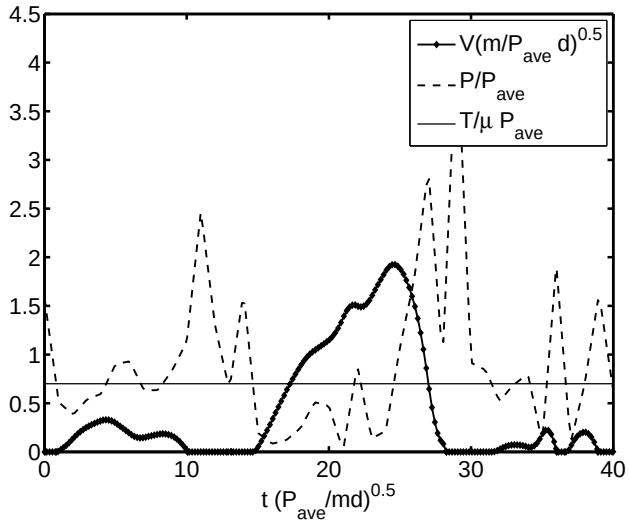

Figure 4.2: *Example of the local dynamics of the system.*

4.4 Discussion

The curves evidence a no-slip limit at low values of the rescaled force T', and a Coulomb limit for $T' \to 1$. The way V'_{ave} approaches 0 depends on the nature of the distribution $p(f)$: if the distribution had an upper cut-off value, it would be easy to conclude that

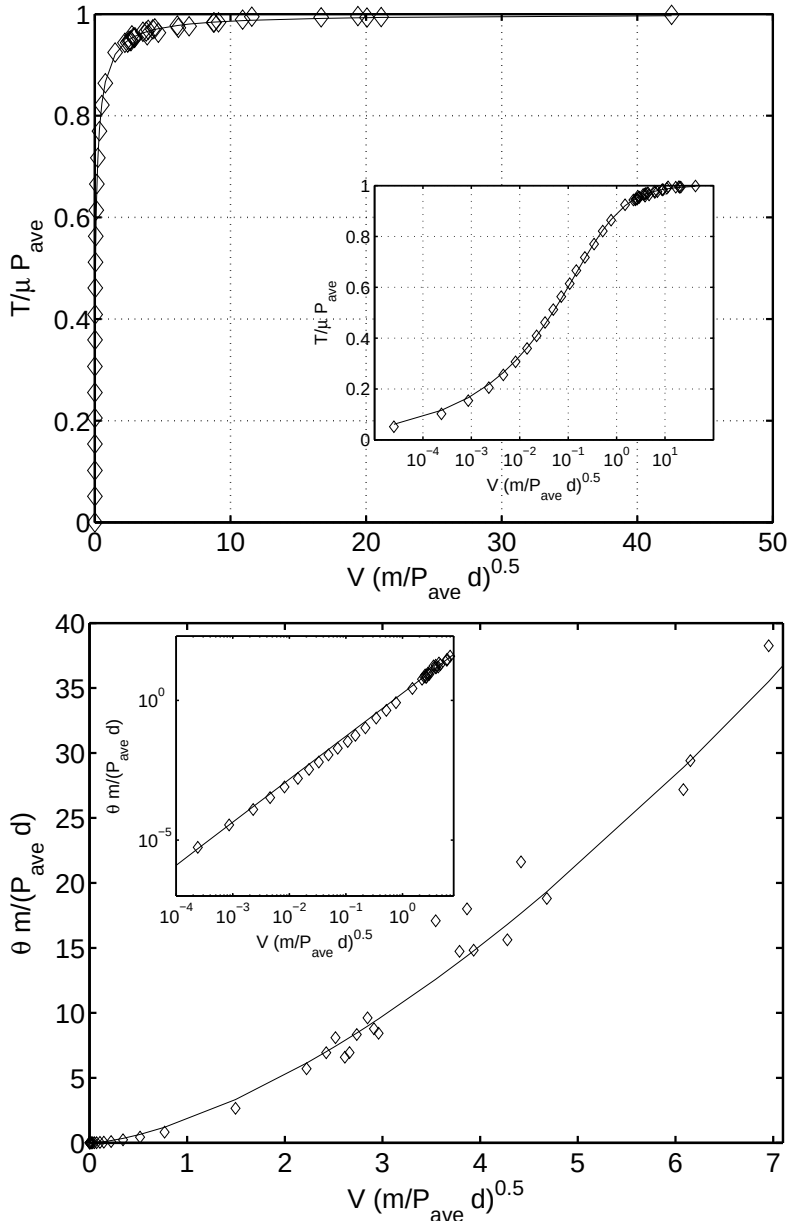

Figure 4.3: *Dependence of statistics of particle velocity on statistics of force. (top) Rescaled average pulling force vs average slip velocity. (bottom) Rescaled velocity variance vs average slip velocity. Best fits from equations 4.7,4.8 are also included.*

the system had a sort of yield-stress behavior at the wall, with a finite range of T' giving $V'_{ave} = 0$; in the other case, without cut-off, the average velocity would be 0 only for $T' = 0$. This is the only point in which the choice of the distribution function qualitatively changes something in the results; however, the fast decrease of the tail in the distribution, if not giving a "plastic" behavior, would give some sort pseudo-plastic behavior, because of the need to impose a certain stress to obtain an appreciable slip. So, with a certain loss of exactness, it is possible to assume also a yield-stress formulation for the BC.

It is interesting to note that also the variance of the distribution of the instantaneous parti-

cle velocities, that corresponds to the concept of granular temperature, which is expressed as $\theta =< (V(t) - V_{ave})^2 >$, where brackets denote time averaging, grows when T' increases, which is similar to the behaviour of the slip velocity. Due to its definition, θ is made dimensionless with the position $\theta' = \theta \frac{m}{P\,d}$. In figure 4.3 correlation between granular temperature and *average* velocity is shown to follow a power-law behavior. From a general standpoint, the boundary conditions can be expressed with the help of the following fitting functions (in the following, subscript *ave* will be eliminated for the sake of simplicity):

$$T' = \left(\frac{V'}{V' + c_1} \right)^{\gamma} \tag{4.7}$$

$$\theta' = c_2 V'^{\beta} \tag{4.8}$$

where $\gamma > 0, \beta < 0.5$ and $c_1, c_2 > 0$ are fitting parameters. A very good fit is obtained for $\gamma \approx 0.28$, $\beta \approx 1.5$, $c_1 \approx 0.51$, $c_2 \approx 1.8$. In the figures the fit is represented as a solid line. Eqq. 4.7 and 4.8 are the simplest expressions for the effective boundary conditions that can be applied at the wall characterised by a particle-wall friction coefficent μ.These functions are an important result of this work: two boundary conditions have been obtained which are characterized by simplicity and direct applicability to continuum simulations of granular flows.

4.5 Dependence on the parameters of the model

In the preceding section it was shown that the average behavior of stick-slip events can be interpreted by means of simple relations between dimensionless stress and velocity. The aim is to propose a simple tool allowing to treat the regime between no-slip and continous sliding in an average sense.

The parameters of the proposed functions should be obtained experimentally, however some issue must be considered which are related to the rather simple model assumed, to see how the obtained relations depend on the assumptions made. First of all, a particular choice of the force distribution $p(f)$ (Mueth et al., 2000) was used, taken from statistics of static granular packings. In fig. 4.4 it is possible to see how the qualitative behavior of the obtained functions is not affected by the particular choice of the force distribution, but seem to come only from the stochastic behavior of the force. Other distributions were also considered, giving the same qualitative behavior. From a more quantitative standpoint, the amount of slip increases as the variance of the distribution increases (increasing β corresponds to increasing the variance of the force distribution). Another issue that shall

be considered is the friction model assumed, which is quite simple. Assuming a different model, with two friction coefficients (a static friction coefficient higher than the sliding friction coefficient), does not affect the results, also quantitatively (see Fig. 4.5). Again, the main feature causing the intermediate, stick-slip, behavior, is the randomness of the force, related to the presence (and the mechanisms of breaking and forming) of force chains. Regarding the variations of the force in time, it was identified as a typical time scale the rearrangement time $\tau = \sqrt{\frac{m\,d}{P_{ave}}}$; this choice might be questionable, particularly in high shear situations (when the inertial number $I >> 1$), where the characteristic time related to shear is small compared to the rearrangement time. Therefore the validity of the approach should be rigorously valid in the limit of small I, while experimental work is needed to verify and extend its validity in other regimes. In this perspective it can be useful to verify whether the time step over which the force changes has an impact on the final curves, though $\Delta t \sim \tau$ seems a reasonable assumption. From results reported in Fig. 4.6 it can be appreciated that the larger the time step, the larger the amount of slip predicted by the model for the same average pulling force. However, it is important to underline the qualitative behavior of the effective boundary conditions does not depend on particular choices for the distribution, the time step or the friction model, and that it can be well represented by means of the proposed Eqs. 4.7 and 4.8. However, the parameters in these equations should be determined experimentally, from local measurements of slip velocity and wall stresses; in this perspective, it can be suggested that to develop boundary conditions more suitable for gravity (i.e. stress) driven flows, slip measurements should be also done in gravity driven situations, for example in the vertical chute configuration.

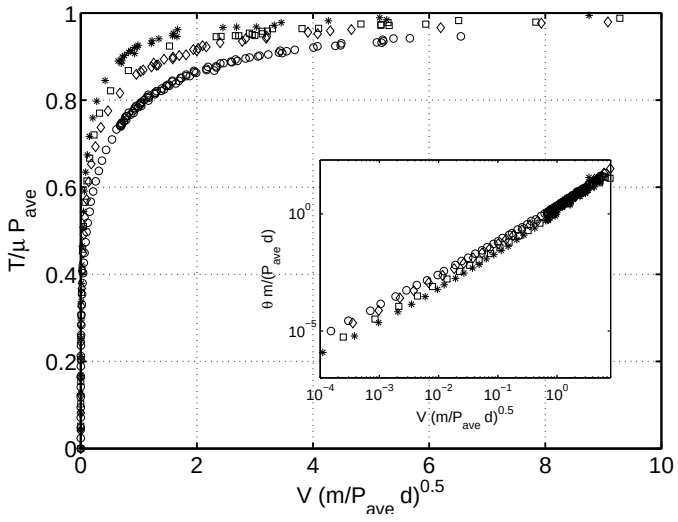

Figure 4.4: *Curves obtained varying the force distribution: Eq. 4.3 (squares), half-gaussian-like (diamonds), same as Eq. 4.3 but with $\beta = 0.15$ (circles), $\beta = 3$ (stars). (outer panel) Rescaled average pulling force vs rescaled average slip velocity (inner panel) Rescaled velocity variance vs rescaled average slip velocity.*

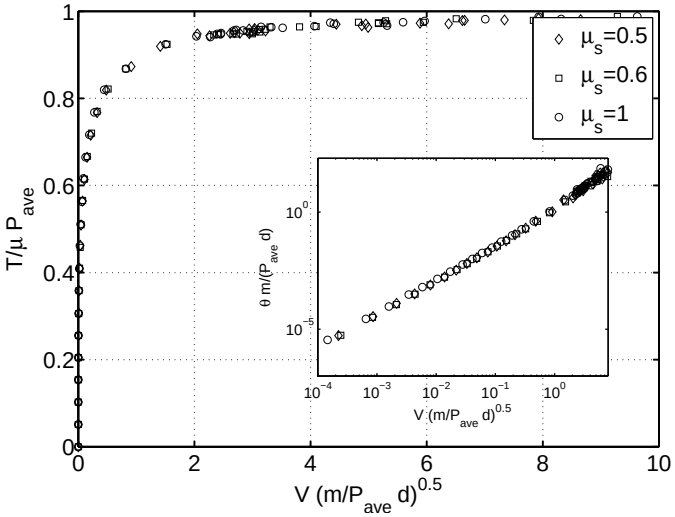

Figure 4.5: *(outer panel) Average dimensionless stress vs average dimensionless velocity and (inner panel) dimensionless granular temperature vs average dimensionless velocity, varying the coefficient of static friction*

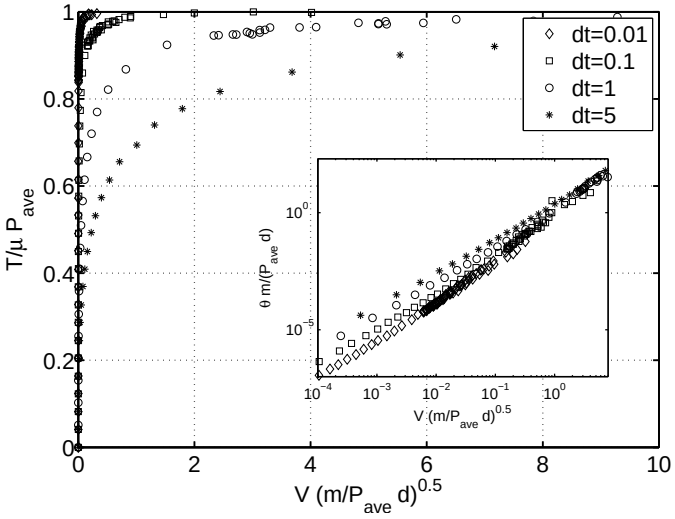

Figure 4.6: *Data obtained varying the time step of force changing. (outer panel) Rescaled average pulling force vs rescaled average slip velocity (inner panel) Rescaled velocity variance vs rescaled average slip velocity.*

4.6 Interpretation of the results by means of a Navier boundary condition

Navier boundary condition, relating the slip velocity and the gradient of the velocity normal to the boundary via a slip length λ, is a common way to characterise slip in fluid flows in micro and nanochannels; however, there is not a single plot of this condition in the V' vs T' diagram, because such a plot needs information on the relationship between stresses

and deformation rates in form of constitutive relations. For a newtonian fluid,

$$V' = \lambda \frac{\mu}{\eta} \sqrt{\frac{mP}{d}} T' \tag{4.9}$$

which is linear and parametric in $\frac{\mu}{\eta}\sqrt{\frac{mP}{d}}$. A Bingham yield-stress fluid will have an explicit relation of the form:

$$V' = \lambda \frac{\mu}{\eta'} \sqrt{\frac{mP}{d}} \, (T' - T'_Y) \quad (for \quad T' > T'_Y) \tag{4.10}$$

where T'_Y is the rescaled yield stress and η' is the viscosity coefficient in Bingham's model. So a Navier condition for Bingham's model in the V' vs T' plot is a line shifted by T'_Y and again parametric in $\frac{\mu}{\eta}\sqrt{\frac{mP}{d}}$.

Both of these relationship obviously do not conform to the behavior obtained from the model developed in the previous pages; assuming a mixing length model as GDR MiDi's, where $\frac{T}{P} = \mu(I)$, with $I = \frac{\dot{\gamma}}{\sqrt{P/md}}$ (the difference in the expression of I of the previous literature is due to the fact that here P is a normal *force*, not a pressure), the assumption of $\mu(I) = \mu_s + \frac{\mu_2 - \mu_s}{I_0/I+1}$ (taken from Pouliquen and coworkers(Jop et al., 2005),(Jop et al., 2006))yields for a Navier BC:

$$V' = \frac{\lambda}{d} \frac{T' - \mu_s/\mu}{\mu_2/\mu - T'} \quad (for \quad T' > \mu_s/\mu) \tag{4.11}$$

which reaches an asymptote for $T' \to \mu_2/\mu$, and is 0 in the range $0 - \mu_s/\mu$. Thus, to unify the curves and represent the results obtained from the simple model of wall friction studied here, λ must be a function of the form:

$$\lambda = k \; d \; \zeta(T') \tag{4.12}$$

where $\zeta(T')$ accounts for the change in the position of the asymptote and can be expressed simply as:

$$\zeta = \frac{\mu_2/\mu - T'}{1 - T'} \tag{4.13}$$

An important result is given in Eq. 4.12: to unify the curves as obtained in the "experiments", λ must be a multiple of d: this is actually an important result, being d the only internal length scale of the system, and so the best choice as a basis for estimating the slip length. The typical form of $V' \; vs \; T'$ curves for the various models is given in figure 4.7.

To resume, the intermediate, efficient boundary condition we are looking for can be qualitatively expressed as Navier slip condition in a mixing length framework, the slip length corresponding to a multiple of the particle diameter. A step further can be made in the direction of determining a value for λ. Let's admit the yield-stress behavior of Pouliquen's

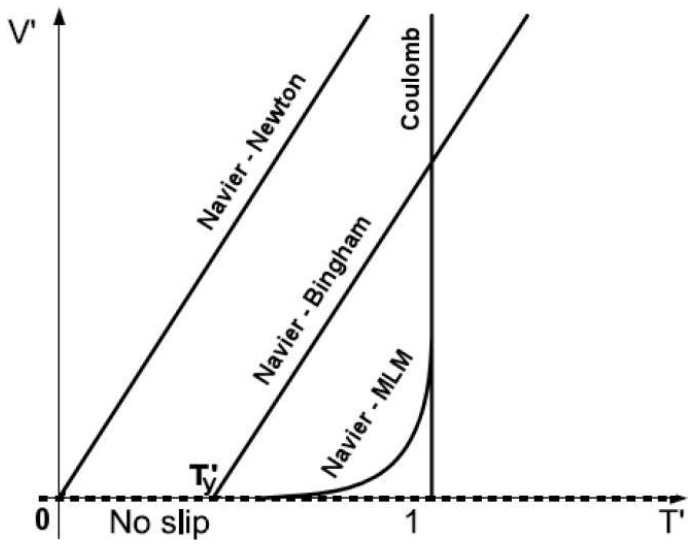

Figure 4.7: *Rescaled average velocity vs average pulling force for different BCs/constitutive laws. The slope of Newton and Bingham lines is* $\lambda\frac{\mu}{\eta'}\sqrt{\frac{mP}{d}}$.

form for $\mu(I)$, and suppose that $\mu_2 \approx \mu$ (remember that μ is the particle-wall friction coefficient). In this perspective the slip length is simply proportional to the particle diameter and the best fit gives $\lambda/d \approx 0.2$. This value gives a sort of minimum slip length; in the case with $\mu_2 > \mu$ the slip length diverges for $T' \to 1$.
It is important to note that V' is an analog of the inertial number I for near wall flows, and T' is an effective wall friction coefficient as $\mu(I)$ is for the bulk; thus it is interesting to note that the shape of the curve $T'(V')$ is very close to that of $\mu(I)$; this can lead to some ideas on the origin of the effective friction coefficient in the bulk remembering that the effective wall friction coefficient derives from the assumption of heterogeneous forces.
Here the aim is not to define the correct functional form for these BCs (even if a very good fit was obtained for this simple case), but it has to be underlined that real boundary conditions (even in simplified setups) are not no-slip or Coulomb-like, and assuming one of these limiting BCs can introduce errors in the physical validity of granular flow models; this slip behavior can be captured by a modified Navier condition, where the slip length is proportional to the particle diameter.

4.7 A possible generalization involving dimensional analysis

In the preceding sections it was shown how simple assumptions on the physics at the boundary led to reasonable expressions for the boundary conditions, which describe the intermediate behavior between Coulomb steady sliding and no-slip. In this section the

approach will be extended in order to understand the validity of the preceding develpment, and give a more general form of the stress-velocity relationship. Being that the physics is too complex to be completely described, one can try to tackle the problem by means of dimensional analysis, which may help in reconstruct, in this case, general behaviors. This attempt is very similar to the mixing length model developed for the bulk and described for example by G. D. R. Midi (2004), which was encountered in Chapter 2, because the relevant phenomena are analysed forming dimensionless numbers and trying to capture the relation between them.

As for the bulk, being that the main dimensional variables are the stress tensor, the shear rate, the density of the material and the particle diameter, it has to be reminded that some dimensionless numbers can be defined involving the simplest physics, the first of which is the effective (bulk) friction coefficient

$$\mu^* = \frac{\tau}{p} \tag{4.14}$$

where p is the trace of the stress tensor, corresponding in 2-D to $p = \frac{\sigma_{xx}+\sigma_{yy}}{2}$, and τ is the shear stress, which will be considered, involving symmetry, as $\tau = \sigma_{xy} = \sigma_{yx}$, and the inertial number(G. D. R. Midi, 2004):

$$I = \frac{\dot{\gamma} d_p}{\sqrt{\frac{p}{\rho_p}}} \tag{4.15}$$

Another, often neglected, dimensionless quantity is the normal stress ratio, which will be discussed later in connection with DEM results (Chapter 7):

$$k^* = \frac{\sigma_{yy}}{\sigma_{xx}} \tag{4.16}$$

which is usually supposed to be 1 in hydrodynamic models of dense granular flow(Artoni et al., 2009c; Bocquet et al., 2002a), but was shown to deviate from unity particularly when the jamming transition is approached(Renouf et al., 2005).

Other dimensionless quantities which shall be considered are the local solid fraction and particle-particle interaction parameters such as friction coefficient, restitution coefficient(s), cohesion parameters. The simple rheology developed by G. D. R. Midi (2004) identifies the inertial number as the center of all the phenomenology influencing directly the solid fraction and the effective friction coefficient. The effect of the normal stress ratio was not studied and no universal relationship was found relating the function $\mu^*(I)$ to particle parameters (therefore the form of the function $\mu^*(I)$ should be determined experimentally, in the intention of the authors, for each material).

At the boundary, another dimensional quantity must be considered, which is the (slip)

velocity v_s. Generally, the slip velocity can be used to define several dimensionless numbers with the quantities already defined for the bulk. As an example, two dimensionless numbers are:

$$\xi^{(1)} = \frac{v_s}{\sqrt{\frac{p}{\rho_p}}} \quad \text{and} \quad \xi^{(2)} = \frac{v_s}{\dot{\gamma} d_p} \tag{4.17}$$

which are related by the inertial number I:

$$\xi^{(1)} = I\xi^{(2)} \tag{4.18}$$

It is easy to see that $\xi^{(1)}$ corresponds to the dimensionless slip velocity used in the previous sections, and that $\xi^{(2)}$ is a dimensionless slip length:

$$\xi^{(2)} = \frac{v_s}{\dot{\gamma} d_p} = \frac{\lambda}{d_p} \tag{4.19}$$

where λ is a slip length in the sense of Navier (1823). Dimensional analysis suggests that a function exists such that:

$$\xi^{(1)} \text{ or } \xi^{(2)} = \mathcal{F}(\mu^*, I, k^*, \phi, \mu_{pw}, \mu_p, ...) \tag{4.20}$$

where the RHS indicates a function of all the dimensionless numbers characterising the system, where μ_{pw} and μ_p represent the particle-wall friction coefficient and the particle-particle friction coefficient. All the quantities are computed at the wall, therefore μ^* corresponds to the effective wall friction coefficient. Other dimensionless numbers which can be considered come from particle-wall and particle-particle interaction laws (coefficients of restitution, cohesion parameters, etc.). Being that $\xi^{(1)}$ and $\xi^{(2)}$ are not independent, one of them can be choosen as a representative dimensionless number of wall partial slip. In the following, differently from what was used in the previous sections, $\xi^{(2)}$ will be taken as a representative number. Keeping the same particle-particle interaction laws and parameters, it can be supposed that:

$$\xi^{(2)} = \mathcal{F}(\mu^*, I, k^*, \phi, \mu_{pw}, ...) \tag{4.21}$$

As regards the effect of the solid fraction on the slip velocity, Tüzün et al. (1988) suggested that it has an important influence for non-Coulomb friction (i.e. when friction depends on local area of contact). Restricting to non-Coulomb friction, it seems not to add important phenomenology, and therefore it will be dropped out in the following.
The need for simplification can then suggest a less general form (here simplified in order to treat inelastic, cohesionless particle-wall interactions):

$$\xi^{(2)} = f_1(\mu^*) f_2(I) f_3(k^*) f_4(\mu_{pw}) \tag{4.22}$$

It can be supposed, considering the results from the simple model of Section 4.3, that the dependence on μ^* and μ_{pw} can be simplified assuming that the relevant dimensionless number is the distance of the effective wall friction coefficient on the particle-wall friction coefficient, $\frac{\mu^*}{\mu_{pw}}$:

$$f_1(\mu^*)f_4(\mu_{pw}) \approx g\left(\frac{\mu^*}{\mu_{pw}}\right) \tag{4.23}$$

Therefore a general form of the boundary condition can be expressed as

$$\xi^{(2)} = g\left(\frac{\mu^*}{\mu_{pw}}\right) f_2(I)f_3(k^*) \tag{4.24}$$

The dependence of the generalized boundary condition on the normal stress ratio $f_3(k^*)$ should be considered when trying to develop refined correlations; for the moment its effect will be neglected for simplicity, because the behavior of k^* is not well known in dense granular flows. It will remain an important topic to be analysed in the future. Some hints will be however obtained from DEM data in chapter 7.

Therefore, neglecting for the moment the effect of the normal stress ratio k^*, the boundary condition takes the form:

$$\frac{v_s}{\dot{\gamma}d_p} = g\left(\frac{\mu^*}{\mu_{pw}}\right) f_2(I) \tag{4.25}$$

or alternatively, for $\xi^{(1)}$:

$$\frac{v_s}{\sqrt{\frac{p}{\rho_p}}} = I\ f_2(I)\ g\left(\frac{\mu^*}{\mu_{pw}}\right) \tag{4.26}$$

If the considerations invoked in the preceding lines hold, an expression for the effective boundary condtion can be determined once the functions f_2 and g are obtained. This should be done experimentally or by means of numerical simulations. It can be easily seen that for the boundary condition to be valid in the low frictional limit,

$$g\left(\frac{\mu^*}{\mu_{pw}}\right) \to \infty \ \text{ for } \ \frac{\mu^*}{\mu_{pw}} \to 1 \tag{4.27}$$

Therefore a hypothetical form for g could be:

$$g\left(\frac{\mu^*}{\mu_{pw}}\right) = c_1\left(\frac{\frac{\mu^*}{\mu_{pw}} + c_2}{1 - \frac{\mu^*}{\mu_{pw}}}\right)^{c_3} \tag{4.28}$$

where $c_1, c_2, c_3 > 0$. Both from experience and previous considerations (Section 4.3), it can be argued that for very frictional walls no-slip condition is approached, therefore implying $c_2 = 0$. Rewriting, a functional form is proposed:

$$g\left(\frac{\mu^*}{\mu_{pw}}\right) = c\left(\frac{\frac{\mu^*}{\mu_{pw}}}{1 - \frac{\mu^*}{\mu_{pw}}}\right)^{\alpha} \tag{4.29}$$

In previous sections, based on considerations involving typical timescales, the boundary condition was written as:

$$\frac{v_s}{\sqrt{\frac{p}{\rho_p}}} = g\left(\frac{\mu^*}{\mu_{pw}}\right) \tag{4.30}$$

implying, in the present development, $If_2(I) = 1$. The analysis carried out in this section shows that such an implication is not fully correct and that some assumptions employed in the simple stochastc model described in Section 4.3 should be revised to get rid of this fact. Apart from these considerations, from general premises, f_2 could a function of the form:

$$f_2(I) = c'I^{\beta} \tag{4.31}$$

where $\beta \leq 0$. Just to point out, $\beta = 0$ does not mean that I has no effect on the slip velocity, because a indirect effect is exerted through the dependence of μ^* on I(G. D. R. Midi, 2004). Moreover, there is no evidence that β is uniform in I. In fact, it can be deduced that the value of the exponent β depends on the relevant timescale of the process. In 4.3, based on the assumption that the time scale of pressure driven rearrangements, $\tau_p = \frac{1}{d_p}\sqrt{\frac{p}{\rho_p}}$ was the controlling one, we proposed that v_s scaled as $\sqrt{\frac{p}{\rho_p}}$. This is in principle valid if $\tau_p << \tau_\gamma$, where $\tau_\gamma = \dot{\gamma}^{-1}$ is the time scale of shear-induced processes (note that these time scales form the inertial number, $\frac{\tau_p}{\tau_\gamma} = I$). If $\tau_\gamma << \tau_p$, it is probable that v_s scales with $\dot{\gamma}d_p$. This can be translated through the function $f_2(I)$, by simply arguing that $\beta \to 0$ as $I \to \infty$ and $\beta \to -1$ as $I \to 0$. From this point of view, it can be argued that two limiting regimes are found, corresponding to the rapid and quasistatic regimes of flow. However, the present considerations do not hold in the rapid flow regime (where other well defined BCs apply), but are intended to apply only on the dense flow where persistent contacts are found. So what we are looking for is a transition from a quasistatic region, where I takes low values, and a dense region where I takes moderate values. It can be supposed that the exponent β in the quasistatic region will tend to -1, while it will be comprised between 0 and -1 in the dense region, where both the effect of shear rate and pressure are important. This can be translated into the functional form, characterised by two limiting power-law behaviors:

$$f_2(I) = c_1'I^{\beta_1} + c_2'I^{\beta_2} \tag{4.32}$$

Therefore the functional form proposed here for the boundary condition extends what was previously suggested by means of simple modeling attempts into a more general form:

$$\frac{v_s}{\dot{\gamma}d_p} = \left(\frac{\frac{\mu^*}{\mu_{pw}}}{1-\frac{\mu^*}{\mu_{pw}}}\right)^{\alpha}\left(c_1''I^{\beta_1} + c_2''I^{\beta_2}\right) \tag{4.33}$$

Such a formulation, due to the fact that it comes from dimensional analysis, can be considered as valid only in an average sense, within the range of validity of all the assumptions involved. Neither its correctness nor the specific parameters can be determined analytically, but shall be evaluated from experiments or numerical simulations. Possible improvements, coming from hints derived by evaluation, could be achieved adding corrections based on the normal stress ratio k^* and on the solid fraction ϕ, whose phenomenological basis was not clear up to this moment. Some discussion will be given in Chapter 7, in comparison with discrete element data.

4.8 Conclusions

To resume the main results of this chapter, a simple model of a particle sliding with the simplest frictional law on a plane has been developed to determine effective boundary conditions for granular flows. To account for the heterogeneity of the medium, the particle is subjected to a random normal force, while a constant tangential force is assumed for simplicity. The dynamics consists of stick-slip events, which are related to the heterogeneity in the stress field; the resulting dependence of the average tangential force on the average slip velocity and on the variance of the velocity of the particle (*i.e.* granular temperature) was reported, thus providing two possible effective boundary conditions for the velocity and granular temperature fields. The results are well fitted by simple laws and represent for the velocity field an intermediate behavior between Coulomb's law (at high velocities) and the no-slip boundary condition. Granular temperature is related to the velocity by a simple power law behavior. The functional form proposed can be adopted as a general tool to quantify this intermediate behavior, as it does not depend on the particular choice of the force distribution, nor the friction model adopted. In addition, it was demonstrated that the curve obtained by numerical simulation satisfies a modified slip-length Navier boundary condition within a mixing length model of granular flow, with the slip length being proportional to the characteristic length of the system, the particle diameter. After having analysed the results obtained by means of the simple stochastic model of wall behavior, a generalization was attempted, based on dimensional analysis, which helped to understand the hypotheses underlying the previous development, and gave a basis for an extension of the boundary condition introducing a dependence on the inertial number I also. Further experimental work is needed to estimate the parameters and test the validity of the boundary conditions developed in real situations. Comparison with DEM results will be given in Chapter 7.

Chapter 5

Coupling between solids rheology and gas flow

Du sable, puis du sable !
Le désert ! noir chaos
Toujours inépuisable
En monstres, en fléaux !
Ici rien ne s'arrête.
Ces monts à jaune crête,
Quand souffle la tempête,
Roulent comme des flots!

Victor Hugo, Le Feu du Ciel, Les Orientales

5.1 Introduction

In this chapter the classical approach to model the problem of countercurrent gas-solid flow in vertical pipes is extended with the explicit computation of the coupling between a flowing gas and the rheology of a moving bed of granular solid. In particular the physics is characterized by a two-fold phenomenology since (a) the presence of shear in the granular material induces a porosity profile that changes the flow pattern in the gas and (b) the gas phase pressure drop has the effect of lowering the effective gravity force acting on the solid. The major novelty of the approach lies in the fact that for the first time the strong relationship between the rheology of the granular medium and its capacity to dilate under flow is taken into account, while in the past the porosity was considered as an independent quantity. The content of this chapter is the subject of a paper submitted to the *International Journal of Multiphase Flow*.

Moving beds experiencing countercurrent gas-solid flow are commonly encountered in industry. Applications span from drying processes, moving bed granular filters(Seville and Clift, 1997), to direct reduction of iron ore(Parisi and Laborde, 2004), or even to pebble-bed nuclear reactors(Rycroft et al., 2006), just to cite few examples. Here, attention will be focused on countercurrent moving beds below the fluidization threshold, when the mixture is rather dense, such that the granular medium can be treated within the context of dense granular flows(G. D. R. Midi, 2004). The simplest set-up which can be imagined is a fully-developed channel flow: from the modeling point of view, steady, one-dimensional gas solid flow is a well estabilished topic in the theory of flow through porous materials and in fluidization. Considering a pipe or a channel filled with a moving granular bed experiencing a countercurrent gas flow, the classical analysis(Gidaspow, 1994) is developed assuming that a granular bed moves with uniform (plug) velocity profiles in the direction orthogonal to the flow, with a gas flow which is uniform too. A drawback of such an assumption, which is a very useful simplification in a variety of occasions, is that it neglects radial profiles of solid velocity and porosity. This leads to a wrong estimation of the gas velocity and subsequently does not take into account gas maldistribution and contact time distribution, which come directly from the existence of such profiles. Previous studies on voidage variations in channels(Faderani et al., 1998a,b) used a simplified model, the so-called “Drift Flux Model” (Wallis, 1969), involving the assumption that the relative velocity of the solids and the interstitial fluid equals the terminal velocity, in order to describe the behavior of nearly buoyant granular materials experiencing gravity driven flow; in this work, such a model cannot be used because (1) the effect of wall friction is going to be considered, which is neglected in the development of that model, and (2) the assumption on the relative velocity is unfeasible because we refer to situations in which generally the bed is far both from fluidisation and free settling. Therefore the full analysis involving the specification of forces on each single phase will be adopted. In the context of fixed beds, the importance of considering radial profiles of porosity in the bed was already introduced by (Vortmeyer and Schuster, 1983), who showed how they can affect the gas flow pattern. In this situation, if the sample is accurately prepared, geometrical reasons alone can explain the development of a non uniform porosity profile. Geometrical constraints impose that for nearly spherical particles and in presence of flat walls, close to the boundary, porosity $\epsilon \to 1$, and ϵ typically fluctuates around a mean profile due to layering effects. This effect vanishes if the wall is fully rough (that is, if the roughness length is comparable with the dimension of the particles in the bulk).

When the granular material is moving in the channel, an additional source of dilation occurs: due to (and in order to allow) the motion, the material needs to dilate close to

the wall, where a shear band develops. In the centre of the channel instead the material remains unsheared and the porosity constant around the random packing limit. In this context, some studies concerning the importance of porosity profiles, for example in the drying process, or for heat transfer, have been carried out(Lacerda et al., 2005; Lira et al., 2007).

However, often an a-prioristic porosity profile, coming from fixed-bed measurements, was assumed, and it was not discussed how this profile could vary with the controlling parameters of the system, such as solid and gas flowrate, material parameters such as wall-particle and particle-particle friction, and the gas phase physical properties. Moreover the coupling between solid rheology and gas flow, as described below, seems to have never been taken into account previously.

It seems of great evidence that deeper understanding of the behavior of the flowing granular material is needed to predict the porosity, and so the gas phase, velocity profile. Moreover, it is evident, for example looking at the experimental works on the dense flow of granular materials collected by the French group GDR MiDi(G. D. R. Midi, 2004), that the dilation of the medium is strongly related to the flow pattern of the materials, and so the porosity profile can not be considered as an a-priori ingredient.

The dilation needs to be evaluated by means of a rheology and a dilatancy rule for granular materials. At constant pressure drop, a more dilated medium means higher velocities of the gas, with consequent preferential channeling near the walls. This is a quite important industrial problem and it will be tackled by means of simple arguments. For the sake of simplicity, efforts will be concentrated on the shear-induced dilation, which seems to be more important than the geometrical one, at least for sufficiently large bin to particle diameter ratios(Paterson et al., September 2000). The dilated zone due to the shear band typically spans for almost ten particle diameters, while the geometrical dilation, averaged over the fluctuations extends for maximum 2 particle diameters(Goodling et al., 1983; Mueller, 1992). Thus, it is reasonable to expect that if the channel is sufficiently large to allow the formation of shear bands ($b/d_p > 20$), the contribution of geometrical dilation is negligible with respect to the shear-induced one; in addition, it was shown(Paterson et al., September 2000) that in such channels, not only the relative weight of the geometrical dilation is low, but also the absolute value is negligible on gas maldistribution.

In summary, the following work deals with the prediction of the flow patterns in the gas and in the solid, when a proper rheology is considered for the solids. It is shown how the simple but effective mixing-length model of granular materials developed by the GDR MiDi(G. D. R. Midi, 2004; da Cruz et al., 2005), can be used to predict velocity and porosity profiles, which strongly affect the behavior of a countercurrent gas flow. The

main scope is to discuss the methodology for the coupling, and evaluate the predictions given by the approach in a simple configuration, with simple (though reasonable) assumptions for the rheology of the granular medium and the gas phase behavior. In view of the framework outlined here, there's strong need for further modeling and experimental work on the subject.

5.2 Physical problem and model

The focus is on a quasi 2-dimensional problem (which is the simplification of a silo), assuming that the flow field of both the gas and the solid is fully developed, and that due to the Jannsen effect, stresses do not vary with height far from the top(Nedderman, 1992). The case without gas has been referred previously as the vertical chute problem; the case of countercurrent gas flow is exemplified in Fig. 5.1. It is important to stress that the coupling between granular and gas flow is given, in this simple configuration, by the following issues:

- assuming constant pressure drop, variation in the porosity of the solid implies variation in the relative velocity between the gas and the solid, because the permeability of a granular medium is an increasing function of the porosity. Being that the velocity profile of the solid is determined from its momentum equations, once that the latter is fixed, the velocity profile in the gas is given. On another side, varying total gas (and solid) flowrate implies a variation in the global gas phase pressure gradient.

- gas phase pressure gradients (due to the frictional drag between the solid and the gas) correspond to drag forces in the solid; in a fully developed flow in a channel, with all gradients in one direction, the gas pressure drop has the effect of lowering the weight of the granular material.

- the action of lowering the weight of the material modifies internal stresses, and so in cascade influences shear rate and velocity profiles in the solid. Therefore, porosity is determined at this step because it depends on the amount of shear in the material.

Another mechanism inducing coupling between the dynamics of the two phases considered could be lubrication of the solid particles by the fluid: if the interstitial fluid is a gas and not a liquid, this effect is reasonably negligible.

Gas phase model Let $\vec{v}_g$ $(= (u_g,\ v_g,\ w_g))$ and $\vec{v}_s$ $(= (u_s,\ v_s,\ -w_s))$ be, respectively, the gas and the solids velocity fields; for the sake of analysing the case of countercurrent

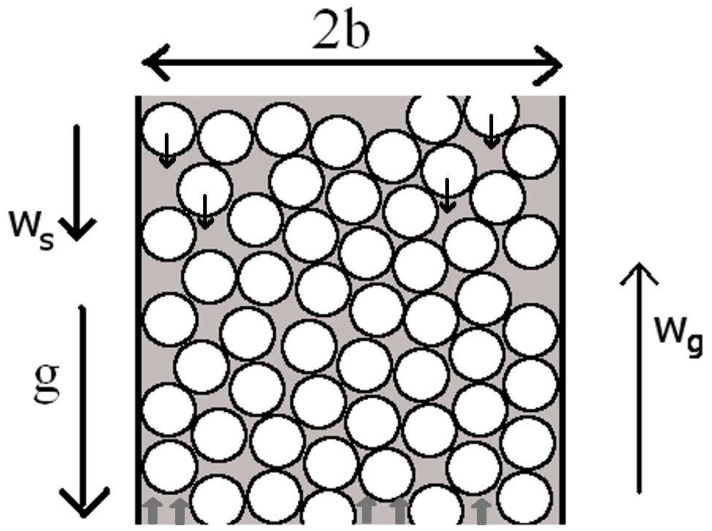

Figure 5.1: *Schema of countercurrent gas solid flow.*

gas flow (with the solid discharging due to gravity), w_s is choosen to be positive when the solids flow downwards and w_g is choosen to be positive when the gas flows upwards, with respect to the absolute reference frame, or, in other words, with respect to the walls of the container.

The gas phase model choosen is a continuum one, mimicking the interaction with the dense assembly of particles by means of lumped, locally averaged, terms. Indeed, the gas flow can be thought to belong to the category of flow in a porous medium, for which a vast Literature exists. The idea, which is common to many variable-porosity modelisation attempts, is that the empirical laws expressing permeability in terms of porosity are considered to hold (locally) even in the case of variable porosity. Even if porosity often shows significant variations along few particle diameters (corresponding to the width of shear bands), it seems reasonable that a lumped empirical law can be thought as a height-averaged expression, thus it is local in the transversal direction, but contains global informations on the direction parallel to the flows. Dealing with gases, walls can be thought as having a small zone of influence on the flow, thus Darcy's law (which neglects viscous effects) can be used instead of Brinkman's. Neglecting viscous effects means neglecting friction of the gas with the wall: this implies that the gas has a finite velocity at the wall. Darcy's law states that:

$$\vec{v}_g - \vec{v}_s = -\frac{k}{\eta_g}\left(\vec{\nabla}P - \rho_g \vec{g}\right) \tag{5.1}$$

So, with the hypothesis of fully developed and stationary flow, for the solid and the gas, which implies:

$$u_g = v_g = 0, \quad u_s = v_s = 0 \quad \left[\frac{\partial w_g}{\partial z} = \frac{\partial w_s}{\partial z} = 0\right] \tag{5.2}$$

the following is obtained:

$$\frac{\partial P}{\partial z} = -\frac{\eta_g}{k}(w_g + w_s) + \rho_g g \tag{5.3}$$

$$\frac{\partial P}{\partial x} = \frac{\partial P}{\partial y} = 0 \tag{5.4}$$

Thus, P is uniform in the transversal direction; neglecting the gravity term, in low gas density flows, and provided that the RHS of Eq. 5.3 does not depend on z, it is possible to use the algebraic relation:

$$\frac{\Delta P}{L} = -\frac{\eta_g}{k}(w_g + w_s) \tag{5.5}$$

in which the permeability is unknown and could be derived, for example, from the Càrman-Kozeny expression(McNamara et al., 2000). Being this relation valid only at low flowrates, we choose to use its extension to high flowrates (and obviously valid below the fluidization limit) provided by Ergun (1952):

$$\frac{\Delta P}{L} = \frac{150\bar{V_0}\eta_g}{d_p^2}\frac{(1-\epsilon)^2}{\epsilon^3} + 1.75\frac{1-\epsilon}{\epsilon^3}\frac{\rho_g \bar{V_0}^2}{d_p} \tag{5.6}$$

where η_g is the viscosity of the gas, $\bar{V_0} = \epsilon(w_g + w_s)$ the superficial (empty column) velocity, d_p the particle diameter. It is important to emphasize that the Ergun equation just written relates the pressure drop to a relative velocity of the gas, which can be higher or lower than the velocity expressed in the "walls reference frame", since it depends on the direction of the motion of the solid phase. It is evident that even if the gas has a zero absolute velocity, a pressure drop occurs due to the *relative* velocity between the two phases imposed by solid motion. The problem was early elucidated in the famous paper by Richardson and Zaki (1954). The Ergun equation can be nondimensionalized into:

$$\frac{\Delta P \rho_g d_p^3}{L\eta_g^2} = 150 Re_p \frac{(1-\epsilon)^2}{\epsilon^3} + 1.75\frac{1-\epsilon}{\epsilon^3} Re_p^2 \tag{5.7}$$

where $Re_p = \frac{\rho_g \bar{V_0} d_p}{\eta_g}$. It is noteworthy to observe that the Ergun equation contains the first issue of the coupling between gas and solid, since it states that the gas flow pattern depends on the porosity of the solid bed. Being that the pressure drop is uniform along the transversal coordinate, if ϵ varies along x, $w_g + w_s$ must vary in order to keep ΔP constant. More precisely if the porosity increases, the relative velocity must increase also. To better understand this point, it is possible to refer to figure 5.2, which displays the behavior of Re_p vs ϵ for constant $\Delta P' = \frac{\Delta P \rho_g d_p^3}{L\eta_g^2}$. The dashed line in the figure represents the onset

of fluidization; this condition is obtained as usual as the point where the pressure drop in the gas balances the weight of the bed. In this case the classical relation(Kunii and Levenspiel, 1969) holds:

$$\begin{aligned} &\tfrac{\Delta P}{L}\big|_{mf} = (\rho_s - \rho_g)\,(1-\epsilon)g \\ &\Rightarrow \Delta P'_{mf} = \tfrac{(\rho_s-\rho_g)\rho_g g d_p^3}{\eta_g^2}(1-\epsilon) = \mathrm{Ar}(1-\epsilon) \end{aligned} \tag{5.8}$$

where Ar is Archimedes number; Eq. 5.8 means that the pressure drop at which fluidization starts decreases linearly with porosity; inserting this result in Ergun relation we obtain the dashed line in Fig. 5.2 which represents the Reynolds number at the minimum fluidization point, Re_{mf}. Being that the material is more dilated near the walls, it follows that the onset of fluidization is generally reached earlier in these zones. So, provided that the system is below the fluidization limit depicted in Fig. 5.2, an algebraic relation holds, which is the Ergun equation, that for a given local porosity and the overall pressure drop, allows to calculate the superficial velocity of the gas (this algebraic relation corresponds to solid lines in figure 5.2). In the next paragraph a method to calculate the porosity and the solid velocity profiles will be presented, in order to close the system of equations.

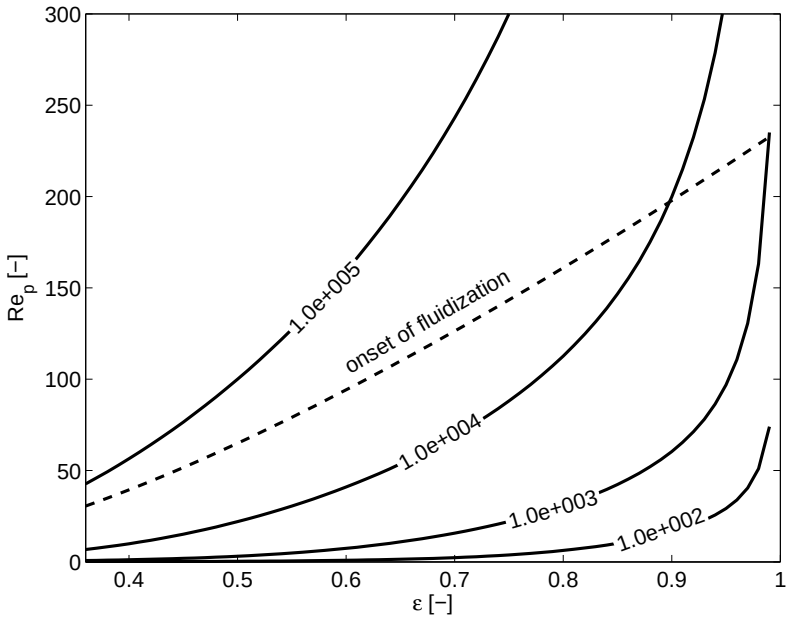

Figure 5.2: *Re_p vs ϵ for four different constant values of $\Delta P' = \frac{\Delta P \rho_g d_p^3}{L\eta_g^2}$, following Ergun equation. The onset of fluidization is obtained with parameters in table 1.*

Solid phase model The vertical chute problem for dense granular flows, neglecting the presence of an interstitial fluid, was already discussed in Chapter 2; apart from the assumption of fully developed flow which affects the velocity field, in this case Jannsen's result(Nedderman, 1992) is employed on the stress profiles as a function of depth in a

granular column, assuming to be far enough from the top of the bed to have uniform wall stresses. As regards stresses, which are:

$$\tau = \rho g' x \qquad p = \text{const.} \tag{5.9}$$

where g' is a rescaled gravity which takes into account the second issue of gas-solid coupling, considering the weight reduced by the drag exerted by the gas, and is given by:

$$g' = g - \frac{\Delta P}{\rho L}. \tag{5.10}$$

The local mixture density ρ depends on the local porosity by means of the relationship $\rho = \rho_g \epsilon + \rho_s(1-\epsilon)$ which, for gases, can be approximated as $\rho \approx \rho_s(1-\epsilon)$. In fact, in the following the pressure drop will be taken as a control parameter (which is equivalent to choose gas flowrate, but is possible only under the fluidization limit). In this case $\frac{\Delta P}{L}$ is a known quantity. As regards boundary conditions for the solid, dealing with frictional contacts, it is likely to assume a Coulomb slip condition stating that that the effective friction coefficient $\mu = \tau/p$ equals a wall friction coefficient μ_w, such that:

$$\mu(x) = \frac{\mu_w x}{b} \qquad p = \frac{\rho(x=b) g'(x=b) b}{\mu_w} \tag{5.11}$$

where b is the channel half-width. It is important to spend some time on discussing the role and nature of the wall friction coefficient μ_w; for the sliding of a mass on a plane, the well known Da Vinci - Amontons - Coulomb law states that the friction coefficient is a constant depending only on the materials in contact (mass and plane). However, when dealing with a granular mass, which consists of a collection of contactors, there can be unsteady motions (stick-slip events) which cannot be characterized (even in an average sense) by a constant μ_w. To account for these effects, the simple time-averaged velocity-dependent formulation proposed in Chapter 4 is used :

$$\mu_w = \mu_w^\infty \left(\frac{v'_{slip}}{c_w + v'_{slip}} \right)^\zeta \tag{5.12}$$

where $v'_{slip} = v_{slip}/\sqrt{p/\rho_s}$ is a dimensionless slip velocity, μ_w^∞ is the steady sliding coefficient, c_w and ζ are dimensionless parameters which in principle are function of the particle-wall pair materials. As a remark, the slip velocity v_{slip} is the velocity of the solids at the wall, which is typically non-zero due to sliding phenomena, and should not be confused with the relative velocity between the solids and the gas, which is also sometimes referred as “slip velocity”. This formulation was developed to take into account the fact that stick slip events are less probable when the normal stress is high (or shear stress is low), so the average velocity tends to zero in this limit, while for $\tau/p \to \mu_w^\infty$ the motion

is more similar to steady sliding.

To obtain the solids' velocity and the porosity field, a rheological model is needed, together with a dilatancy rule for the porosity. In order to treat the flowing behavior of granular materials, many rheologies have been proposed. Here absolute predictions are not sought, but rather it is tried to estabilish a methodology. In order to do so, a simple (though well estabilished) closure is used in the following(G. D. R. Midi, 2004). Considering the rheology proposed by da Cruz et al. (da Cruz et al., 2005), which is a simple zero order closure for the behavior of granular materials in dense flow:

$$\mu = \mu_0 + \beta I \tag{5.13}$$

where $I = \dot{\gamma} d_p / \sqrt{p/\rho_s}$ is a dimensionless parameter called *inertial number*, μ_0 and β parameters of the model; the inertial number profile is thus:

$$I = \frac{\mu_w \frac{x}{b} - \mu_0}{\beta} \quad \text{for } x > \frac{\mu_0 b}{\mu_w} \tag{5.14}$$

and is otherwise zero. Using a linear dilatancy law $\epsilon(I)$ as suggested by da Cruz et al. (da Cruz et al., 2005):

$$\epsilon = \epsilon_{min} + \alpha I = \epsilon_{min} + \alpha \frac{\mu_w \frac{x}{b} - \mu_0}{\beta} \quad \text{for } x > \frac{\mu_0 b}{\mu_w} \tag{5.15}$$

where ϵ_{min} corresponds to the random packing porosity (which for spheres can be approximated by 0.36), and α is a parameter. To obtain the velocity profile for the granular material, the shear rate has to be extracted:

$$\dot{\gamma} = \frac{1}{d_p} \sqrt{\frac{p}{\rho_s}} \frac{\mu_w x/b - \mu_0}{\beta} \quad \text{for } x > \frac{\mu_0 b}{\mu_w} \tag{5.16}$$

(and zero otherwise) and integrate it along the channel width:

$$w_s(x) = w_s(x = b) - \int_x^b \dot{\gamma} \, dx'$$

which becomes, finally:

$$w_s(x) = \begin{cases} v_{slip} - \frac{1}{\beta d_p} \sqrt{\frac{p}{\rho_s}} \left(\frac{\mu_w b}{2} - \mu_0 b - \frac{\mu_w x^2}{2b} + \mu_0 x \right), \text{for } \; x > \frac{\mu_0 b}{\mu_w} \\ v_{slip} - \frac{b}{\beta d_p} \sqrt{\frac{p}{\rho_s}} \left(\frac{\mu_w}{2} - \mu_0 + \frac{\mu_0^2}{2\mu_w} \right), \; \text{for } x \leq \frac{\mu_0 b}{\mu_w} \end{cases} \tag{5.17}$$

The velocity profile is determined numerically with an iterative procedure, because in Eq. 5.17 the profile depends on p,v_{slip} and μ_w, which are related by the non linear boundary

condition, Eq.5.12. The solids flowrate and the mass weighted average velocity can be determined by:

$$\dot{Q} = \int_0^b (1-\epsilon) w_s dx, \quad \bar{w}_s = \frac{\dot{Q}}{b} \tag{5.18}$$

An example of the results on velocity and porosity profiles of the two currents are reported in Fig. 5.3; the curves are computed with the parameters of Table 1 and for constant $Fr_s = 0.2$, which is an average Froude number defined as:

$$Fr_s = \frac{\bar{w}_s}{\sqrt{gb}} \tag{5.19}$$

The different curves represent different values of the dimensionless pressure drop $\Delta P'$. As regards limiting cases, at first, there is a finite positive value of the gas phase pressure drop for which $w_g = 0$ almost everywhere; moreover, for high enough pressure drop, the pressure drop at minimum fluidization is reached, which occurs when the effective gravity $g' = 0$ (and this occurs first near the wall, so a local fluidization occurs there). Figure 5.3a displays porosity profiles of the solid: it is clear that the gas tends to expand the bed enlarging zones with porosity higher than the minimum (random packing) limit, which are localized near the walls. In the model this is due to the lowering of solid stresses induced by the lowering of effective gravity (Fig. 5.3b). Also, effective gravity, which depends on porosity, is not perfectly uniform in the transversal direction, but is slightly lower where the porosity is higher. As it can be deduced from Figure 5.3c, the variation in the size of dilated zones is mirrored also by the size of shear bands, which are larger when more gas is inflated. Although it was choosen to model smooth walls (by means of the boundary conditions used), shear bands are clearly evident; the rougher the walls, the greater will be their effect on dilation and gas flow maldistribution. The slip velocity, in this case, decreases as the gas pressure increases: this is due to flowrate conservation and enlargement of shear bands. As expected, In Fig. 5.3d gas velocity is shown to depend obviously strongly on the applied pressure drop, increasing the total flowrate; moreover the presence of dilated zones influences gas distribution, increasing pressure drop enhances the maldistribution because of higher gas velocity in proximity of the wall. The model predicts a strong coupling between solids and gas flow, with an appreciable variation of the shear bands on one side, and a strong change in the maldistribution on the other side. Some comment is needed on the choice of the parameters in Table 1. The difference in density between the material and the gas is typical, and corresponds to choose air as a gas (the order of magnitude of viscosity too was choosen from air properties) and polyethlyene pellets as a granular material. $1\ mm$ sized particles can be considered as a typical size for cohesionless particles. The reason for this choice is that the research was originally driven by applications involving particles of similar or larger size such as

in plastic pellets drying and in metallurgical ore reduction. These applications involve moving unfluidized beds where quantification of the amount of maldistribution coming from shear-induced dilation is preliminar to mass and energy transfer calculations. Being that shear induced dilation, from the model used here, tends to increase as the particle diameter decreases, smaller particles will induce a more dilated medium and therefore possibly increase gas maldistribution. Rheological parameters are adapted from the work of da Cruz et al. (2005), while parameters for the boundary condition for solids flow, Eq. 5.12 were choosen after the considerations included in Chapter 4. Obviously, when trying to model real configurations, all of these parameters should be determined experimentally by means of appropriate testing facilities. The channel half-width was choosen equal to 100 particle diameters, as a value which is large enough to allow neglecting of geometrical dilatancy, and characterizes a number of practical applications.

Experiments to measure directly the flow patterns of the two currents are very difficult to carry out, in a true moving bed configuration. Moreover, it is simpler to understand the problem of maldistribution by means of global measures rather than looking at the flow profiles. Thus, in the next sections, the analysis is devoted to study the maldistribution in two ways: first with a lumped parameter, to have an approximate measure of the distribution, and then in terms of residence times.

Table 5.1: *Parameters used in this work.*

ρ_s	1000	kg/m^3
ρ_g	1	kg/m^3
η_g	$1E-5$	$Pa \cdot s$
d_p	$1E-3$	m
μ_0	$.1$	$[-]$
ϵ_{min}	$.36$	$[-]$
α	$.5$	$[-]$
β	2	$[-]$
b/d_p	100	$[-]$
L/d_p	1000	$[-]$
μ_∞	$.3$	$[-]$
ζ	$.5$	$[-]$
c_w	1	$[-]$

5.3 Macroscopic analysis of gas flow maldistribution

In the preceding section a simple model of countercurrent gas-solid flow was outlined, which involved the coupling between the two phases. The analysis developed is quite

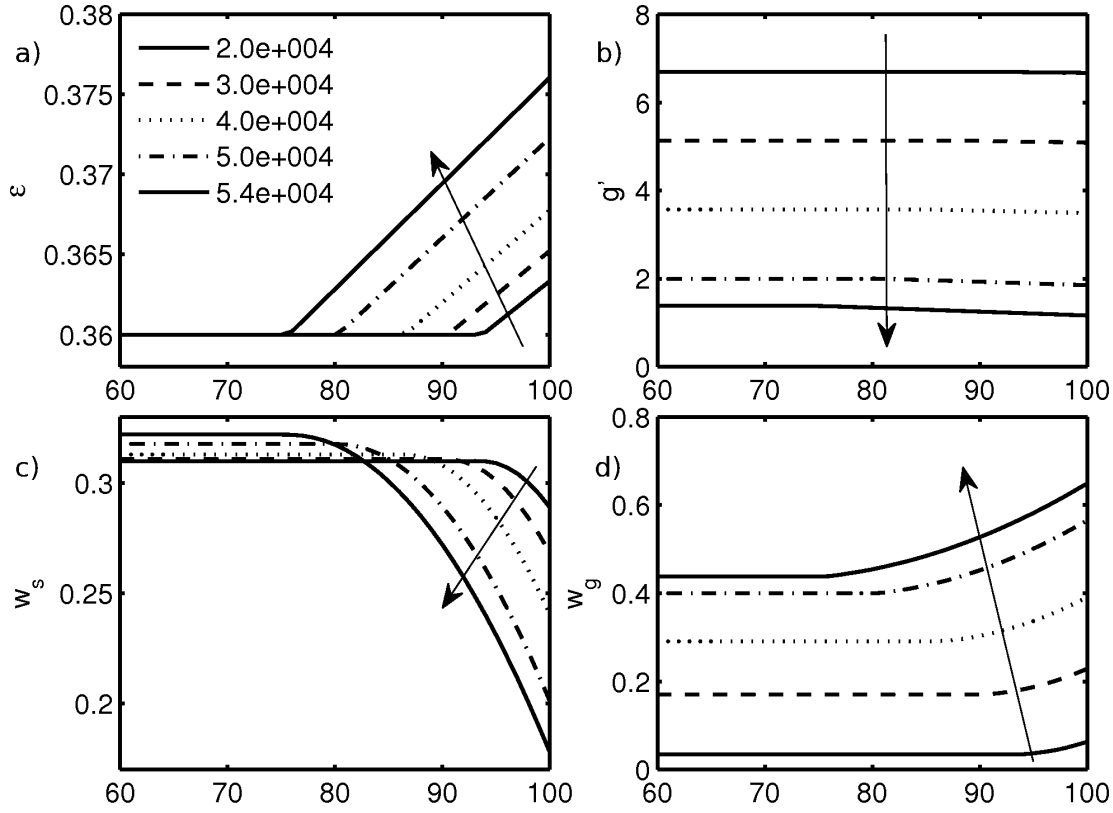

Figure 5.3: *Profiles obtained varying dimensionless pressure drop $\Delta P'$, with constant $Fr_s = 0.2$. Profiles are zoomed near the wall to better appreciate the differences. The x-axis is the transversal coordinate expressed in particle diameters, x/d_p.*

simple, both for the geometrical configuration choosen and the rheological-dilatancy laws adopted. Refinement is required, once the methodology has been proved to be succesful, the demonstration of which is the subject of the present work. In the following a procedure to analyse the results obtained by means of the model is described. Two types of analysis will be developed: a simple one based on approximated measures of the gas maldistribution, yielding global informations on the effect of gas and solid flowrate, and a more specific one regarding the shape and the variations in the full residence time distribution of the gas.

Considering the superficial velocity $\bar{V_0}$ obtained from the Ergun equation, the absolute local velocity of the gas can be expressed as:

$$w_g(x) = \frac{\bar{V_0}(x)}{\epsilon} - w_s(x) \tag{5.20}$$

There are two main control parameters, from the fluid dynamics standpoint: the pressure of the gas at the inlet and the flowrate of the solid going down the bin. The residence time of the gas and of the solid in the bin are respectively:

$$\theta_g = \frac{L}{\epsilon w_g} \qquad \theta_s = \frac{L}{(1-\epsilon)w_s} \tag{5.21}$$

which are obviously two functions of x. As an approximate measure of the skewness of the residence time distribution, and so of the amount of gas maldistribution, the dimensionless number could be choosen:

$$A = \frac{\theta_g(x=b)}{\theta_g(x=0)} \tag{5.22}$$

Due to the combined effect of enlarged porosity and slower motion of the solid, the absolute velocity of the gas is always higher near the wall than in the bulk, so it is always $A \leq 1$. If we are interested in avoiding the maldistribution, A should be operatively kept close to unity; in fact, it is preferable to use an integral criterion representing the *amount* of maldistribution, such as the bypass percentage, as defined by Vortmeyer and Schuster (1983). Being $w = \epsilon w_g / \bar{w_g}$, it can be written as:

$$\%\text{bypass} = \frac{1}{2b} \int_0^b |w-1|\, dx \cdot 100. \tag{5.23}$$

To study the effect of solid flowrate and gas pressure drop two maps have been constructed and reported in Figg. 5.4 and 5.5. Fig. 5.4 shows a contour plot of of the bypass percentage versus the already defined average Froude number Fr_s and versus $\Delta P'$, while Fig. 5.5 shows a contour plot of the bypass percentage as a function of Fr_s and Re_p^*, which is a global particle Reynolds number defined as $Re_p^* = \frac{\rho_g \bar{w}_g d_p}{\eta_g}$, where analogously to the solid $\bar{w}_g = 1/b \int_0^b \epsilon w_g dx$ represents an average velocity of the gas.

When dealing with both solid and gas flowing countercurrent, the minimum fluidization velocity is a combination of the velocity of the gas and of the solid. For high solid flowrates, almost all of the imposed pressure drop is necessary to overcome the drag induced by the descending solid, in order to have an upward gas flux; moreover, a little gas flowrate will determine a high relative velocity, possibly reaching the fluidization limit. For this reason if represented in a non-dimensional gas flowrate *vs* non-dimensional solid flowrate chart (Fig.5.4), the region under the fluidization regime can be approximated by a triangle, while in a pressure drop - solid flowrate chart (Fig. 5.5) the limit is a nearly horizontal line defining the maximum admitted pressure drop below the fluidization limit. However, not all the area of the triangle is feasible, because at high solids flowrate and relatively low gas velocity, the gas at the center of the channel reaches zero velocity with

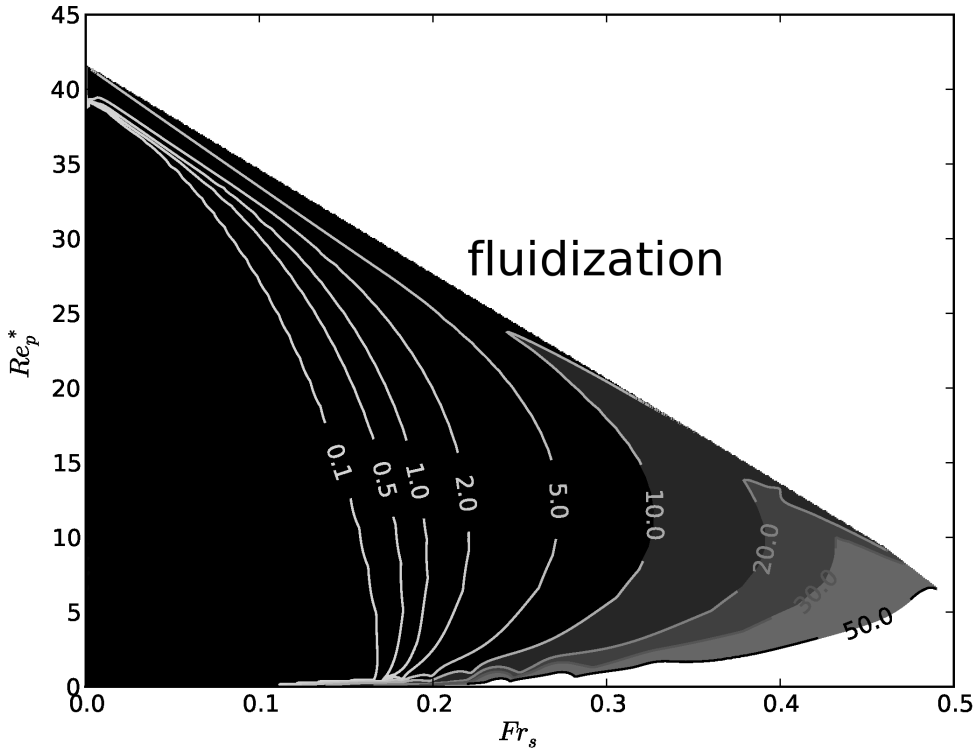

Figure 5.4: *Variation of the bypass percentage characterising the gas maldistribution with average Reynolds number of the gas and average Froude number of the bed.*

respect to the absolute reference frame.

In the pressure drop *vs* solid velocity diagram it is possible to identify also a lower curve denoting the minimum pressure drop required to force an upward gas flux (i.e. to have not zero gas velocity with respect to absolute reference frame), for each solid velocity; this curve is monotonically increasing due to the fact that, as already stated, the higher the solid flowrate, the higher the drag exerted on the gas by the descending medium, so the higher is the pressure drop is needed to overcome the drag exerted by the granular material to force an upward gas flux. This lower curve and the maximum pressure drop line intersect in one point which represents the limiting condition of zero absolute gas flow rate described above.

In this perspective, it is possible to give an estimation of the minimum pressure drop necessary to have an upward gas velocity, on the basis of the analysis developed: if the solid has sufficient drag, it will reverse the gas flow direction preferentially at the center of the bin, where the gas velocity is lower. In this zone it was assumed that $\epsilon = \epsilon_{min}$, thus the pressure drop is given by Ergun equation:

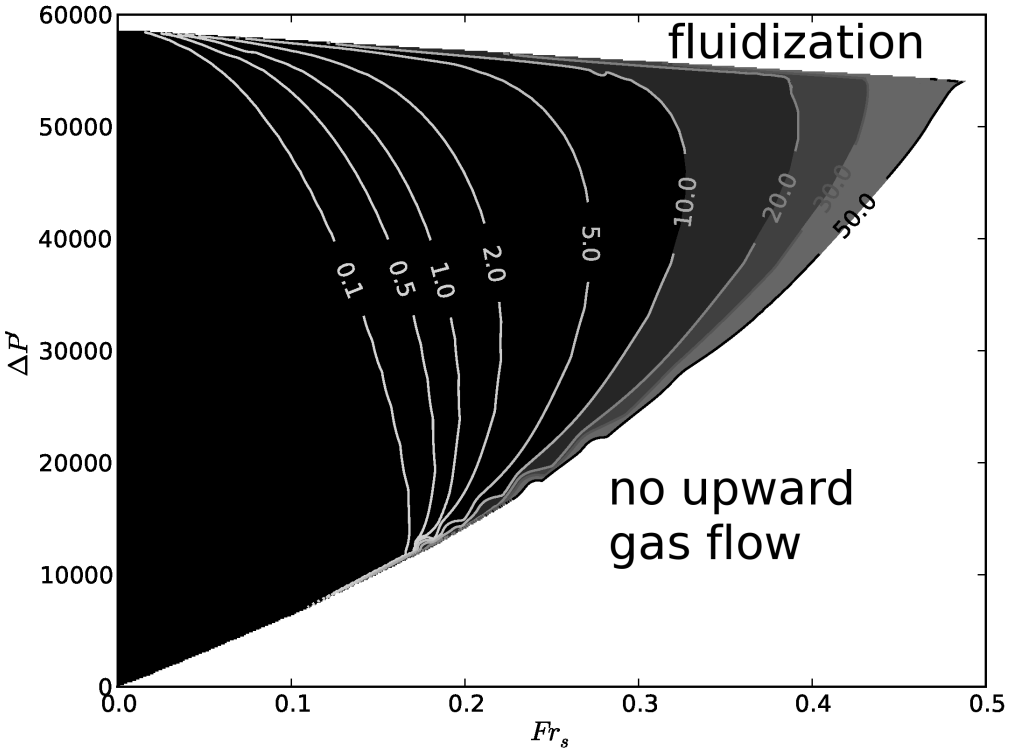

Figure 5.5: *Variation of the bypass percentage characterising the gas maldistribution with dimensionless gas-phase pressure drop and average Froude number of the bed.*

$$\frac{\Delta P_{min}}{L} = 150\frac{\epsilon_{min} w_{s0}}{d_p^2}\frac{(1-\epsilon_{min})^2}{\epsilon_{min}^3} + 1.75\frac{1-\epsilon_{min}}{\epsilon_{min}^3}\frac{\rho_g \epsilon_{min} w_{s0}}{d_p} \tag{5.24}$$

where w_{s0} is the solids velocity at the center of the channel.

Being that shear bands are the reason for gas maldistribution when the granular material is in motion, it is clear that the amount of maldistribution (as it was already partially shown, e.g. in Fig. 5.3) depends on the shear band width, and particularly on the ratio between this width and the width of the channel, b. In Fig. 5.6 the bypass percentage is plotted *vs.* the bin width - particle diameter ratio, for different values of the width-averaged particle Reynolds number. Some interesting issues can be derived from the analysis of this figure. First, increasing gas flowrate reduces the maldistribution; this was already shown for the gas flow through a static packing by Vortmeyer and Schuster (1983), which showed also that the bypass percentage decreases when increasing the channel width. This happens also in the present case, when the granular material is flowing, because the ratio shear band width - channel width predicted by the model decreases with increasing channel width. In reality, shear bands seem to have a fixed width of approximately 10-15 particle diameters, thus when the bin width increases, the ratio shear

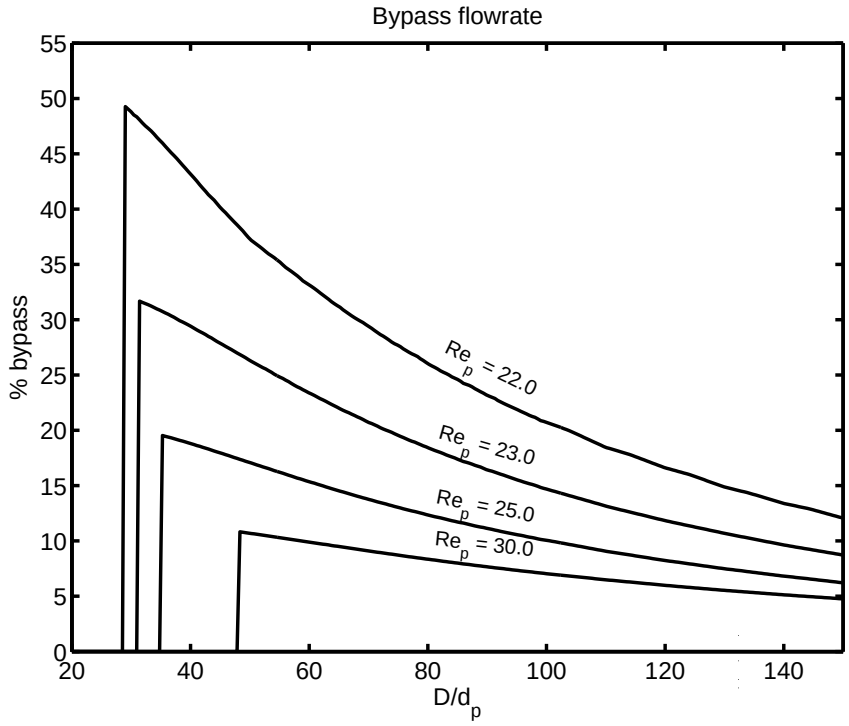

Figure 5.6: *Percentage of bypass flow versus dimensionless channel width for different values of width averaged Re_p. The solid average velocity is the same for all curves.*

band width - channel width decreases. Thus qualitatively the behavior predicted by the model is in agreement with experience. In fact the rheological model proposed by da Cruz et al. (2005) does not predict such an upper limit for the shear band width, which increase indefinitely with channel width, thus the model will be probably overestimating the bypass flowrate for very large widths. Refinements in the rheological model are needed to get quantitative predictions, however it seems that the approach is rather promising. Another extension of the approach has to be discussed having another glimpse at Fig. 5.6. For low values of the channel width, the rheological model (in agreement with experimental knowledge) predicts that no shear bands can form; in real moving beds this is due to the lack of space necessary for the particle rearrangement. Without shear bands, the material is not dilated by shear, thus the model predicts that there is no maldistribution. This is not the case of real packed bed because as said above dilation induced by shear is not the unique reason for maldistribution: it is well known that for static packings, the arrangement of particles near the walls is not perfect, inducing a static porosity profile which tends to 1 at the wall, then oscillates around from the maximum packing up to 5 particle diameters from the wall (for uniformly distributed spheres, less for not monosized ensembles)(Goodling et al., 1983; Mueller, 1992), while the deviation from the maximum packing of the porosity profile averaged over the fluctuations extends nearly for 2 particle diameters. For low values of the channel width, this phenomenon should be taken into

account, as it was done, for example, by Vortmeyer and Schuster (1983); however, the relationship between this "geometrical" dilation and the shear-induced one is not clear and should be studied experimentally, because when sheared the material cannot attain a stable geometrical configuration, thus the phenomena cannot be seen as independent. A possible improvement of the model would be the introduction of a geometrical factor of dilatancy near the walls should be added in order to account for maldistribution in absence of shear bands.

5.4 Residence time distribution of the gas

In the preceding section the development of maldistribution in gas flowing through a moving bed of granular material was analysed in terms of single measures of the maldistribution. In this section it is examined what happens to the residence time distribution of the gas in the column if the bed is moving with a velocity and porosity profile. A certain number of studies have been devoted to the subject; Paterson et al. (Paterson et al., September 2000) reported the measured RTD for fixed and frozen (i.e. carefully stopped during moving) beds of spherical particles to account for the maldistribution of the gas, seen as the deviation from the fixed column distribution. They showed that it is the presence of velocity profiles in the gas to induce a deformation in the RTD, and that increasing wall friction increases the amount of maldistribution.
In order to obtain the RTD for our model the procedure given by Paterson et al. (September 2000) is followed; it is assumed that the column operates at atmospheric pressure, and that the superficial velocity does not change significantly by moving in the axial direction. In the case of a fixed bed it is common to use a simple axial dispersion model for the passive tracer, for which the RTD was obtained byLevenspiel and Smith (December 1995) to be

$$E(t) = \frac{1}{2\theta_g}\sqrt{\frac{Pe_l}{\pi}} exp\left[-\frac{Pe_l}{4}\left(1-\frac{t}{\theta_g}\right)^2\right] \tag{5.25}$$

where Pe_l is the macroscopic Peclet number $Pe_l = \frac{w_g \epsilon L}{D_{eff}}$. In fixed beds the effective dispersion coefficient D_{eff} can be calculated from fixed bed correlations, such as the one proposed by Wen and Fan(Paterson et al., September 2000):

$$\frac{1}{Pe_p} = \frac{0.3}{ScRe_p} + \frac{0.5}{1+\frac{3.8}{ScRe_p}} \tag{5.26}$$

where $Pe_p = \frac{w_g d_p}{D_{eff}}$ is the particle Peclet number and $Sc = \frac{\eta_g}{\rho_g D}$. Being that neither gas velocity nor porosity are uniform along the transversal direction, for each x position a local RTD can be defined, $E^*(t,x)$, which is a function of local velocity and porosity.

The global RTD can be calculated by means of the flowrate weighted expression:

$$E(t) = \frac{\int_0^\infty w_g(x)\epsilon(x)E^*(t,x)dx}{\int_0^\infty \int_0^\infty w_g(x)\epsilon(x)E^*(t,x)dxdt} \tag{5.27}$$

For better comparison, curves are rescaled with the choice $t' = t/\theta_g$, $E' = \theta_g E$.

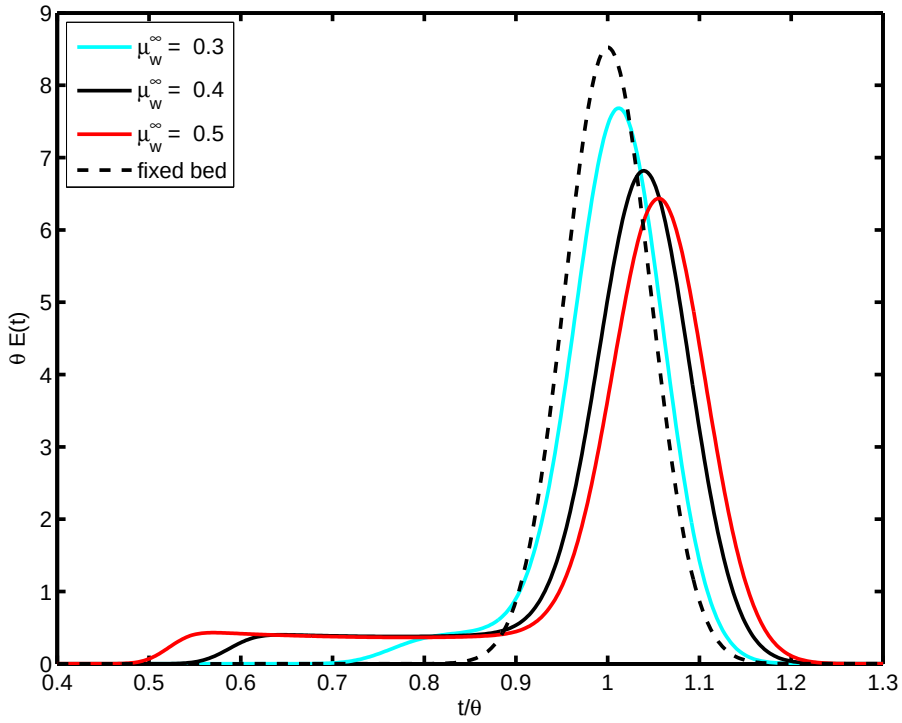

Figure 5.7: *Variation of the RTD for fixed and moving columns, for $\Delta P' = 4.0E+04$, $Fr_s = 0.2$ (in the moving case), for different values of the wall friction coefficient μ_w^∞ .*

As shown in Fig. 5.7 the present approach well predicts the shape and behavior of the RTD as reported by Paterson et al. (September 2000). In this case, increasing wall friction corresponds to increasing dilation in the shear band, thus increasing the velocity of the gas in that zone; when the wall instead is sufficiently smooth, the material slides as a block on the wall without forming shear bands, and this yields that, consistently with the experiments by Paterson et al. (September 2000), in the smooth-walls limit the RTD does not differ from the packed bed case.

To understand the effect of the velocity of the solid and the gas, which has already been represented in Figs. 5.4,5.5, the obtained RTD are represented in Figs 5.8,5.9. From fig. 5.8 it is clear that increasing solids flowrate at constant pressure drop slows down the gas, which uses a higher fraction of the total pressure drop to gain an upward flux; moreover the distribution of the gas is very bad at high flowrates, while it is similar to the fixed bed case when the solid flowrate tends to zero. On this issue, Paterson et al. (September 2000) reported a weak dependence of the RTD on the solids flow rate, in the

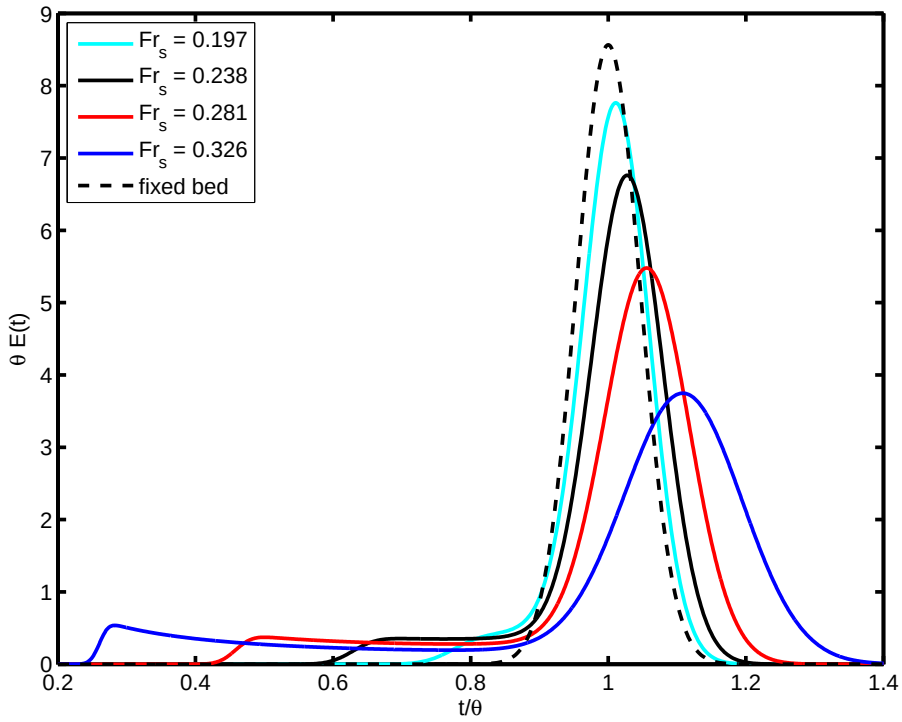

Figure 5.8: *Variation of the RTD for fixed and moving columns, for $\Delta P' = 4.0E + 04$ (in the moving case), for different values of the solids' Froude number.*

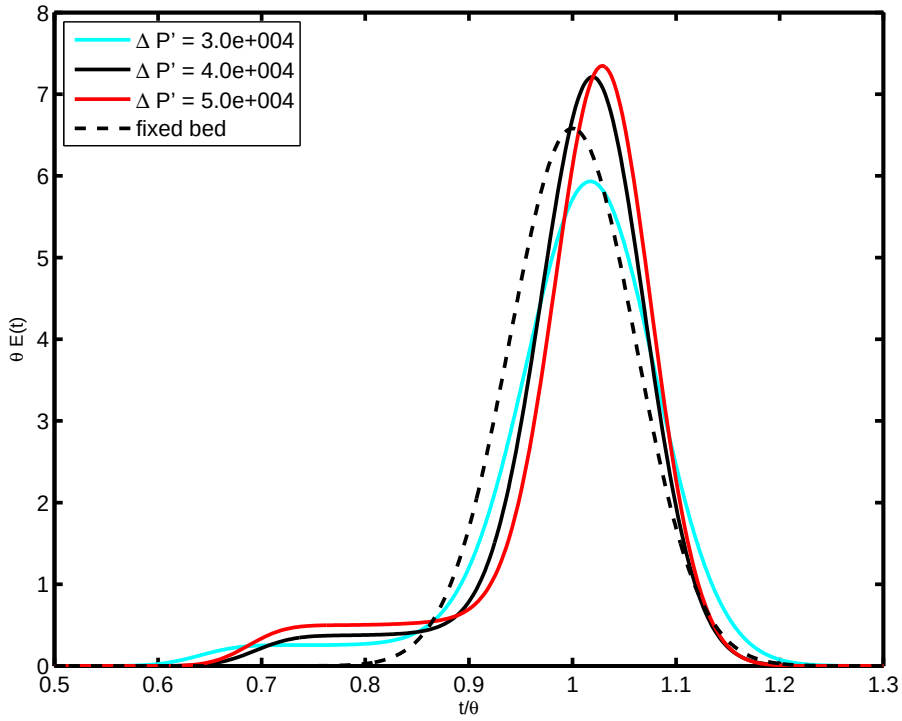

Figure 5.9: *Variation of the RTD for fixed and moving columns for $Fr_s = 0.22$ (in the moving case), for different values of the applied gas pressure drop. Fixed bed result is for the gas flowrate of the moving case with $\Delta P' = 3.0E + 04$*

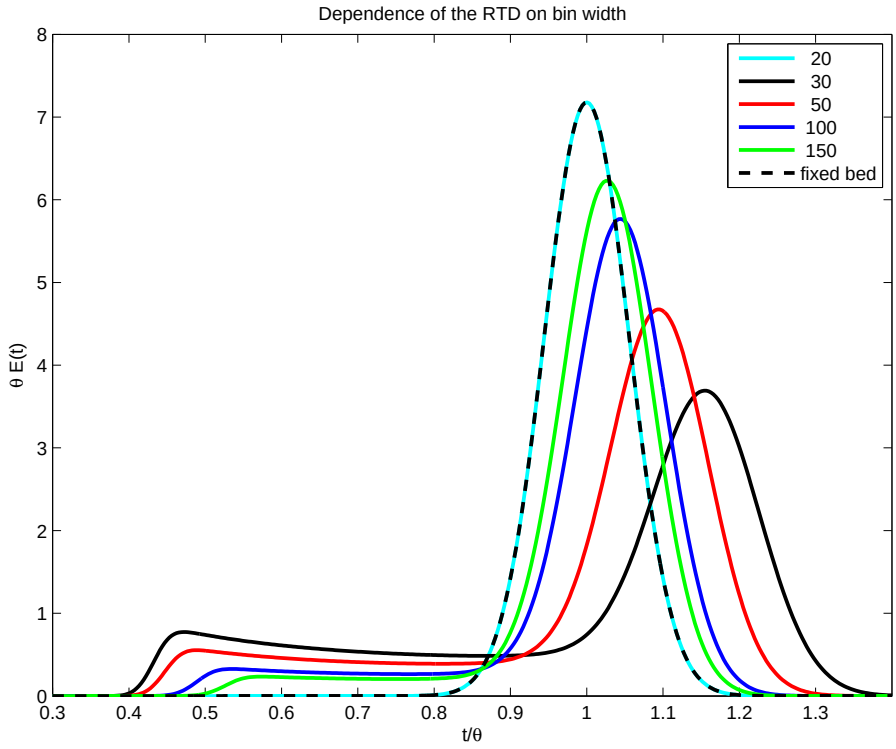

Figure 5.10: *Variation of the RTD for fixed and moving columns, for* $\Delta P' = 3.0E + 04$, $\bar{w}_s = 0.2\ ms^-1$ *(in the moving case), for different values of channel width (expressed in particle diameters).*

range of velocities they considered, which was even weaker in the presence of smooth walls. Further studies should be conducted in a wider range of solids flowrates, also changing the gas phase pressure drop. It is expected that a combination of flowrates exists where dilation strongly depends on the flowrate itself. Moreover, from hints coming from the mechanics of granular materials, we think that the technique of the frozen bed to measure properties of the moving bed is somewhat questionable, because stopping (though carefully) the material gives rise to a relaxation phenomenon which could densify the medium.

The result obtained by varying the pressure drop at constant solids flowrate is evidenced in fig. 5.9; it is clear that increasing the pressure drop has the effect of augmenting the gas velocity, thus shifting the average residence time towards zero (not shown due to rescaling of the axes). When rescaling the curves, it is evident that the pressure drop has a complex (non-monotonic) effect on the gas maldistribution, as it could be noticed on figure 5.5. In fig. 5.10 also the behavior obtained by changing the width of the channel is studied, keeping constant the average solids velocity. It is easy to see that little spacing between the walls has a behavior similar to the fixed bed one (see the curve for $b/d_p = 20$); increasing the width, an abrupt change in the behavior is obtained, with a strong maldistribution of the gas, and increasing again the behavior returns towards the fixed bed case; this limiting

behavior for great diameters is well known, for example in the drying literature(Lacerda et al., 2005; Lira et al., 2007). It is not difficult to explain the behavior obtained for little spacings, which is due to the disappearance of shear bands in this limit; it is well known from experience that for narrow separated walls no shear band can form(Jop et al., 2005) but the material can slide down as a block or alternatively stop due to the formation of arches. This dependence on the maldistribution on the ratio b/d_p is the same which was evidenced about Fig. 5.6.

5.5 Conclusions & Perspectives

In summary, in this chapter an approach to model the problem of countercurrent gas-solid flow in vertical pipes was developed. The approach consists in the explicit computation of the coupling between the flowing gas and solid, including the phenomenology that (a) the presence of shear in the granular material induces porosity profile that change the flow pattern in the gas, and that (b) the gas phase pressure drop has the effect of lowering the effective gravity force acting on the solid.

Using the simplest approach containing the phenomenology, combining Darcy's model for the gas phase and a simple rheology (taken from the work of da Cruz et al. (2005)) for the solids, the development of gas flow maldistribution was studied theoretically, both globally (by means of lumped measures of the maldistribution) and specifically (using the theoretical RTD of the gas in the system). Qualitative comparison with Literature data by Paterson et al. (September 2000) for RTD in frozen beds (i.e. carefully stopped moving beds) was made, where good agreement was found. Future developments will deal, from the modeling point of view, with more complex treatment of the two phases: for the fluid phase, it would be important to relax the hypothesis of inviscid flow, to extend the applicability of the approach to liquids and to account explicitly for friction induced by the wall on the fluid. As regards the granular medium, more complex rheologies should be used which apply more specifically to confined flow situations, such as the one developed in Chapter 3. This will be partly addressed also in comparison with experimental data of pressure and solids flow patterns in Chapter 6. Moreover, the results presented here, and the future ones, should be compared with experimental data addressing specifically the maldistribution. It should be stressed that the technique of the frozen bed(Paterson et al., September 2000), even if very clever, can be somewhat critic, because even if carefully stopped, the material undergoes a relaxation; future experimental efforts should deal with the attempt to overcome this technique and study real moving bed configuration.

Finally, future efforts should deal with the coupling of the momentum transport phenomena described here with heat and mass transport phenomena which actually occur in

moving-bed-like industrial configurations.

Chapter 6

Pilot scale silo experiments

O God, I could be bounded in a nut shell and count myself a king of infinite space, were it not that I have bad dreams.

Shakespeare, *Hamlet.*

6.1 Introduction

Granular materials are handled commonly by means of a large number of industrial chemical and related processes. Applications span from operations expected to be elementary, like transport or discharge from storage silos, to more complex ones like moving beds, rotating ovens, mills, granulators, mixers, etc. As it was already noticed in previous chapters, difficulties in predicting the flow of such material surprisingly persist, despite quite a large amount of theoretical and semi-empirical studies. Thus, besides working on refined rheological models which have to represent the flow behavior in the largest variety of configurations, it appears to be useful also to perform experiments on pilot plants of reduced dimensions(Johanson, 1972). It is therefore fundamental to develop scaling principles in order to correctly design small scale testing facilites which represent in some way the behavior of the corresponding industrial scale objects. This chapter deals with experiments on small scale silos for countercurrent gas-solid flow. Part of the research contained in this chapter was motivated by interaction with an industrial partner (Centro Ricerche Danieli), focused on the understanding the flow behavior of both the solids and the gas in an industrial, metallurgical set-up. First, scaling rules were studied at the University of Padova in order to give reasonable hints for properly rescaling design variables, material properties and flow, operating variables (gas and solids flowrates) to set-up a

model silo. This is described in the first section of the chapter. Next sections describe experiments carried out on the pilot facility, which was built by CRD. Experiments required spaces and skills which obliged to perform them at CRD; while general features (sizing, choice of the measurement techniques,...) have been the subject of a joint work, the practical experimental campaign was carried out by Alberto Zugliano and Alessandra Primavera at CRD. In the following sections data obtained from the experiments are analysed and compared with the results from the rheological model described in Chapter 3, both regarding stress and flow fields, with godd agreement between them. The description of the experimental results compared with modeling predictions is the subject of a joint paper submitted to *Chemical Engineering Science*.

6.2 On the scale-up of silos for granular-gas flow applications

This section deals with applications of various concepts recently (or less recently) developed to the scaling of silos. Once a small scale pilot silo has been constructed, results from this configuration can be used as test cases for flow models, but also (and directly) provide important information for the larger-scale plant. Hereafter, at first the procedure is developed for granular flow alone, then countercurrent gas flow is introduced; finally, the design procedure is resumed with a simple example of a moving bed reactor. Needless to say, the technique proposed for the scale-up is a first attempt which should be refined with specific experimental studies.

6.2.1 Non-Aerated Granular Flow

Geometrical similarity.

The need of feasibly performing experiments on a pilot silo requires small dimensions. This is obviously embedded in the notion of small scale pilot facility, but it is important to stress that in the case of granular flow this is mainly due to (1) need for less granular material to treat, so lower power consumption in bulk solids handling, (2) low weight of the structure (with respect to huge industrial buildings), (3) possibility of operating at atmospheric pressure, while larger structures (due to the large pressure drops, and for the peculiar operations being held) can need high pressure equipment. In this paper design procedures are developed for dry cohesionless granular materials.

Before describing the concept of geometrical similarity, it is clear that a lower limit for the small scal silo is given by the width of the bottom hole, which must be large enough to allow continuous flow. This means that, according to practice, the bottom hole shall be

larger than 10 particle diameters. From this sentence it starts to be clear that the scaling involves choice of the particle diameter, which is therefore an independent quantity. Starting from the analysis of a simplified configuration, the fully developed gravity driven flow in a channel, it is clear from many experimental and theoretical efforts(Natarajan et al., 1995; Nedderman and Laohakul, 1980; Pouliquen and Gutfraind, 1996; G. D. R. Midi, 2004), that characteristic lengthscales of flow profiles (such as shear bands in silos) depend linearly on the particle diameter, thus, in order to have comparable flow profiles rescaling from the full scale to the small scale, that is:

$$\left.\frac{\Delta_{sb}}{D}\right|_{ls} = \left.\frac{\Delta_{sb}}{D}\right|_{ss} \Rightarrow \left.\frac{d_p}{D}\right|_{ls} = \left.\frac{d_p}{D}\right|_{ss} \tag{6.1}$$

where ls and ss stand for large and small scale, Δ_{sb} is the dimension of typical shear bands in silos, d_p the particle diameter, D the silo diameter. Equation 6.1 means that, in order to reproduce comparable flow profiles, particle diameter and the diameter of the cylindrical section of the silo cannot be choosen independently. This limits our freedom to choosing the couple $(D, d_p)_{ss}$, which is further limited by the following issues:

1. D is limited by feasibility of operations: large D requires strong resources for handling, small D can become problematic for gas injection, for example when typical dimensions of injectors are comparable with silo width.

2. d_p is lower-limited by the size at which cohesion becomes important (so a different phenomenon is intoduced which is not present in the large scale), so typically it shall be $d_p > 100\mu m$. On the other side this sets up a lower limit for the silo width, which can not be too small.

Scaling all the dimensions of the silo with the particle diameter results also in maintaining the same condition of flow a the outlet, which is determined by the ratio “hole width/particle diameter”. From the given discussion, it is clear that the exact material that is processed in the industrial set up cannot be used in the small scale plant, at least regarding particle size. Other material properties which must be taken into account are angle of internal friction, angle of wall friction and bulk density. As regards the angle of internal friction, it is reasonable to assume that

$$\delta_{int}|_{ss} = \delta_{int}|_{ls}\,, \text{ or } \mu_{int}|_{ss} = \mu_{int}|_{ls} \tag{6.2}$$

where $\mu_{int} = \tan(\delta_{int})$ is the coefficient of internal friction. So though being different in size it shall be preferable that the internal friction character of the materials was the same. As regards the angle of wall friction and particle mass density, they will be discussed in the following, with respect to their effect on the dynamics of the medium.

Dynamic similarity

Once the dimensions of the model silo have been defined, and the size of the particles has been fixed, the granular material has to be choosen, and the discharging velocity of the material needs to be properly rescaled. As it was already said in previous chapters, in the cylindrical section of the silo, which will be taken as a reference in the following, the velocity profile is typically a plug flow at the center with shear bands near the walls(Nedderman and Laohakul, 1980; Natarajan et al., 1995; Pouliquen and Gutfraind, 1996). Linearizing the velocity profile, in the shear band the average shear rate is given by (out of the shear band the shear rate is zero):

$$\dot{\gamma} = \frac{u_{max} - u_{slip}}{\Delta_{sb}} \tag{6.3}$$

Considering that the slip velocity is a fraction of the maximum velocity $u_{slip} = \alpha u_{max}$, the average shear rate is

$$\dot{\gamma} = (1 - \alpha)\frac{u_{max}}{\Delta_{sb}} \tag{6.4}$$

Average normal stresses, considering at the moment $\sigma_{zz} = \sigma_{rr}$, correspond in the shear band to the value

$$p = \frac{\rho_s(1 - \epsilon)gD}{\mu_w} \tag{6.5}$$

where μ_w is the wall friction coefficient, ϵ the average porosity in the band. It is reasonable to assume that the average porosity outside the band corresponds to a close packing value, ϵ_{min}. In the shear band, the porosity can be assumed to depend on the inertial number I, which was defined as:

$$I = \frac{\dot{\gamma} d_p}{\sqrt{p/(\rho_s(1 - \epsilon))}} \tag{6.6}$$

Several studies pertaining to the physics literature(da Cruz et al., 2005; G. D. R. Midi, 2004) showed how such a dependence can be approximated by a linear dilatancy law:

$$\epsilon = \epsilon_{min} + const. \times I \tag{6.7}$$

Having linearized the velocity profile, the inertial number in the shear band becomes:

$$I = (1 - \alpha)u_{max}\frac{d_p}{\Delta_{sb}}\sqrt{\frac{\mu_w}{gD}} \tag{6.8}$$

In order to keep dynamic similarity between the small and the large scale, it is reasonable to assume that the same flowing regime has to be assured in the two geometries. The inertial number determines the relative importance of inertial and rearranging phenomena, and so in the shear band it should be kept equal. Taking into account the fact that shear band width is nearly independent on flowrate, and depends mainly on the particle

diameter, it is reasonable to assume $d_p/\Delta_{sb} \approx const. \approx 1/10$. With this in mind, in order to keep dynamic similarity in the shear band, the maximum velocity of the grains (and so the solid flowrate) shall be rescaled in order to have

$$(1-\alpha)u_{max}\sqrt{\frac{\mu_w}{D}} = const. \tag{6.9}$$

It can be assumed that (see also Chapter 7 for numerical data) the parameter α depends mainly on wall friction. In general, the wall friction coefficient can be fixed separately, and the flowrate has to be decided according to Eq. 6.9, where however the dependence of α on μ_w is not clearly defined. So, it is reasonable to choose the couple of materials constituing particles and walls respecting the relationship:

$$\delta_w|_{ss} = \delta_w|_{ls}\,, \text{ or } \mu_w|_{ss} = \mu_w|_{ls} \tag{6.10}$$

If the materials were choosen in order to equal wall friction coefficients, rescaling followed the law

$$u_{ss} = u_{ls}\sqrt{\frac{D_{ss}}{D_{ls}}} \tag{6.11}$$

which corresponds to keeping constant the Froude number in the silo (and in fact the inertial number, in this configuration, is strictly related to the Froude number, adding to the description the effect of friction). If the solids velocity was scaled with Eq. 6.11 the residence time in the geometry scaled as $\frac{1}{\sqrt{D}}$, which means that the material spent more time in the small scale than in the full scale silo. Slower motion is needed to keep the inertial number the same because compressive forces are lower in smaller silos.

Therefore, from the hints developed in the previous discussion, material properties, geometrical features and process parameters have been imposed in order to preserve similarity. One quantity which was not determined is the particle density. In fact, it is clear from the dimensional analysis involving the inertial number I that the intrinsic density of the material has no effect on the scaling (but must be taken into account in calculating mass flowrate). In the next section, studying the effect of gas flow, it will be shown that the injection of fluid imposes additional restrictions. Before quitting this section, it has to be noted that previous scaling rules developed by Johanson (1972) yielded a different scaling for the solids flowrate which is rather different from the one developed here. Johanson developed his rules considering the acceleration of the particles at the outlet, while the development in this work is based on the problem of the existence of velocity profiles in the cylindrical section of the silo.

6.2.2 Aerated flow

In this section the previously developed scaling procedure will be extended in order to include countercurrent gas flow. The focus is always on dense flows, which means that

only flows below the fluidization threshold will be considered, above which other scaling considerations apply(Kunii and Levenspiel, 1969).

Granular rheology

When considering countercurrent gas-solids flow, the rheological equations for the solids are the same than in non-aerated flow, with the exception that drag forces from the gas to the solids must be taken into account (as it was discussed in Chapter 5). Eq. 6.8 must be modified introducing an effective gravity which considers fluid drag:

$$g' = g - \frac{\Delta P}{\rho L} \tag{6.12}$$

where the density is $\rho \approx \rho_s(1-\epsilon)$ and $\Delta P/L$ is the applied pressure drop. In order to preserve constance of the inertial number between different scales, some constraint has to be imposed on the applied pressure drop. In fact, reconsidering Eq. 6.9 with the inclusion of the effective gravity, assuming similar frictional characteristics of the materials, yields:

$$u\sqrt{\frac{1}{g'D}} = const. \tag{6.13}$$

Therefore if the effective gravity is different between different scales, the solids flowrate must be scaled accounting for this issue.

6.2.3 Global scaling

As a dynamical similarity principle, the most reasonable choice is to preserve the ratio of weight forces to drag forces. From the solids velocity point of view, this implies keeping the effective gravity, Eq. 6.12, the same from one scale to another, and so scaling the velocity of the solids with Eq.6.9 instead of 6.13. Obviously when dealing with a granular bed one cannot consider the forces acting on each particle as if it was isolated, but is obliged to consider force balances for the entire bed. Following the above mentioned criterion, the dimensionless number which must be conserved is the ratio between weight and drag forces, that is :

$$\chi = \frac{\Delta P}{L(\rho_s - \rho_g)g(1-\epsilon)} \tag{6.14}$$

This means that to keep the same ratio χ, apart from the pressure drop, one can tune also solids and gas density (the first having the greatest effect, being that for gases $\rho_g << \rho_s$). The information contained in χ can be transferred to a scaling law for gas flowrate by means of Ergun equation (which was already introduced):

$$\frac{\Delta P}{L}\frac{\rho_g d_p^3}{\eta_g} = 150\mathrm{Re}_p\frac{(1-\epsilon)^2}{\epsilon^3} + 1.75\mathrm{Re}_p^2\frac{(1-\epsilon)}{\epsilon^3} \tag{6.15}$$

When using dimensionless number χ as a guidance to scale gas flowrate, it is sure that the small scale is below the fluidization threshold as the full scale is. It has to be remembered that the scaling procedure is developed for non fluidized flows (incipient fluidization corresponds to $\chi = 1$). It can be shown that depending on the gas flow regime (viscous or inertial), conservation of χ implies different scalings for the gas flowrate.
Indeed, in the viscous limit, Ergun equation can be approximated as:

$$\frac{\Delta P}{L}\frac{\rho_g d_p^3}{\eta_g} = 150\mathrm{Re}_p\frac{(1-\epsilon)^2}{\epsilon^3} \tag{6.16}$$

from which it folllows that

$$Re_p = \frac{\chi}{150}(\rho_s - \rho_g)g\frac{\rho_g d_p^3}{\eta_g^2}\frac{\epsilon^3}{(1-\epsilon)} \tag{6.17}$$

which becomes, expliciting gas velocity:

$$u_g - u_s = \frac{\chi}{150}(\rho_s - \rho_g)g\frac{d_p^2}{\eta_g}\frac{\epsilon^2}{(1-\epsilon)} \tag{6.18}$$

Therefore, the final scaling of gas velocity is not simple because of the presence of the solids velocity which scales as $\sqrt{D}$. If the solids velocity is negligible with respect to the gas velocity, it appears that (considering that solids flowrate was scaled with Eq. 6.9, thus implying same porosities):

$$u_g \sim (\rho_s - \rho_g)\frac{d_p^2}{\eta_g} \tag{6.19}$$

On the other hand, in the inertial regime, Ergun equation reduces to:

$$\frac{\Delta P}{L}\frac{\rho_g d_p^3}{\eta_g} = 1.75\mathrm{Re}_p^2\frac{(1-\epsilon)}{\epsilon^3} \tag{6.20}$$

from which the particle Reynolds number can be obtained and so the relative velocity of the gas and the solids:

$$(u_g - u_s)^2 = \frac{\chi}{1.75}\frac{\rho_s - \rho_g}{\rho_g}g\epsilon d_p \tag{6.21}$$

From which the scaling of gas velocity on particle diameter (or, more generally, on a characteristic length, according to Eq.6.1) can be verified to be:

$$u_g \sim \sqrt{d_p} \tag{6.22}$$

Therefore, if scaling gas flowrate is made following Eq. 6.19 or 6.22, it has to be considered that the scaling law for flowrate depends on the flow regime of the gas. The better choice would be calculating gas flowrate from scaling based on χ, rather than using Eq. 6.19 or 6.22. For the same reason, another simple scaling law based on the dimensionless number $\frac{u_g}{u_{mf}}$, where u_{mf} is the minimum fluidization velocity, is correct only if the same

regime pertains to the fluidization and to the operating velocity both in the full and the model scale. This is not obvious because reducing particle size, also the Reynolds number at minimum fluidization is reduced. Indeed, the minimum fluidization threshold was defined through different correlations(Kunii and Levenspiel, 1969; Zenz, 1997; Richardson et al., 2002). An example is the correlation(Basu, 2006) (Basu,, 2006)

$$Re_{mf} = \frac{du_{mf}\rho_g}{\mu} = \sqrt{C_1^2 + C_2 Ar} - C_1 \tag{6.23}$$

where the constants take values $C_1 = 27.2$ and $C_2 = 0.0408$, and Ar is the Archimedes number:

$$Ar = \frac{\rho_g(\rho_s - \rho_g)gd^3}{\mu^2} \tag{6.24}$$

Eq. 6.23 is directly derived from Ergun equation, made dimensionless. It shows clearly that particle Reynolds number at minimum fluidization depends on particle diameter with a $3/2$ power, therefore if the size is reduced, one can pass from a configuration dominated by inertial contributions to pressure drop to one dominated by the viscous part of Ergun equation.

The results obtained here means that once the geometrical configuration is fixed, gas flowrate is fixed too once the materials are choosen. Therefore playing on the different ρ_s/ρ_g between the small and the large scale gives another degree of freedom. For example, a solid material with a different density can be used for particular reasons, implying a different gas flowrate to be injected to preserve the ratio between weight of the material and drag forces.

Local fluidization

Even if the global fluidization behavior allows to scale properly the gas flowrate, it could be that locally the behavior in the large and small scale differ, if *e.g* near the injectors the material is near the fluidization threshold. Therefore also the scaling

$$u_{ss}^{g,in} = u_{ls}^{g,in}\frac{u_{g\ ss}}{u_{g\ ls}} \tag{6.25}$$

should be considered (where $u^{g,in}$ is the gas velocity at the injectors); this means that the shape and the number of injectors should be designed, if possible, to reproduce the same situation in the large scale and in the small scale plant. If gas drag is sufficient to induce local fluidization (which probably will not occur due to the weight of the material), a criteria to determine the qualitative state of the system could be using the criterion for bubbling fluidization by Wilhelm and Kwaku (1948) based on gas Froude number $Fr_{mf}^{g} = \frac{u_{mf}^{g}}{d_p g}$.

Gas maldistribution

Building a small scale version of an industrial silo for countercurrent gas-flow applications might be useful for the purpose of understanding from the empirical point of view the amount of gas maldistribution and its dependence on process parameters. Due to the fact that developing techniques for avoiding maldistribution is a reason for which downscaled versions of moving bed reactors are built, it has to discussed whether or not the simple scaling relationship for the gas flowrate to be used is valid also for systems in which gas is maldistributed. As it was discussed in Chapter 5, maldistribution of the gas is often related to channeling effects near the walls, which appear when the medium has locally a higher porosity, which mainly due to two contributions: (1) a geometrical reason (which appears in moving bed as well as in static packings), which obliges particles next to a wall to be more dilated due to the ordering induced by the wall, and (2) a rheological reason, related to the dilatancy behavior of granular flows, which need to dilate in order to be sheared (so this occurs mainly near the walls). In moving beds, the second mechanism is probably the most important, and can be assessed by means of rheological and dilatancy rules as it was done in Chapter 5.

The relationships used above were developed with the assumption of perfect distribution of the gas; let's see what happens when gas flow maldistribution is accounted for in a simple manner. Assuming a linearized velocity profile in the solids, the material can be divided in two zones, one with porosity $\epsilon_1 = \epsilon_{min}$ in the center, one with porosity given by eqs. 6.7 and 6.8:

$$\epsilon_2 = \epsilon_{min} + \beta(1-\alpha)u_{max}\frac{d_p}{\Delta_{sb}}\sqrt{\frac{\mu_w}{gD}} \tag{6.26}$$

where β is the constant involved in Eq. 6.7. Being that the pressure drop is uniform in the radial direction, two zones with different particle Reynolds number appear, each one given by the solution of the equation

$$\frac{\Delta P \rho_g d_p^3}{L\eta_g^2} = 150 Re_p \frac{(1-\epsilon)^2}{\epsilon^3} + 1.75\frac{1-\epsilon}{\epsilon^3}Re_p^2 \tag{6.27}$$

where the particle Reynolds number is given by $Re_p = \frac{\rho_g \bar{V_0} d_p}{\eta_g}$, where $\bar{V_0} = \epsilon(w_g - w_s)$ is the superficial relative velocity of the gas. Let's assume that the solids flowrate is rescaled according to Eq. 6.9 or 6.11: then the inertial number profile is conserved between the different scales, so also the porosity profile is the same. If conservation of the same ratio between weight and drag forces through the χ number is used for scale-up (which allows to change $\Delta P/L$ and ρ_s), as suggested previously, the particle Reynolds number profile will not be in principle preserved. Typically, it could be that for low particle diameters ($d_p \sim 1mm$), $Re_p < 100$, while for particles of centimeter size $Re_p > 1000$. More-

over, if two different regimes of gas flow characterized the model and the full scale silos, not only the Reynolds number profiles were different, but , also, the profiles were not autosimilar. On the other hand, if $\frac{\Delta P \rho_g d_p^3}{L\eta_g^2}$ was kept the same between the scales, then the particle Reynolds number profile was the same between the scales. In fact, $\frac{\Delta P \rho_g d_p^3}{L\eta_g^2}$ cannot be easily kept constant between the scales because the pressure drop is limited by $\frac{\Delta P}{L} < (\rho_s - \rho_g)g(1-\epsilon)$, therefore it will be easily that decreasing the particle diameter following equation 6.1, trying to increase $\Delta P/L$ to preserve the dimensionless number $\frac{\Delta P \rho_g d_p^3}{L\eta_g^2}$ will bring the material to a fluidized state in the model silo. Thus a criterion based on the previously introduced dimensionless numbers is not directly useful for studying gas maldistribution. In fact, in order to have a similar distribution of the gas in the full and the model scale, if one considers an average maldistribution measure such as the bypass percentage as defined by Vortmeyer and Schuster (1983), it is sufficient that the velocity profile of the gas is similar between the scales (this means that $v_g^{ls}(x)/v_g^{ss}(x) = \text{const.}$). This is possible, from Ergun equation, only if the same scaling of Re_p on porosity belongs to the two configurations; this means that gas flow in the model and the full scale silo should pertain to the same (inertial or viscous) regime. When resizing, if design considerations lead the pilot facility in a different flow regime (as it is likely to happen due to particle size reduction), this effect must be taken into account: the amount of maldistribution in the pilot facility will be in principle different than in the full scale plant, and this, together with the great difference in the particle Reynolds number could become a problem, particularly when dealing with experiments involving also mass transfer and reactive problems. Therefore these scaling procedures are limited probably to the study of solids and fluid dynamics issues. However other scaling procedures neglecting the existence of porosity profiles in the solid or not implying scaling the particle diameter may also rise issues about maldistribution related to geometrical reasons. For these reasons, when its implications are kept in mind, it seems that dynamic similarity remains a sufficiently reasonable criterion for scaling.

6.2.4 Example. Cylindrical moving bed reactor

As an example let's consider a cylindrical geometry, whose parameters, together with the material ones, are reported in Table 6.1. This example describes a moving bed reactor which is a channel with a diameter of 2 m in which granules with a mean particel diameter of 2 cm are characterised by a relatively high velocity and the gas too has a strong drag on the particles (though being below the fluidization threshold). On the other hand, a relatively high frictional wall is assumed, for which the coefficient α is supposed to be low. When trying to rescale such a geometry, the procedure can be divided in the subsequent

D (diam.)	$[m]$	2
Δ_{sb}	$[m]$	0.2
$\Delta P/L$	$[Pa/m]$	5.00E+003
ρ_s	$[kg/m3]$	1.00E+003
ρ_g	$[kg/m3]$	1
η_g	$[Pa \cdot s]$	1.85E-005
d_p	$[m]$	2.00E-002
v_s (mean)	$[m/s]$	0.1
μ_w	$[-]$	0.6
α	$[-]$	0.1
β	$[-]$	1.00E+000

Table 6.1: *Data for an arbitrary full scale geometry.*

steps:

- a goood choice for the couple channel-particle diameter is defined as $d_p = 1$ mm and $D = 10cm$. A lower size would imply problems both in handling solids and in performing measurements on the pilot plant. All the other dimensions are rescaled keeping constant the ratio d_p/L.

- in this case, a material with the same density and wall coefficient of friction is used for simplicity

- the solids flowrate is rescaled according to Eq. 6.13, and being that the scaling of the gas pressure drop will be made using number χ, the same effective gravity will act in the model and the full scale. Resulting solids velocity is reported in Table 6.2. It can be verified that the scaling implies the same inertial number and porosity in the shear band.

- the gas pressure drop is rescaled by keeping constant χ. Having choosen (arbitrarily) to keep the same material density, this results in keeping constant the pressure drop. From the profile of χ, it can be seen how the material is (not too much) below the fluidization threshold. The resulting approximate maldistribution is in general low ($\sim 1\%$), and it is higher in the model than in the full scale system.

This can be more appreciated if a larger dilation is supposed (a 10 $\%$), as reported in Table 6.3. Generally the model seems to behave worse as regards maldistribution. In both cases maldistribution is not negligible, and in the model it is approximately doubled. The reason for this is that the gas flow is in the viscous regime in the model and in the inertial regime in the full scale. If the same regime should be obtained (e.g. for reactive or heat/mass transfer reasons), then probably the scaling of particle diameter

	full scale		model scale	
D $[m]$	2		0.1	
d_p $[m]$	2.00E-02		1.00E-03	
ρ_s $[kg/m3]$	1.00E+03		1.00E+03	
ρ_g $[kg/m3]$	1		1	
η_g $[Pa \cdot s]$	1.85E-05		1.85E-05	
$\Delta P/L$ $[Pa/m]$	5.00E+03		5.00E+03	
β $[-]$	1		1	
μ_w $[-]$	0.6		0.6	
α $[-]$	1		1	
	bulk	shear band	bulk	shear band
Zone width $[m]$	0.8	0.2	0.04	0.01
ϵ $[-]$	0.36	0.365	0.36	0.365
χ $[-]$	7.97E-001	8.50E-001	7.97E-001	8.50E-001
Re_p $[-]$	2723.07	2802.02	9.99	10.51
v_g (int) $[m/s]$	6.98	7.08	0.51	0.53
v_g (sup) $[m/s]$	2.51	2.58	0.18	0.19
v_s $[m/s]$	0.1		0.02	
I $[-]$	4.93E-03		4.93E-03	
v_g (sup) ave. $[m/s]$	2.54		0.19	
% bypass $[-]$	0.66		1.18	

Table 6.2: *Results from the rescaling procedure for the cylindrical moving bed.*

	full scale		model scale	
	bulk	shear band	bulk	shear band
Zone width $[m]$	0.8	0.2	0.04	0.01
ϵ $[-]$	0.36	0.4	0.36	0.4
χ $[-]$	7.97E-001	8.50E-001	7.97E-001	8.50E-001
Re_p $[-]$	2723.07	3412.45	9.99	14.84
v_g (int) $[m/s]$	6.98	7.87	0.51	0.68
v_g (sup) $[m/s]$	2.51	3.15	0.18	0.27
v_g (sup) ave. $[m/s]$	2.74		0.22	
% bypass $[-]$	5.35		9.52	

Table 6.3: *Effect of rescaling on gas flow behavior, for a highest value of dilation (*10%*).*

should be relaxed (implying coarser particles), but the effect of such a choice on the flow of granules and on maldistribution (e.g. emergence of geometrical maldistribution) should be considered.

6.3 Experimental methods

Based on the scaling laws described in Section 6.2, a pilot facility was built at CRD to perform experiments on wall stresses and flow profiles, in order to gather information on the full scale flow configuration, and to test and validate the model presented in Chapter 3 . The silo (shown in Fig. 6.1) was almost 2.5 meters tall and had a variable diameter (a cylindrical zone at the top, an enlarging zone in the middle, a convergent part at the bottom) that in the upper part spanned from ~ 0.4 m to ~ 0.5 m. Such facility had also the possibility to include internal devices (tubes passing side-to-side in the pilot plant) and air flowing upwards. Internal devices such those used in this work are installed in industrial plants (1) to try to induce mixing of the descending bulk solids and (2) to reduce peak stresses at the junction between the cylindrical and the convergent part of the silo(Johanson, 1968). Some published studies can be found on the use of similar devices and on their effect on the flow and stress fields(Tüzün and Nedderman, 1985a,b).
The main granular material was steel grit while the tracer was zinc grit both with a mean particle diameter of $825\mu m$. The material properties are reported in Table 6.4. Zinc grit was chosen as tracer for four reasons: 1) it was available in the same size as the steel grit; 2) it has physical properties comparable to those of steel grit in terms of particle density and wall friction angle (see Table 6.4); 3) it has a color clearly contrasting with that of steel and 4) it has not magnetic properties, differently from steel. The last property was important in order to separate zinc from steel grit, and so to reuse the two materials in subsequent runs.

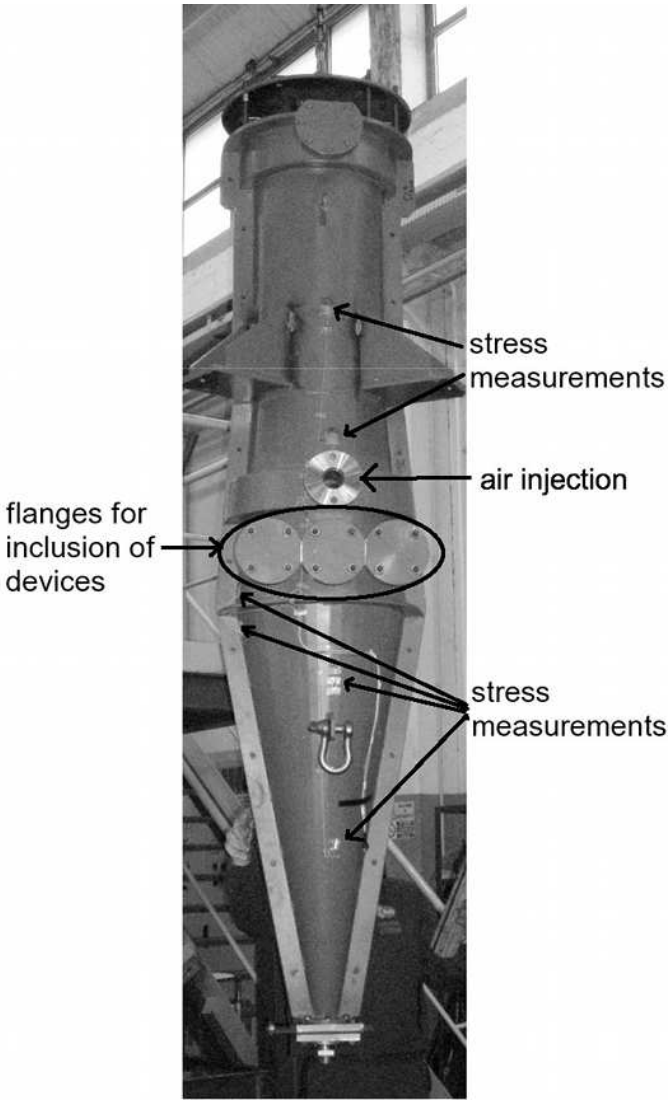

Figure 6.1: *Picture of the pilot silo with description of the main features.*

	Steel grit	Zinc grit	
d_p	0.825	0.825	mm
ρ	7800	7100	$kg\ m^{-3}$
δ	25.29	35.22	$^\circ$
δ^w	17.75	16.41	$^\circ$

Table 6.4: *Properties of the materials used in the experiments.*

As attention was focused on flow and stress profiles, the experimental set-up was arranged in order to measure both of these quantities in the pilot scale silo. As regards flow profiles, many different experimental techniques can be found in the literature to study velocity profiles of granular materials in confined geometries. Among these, tomographic techniques allow to understand what happens inside the material, with both non-invasive and invasive methods.

Non-invasive methods such as PEPT, NMR, γ-ray tomography, X-ray tomography (Yang et al., 2007; Ingrama et al., 2005; Nakagawa et al., 1997; Nikitidis et al., 1998; Langston et al., 1997; Dyakowski, 1996) have not been considered in this work partly because of their cost and difficulty of use, but mainly because they seem not to be useful for medium/large scale geometries (i.e. a device with a diameter of 0.5 m and 2.5 m high), which are in the focus of this work. As regards the techniques based on capacitance measurements, they allow to obtain both local and global (averaged) information on velocity and porosity (Dyakowski, 1996; Hage and Werther, 1997; Zhu et al., 2004, 2003). Being interested in local information, techniques yielding spatially averaged information where discarded. Many of those yielding local information however where considered too invasive on the flow field because of the insertion of capacitive probes in the moving bed for example. Other, non-tomographic, techniques usually adopted to determine velocity profiles are optical ones; typically a transparent wall is required on the wall of the silo, so that particles can be directly observed and their motion recorded through a CCD camera. The velocity field can be then reconstructed by means of numerical techniques, which can be divided in PIV (particle image velocimetry) (Steingart and Evans, 2005; Slominski et al., 2007) and PTV or SPT (particle tracing velocimetry or single particle tracking) (Machin et al., 2006) ones. The need for a transparent wall however limits the experiments to situations (such as quasi 2-D silos) which may be not realistic. In this work, the technique chosen to determine the flow field was based on the use of a tracer. For a relatively large structure, a tracer technique is probably the best choice because of the simplicity of the operations. These techniques can be found in literature both on real scale (Chen et al., 2005; Ooi et al., 1998) and pilot scale(Johanson, 1964; Slominski et al., 2007) plants.

Since the focus was to use a vessel of pilot scale size, it was possible to use the procedure described by Johanson (1964), which consists of using a vessel which can be splitted along the longitudinal plane into two halves. Two materials (the main one and the tracer) are loaded into the unsplitted vessel so that to form a stratified bed of alternated bands. The flow is then started for a given time and then stopped. The material is then constrained at the top and at the bottom of the vessel so that to avoid any further macroscopic motion of the material. The plant is then turned horizontally and splitted removing the upper shell. The excess material is then carefully swept away obtaining the final result shown in Figure 6.2. The final position and morphology of the bands was then registered by visual inspection.

This approach although it may appear tedious, it allows to observe the profiles resulting from a fully 3-D geometry without any bias due to the use of invasive probes. In this case, for each single test, some tracer bands of zinc grit were prepared at different heights and

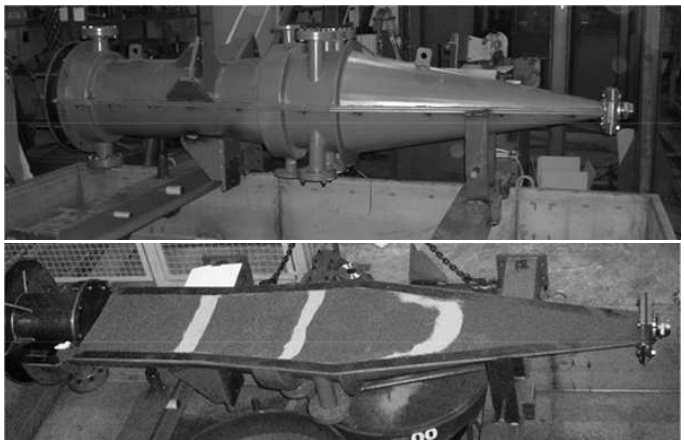

Figure 6.2: *Pictures from the profiles study phase of the tests. The silo is closed and moved with a crane, then (top) put in horizontal position and finally (bottom) the material is removed until the middle line is reached.*

then the stratified bed was made flowing downwards by means of a screw conveyor at the bottom end, which allowed for a constant flowrate. Meanwhile fresh material was continuously charged at the top with a hopper to preserve the level inside the pilot plant. After each run zinc was divided from steel grit at the end of a conveyor belt using a magnetic pulley as sketched in Figure 6.3.

In order to measure the stress profile at the wall, normal stresses were recorded at six

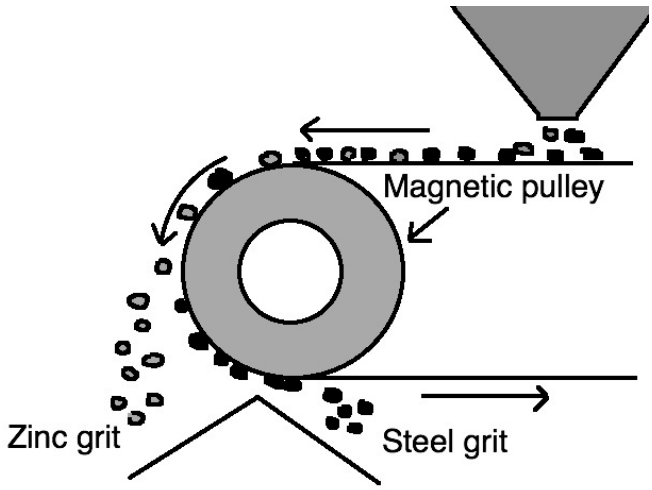

Figure 6.3: *Schema of the method used to separate steel grit from zinc grit.*

different positions by means of strain gauges placed on steel plates strained by the material acting on them. Six rectangular holes were made on the wall at different heights (starting from the bottom at 0.50, 0.95, 1.12, 1.24, 1.64 and $2.04\ m$ respectively) and at different angular positions (see Fig. 6.1) and where closed by rectangular steel plates $0.5\ mm$ thick. The plates could move elastically deforming and straining except at their

upper extremity where they were fixed at the wall (see Figure 6.4). The estensimeters were fixed on the outer side of the steel plates, as close as possible to the junction between steel plate and wall where the strain gradients were larger. The width of the sheets was fixed ($10\ mm$) while the length was variable ($25 - 35\ mm$) so that to increase the sensitivity (longer sheets were placed in zones with lower stresses) and to avoid plastic deformation of the steel plates (shorter sheets were placed in zones with higher stresses). The estensimeters were connected to a Wheatstone bridge, whose signal was converted in a tension signal ($\pm 5V$) by an apposite module (Analog devices 5B38) and stored on a laptop PC by means of a data acquisition card (NI DAQCard-6062E).

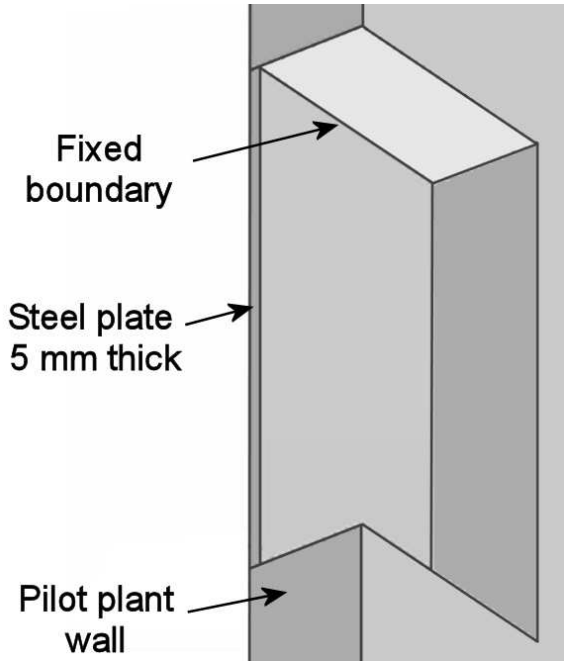

Figure 6.4: *Schema of the installation of plates for strain measurement.*

Test	Internals	Duration	Gas
T1	no	long†	no
T2	no	short††	no
T3	yes	long†	no
T4	yes	short††	no
T5	no	long†	yes
T6	no	short††	yes
T7	yes	long†	yes
T8	yes	short††	yes

† $\sim 110min$, 1 band 200 mm high, placed at height 2.3 m
†† $\sim 45min$, 3 bands 70 mm high, placed at heights 1.23, 1.8,2.37 m

Table 6.5: *Main kinds of test performed*

During the experimental campaign 8 different tests were made according to Table 6.5. Each run was repeated three times. In all of these tests a constant flowrate of 6kg/min was choosen, corresponding to a velocity of the granular material at the outlet of about 0.008ms^{-1} which is a very slow draining.
Also the effect of gas flowing countercurrent on the dynamics of the descending granular material was studied, injecting air in the silo at the middle (see Fig. 6.1) through a circular jacket communicating with the silo by means of 64nozzles. Air temperature was controlled by means of a heat exchanger, and air pressure before the heat exchanger was of 0.40 barg, the nominal flowrate being of 392.00 Nm3/h. In the next sections, at first the main experimental results will be resumed, which will serve also as a methodological guidance for the following steps. Then the procedure for calculations will be described together with the estimation of model parameters, and finally a comparison between modeling and experimental results will be performed, at first for the case without air, then for the full gas & solids flow.

6.4 Experimental results

6.4.1 Granular flow without air

As regards wall normal stress profiles, which are displayed in Figure 6.5, they were obtained for the two different flow configurations (with or without internal devices) by averaging all the six tests referring to each set-up (T1-T2 and T3-T4). As for the average profiles for the case without internals, the expected profile was found(Nedderman, 1992) with a stress peak at the junction between the enlarging and the convergent part. The effect of introducing the tubes passing from side to side was quantified in a strong reduction of the stress peak, while far from the internals the stress remains unchanged. The lowest wall normal stress was measured in this case in the position just below the internals, probably because of the particular geometry, characterised by an enlargement of the section with depth (see Fig.6.5). As it is easily noticeable from the error bars in the figure, in the case without internals wall data can be very different from one test to another near the junction. This happens probably because of the well known large fluctuations of forces in this zone(Nedderman, 1992; Nielsen, 1998); the insertion of the devices diminishes not only the average value of the stresses near the devices, but also their variability, therefore further reducing the possibility of structure damage.

As regards the flow field, from a general point of view, tracer experiments (displayed in Figures 6.12 and 6.17 in comparison with modeling results) confirmed that the silo is in mass flow with no formation of stagnant zones, with a deformation of the bands induced

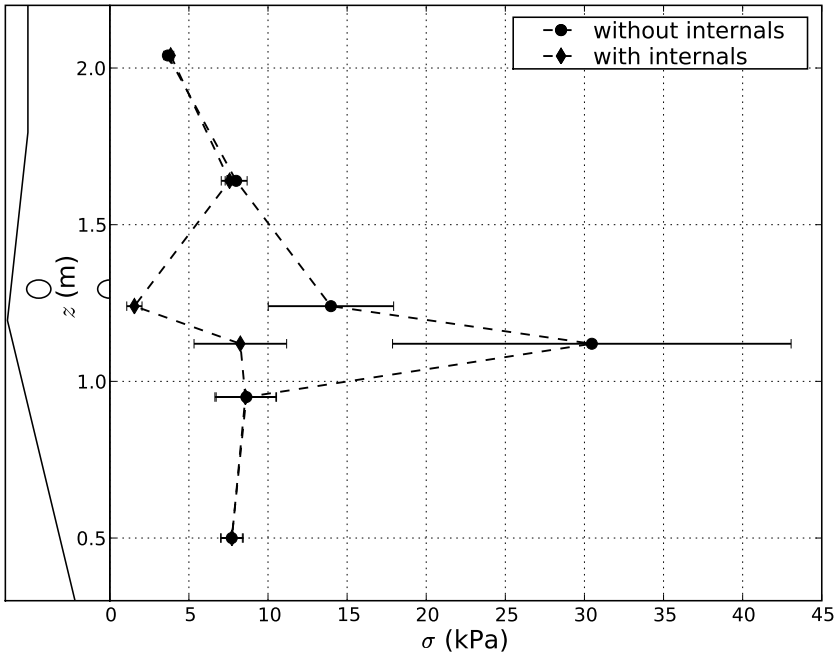

Figure 6.5: *Comparison of experimental results of wall normal stresses with and without internal devices, with no air flowing (without: average of tests T1-T2, with: average of tests T3-T4). Error bars represent standard deviations.*

by the presence of a divergent and a convergent part in the silo. In the cylindrical (upper) part of the silo, from direct inspection of the position of the bands (as it can be noticed in Figure 6.6), it was however clear that while nearly all the material is in plug flow, in the region very close to the wall a velocity profile exists, with a so-called *shear band*.
With respect to this, visual inspection confirmed that the shear bands are confined by the wall to a thickness which corresponds to about ten diameters. This means, as expected, that more of the 90% (by weight) of the material in the upper section of the pilot plant is not subjected to shear, and descends as a plug flow. Because of the shear induced dispersion of the particles it was not possible to determine unambiguously the slip velocity at the wall. For this reason it was not possible to compare the profiles obtained from the experimental results with the modeling ones in the shear band zone and the issue of assessing the performance of the model in this narrow area remained unresolved. This specific aspect however was not in the scopes of this work. The need for the experimental set-up of being of industrial relevance and the choice of the technique for studying the flow are clearly devoted to the study of the bulk behavior. The exact estimation of velocity profiles in the shear zone and the precise quantification of slip velocity would have needed different and more idealized configurations of flow. Moreover, it must be pointed out that from a practical standpoint it is much more important for the rheological model to be able to predict the correct behaviour of the profiles of tracer in the other zone of the silo which

means to predict a plug flow (or mass flow in powder mechanics terminology) behaviour. However, the width of the shear band, which is somewhat possible to extrapolate, at least as an indication, remains a result of fundamental importance which has to be reproduced by the model.

In Figure 6.6 an example of the behavior of the tracer in the convergent section is reported. Here the flow field is seldom symmetrical and large fluctuations of the profiles can be observed. This feature is not usually embodied in continuum models, which instead provide symmetric profiles that have to be considered as a time averaged representation of the behaviour of the system.

As regards the effect of the inclusion of internals on the flow field, experiments suggest

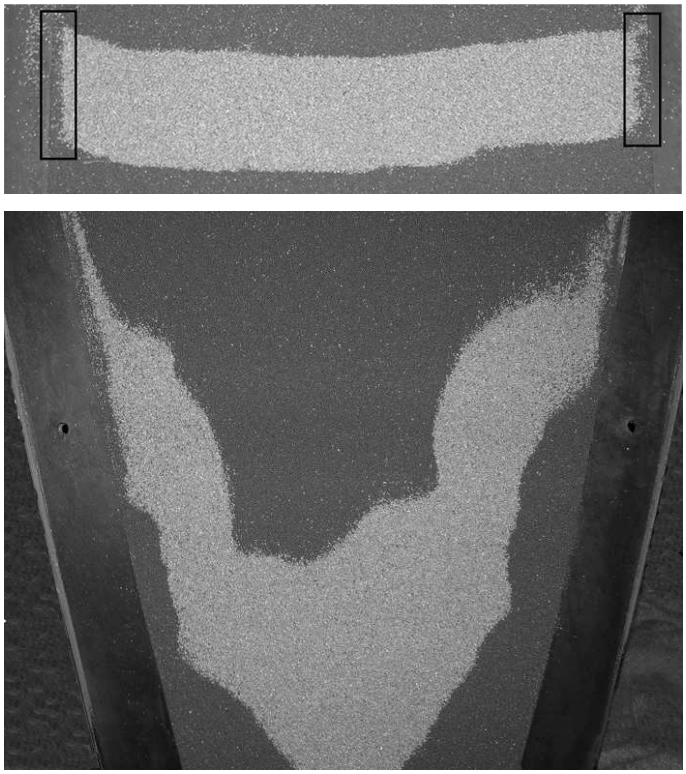

Figure 6.6: *Example of tracer profiles results: (top) shear band width, (bottom) fluctuations in the convergent part of the silo.*

that the introduction of internal devices does not impact significanlty on the flow profiles; in fact, two zones of limited extension exist just above and below the internals, where the blocking effect due to the external body is clear. These zones (an example of which is displayed in Fig. 6.7) seem in this case to be limited as shear bands areto a width of a tenth of particle diameters.

Figure 6.7: *Particular of the zone above (top) and below (bottom) an internal device, with a measurement grid superimposed*

6.4.2 Gas-granular flow

As regards wall normal stress profiles of the tests with air, which are displayed in Figure 6.8, obtained as an average of all the tests T5-T6 and T7-T8 for the case without or with internals, results show that generally pressures grow in all the silo with respect to the case without air. This is obvious because strain gauges measure the sum of solids pressure and of air, which is fed in the silo at a relatively high pressure. As for the inclusion of internal devices, tests seem to point that the inclusion of devices increases stress. A reason for this behavior is hard to be found: in fact, it is possible that the increase in pressures comes from problems in gas flowrate regulation, being that it has an effect on the whole silo, while normally the inclusion of devices (see previous subsection) has only an effect near the place where they are positioned. Wall pressures are very sensitive to gas pressures because gas is injected at a pressure ot more than 10 kPa.

As regards tracer results, reported in Fig. 6.17 in comparison with modeling results, it is possible to say that the gas flowing into the silo does not practically affect the solids behavior as profiles are similar to the case without air. In tests T5 and T7, the experimental conditions were the same, therefore data are areported as an average of different tests. Some problems of flowrate control were evidenced in test T6, where solids flowrate was often higher than the nominal value; in Figure 6.17 only one tracer profile is reported which is the one with the lowest flowrate. One test of the T8 set-up ended early, therefore

on the figure the comparison is made between tests at different residence times. As regards possible maldistribution of the gas, including channeling near the walls or preferred paths due to the lateral positionment of the injectors, gas velocity was observed also into the bulk by means of anemometers (not shown here), approximately finding a good distribution of the gas.

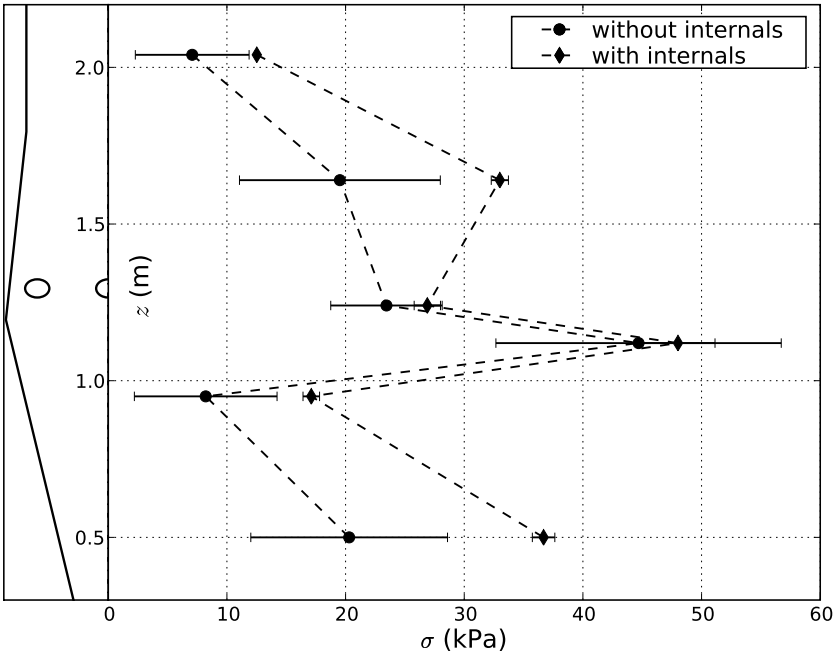

Figure 6.8: *Comparison of experimental results of wall normal stresses with and without internal devices (without: average of tests T5-T6, with: average of tests T7-T8), with air flowing upwards. Error bars represent standard deviations.*

6.5 Numerical procedure & parameter estimation

The system of PDEs can be conveniently solved through any general purpose solver. A commercial CFD software(COMSOL, 2005) was used in this case as in Chapter 3. Momentum balance has been closed by Navier slip relation, Eq. 3.26, at the wall and by a tangential stress free upper boundary, while the outlet velocity was fixed (this corresponds to the experimental case were a screw feeder was adopted to control flowrate). For the fluctuating energy equation it was choosen to impose 'insulation' conditions at the walls and a fixed temperature at the top (determined as the average temperature value in the cylindrical part of the pilot plant). During the calculations the height of the material was supposed to be constant, as in experiments where fresh material was nearly continuosly fed at the top. As regards the strategy used to compare numerical and experimental re-

sults, in this case (1) some parameters were fitted to reproduce the behavior of stresses and velocity profiles in the pilot plant without air and without internals, then (2) the obtained parameters were used to test the predictions against data obtained for granular flow in the plant with internals and with air. The parameters that need to be calibrated in the model are, in principle five: μ, η_0, θ^*,k',λ. However, considerations developed in previous chapters allow to modify and reduce the number of these parameters, because:

- in Chapter 3 it was shown that for cohesionless materials the relation $\mu \approx \tan\delta$ can be adopted for the parameter μ, where δ is the internal angle of friction of the material, that can be determined experimentally.
- it can be assumed that $\theta^* \approx k_\theta g d_p$, where k_g is a dimensionless parameter, which mainly influences the velocity profiles (as it can be noticed from the sensitivity analysis, figure 6.9).
- λ has to be a linear function of the particle diameter: $\lambda \approx k_\lambda d_p$ (as it was shown in Chapter 4).

This means that the parameters to be calibrated are reduced to four: η_0, k_θ,k',k_λ. As regards the value of the parameter μ, due to the large prevalence in the pilot plant of the main material (steel grit) with respect to the tracer, the value of the angle of internal friction was taken as that of the main one, which from Table 6.4 can be estimated as 0.5. The sensitivity of both wall normal stresses and velocity profiles on these parameters can be appreciated in figure 6.9. As regards a more detailed sensitivity analysis of stress profiles predicted by the model varying parameters μ and flowrate, the reader can refer to Chapter 3. As it can be deduced from the results displayed in figure 6.9 the parameter having the highest sensitivity on the results (both on stress and on velocity profiles) is the slip length parameter k_λ.

As regards the use of experimental data for parameter estimation, as it was previously discussed, data available for calibration and verification are (1) the pressure data at the walls (2) the width of the shear band close to the walls, which can be *grosso modo* estrapolated from the experimental tracer profiles, and on (3) the tracer profiles in the central part of the pilot plant.

In particular, in this work the parameters of the model were first calibrated on the case without internals, then the model was predictively used with the same parameters, on the case with internals, being that the material was unchanged between the two cases. A good fit for the parameters was obtained as $k_\lambda = 5$, $\eta_0' = 2$,$k' = 2$, $k_\theta = 100$.

In order to simplify the calculations, both cases with and without internals were treated as axisymmetrical, which is correct for the situation without internal devices, while it is

incorrect for the other configuration in which the devices pass from side to side. However, at least on the simmetry plane where the pilot plant was opened for measurement of tracer profiles, results may be thought as comparable.

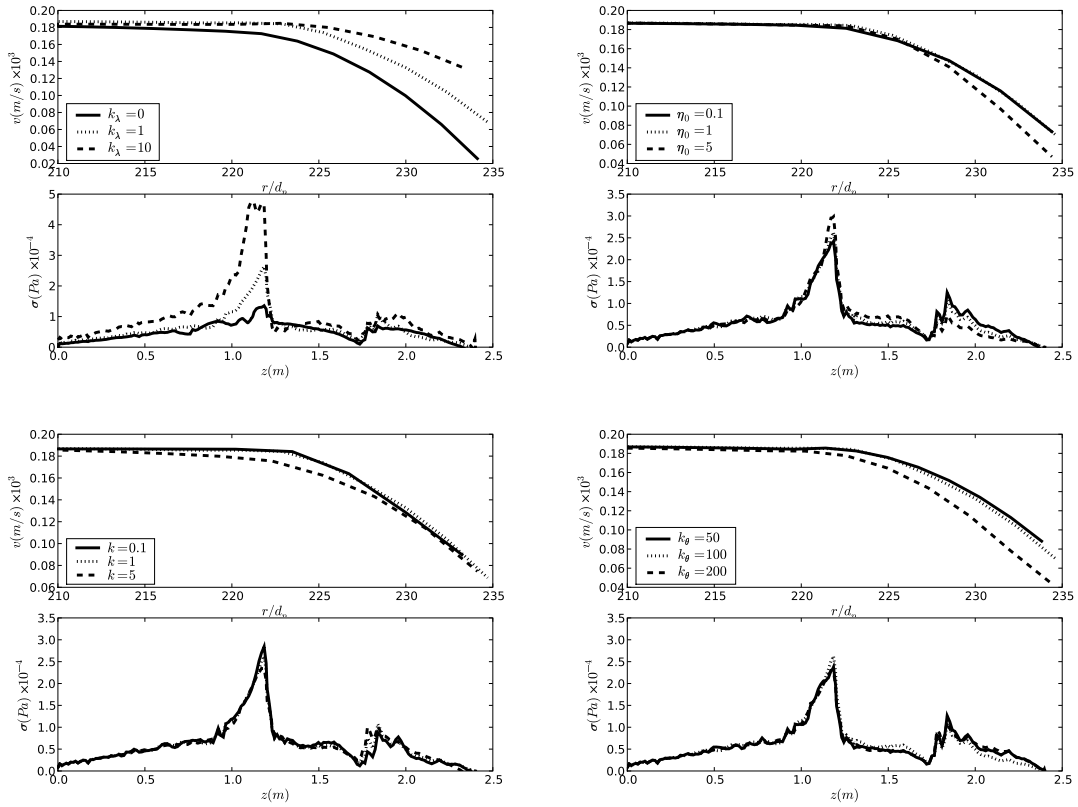

Figure 6.9: *Sensitivity of radial velocity and vertical wall stress profiles on (from left to right and from top to bottom) parameter k_λ,η_0',k',k_θ.*

6.6 Comparison between the model and the experiments

6.6.1 Granular flow only

Stress profiles

Comparison of normal stress profiles with and without internals are shown in Figures 6.10,6.11. As regards profile without internals (Fig.6.10), there is experimental evidence of good agreement between data and model predictions; in this case the parameters were fitted in order to reproduce the results, so quantitative agreement is somehow obvious, while it has to be stressed the ability of the model to reproduce the correct shape of the stress profiles. The case with internals (Fig. 6.11) is even more significant because the same parameters of the previous case have been used: it is clear that the reduction of the peak stress due to the presence of the internals is fairly well predicted by the model, both

qualitatively and quantitatively. Indeed, predicted profiles with and without internals are the same far from the internals and very different only in the region close to the devices. Simulations therefore confirms that internals contribute to sustain part of the weight of the material lowering the load acting on the walls, exactly as in reality. Departure from the experimental profile in the upper part of the silo could be attributed to the difficulty of clearly determining the correct position of the top surface, the material being continuosly fed during the experiments.
However, it can be assessed that, as regards stresses, quantitative agreement exists between experiments and the model predictions.

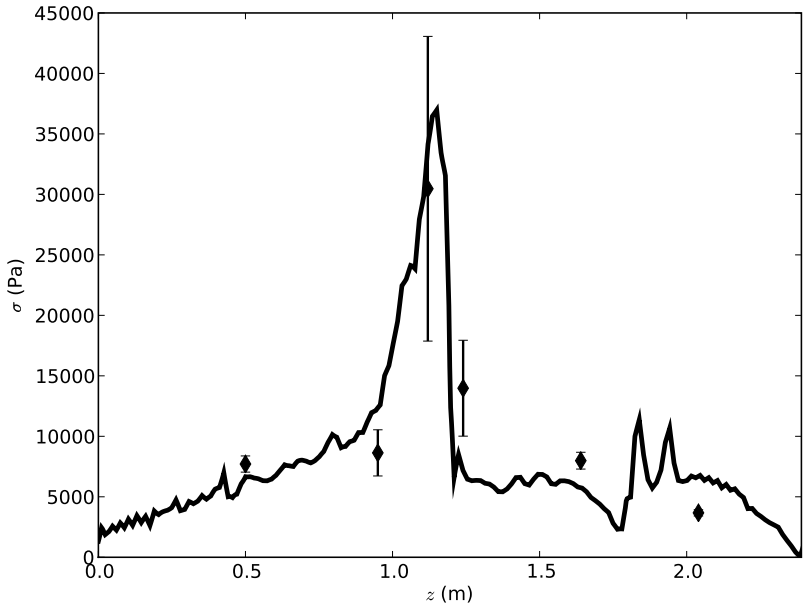

Figure 6.10: *Comparison of experimental results(average of tests T1-T2, diamonds) and numerical calculations (solid line) for wall normal stresses in the silo without internals with no air flowing.*

Tracer profiles

In Fig. 6.12 tracer profiles predicted by the model can be appreciated, compared with the experimental results. Comparison between the model and experiments is qualitatively successful, considering the presence of an uncertainty in the determination of the exact flowrate (the screw conveyor had a 10% precision); in order to get results closer to experiments, a slightly different outlet velocity (with a variation of less then 10% with respect to the nominal value) was assumed which allowed to quantitatively recover experimental profiles. Keeping in mind mass conservation issues, it can be judged that the bias can be eliminated easily, with no need of correcting the outlet velocity in the model, if the flowrate is correctly determined. Therefore both the experiments and the model agree in

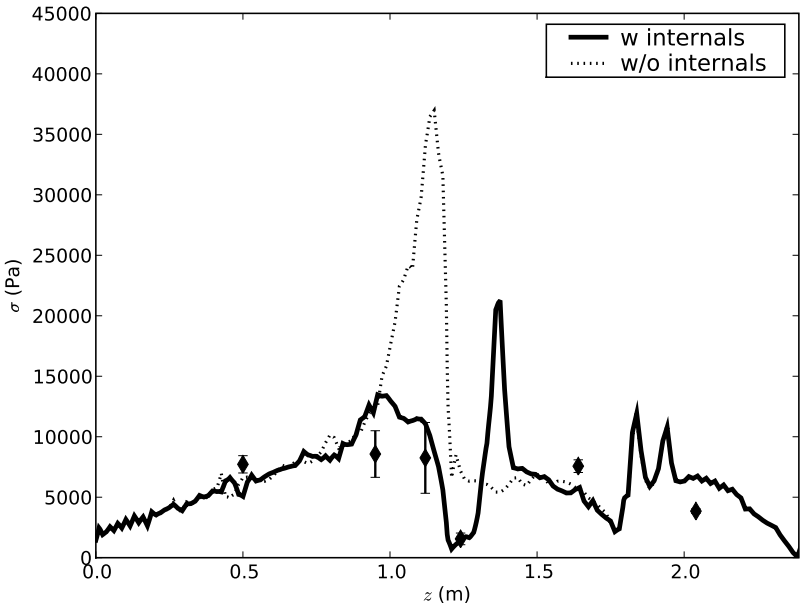

Figure 6.11: *Comparison of experimental results(average of tests T3-T4, diamonds) and numerical calculations (solid line) for wall normal stresses in the silo with internals with no air flowing. Dotted line is the profile without internals (Fig. 6.10), displayed as a reference.*

showing that the silo is characterised by mass flow, the model predicting also the effect of the changes in diameter of the silo. Regarding the effect of the inclusion of internal devices on the flow field, the model is able to reproduce also the fact that internal devices have a very local effect on the flow field, determining only a local drag on the particles. Therefore, when compared to experiments, the model predicts reasonably well the macroscopic deformation of the material, as well as the size of disturbances on the flow field (such as the "wake" induced by internals, but also the size of shear bands).

6.6.2 Gas-solids flow

Model

The model used for the gas-solid flow extends the rheological model adopted for granular flow (in the same spirit of what was done in Chapter 5) alone by means of a drag term in the momentum balance, $\mathbf{F}_D$:

$$\rho\partial_t\left(\bar{\mathbf{v}}\right) + \rho\bar{\mathbf{v}}\cdot\nabla\bar{\mathbf{v}} = -\nabla p - \nabla\cdot\underline{\underline{\tau}} + \rho\mathbf{g} + \mathbf{F}_D \tag{6.28}$$

which is a specific drag force which is given by the pressure drop in the gas:

$$\mathbf{F}_D = \nabla P_g \tag{6.29}$$

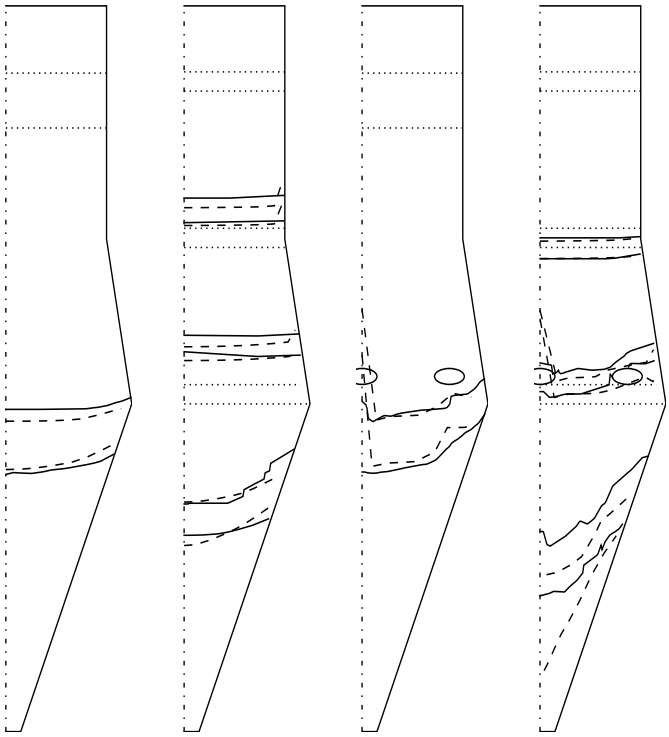

Figure 6.12: *Comparison between tracer experiments (solid lines) and simulations (dashed lines) for tests without air (from left to right: T1,T2. T3, T4). Dotted lines represent initial positions of the bands. Axes are not on scale.*

On the other side, to characterize the 2-3D gas flow the Brinkman equation was adopted:

$$\rho_g \frac{\partial \vec{u_g}}{\partial t} + \frac{\mu_g}{k_p}\vec{u_g} = \nabla \cdot (-p\mathbf{I} + \mu(\nabla \vec{u_g} + (\nabla \vec{u_g})^T)) + \rho_g \vec{g} \tag{6.30}$$

The porous medium is described in Brinkman equation by the the term $\frac{\mu_g}{k_p}\vec{u_g}$, where k_p is the permeability. In order to define the permeability, Ergun equation can be used:

$$k_p = \left(\frac{dP/dx}{u_0}\right)^{-1} = (E_1 + E_2 u_0)^{-1} \tag{6.31}$$

where u_0 is the superficial velocity, and:

$$E_1 = \frac{150\mu_g(1-\epsilon)^2}{d_p^2 \epsilon^3} \tag{6.32}$$

$$E_2 = \frac{1.75\rho_g(1-\epsilon)}{d_p \epsilon^2} \tag{6.33}$$

Permeability is thus a function of porosity and superficial velocity. This expression for the permeability is used to solve Eq. 6.30 by means of COMSOL Multiphysics. At

this moment, there are no tuning parameters except the ones contained in the granular rheology. In fact, a local value of porosity is needed from the permeability expression, and, as a simple choice, it is possible to use the linear dilatancy law already introduced, Eq. 6.7, relating porosity and the inertial number I. This can be seen to be in conflict with a main hypothesis of the rheological model, that the flow is uncompressible. In fact, due to the increasing complexity of the models, it is choosen to allow for porosity variations only in their effect on the gas dynamics, and to keep the rheological model the same without relaxing the uncompressibility hypothesis. This can be reasonable when porosity variations are less than $10\ \%$, which is a value below which the rheological model can be considered incompressible, but the little variation in ϵ can imply a strong effect on gas distribution.
Therefore the model is closed when the dilatancy parameters ϵ_{min} and β are specified. Based on experience and literature, in the following it will be assumed that $\epsilon_{min} = 0.54$ and $\beta \approx 1$. The other parameters of the full model were taken the same as determined in the previous Sections.

Stress profiles

Comparison of modeling and experimental results regarding stress profiles is given in figures 6.13 and refc6stress2. The model predicts the change in the wall stress profile due to gas pressure with good agreement, apart from one position (the fifth estensimeter starting from the top) which is very far from the other experimental points also, and which is characterised with great probability by experimental errors. The fact that the fifth estensimeter seemed to have some problems was noticed when recording signals by A. Zugliano at CRD. When studying the inclusion of internals, the model as expected, predicts that wall stress change only in the zone close to the devices (as for the case without air), and therefore results in a rather different profile than the experimental one (Fig. 6.14). The model results support the idea that gas flowrate (or inlet pressure) is different in the two set-ups. However, this topic would require repeating the campaign to collect new, more precise, data. Having noticed a certain agreement between experimental and modeling results, the model was used in order to understand the effect of having a pressurized bottom (typical of industrial set-ups, but which was unfeasible in the experimental set-up, where gas could exit both at the top and at the bottom); this was done in order to understand if "closing" the vessel for gases at the bottom changed flow patterns and the stress field. As shown in Figure 6.15, the model predicts that the influence of closing the bottom is limited to the hopper, and generally it acts (as expected) increasing stresses in that part of the silo. As regards the way the injection of gas changes wall stress with

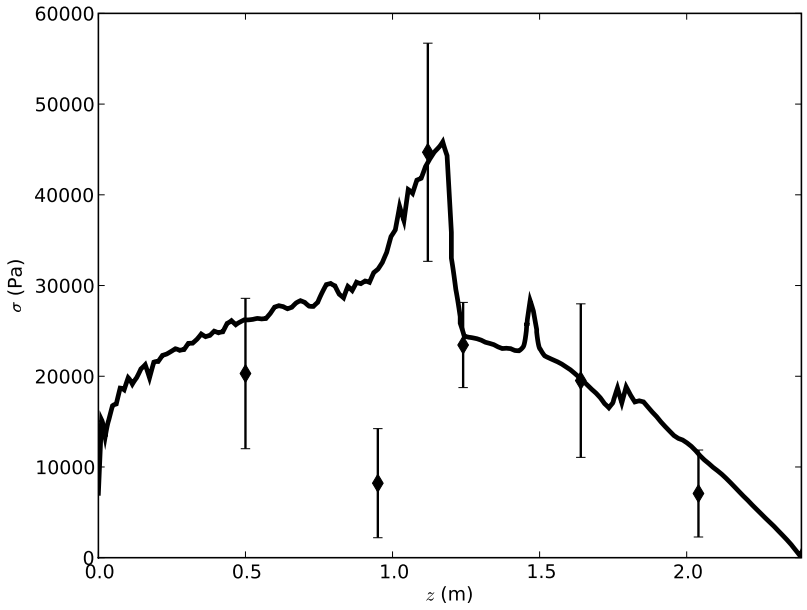

Figure 6.13: *Comparison of experimental results(average of tests T5-T6, diamonds) and numerical calculations (solid line) for wall normal stresses in the silo without internals with air flowing upwards in the silo.*

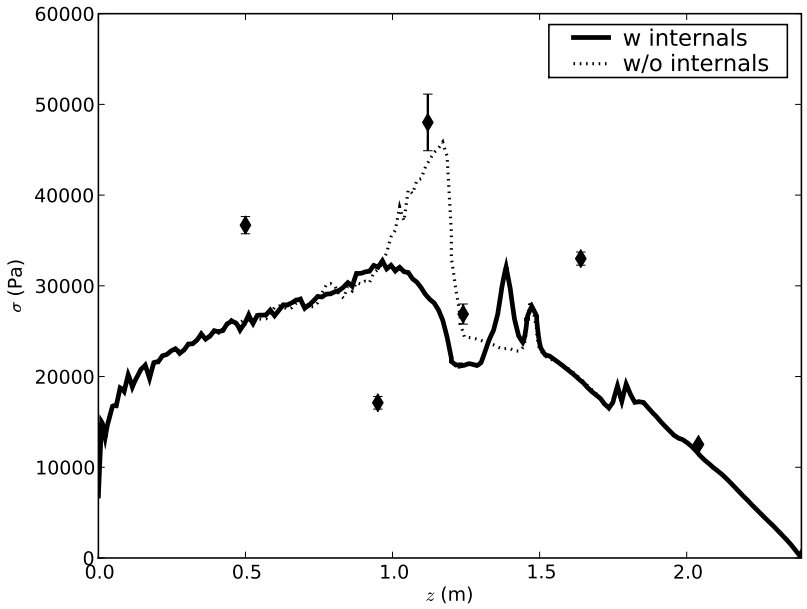

Figure 6.14: *Comparison of experimental results(average of tests T7-T8, diamonds) and numerical calculations (solid line) for wall normal stresses in the silo with internals with air flowing upwards in the silo. Dotted line is the profile without internals (Fig. 6.13), displayed as a reference.*

respect to the configuration without gas, Figure 6.16 can give some hints, showing the decomposition of the wall stress obtained by the model (for the case with “open” bottom)

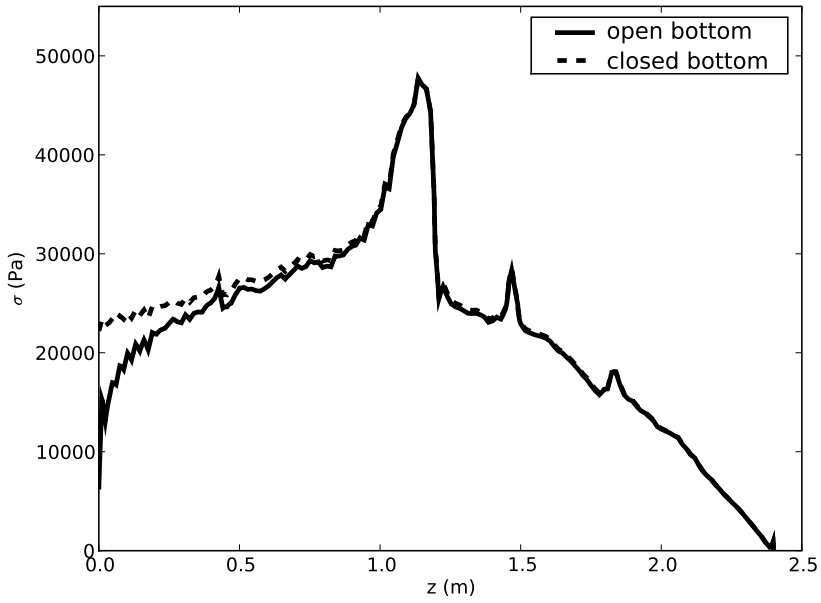

Figure 6.15: *Comparison of model results for wall normal stresses regarding open/closed bottom conditions.*

into particle stress and air pressure. At first, it is clear that the stress increases mainly due to air pressure contribution. As regards the particle stress, it is very interesting to notice that, from the switch to the top of the silo, air injection reduces the stress with respect to the case without air. In the model, this is reasonably given by the fact that gas pressure drop reduces the effective gravity. In the hopper, stresses are equal in both cases, apart near the outlet, where the particle stress is higher in the case with air. This is probably due to the presence of a pressure gradient reversed with respect to the upper part.

Tracer profiles

In Fig. 6.17 tracer profiles predicted by the model can be appreciated, compared with the experimental results. Again, as for the case without air, a good qualitative agreement is obtained, and adjusting the solids flowrate by less than 10 $\%$ results also in a quantitative agreement. For test T6, where a higher (and unknown) flowrate was experienced, comparison with the model was unsuccesful until flowrate was adjusted by more than 10 $\%$. Again, both the experiments and the model agree in showing that the silo is characterised by mass flow also in the case with air, with the same scarce effect of inserts on the flow field. It seems that the model behaves well even when extended to treat gas flow, and therefore it could be used also for more complex couplings including mass transfer, reactions, and so on.

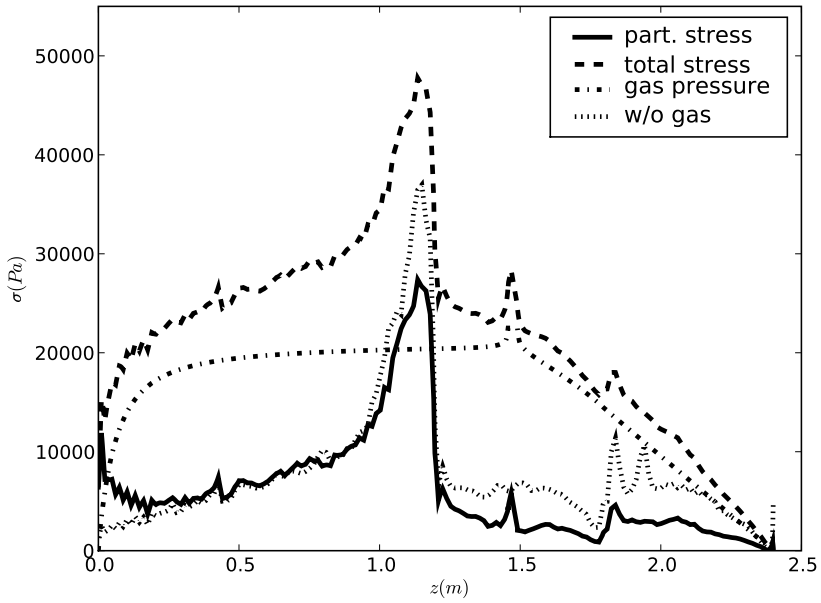

Figure 6.16: *Decomposition of the wall stress into the various contributions for the case with air injection, without internals, from model calculations, and comparison with the case without air and without internals.*

Gas flow pattern

As regards the flow pattern of the gas in the model silo, the model predicts (please see Figure 6.18) that just above the injector the gas is well distributed both suggesting that neither wall channeling nor "dead zones" in the center are present. From first observations made with anemometers in the bed (not shown here), it seems that the picture given by the model is correct, with no velocity difference from the center to the wall. However, these analyses need to be refined in order to arrive to a satisying comparison.
Regarding the possibility of pressurizing the bottom in order to avoid gas flowing downwards, from figure 6.18c it can be said that apart being increased the upwards flowrate, no macroscopic effect on the distribution exists, and also no dead zones form in the center.

6.7 Conclusions and Perspectives

This chapter dealt with the development of scaling procedures for silos for gas-solids applications, and with the comparison of experimental results of stress and flow profiles of a pilot scale silo with the predictions of the rheological model described in Chapter 3, also extended in order to treat gas-solid coupling. Several issues were discussed regarding scaling laws, ending with original scalings, whose range of validity was analysed.
Experiments on a pilot silo built by an industrial partner were performed studying the

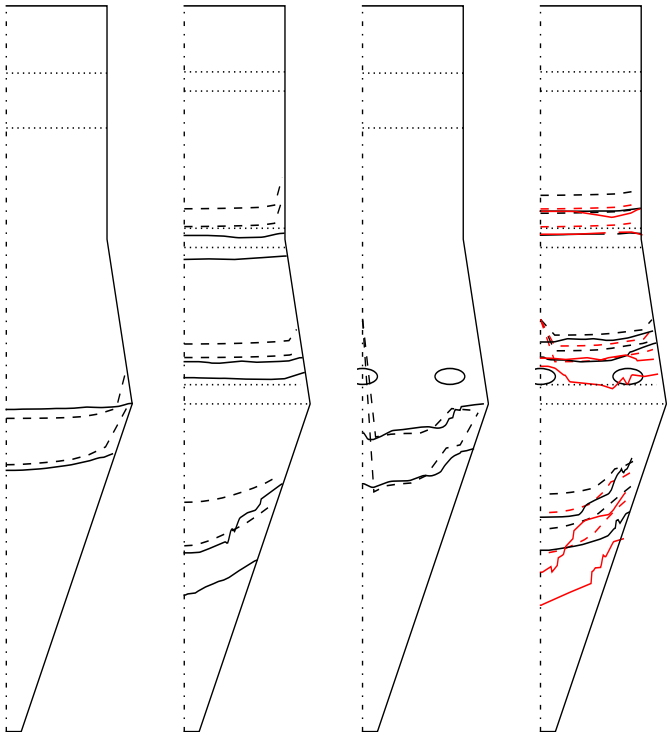

Figure 6.17: *Comparison between tracer experiments (solid lines) and simulations (dashed lines) for tests with air (from left to right: T5,T6,T7, T8). Dotted lines represent initial positions of the bands. Axes are not on scale.*

effect of including internal devices and injecting air. First the experiments were analysed providing interesting hints, then the model was first calibrated on data without internals and air and then used to predict the profiles for the case with internals and with air. Both stress and flow profiles with and without the devices and with and without air performed reasonably well (qualitatively and quantitatively) in comparison with experiments.
This experimental campaign, which is rather unique for skills, dimensions, etc. confirms that the rheological model is well-behaving in the case of confined flow such as flow in a silo, both for stress and velocity fields, assessing with an experimental comparison what was previously claimed on the basis of experience and Literature correlations. Future experimental and theoretical works will deal with better understanding of local scale phenomena (i.e. phenomena occurring near the walls), also in order to verify the predictions of the model in the shear band zone. These topics will also be the subject of the next chapters.

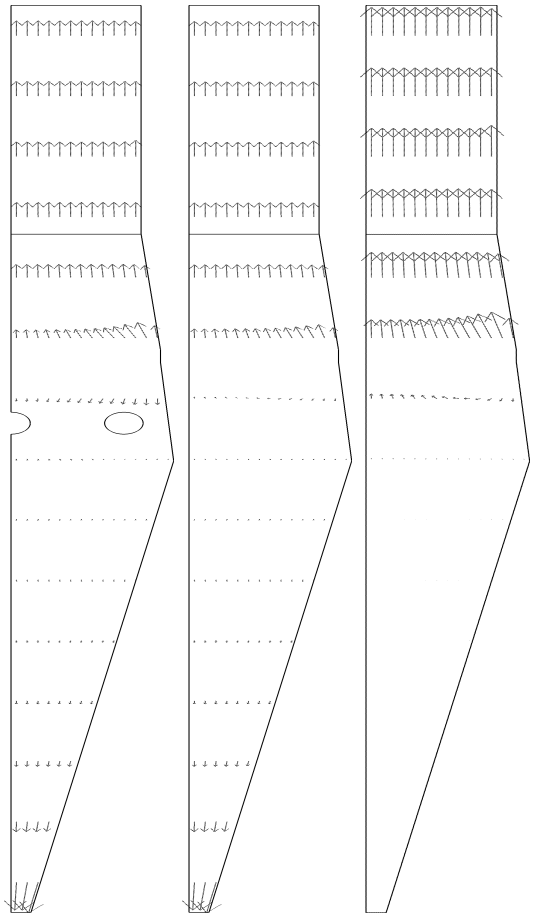

Figure 6.18: *Vector plots of gas velocity, a) with e b) without internals, c) without internals and closed bottom. Axes are not on scale*

Chapter 7

DEM methods for dense flows: application to the vertical chute configuration

O mais c'est qué, voyez-vous bien, je n'ai point sujet d'être mécontent de mes polyèdres : ils font des petits toutes les six semaines, c'est pire que des lapins. Et il est bien vrai de dire que les polyèdres réguliers sont les plus fidèles et les plus attachés à leur maître ; sauf que l'Icosaèdre s'est révolté ce matin et que j'ai été forcé, voyez-vous bien, de lui flanquer une gifle sur chacune de ses faces. Et que comme ça c'était compris. Et mon traité, voyez-vous bien, sur les mœurs des polyèdres qui s'avance : n'y a plus que vingt-cinq volumes à faire.

Alfred Jarry ,*Ubu Cocu*, Acte I, Scene I.

7.1 Introduction

In previous chapters all modeling attempts invoked the use of continuum models, which typically consist of conservation equations for mass, momentum, et cetera, equipped with constitutive relations for the unknowns which appear in balance equations (transport, generation/dissipation terms,...). As it was already introduced in Chapter 1, this is not the only way to model granular materials in flow. Being that a bulk solid consists of individual particles, another way of modeling its behavior is to model all particle-particle interactions. This is what is usually done by means of DEMs (Discrete Element Methods), which solve the equation of motion for each particle in a given system computing, apart from body forces, also the interactions between particles. Though in principle this seems to be the most rigorous way to treat granular materials, in the development of DEMs many problems exist which are often solved by means of modeling choices, and therefore end in creating approximated, analog systems. As to cite a few, contacts are often treated in

simplified ways (e.g. by means of spring-dashpot models), there are still difficulties in simulating irregular particles, interaction laws are coded with simple assumptions when the physics (particularly in presence of cohesion, liquid bridges, wear) is rather complex. Then, DEMs are limited by the number of particles: typically a bulk solid(Schulze, 2008) consists of, say, 10^9 particles, while up to now DEM codes arrive (with a very large calculation time) to treat 10^5 particles. Research on DEM, both on extending computational feasibility (which is however hardware-dependent), and on implementing more complex behavior, is currently being carried out; surely DEM methods are a very important tool when (1) the number of particles in the system allow to treat them all, or (2) a local behavior has to be studied, as wall slip or shear banding. In this chapter a DEM code is used , LMGC90, which I learned to use during my stay at the Laboratoire de Materiaux et Structures du Genie Civil in Montpellier, under the supervision of F. Dubois. The code is used to understand the effect of varying flowrate, particle shape, wall friction, and other parameters, on stress and velocity profiles for the flow in a vertical chute, for the purpose of giving insights on the rheology of granular materials in confined geometries. In this case the DEM method is used as a source of virtual experiments, which can give informations which cannot be simply extracted from experiments (in particular, this is the case of stress fields inside the material). It is intended here as a benchmark for continuum models.

Due to the need of performing a number of analyses, it was preferred to simulate 2D granular flows. DEM simulations of disks in silo flow were already done by François Chevoir's group at LCPC(Prochnow, 2002), using a silo with flat bottom and controlling flowrate by means of a hole. Simulations of flow of spheres in pebble flow in a silo and in a vertical chute were done for example by Rycroft et al. (2006, 2009). At this moment, no simulations exist in Literature for polyhedric/polygonal grains in a vertical chute geometry. This geometry is rather interesting because (1) from the practical point of view it is a common configuration (e.g in silo discharge) and (2) it seems that promising rheological models(G. D. R. Midi, 2004; Pouliquen et al., 2006) fail to predict the shear banding phenomenon which occurs near the walls.

As noticed in previous chapters, vertical chute flows are characterised by a plug flow at the center and shear bands near the walls(G. D. R. Midi, 2004). The width of these shear zones has been subject of several studies(Pouliquen and Gutfraind, 1996; Nedderman and Laohakul, 1980; Natarajan et al., 1995; Ananda et al., 2008), which are sometimes in contradiction regarding the influence of several parameters. However, synthesizing, the typical result is that shear band do not depend on flowrate, while they are weakly dependent on channel width and strongly dependent on wall roughness. Their typical size is

however related mainly to the particle diameter, and results show typically bands ranging from 5 to 15 particle diameters.
A number of modeling studies were devoted to this type of flow(Savage, 1998; Pouliquen et al., 2006). The main problem in the performance of rheological models in this configuration is probably related to the fact that shear is not uniform, and moving from the wall to the center of the channel the material changes flow regime (from dense to quasistatic). When dealing with continuum models, another topic which must be assessed is the issue of boundary conditions. In view of the considerations developed in Chapter 4, detailed numerical simulations can surely help in better understanding wall dynamics, in order to improve our knowledge of boundary conditions, both in smooth and bumpy walls configurations. The simulations described in this chapter are devoted to the case of smooth walls, which are of direct practical impact. First the geometry, computational strategy and numerical method are presented, then the main results (which are however always in development) are resumed and compared with rheological considerations.

7.2 Geometry & computational strategy

For the sake of reducing computational cost due to the need of performing a large number of simulations to study sensitivity of results to parameters, it was choosen to model a two dimensional vertical chute configuration. The geometry of the simulations is sketched in figure 7.1. The reference case chute was 39×115 particles large, filled with 4425 particles, while a larger configuration (80×120, ~ 9000 particles) was also simulated in order to study the effect of channel width, and also smaller configurations were simulated for the analysis of the boundary conditions.
In order to understand the importance of particle shape, both polygonal and circular particles were used, with a particular attention on the former, while the latter were taken for a comparison. Generally a slightly polydispersed sample was choosen in order to avoid layering effects. As regards polygons, it was choosen to model regular penthagons. The method choosen to control flowrate and provide steady flow is simple: (1) after an initial compaction, the bottom wall is removed and the material let flow due to gravity, (2) when the material passes a certain line at the bottom, its velocity is prescribed, thus controlling the flowrate, and (3) when the material passes another line at the botttom, it is recirculated at the top. This strategy (sketched in Figure 7.1) revealed to be very useful because flowrate control is much direct and simple than, for example, by means of a variable hole at the bottom. Contacts between particles and between particles and walls were considered inelastic using the “inelastic quasi-shock” approach developed by Michel Jean(Jean, 1999). Due to the particular attention devoted to the problem of boundary conditions, it

was not choosen to model walls as a collection of fixed particles, as it is often done in order to impose a sort of ‘no slip´ boundary condition, but to model smooth frictional walls, which are more similar to boundaries tipically found in reality. A number of simulations were carried out, varying flowrate, wall friction, particle shape, channel width. Solid fraction, average velocity, granular temperature were computed for each simulation.

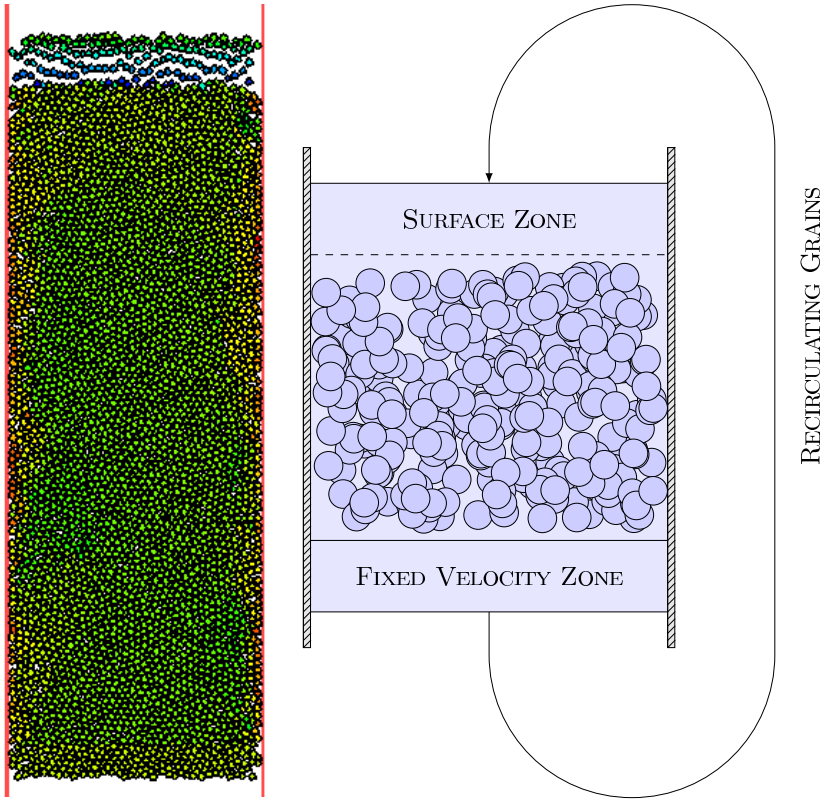

Figure 7.1: *(left) Snapshot of the geometry during a simulation and (right) Sketch of the strategy used to recirculate grains and control flowrate.*

7.3 Numerical method & averages

The DEM method used in this work is the method developed by Michel Jean (1999) and implemented in the open source platform LMGC90(Renouf et al., 2004). The code is used by a growing community of researchers and was used in several publications(Renouf et al., 2005; Azema et al., 2009). The code, developed in Fortran 90, has a Python interface which allows implementation of non-common features such as the fixed velocity + recirculation strategy used in this work. LMGC90 uses a method which is different from the original DEM strategy developed by Cundall and Strack (1979), based on spring-dashpot models of contact, and which is called Non-Smooth Contact Dynamics. Description of

the approach is not in the scope of this thesis, however it can be summarized that classical DEM treats forces as explicit functions of local deformations of the contact surface through Hertz law (which are calculated from particle displacements), while NSCD considers that contacts are rigid and forces are implicitly calculated from a local balance.
Being that, in this work, the main focus is the development of continuum models of granular flows, also the quantities extracted from the simulations were choosen as continuum averaged variables, in order to compare the results with rheological models and collect hints for further development of such models. Mean variables extracted from the simulations were velocity, solid fraction, granular temperature, stress tensor; then also statistical evaluations were performed on spatially averaged fields due to the fact (1) some models involve closures based on granular temperature(Losert et al., 2000), (2) some models are explicitly stochastic(Kamrin and Bazant, 2007), (3) some models involve randomness of the force in developing rheology(Savage, 1998) or boundary conditions (like in Chapter 4). Therefore averaging was made in two steps: (1) fixed grid (Eulerian) interpolation (2) time averaging and statistics.
Averaging methods for granular materials have been subject of many research attempts. A general framework can be identified in the work of Babić (1997), who defined the time-space mass weighted average. In this chapter, being that the method of controlling flowrate assures constant velocity, which was verified to hold by means of analysis of the total kinetic energy of the sample, after an initial transient the system is thought to be at steady state: therefore time-averages are obtained simply as a mean of the instantaneous values.
Instantaneous, locally spatially averaged solid fraction is computed by means of the expression:

$$\phi = \sum_{i \in \Omega_R} w_i A_i \tag{7.1}$$

where w_i is a weight function, A_i the area of the *i*-th particle. Velocity field is obtained similarly by means of the mass weighted expression:

$$\vec{u} = \frac{\sum_{i \in \Omega_R} w_i A_i \vec{u}_i}{\sum_{i \in \Omega_R} w_i A_i} \tag{7.2}$$

Granular temperature is defined in this work as:

$$\theta = \frac{1}{3} < (\vec{u} - < \vec{u} >)^2 > \tag{7.3}$$

where $<>$ denote time averaging. While flow properties as porosity, velocity, granular temperature are averaged in the simple way already described and are not sensitive to the averaging procedure, stresses require more attention. The main problem is that averaging

methods (such as for example, the framework estabilished by Babić (1997)) are generally developed without considering the presence of boundaries such as walls(Zhu and Yu, 2002). Generally this induces, if forces due to boundaries are not considered, a force imbalance, i.e. deviation from momentum conservation(Luding et al., 2001).
In principle, the stress tensor is a sum of a contact and of a kinetic contribution. The contact contribution to the stress tensor for the case without walls can be defined as:

$$\underline{\underline{\sigma}}^C = \sum_i \sum_{j>i} w_{ij}^* \vec{f}_{ij} \otimes \vec{l}_{ij} \tag{7.4}$$

where w_{ij}^* is a weighting function for contact forces, f_{ij} is the contact force between particles i and j, $l_{ij} = \vec{x}_i - \vec{x}_j$ is the distance between particle centers. Restricting to quasistatic and dense flow, the kinetic contribution to the stress tensor vanishes, so $\underline{\underline{\sigma}} \cong \underline{\underline{\sigma}}^C$. The weighting function w_i can be expressed simply as:

$$w_i(\vec{x_i} - \vec{x_0}; R) = \frac{1}{A_R} \mathcal{H}(R - |\vec{x_i} - \vec{x_0}|) \tag{7.5}$$

where $\mathcal{H}$ is the Heaviside step function; this means that a circular selection of radius R is drawn surrounding the averaging point $\vec{x}_0$ and only the area of the particles whose center $\vec{x}_i$ resides in the circular selection is considered for the computation. A_R is the area of the circular selection corrected to take into account only the part of the circle residing in the sample, to give correct estimates near the walls. A more smooth expression of w_i (taking into account partial presence of a particle in the circular area of interpolation) can be expressed as:

$$\begin{aligned} w_i(\vec{x_i} - \vec{x_0}; R, r_i^P) = \tfrac{1}{A_R} \big[& \mathcal{H}(R - |\vec{x_i} - \vec{x_0}| - r_i^P) + \\ & + \mathcal{H}(|\vec{x_i} - \vec{x_0}| + r_i^P - R) \cdot \\ & \cdot \mathcal{H}(R - |\vec{x_i} - \vec{x_0}| - r_i^P) \tilde{f}(|\vec{x_i} - \vec{x_0}|; r_i^P, R) \big] \end{aligned} \tag{7.6}$$

where $\tilde{f}$ is a function giving the fraction of area of the particle i to be computed when the averaging selection intersects the particle. A possible choice for this function is the approximated expression (derived analitically for disks in the limit $r_i^P << R$):

$$\tilde{f}(|\vec{x_i} - \vec{x_0}|; r_i^P, R) = \frac{1}{\pi} \left[x\sqrt{1-x^2} + \sin^{-1} x \right]_{-1}^{\frac{R - |\vec{x_i} - \vec{x_0}|}{r_i^P}} \tag{7.7}$$

This formula is the one used in this work to have smoother profiles for low values of R. The weighting function used in stress computation can be defined approximately as the fraction of the segment linking the two particle centers residing in the circular selection (if at least one particle is inside the selection), or by the more precise expression(Goldhirsch and Goldenberg, 2002; Zhu and Yu, 2002):

$$w_{ij}^* = \int_0^1 ds \; w\left[\vec{x}_i - \vec{x}_0 + s(\vec{x}_j - \vec{x}_i); R\right] \tag{7.8}$$

In the presence of walls, the strategy used in this work is to consider the force between a particle and a boundary as if it was shared by two particles, one of which is the real particle, the other is a disk with the same dimension located along the line connecting the centre of the other particle and the contact point(Zhu and Yu, 2002).

The particle parameters which were maintained constant in all the runs are resumed in

ρ_p	1000	$kg\ m^{-3}$
d_p	0.02	m
μ_p	0.3	$[-]$

Table 7.1: *Parameters of the particles considered in this work which were maintained constant in all the runs.*

Table 7.1. The plan of the simulations carried out by means of LMGC90 is reported in Table 7.2, mainly in chronological order. Simulations with 4400 particles required nearly 15 hours on a common quad-core workstation with no parallelization; as many simulations had to be performed, it was not needed to use a parallelized version of the code, but different simulations were performed in parallel each one using a core. On the other hand, 3D simulations, which are more computationally expensive, require parallelization. At prescribed times, positions, velocities and forces acting on each particle were stored in external files as allowed by the code; after the simulation these files were processed by means of appropriate routines in Fortran to perform averages. Time statistics were computed with routines written in Python.

7.4 Stresses in a continuum framework

In order to compare DEM and continuum results regarding stresses, it is important to understand if in a given geometry continuum models can profit of some assumptions reducing dimensionality, such as the assumption of fully developed flow. Usually in solving rheological models this assumption is adopted, which means that we are far enough both from the entrance and the outlet, such that profiles (of stress, velocity, porosity and so on) do not depend on height. Therefore it is important to test the applicability and validity of such an assumption, if we are interested in comparing the results to rheological models or in building a rheology from insights coming from DEM simulations. To understand the basis of such an assumption, a starting point is the momentum balance:

$$\frac{\partial \rho \vec{u}}{\partial t} + \nabla \cdot \rho \vec{u}\vec{u} = -\nabla \cdot \underline{\underline{\sigma}} + \rho \vec{g} \tag{7.9}$$

The vertical chute problem is usually tackled with steady state assumption, $\frac{\partial}{\partial t} = 0$, and with the hypothesis (which is valid in the dense and quasistatic regimes) of negligible

	$\mu_{pw}\,[-]$	$< v > [m/s]$	shape	grav. $[m/s^2]$	$D/d_p\,[-]$
S1	1.0	1	penthagon	9.81	40
S2	0.6	1	penthagon	9.81	40
S3	0.4	1	penthagon	9.81	40
S4	1.0	0.5	penthagon	9.81	40
S5	0.6	0.5	penthagon	9.81	40
S6	0.4	0.5	penthagon	9.81	40
S7	1.0	2.0	penthagon	9.81	40
S8	0.6	2.0	penthagon	9.81	40
S9	0.4	2.0	penthagon	9.81	40
S10	1.0	0.1	penthagon	9.81	40
S11	0.6	0.1	penthagon	9.81	40
S12	0.4	0.1	penthagon	9.81	40
S13	0.6	1.0	penthagon	9.81	80
S14	0.6	1.0	penthagon	98.1	40
S15	0.6	1.0	penthagon	18.1	40
S16	0.8	1.0	penthagon	9.81	40
S17	0.8	0.5	penthagon	9.81	40
S18	1.2	1.0	penthagon	9.81	40
S19	1.2	0.5	penthagon	9.81	40
S20	1	1.0	penthagon	9.81	20
S21	0.8	1.0	penthagon	9.81	20
S22	0.6	1.0	penthagon	9.81	20
S23	0.8	$10^{(*)}$	penthagon	98.1	20
S24	0.7	1.0	penthagon	9.81	20
S25	$0.7^{(**)}$	1.0	penthagon	9.81	20
S26	0.5	1.0	penthagon	9.81	40
S27	0.55	1.0	penthagon	9.81	40
S28	0.45	1.0	penthagon	9.81	40
S29	1.0	1.0	disk	9.81	40

$(^*)$: $d_p = 0.2$ m
$(^{**})$: restitution coefficient, $e = 0.5$.

Table 7.2: *Plan of the simulations.*

inertial effects, $\nabla \cdot \rho\vec{u}\vec{u} = 0$. The resulting momentum balance equations are:

$$\nabla \cdot \underline{\underline{\sigma}} = \rho\vec{g} \tag{7.10}$$

which can be written as:

$$\begin{cases} \frac{\partial \sigma_{xx}}{\partial x} + \frac{\partial \sigma_{xy}}{\partial y} & = 0 \\ \frac{\partial \sigma_{yx}}{\partial x} + \frac{\partial \sigma_{yy}}{\partial y} & = \rho g \end{cases} \tag{7.11}$$

The typical assumption which is made in the solution of the vertical chute flow is that of "fully developed flow", that is $\frac{\partial}{\partial y} = 0$. This simplifies the equations into:

$$\begin{cases} \frac{\partial \sigma_{xx}}{\partial x} = 0 & \Rightarrow \sigma_{xx} = \text{const.} \\ \frac{\partial \sigma_{yx}}{\partial x} = \rho g & \Rightarrow \sigma_{yx} = \rho g x \end{cases} \tag{7.12}$$

Eq. 7.12 do not tell anything about σ_{yy} and σ_{xy}; as regards σ_{xx}, it is stated that it is uniform along the cross section, without precising its value, which will depend on the boundary conditions. It is important to stress that the previous soultion is valid only in the case of fully developed flow, thus a nonlinear shear stress profile will probably be due to the unfulfilment of this assumption. In order to fully specify the stress tensor, in this configuration, rheology has to be used; typically rheologies involve (1) considerations about symmetry (or not) of the stress tensor (thus telling something about the behavior of σ_{xy}), and (2) thoughts on the normal stress ratio (in order to fix the undeterminacy of σ_{yy}).
As regards the first topic, asymmetry of the stress tensor, i.e. $\sigma_{xy} \neq \sigma_{yx}$, would be the symptom of the presence of couple stresses, suggesting that the proper rheology should involve angular momentum balances(Mohan et al., 2002). Hydrodynamic models such as the one developed in Chapter 3 usually assume symmetry of the stress tensor, thus it is very important to understand, in this case from numerical calculations, if and when the stress tensor can be assumed to be symmetric.
As regards the other type of considerations, i.e. about normal stress ratio, the reader familiar with Janssen's theory(Janssen, 1895) will remember that the value of the ratio $K = \sigma_{xx}/\sigma_{yy}$, which is called Janssen's constant(Nedderman, 1992), is considered to take values above and below 1, respectively in the so-called passive and active states. While this picture is valid and useful for statics, in the moving case is not so clear whether this picture applies or not. In this confusion, hydrodynamic models usually cut the Gordian knot by assuming $K = 1$. The validity of this assumption can be tested in this case by means of numerical simulations. Another topic of interest, which deals with boundary conditions, is the value of the wall friction coefficient, defined as $\mu_w = \sigma_{xy}/\sigma_{xx}$. In statics, typically the value of the coefficient is easily determinable(Nedderman, 1992), while when the material is moving its value is no more a material (pair) property, but depends also on flow characteristics, as it was argued in previous chapters. The stress analysis held in this work aims at evaluating also this coefficient and its dependence on the parameters of the system.

7.5 Results

The following subsections resume the main results obtained from the simulations. First stress fields are analysed, then flow profiles and statistics (pdfs, time correlations); in the end boundary conditions are studied.

7.5.1 Stress field

The possibility of computing the stress field in a moving granular material is very interesting because of the possibility of relating stresses and strains by means of a dedicated rheology. Based on the notes given in Section 7.4, when studying the dependence of stresses on the parameters of the system such as flowrate and wall friction coefficient, some issues which should be considered are (1) the range of validity of the fully developed assumption, (2) existence of symmetry in the stress tensor, (3) the value of the normal stress ratio.
An example of the stress field obtained for $v = 1m/s$, and two values of the particle-wall friction coefficient (respectively $\mu_{pw} = 0.4$ and $\mu_{pw} = 1.$) is reported in Figures 7.2 and 7.3. It is clear that the wall-particle interactions strongly affect the stress field; in particular (as it will be discussed in the following) less frictional walls, as occurs in statics, tend to shift downwards the saturation of stress: it can be judged that in the less frictional case the assumption of fully developed stress profiles does not hold in this particular geometry because stress never reaches an asymptote. This is even clearer looking at Figures 7.4 and 7.5, which collect stresses at the walls of the container as a function of height, varying wall friction and flowrate. The case with $\mu_{pw} = 0.4$ displays wall stress profiles which are nearly a linear function of z, while the other situations show (starting from the top) an increase, a saturation (the well known Janssen effect), and then a decrease, probably due to the fact that the material is pulled down. Again looking at Figure 7.3 it is possible to say that, for the most frictional walls, the saturation of stresses occurs not only at the wall but also in the center of the bin, but not for σ_{yy}, which evidently increases with depth in the center of the geometry; the existence of fully developed profiles (in terms of stresses) is so somewhat questionable, and further analysis would require a higher height/width ratio. Therefore generally in this configuration the classical vertical chute solution does not apply: practically, this means that, for example, to compare a solution of a continuum model with these results, the model must be solved on the whole geometry, not on a quasi-2D approximation of it, because the DEM configuration does not support a quasi-2D reduction. A higher chute should be simulated to allow for such an assumption to hold. However, the validity of DEM data does not suffer from these considerations: simply, when solving the

correspondent continuum model it has to be reminded that the solution procedure cannot profit from fully developed flow assumption.

As regards variation of wall stress with flowrate, in Figure 7.5 it can be noticed that

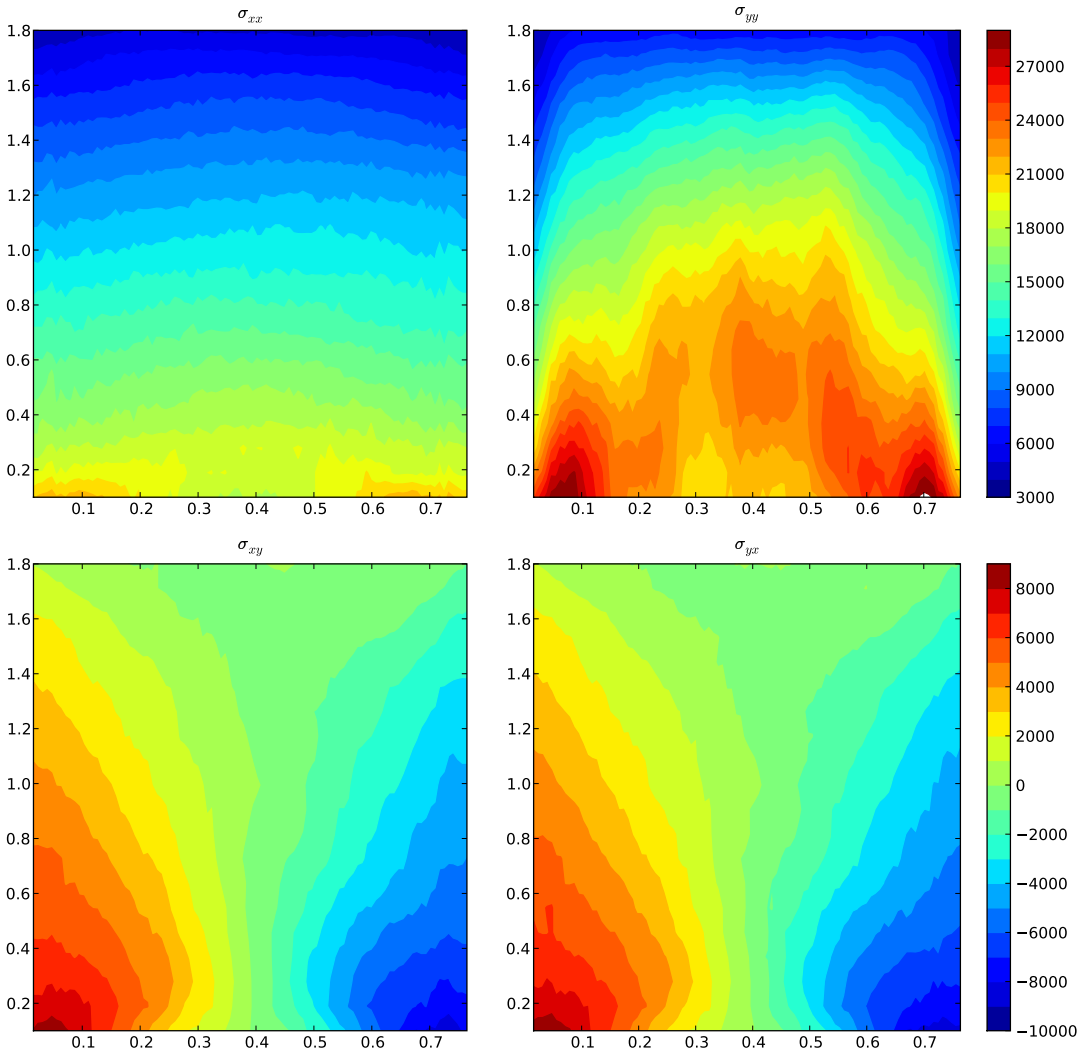

Figure 7.2: *Stress field obtained for* $v = 1m/s$, $\mu_{pw} = .4$.

the shape of the profiles does not depend on flowrate, except for the lowest part of the bin where for high values of the flowrate stresses decrease with depth, while for low values of the flowrate stresses increase with depth rather than decreasing. This is certainly due to the method of controlling flowrate: for higher velocities, material is somewhat pulled down, while for low velocities the weight of the material is more supported by the walls.

As it was already said, a first step in analysing stress data is to study whether the stress tensor is symmetric and the value of the normal stress ratio.

By looking at Figure 7.6, where the field of the normal stress ratio is contoured for two values of the particle-wall friction coefficient, it can be judged that the normal stress ratio

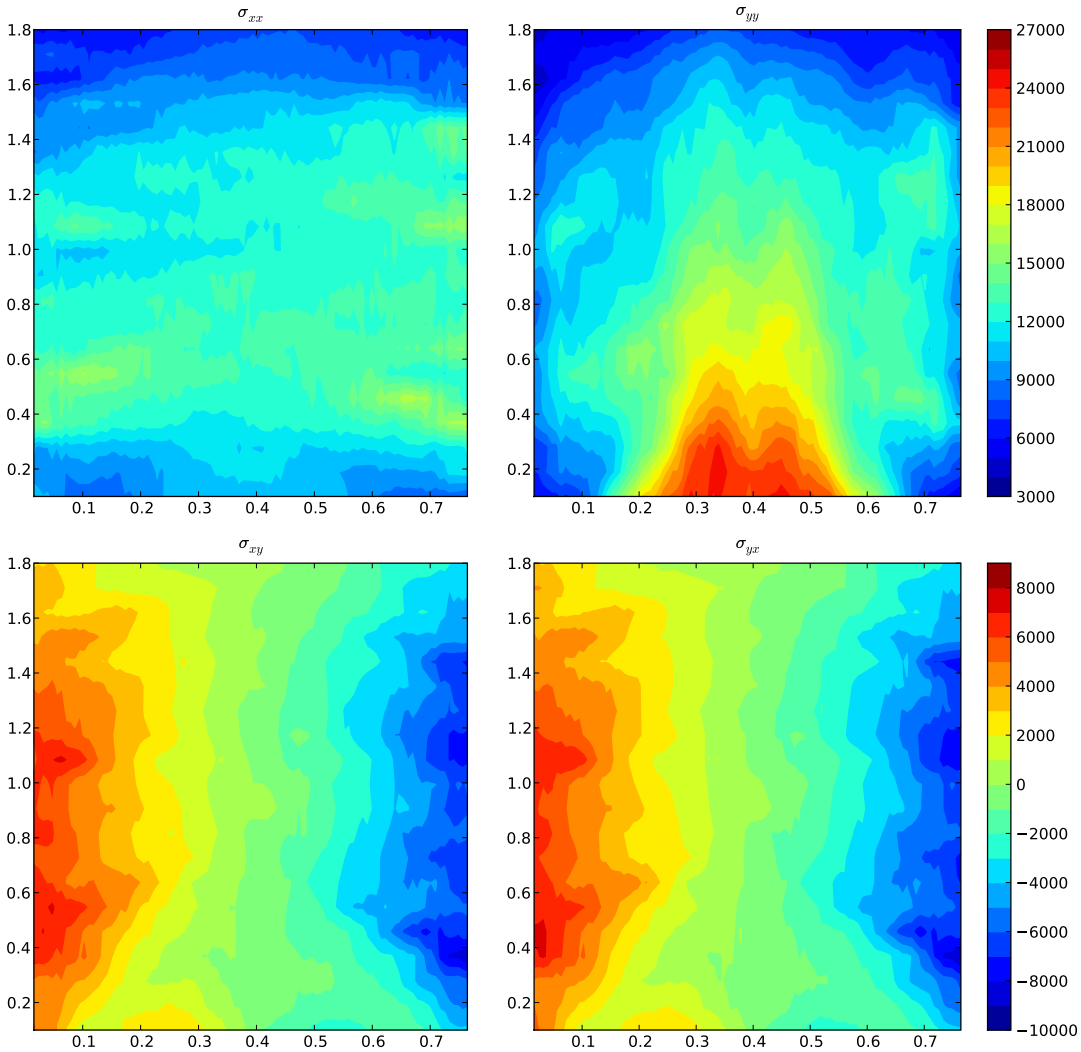

Figure 7.3: *Stress field obtained for* $v = 1m/s$, $\mu_{pw} = 1.0$.

is not uniform and takes values above and below 1. In fact, it is obvious that even for simple fluids the normal stress ratio in a non-fully developed flow is not a constant: for a generalized Newtonian fluid the normal stress ratio depends on velocity gradients, and only for a fully developed flow it is 1:

$$K = \frac{\sigma_{xx}}{\sigma_{yy}} = \frac{P + \tau_{xx}}{P + \tau_{yy}} = \frac{P - 2\eta\frac{\partial u}{\partial x}}{P - 2\eta\frac{\partial v}{\partial y}} \tag{7.13}$$

Therefore, when trying to gather rheological insights from analysis of the normal stress ratio, the existence of a non-fully developed flow is a complication which has to be carefully taken into account, and which should be avoided in future simulations with an higher channel height to width ratio. Regarding the effect of wall friction, Fig. 7.6 allows to recognize that frictional walls sustain the material while less frictional ones let the material to be supported more by the bottom. This fact is even clearer when looking at the princi-

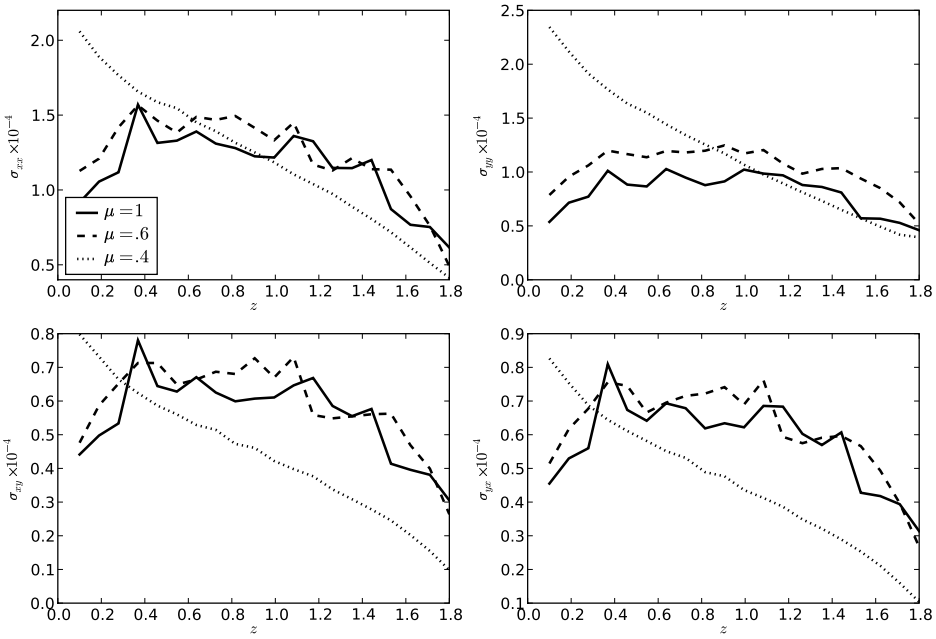

Figure 7.4: *Variation of wall stresses with particle-wall friction coefficient.*

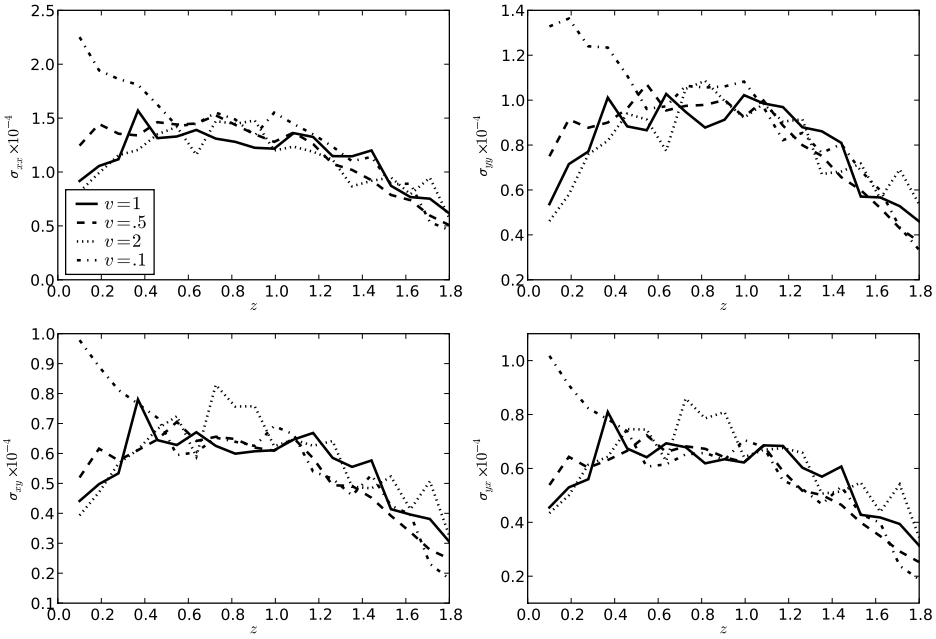

Figure 7.5: *Variation of wall stresses with flowrate, for the case with* $\mu_{pw} = 1.0$.

pal directions of stresses extracted from the simulations (Fig. 7.7).

Far enough from the top and the bottom, figure 7.8 allows to say for reasonably frictional walls and in the dense regime (not in the quasistatic) the normal stress ratio is approx-

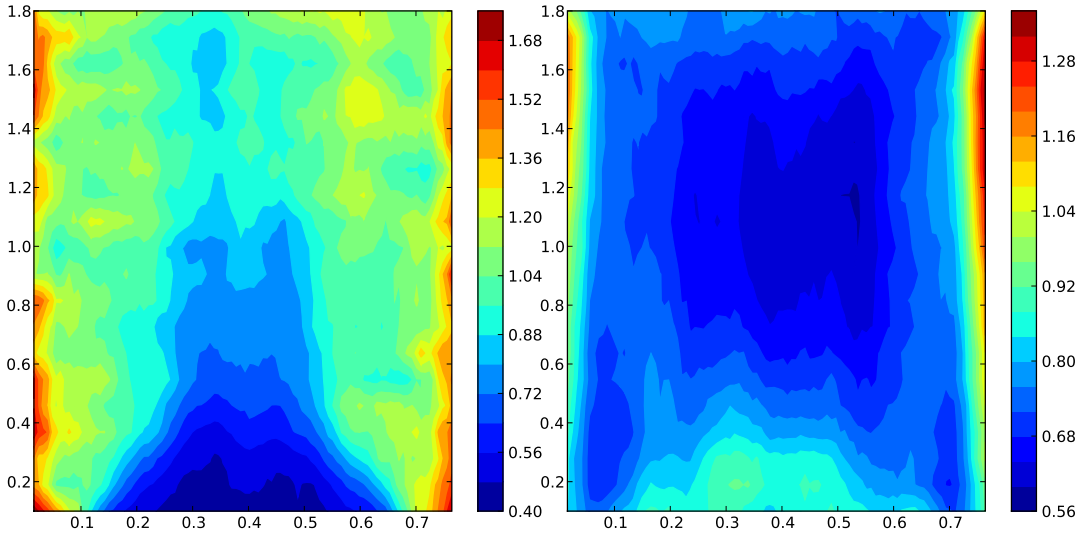

Figure 7.6: *Normal stress ratio for* $v = 1.$ *m/s and (left)* $\mu_{pw} = 1.0$*, (right)* $\mu_{pw} = 0.4$*.*

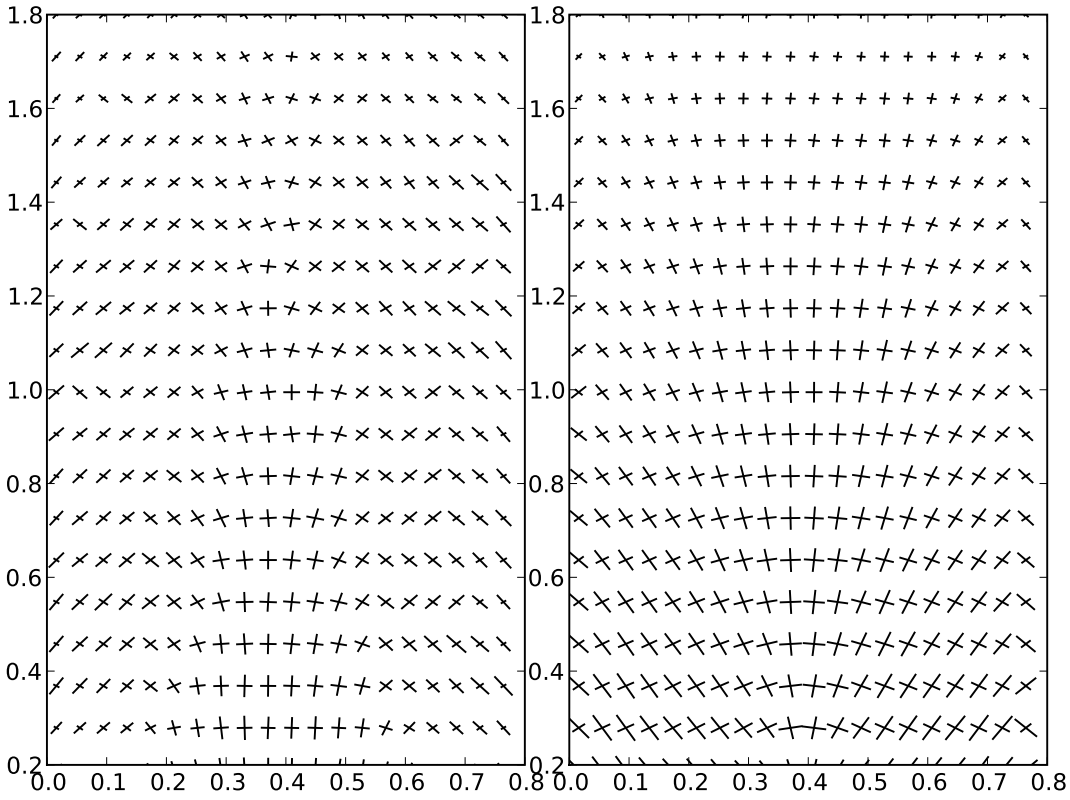

Figure 7.7: *Principal directions of stress for* $v = 1.$ *m/s and (left)* $\mu_{pw} = 1.0$*, (right)* $\mu_{pw} = 0.4$*. The x and y axis are not on scale.*

imately around 1. This results serve as a hint that the choice $\sigma_{xx} = \sigma_{yy}$ under many rheological models may be critical, and sometimes lose its validity; however, Fig. 7.8 seems to suggest that a region might exist where assuming the stress ratio as 1 is not a bad approximation.

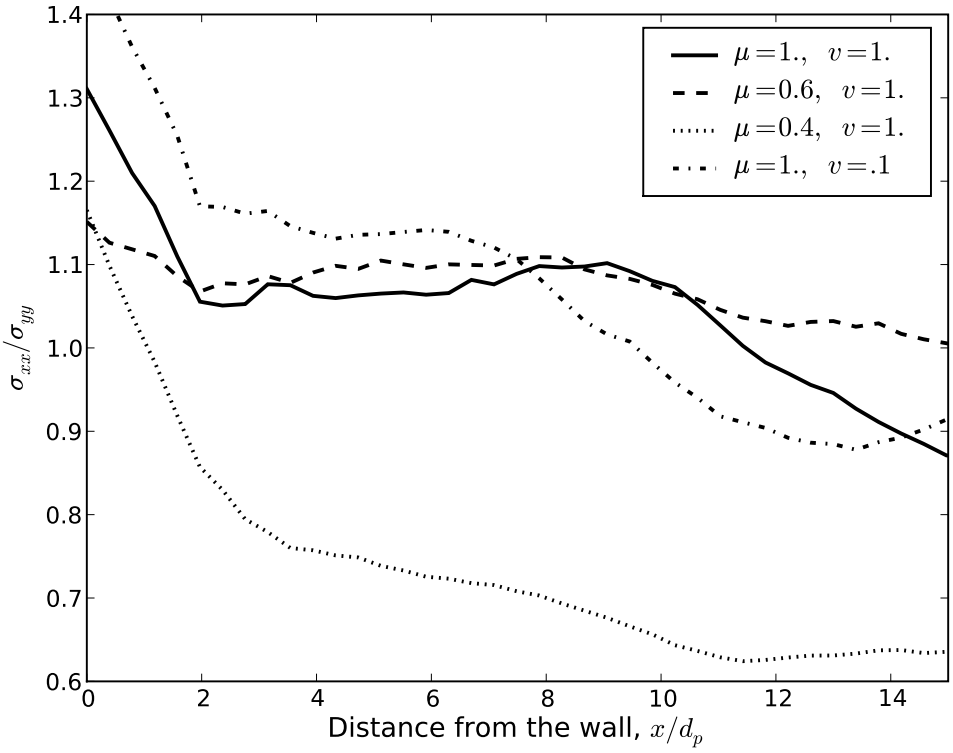

Figure 7.8: *Normal stress ratio profile far from top and bottom as a function of distance from the wall for different flowrates and particle-wall friction coefficient.*

On the other side, Fig. 7.9 displaying the ratio of the shear components of the stress tensor allowing to say that the stress tensor is within good approximation symmetric in the case under study. This seem to happen both when the flow is nearly well developed and when it is not (low values of the coefficient of friction), and seem not to depend on flowrate; therefore the assumption of symmetric stress tensor seems to be strong and general, at least in the case considered. This is a nice result confirming that hydrodinamic models may be - in principle - consistent with the problem of confined gravity-driven flow, because couple stresses are negligible. This does not mean that particles do not rotate, but that the medium is not able to transmit couple stresses, i.e. couple stresses are only local.

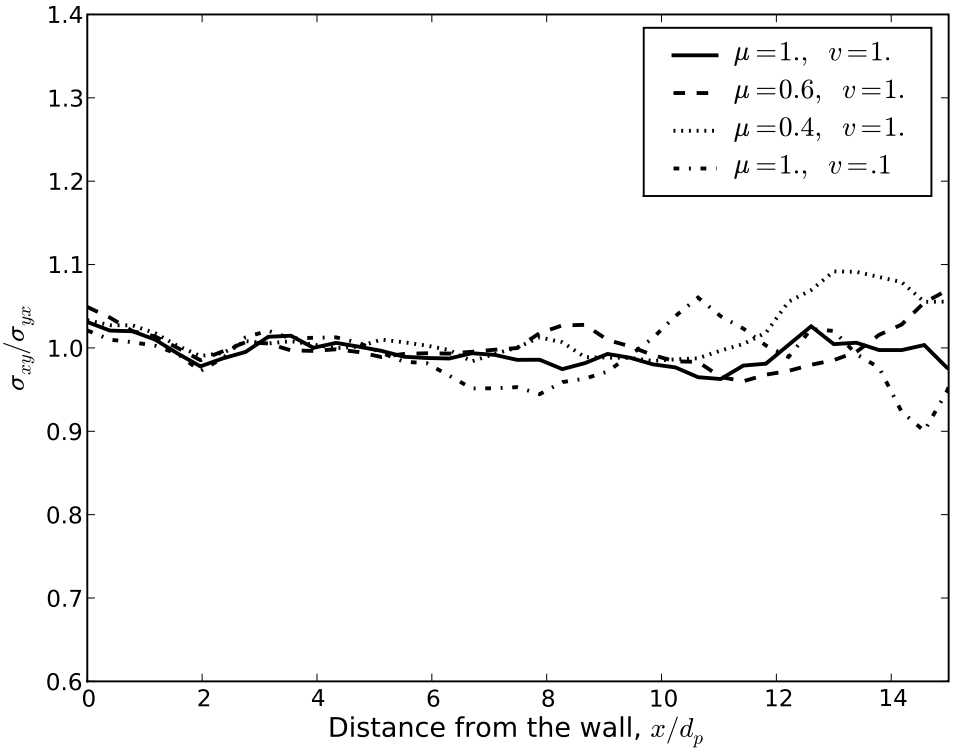

Figure 7.9: *Shear stress ratio profile far from top and bottom as a function of distance from the wall for different flowrates and particle-wall friction coefficient.*

7.5.2 Average profiles

In this section, average profiles of velocity, granular temperature, solid fraction are analyzed. From figure 7.10 one can appreciate that while variables as solid fraction and velocities are well developed in the center of the channel, granular temperature is not. A larger height-to-width ratio should be (probably) simulated in order to have well developed profiles (at the moment it is nearly 3 times high than large). This will be done in the future; to have an idea of the variations of profiles with the main parameters, in the following profiles will be evaluated in the middle, far enough from the top and the bottom.

From Figure 7.11 it can be appreciated that varying flowrate implies no change on the rescaled velocity profile, which means that the shear bands remain of constant width, in this case around 5 particle diameters. Even if the rescaled velocity has the same profile, it appears clearly that the medium in the shear band is more dilated the higher the flowrate. From the granular temperature profile it is possible to judge that not only the average temperature (not shown), but also the disproportion between the temperature a the wall and in the center of the channel increases when increasing flowrate.

The importance of wall friction is shown in figure 7.12: for low values of the wal friction

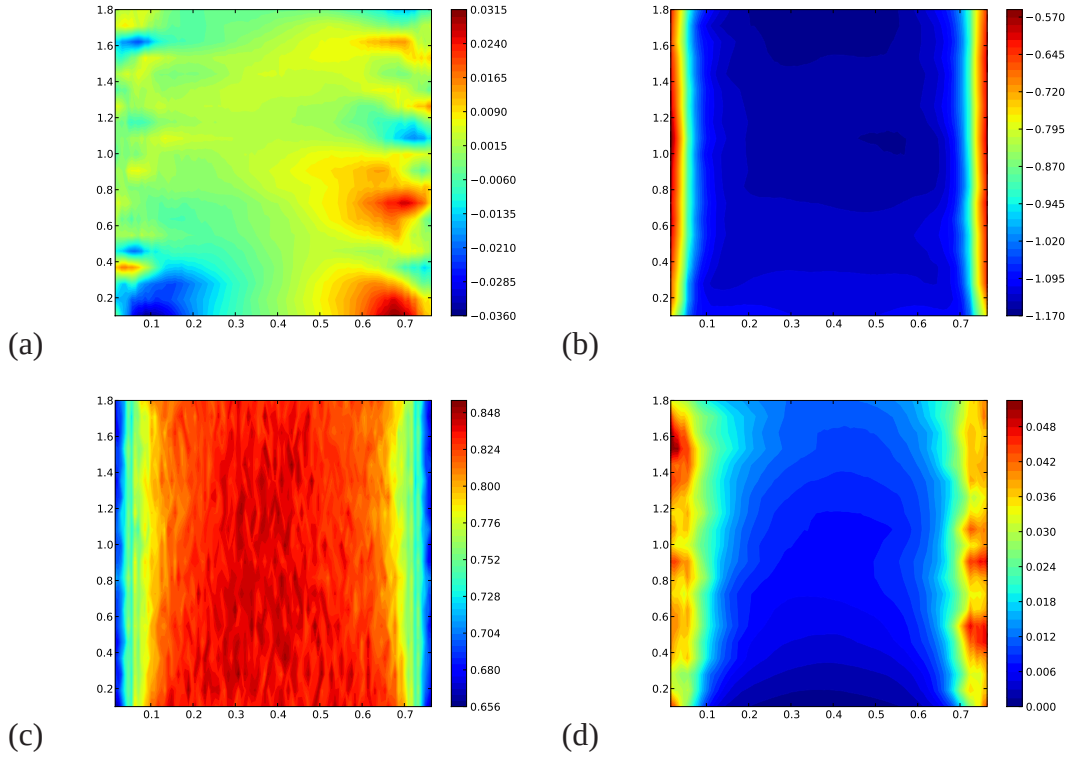

Figure 7.10: *Fields obtained for $v = 1.$ m/s and $\mu_{pw} = 1.0$: (a) horizontal velocity (b) vertical velocity (c) solid fraction (d) granular temperature.*

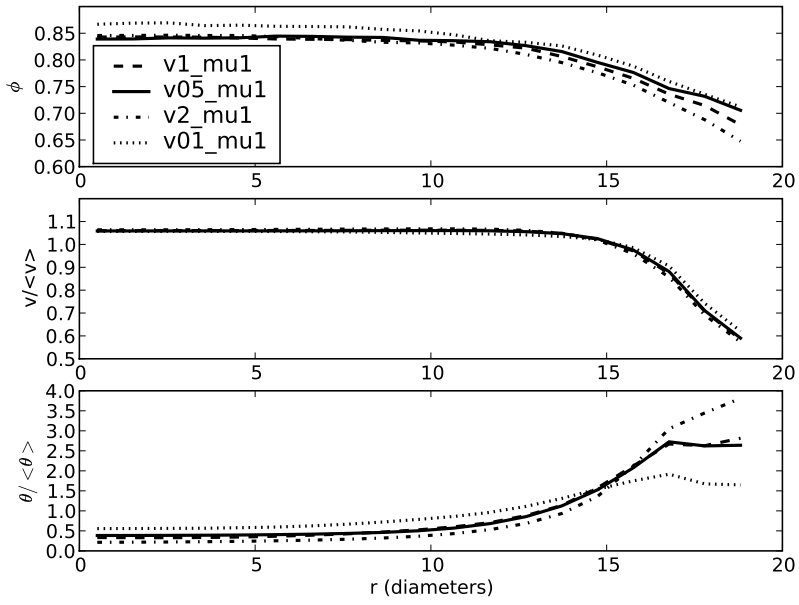

Figure 7.11: *Profiles obtained varying flowrate*

coefficient, the medium nearly experiences perfect slip, with flat velocity and temperature profile. The solid fraction is not constant in this limit surely because of geometrical

effects. Increasing wall friction has the effect of dilating the medium increasing ϕ in the shear band, but also increasing the shear band width. Finally, the higher the friction, the higher the average temperature (not shown) and the disproportion in granular temperature between the center and the walls.

Figure 7.13 offers a comparison between results obtained for disks with diameter $d_p = 0.02m$ and penthagons used in the other simulations. In this case, the shape of the particles seems to play a strong role on the shear behavior of the granular material: shear bands are larger for polygonal particles, and also more dilated. Rescaled temperature profiles are very similar, while the average temperature (not shown) is higher in the case with penthagons. This result strongly suggests that in order to gain accurate predictions from DEM methods for irregular particles researchers must deal with shapes different from the ideal ones (disks and spheres), because predicted profiles can be very different, as this is the case.

Profiles obtained varying the channel width are shown in Fig.7.14. It can be inferred

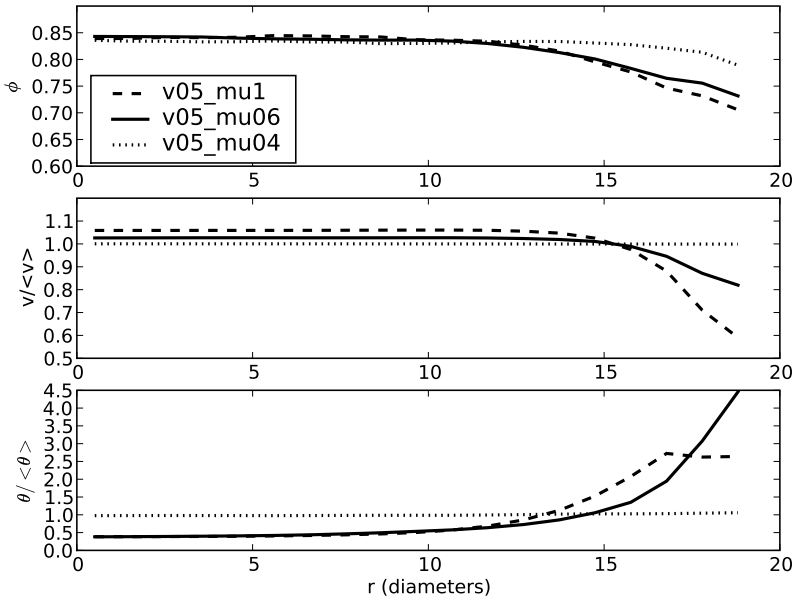

Figure 7.12: *Profiles obtained varying wall friction coefficient*

that the width of the shear band slightly increases as the channel width increases, and also the width of the dilated zone. This supports recent findings by Ananda et al. (2008), together with older experiments by Nedderman and Laohakul (1980), towards the idea that, though being generally limited to a size of ~ 10 particle diameters, the shear band has no universal size, but depends on the size of the system. Profiles obtained varying the gravitational constant are shown in Fig. 7.15. It is clear that increasing gravity of an order of magnitude has a negigible effect on the size of shear bands, while the global amount

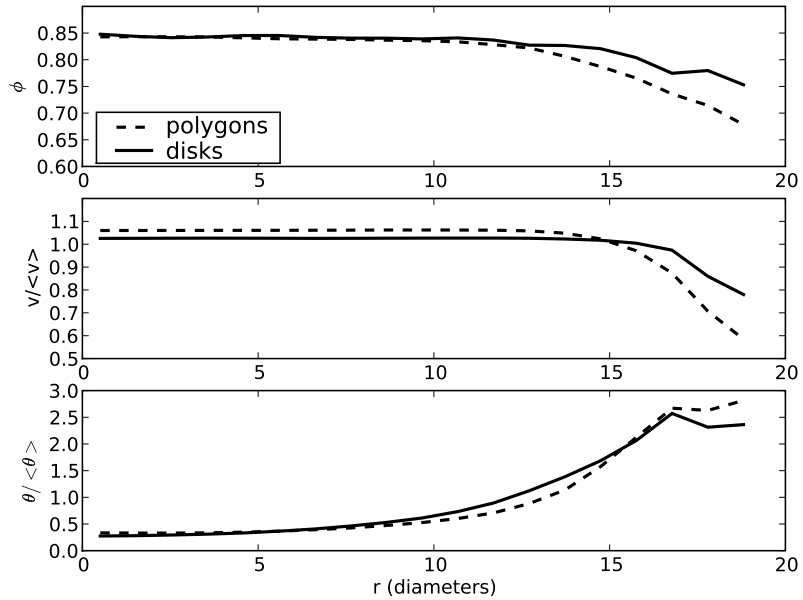

Figure 7.13: *Profiles obtained for disks and polygons*

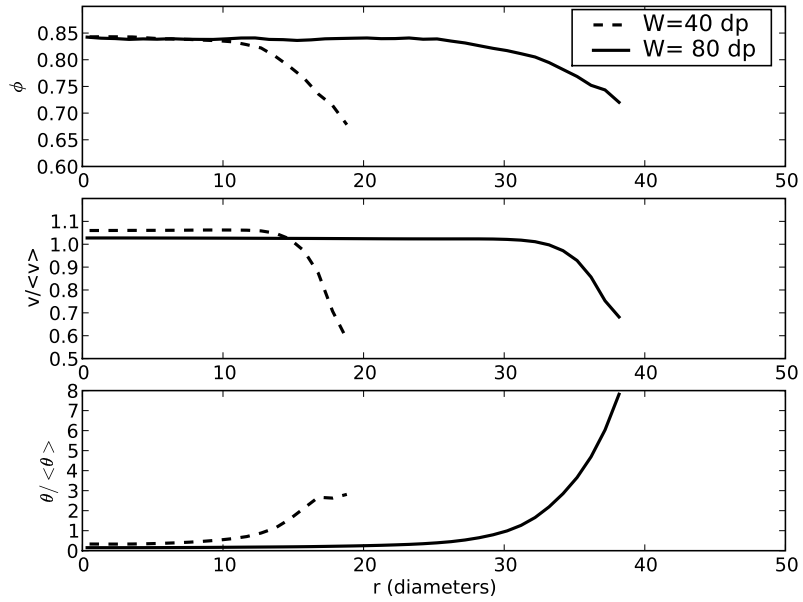

Figure 7.14: *Profiles obtained for different channel widths.*

of shear and the dilation decrease; increasing gravity in this geometry, where the flowrate is controlled, has the effect of increasing compressive forces thus reducing dilation (and pushing the inertial number I towards zero).

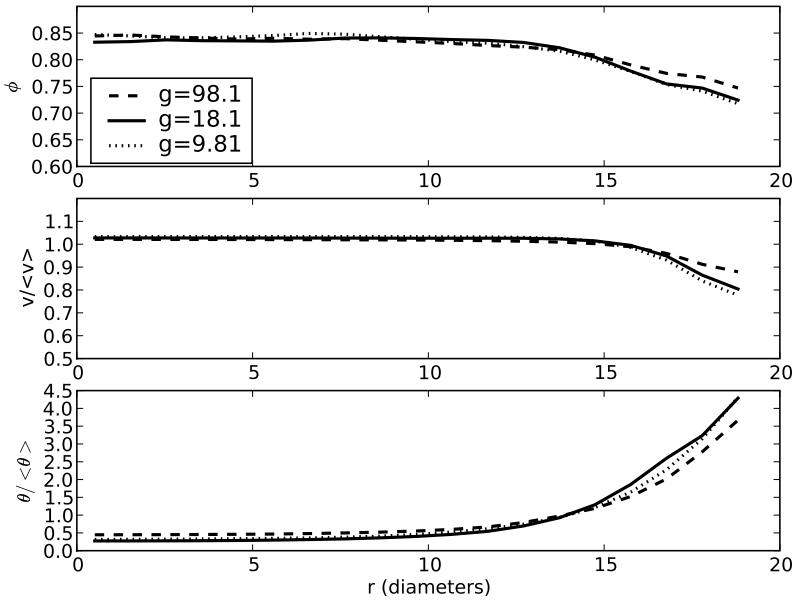

Figure 7.15: *Profiles obtained for different values of the gravitational acceleration.*

7.5.3 Pdfs of the velocity field

It can be interesting to have a look to the statistics of the spatially averaged velocity field in terms of probability density functions. In figure 7.16 variation of the pdf at different positions in the channel is displayed. It is clear that the two components of the velocity field behave differently: while generally the shape of the pdf is the same, symmetric around the mean value, and the variance is higher near the walls, the horizontal component pdf varies less than the vertical one, thus having a smaller variance near the walls, and a larger variance in the center. This can be due to "solid-like fluctuations", which reasonably can propagate better on the direction of the confinement. It is clear from this figure that characterising the fluctuating behavior only with the concept of granular temperature (which corresponds to a global variance not informing about the single components) is a simplification which reduces all the directional information contained in the pdf; wether or not this reduction is viable, it can be a matter of debate.

Variation of the pdfs with flowrate for a point near the walls is reported in fig.7.17. In this case the pdfs seem to vary in a similar way, with no further differences with respect to the preceding figure. Generally, as it was already stated about temperature profiles, the variance increases as the flowrate increases, because more shear is applied to the particles.

Variation of the pdfs with wall friction is displayed in fig.7.18. It appears clearly that increasing wall friction the variance of the pdf increases, the most important result being an abrupt change in the fluctuating behavior for low values of μ_w, with nearly negligible

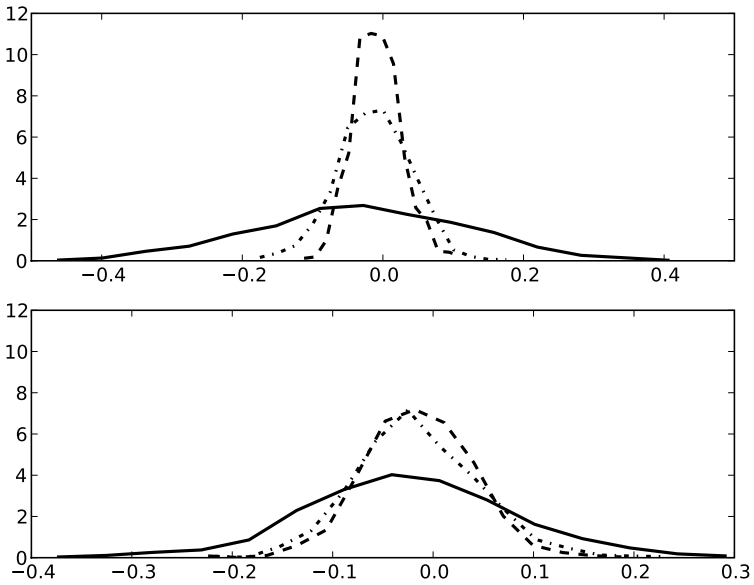

Figure 7.16: *Pdfs of the components of the locally spatially averaged velocity field at different transversal positions in the channel.*

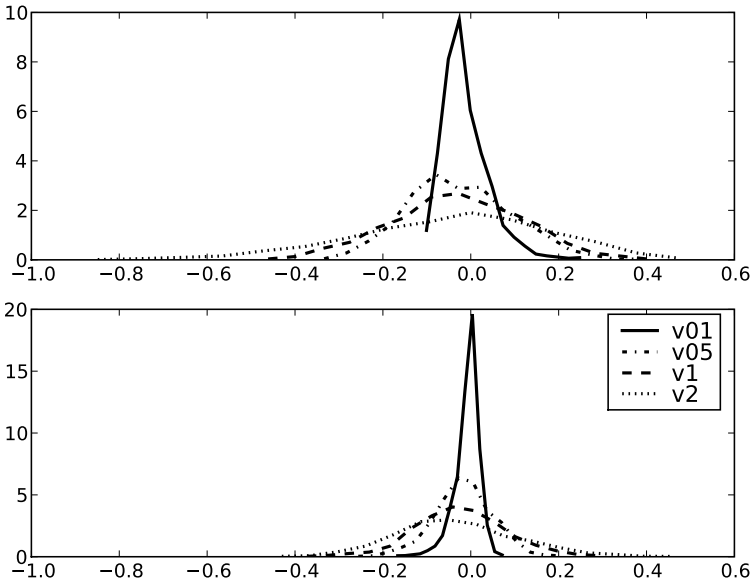

Figure 7.17: *Pdfs of the components of the locally spatially averaged velocity field for different values of the flowrate.*

fluctuations. In this case the material acts nearly as a solid body (as it can be seen also from time statistics). The pdfs obtained varying gravity are shown in Fig.7.19. It can be seen that increasing gravity of a factor 10 has not a strong effect on the pdfs, but however implies increasing the vertical component variance. Thus even if average shear (fig.7.15)

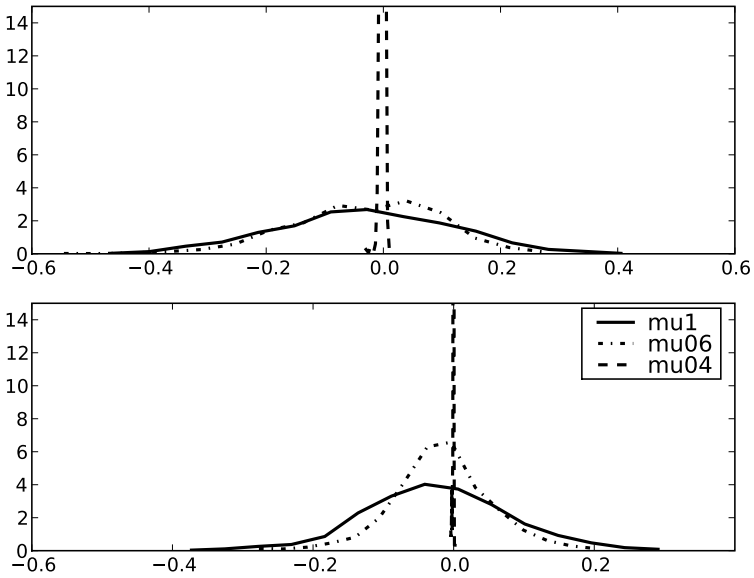

Figure 7.18: *Pdfs of the components of the locally spatially averaged velocity field for different values of the wall friction coefficient.*

is reduced, granular temperature increases. In fact gravity acts both on compressive and shear forces, thus it is probably the second effect which is more important in this case.

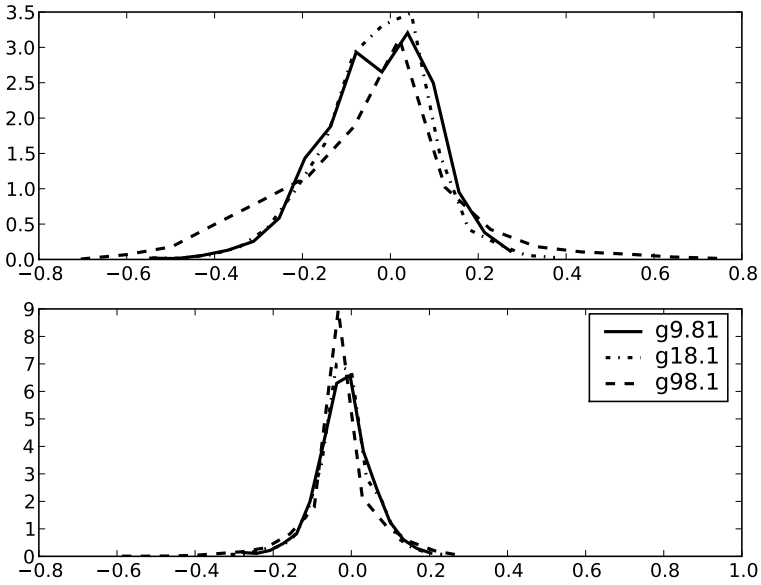

Figure 7.19: *Pdfs of the components of the locally spatially averaged velocity field for different values of the gravitational acceleration.*

7.5.4 Time statistics

Apart from studying probability distribution of the velocity field, it can be interesting to study time statistics, in order to understand how the velocity changes in time. Indeed, to characterise a random signal both the pdf and time statistics are needed. The following figures report autocorrelation plots, Generally, no great difference was noticed between the two components in term of autocorrelation, so in the following only one component (the vertical one) is reported. In particular, figure 7.20a shows the autocorrelation function for different flowrates, supporting the idea that the higher the flowrate, the fastest the process of losing memory of the past. In particular, for the lowest value of the flowrate, the correlation is significantly different; as it will more clear from the followig figure, this could be due to the fact that the higher the flowrate, the larger the distance from the solid like state, so memory of the velocity field fades out more rapidly.

The same informations can be extracted from figure 7.20b. When varying the wall friction coefficient, if walls are less frictional, the material loses memory in a larger time, because shear has less rearranging efficiency. Moreover, the effect of gravity is displayed in fig. 7.20c. Increasing gravity has the same effect of increasing shear, reducing the

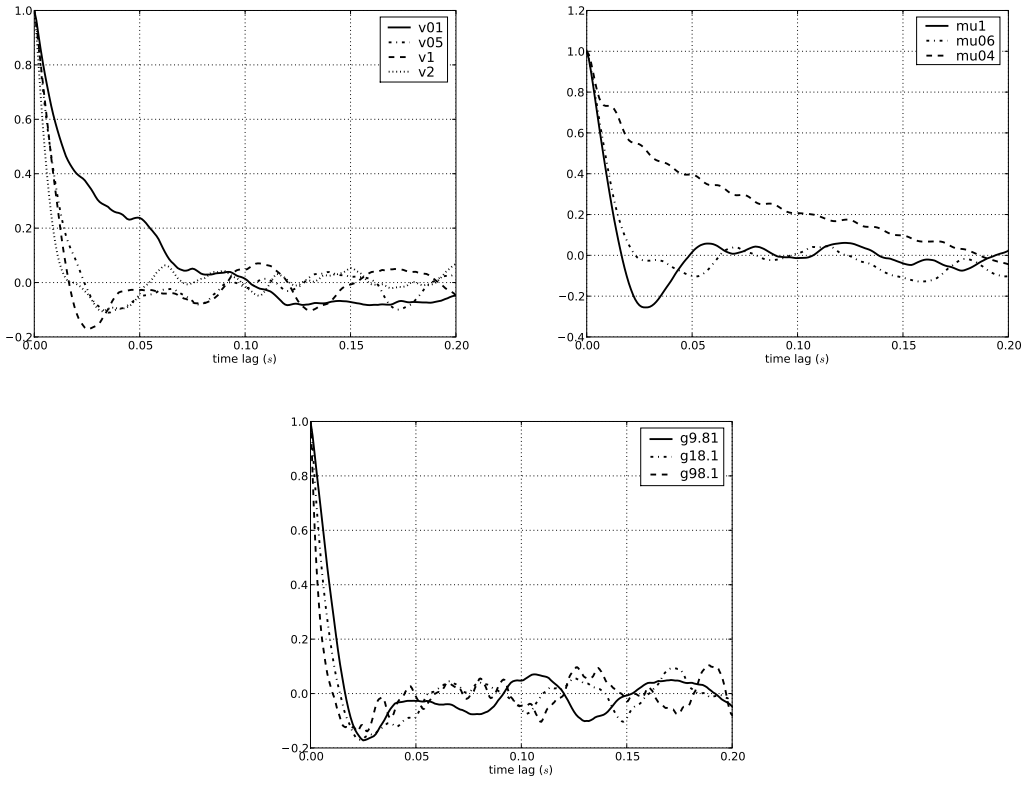

Figure 7.20: *Autocorrelation of the spatially averaged vertical velocity at a position near the wall, a) for different values of the flowrate, b) for different values of the wall friction coefficient, c) for different values of the gravitational acceleration.*

correlation time. As for the pdf, this could be due to the fact that gravity acts on shear forces also, thus increasing shear stress. These topics require further analysis in terms of stresses, which are not subject of the present work. However, it can be recalled that(Artoni et al., 2009b; G. D. R. Midi, 2004) two timescales can be defined for dense flows, the timescale related to shear $\tau_\gamma = |\dot{\gamma}|^{-1}$ and the timescale related to pressure rearrangements $\tau_p = \sqrt{\frac{m}{P}} \sim \frac{1}{\sqrt{g}}$. It is reasonable to assume that when gravity is larger, $\tau_p << \tau_\gamma$, such that τ_p is the controlling time scale, thus determining also the correlation time. Dependence of the correlation time on τ_p justifies the behavior displayed in fig.7.20c.

7.5.5 Boundary conditions

Generally, an issue which can be noticed in all the figures presented up to this point, is that strong slip appears at the walls; this is obvious, because the simulations deal with flat walls, but it is not obvious how this slip can be characterized from a continuum point of view. Data from all the 29 runs were used to gather informations about effective boundary conditions in the spirit of the ideas described in Chapter 4. A best-fit for functions $f_2(I)$ and $g(\mu^*/\mu_{pw})$ were estimated from the data to be :

$$f_2(I) = 0.004 I^{-1.317} + 3.146 I^{-0.138} \tag{7.14}$$

$$g(\mu*/\mu_{pw}) = \left(\frac{\mu*/\mu_{pw}}{1 - \mu*/\mu_{pw}} \right)^{0.524} \tag{7.15}$$

From figures 7.21 and 7.22 it can be appreciated that many different data collapse reasonably on two curves. The supposition that f_2 has a ~ -1 power law behavior for $I \to 0$ is confirmed together with the exponent tending towards 0 for high I. Divergence of $g(\mu*/\mu_{pw})$ for $\mu^*/\mu_{pw} \to 1$ is not denied by results, as well as tendence towards 0 for $\mu*/\mu_{pw} \to 0$. Results seem therefore to confirm that the slip velocity passes from scaling with pressure to scaling with shear rate:
This is only a first analysis indicating that the thoughts developed at the end of Chapter 4 may be a correct way to extend the results from the simple stochastic model to a large number of configurations. In the future, different functional forms should be tried, as well as different fitting methods, but first results seem encouraging. Work is currently being carried out on a different geometry, the inclined chute, for the same reason of collecting wall slip data: results will be used together with the ones presented here in the future. Together with DEM data also experimental data should be collected.

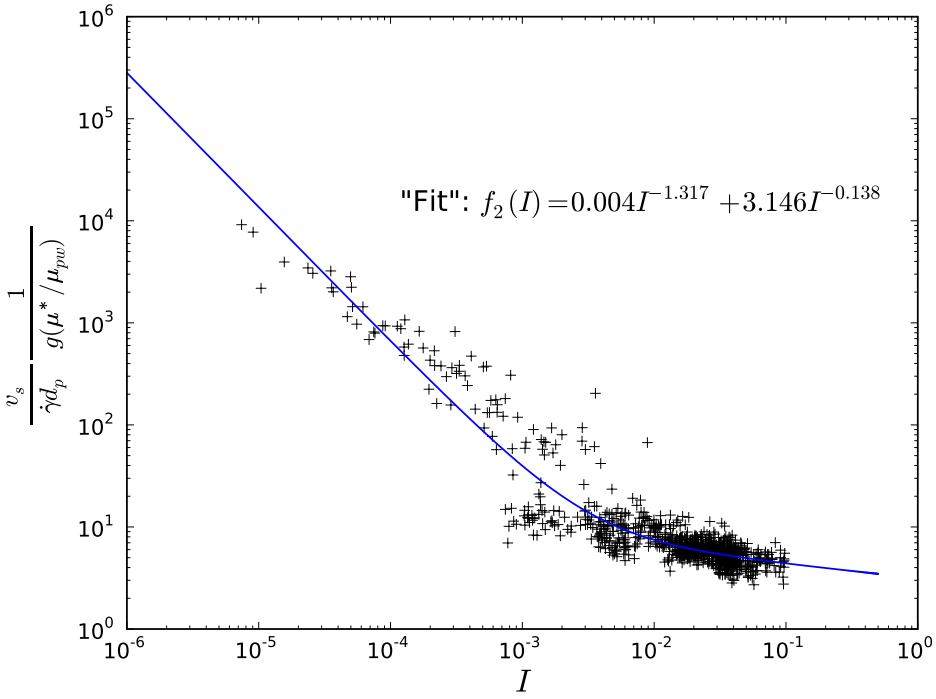

Figure 7.21: *DEM data (crosses) and fitting of $f_2(I)$ function.*

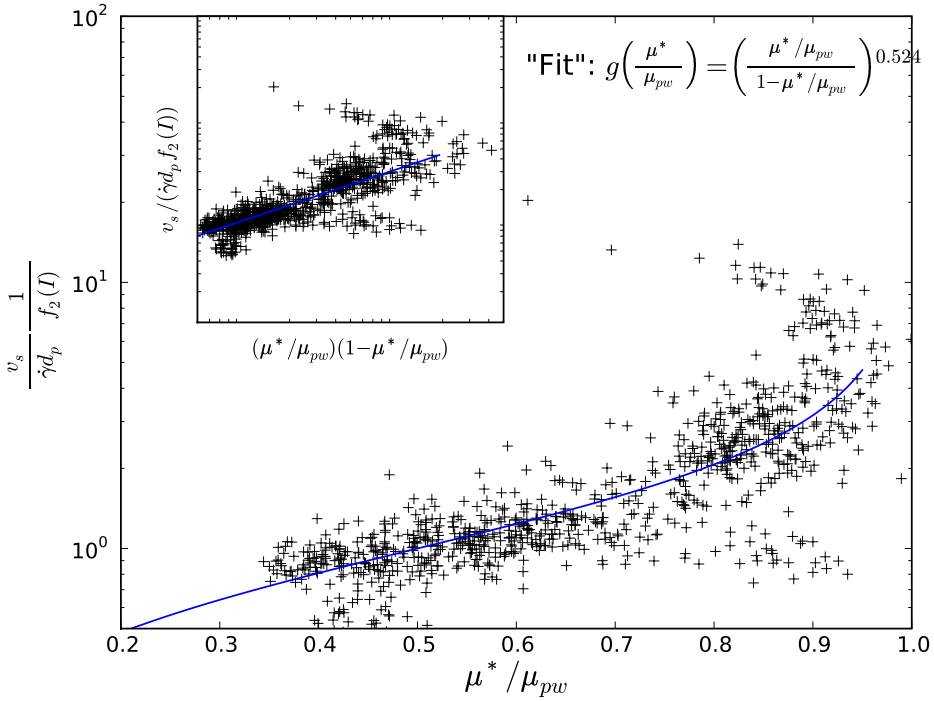

Figure 7.22: *DEM data (crosses) and fitting of $g(I)$ function.*

7.6 Rheology

Many rheological insights can be derived from the results obtained from DEM simulations. Regarding the structure of the stress tensor, it was already suggested that the results

support that the stress tensor is symmetric, and that the assumption of normal stress ratio equal to unity is somewhat questionable. Analyzing the stress-strain rate relationship, an usual assumption (Nedderman, 1992) is the colinearity of stress and strain rate tensor, i.e. the principal directions of stress and strain rate coincide (see also Chapter 3). By looking at Figure 7.23, one can judge that for the case with $\mu_{pw} = 1.0$, this is a reasonable assumption, which seems however to fail in the regions where the orientation changes (for example in Fig. 7.23(left), passing from a zone near the walls with stresses oriented at 45^o, to a zone near the bottom with principal directions aligned with the boundaries).

Among the recent attempts, the simplest rheology using the principle of colinearity is the

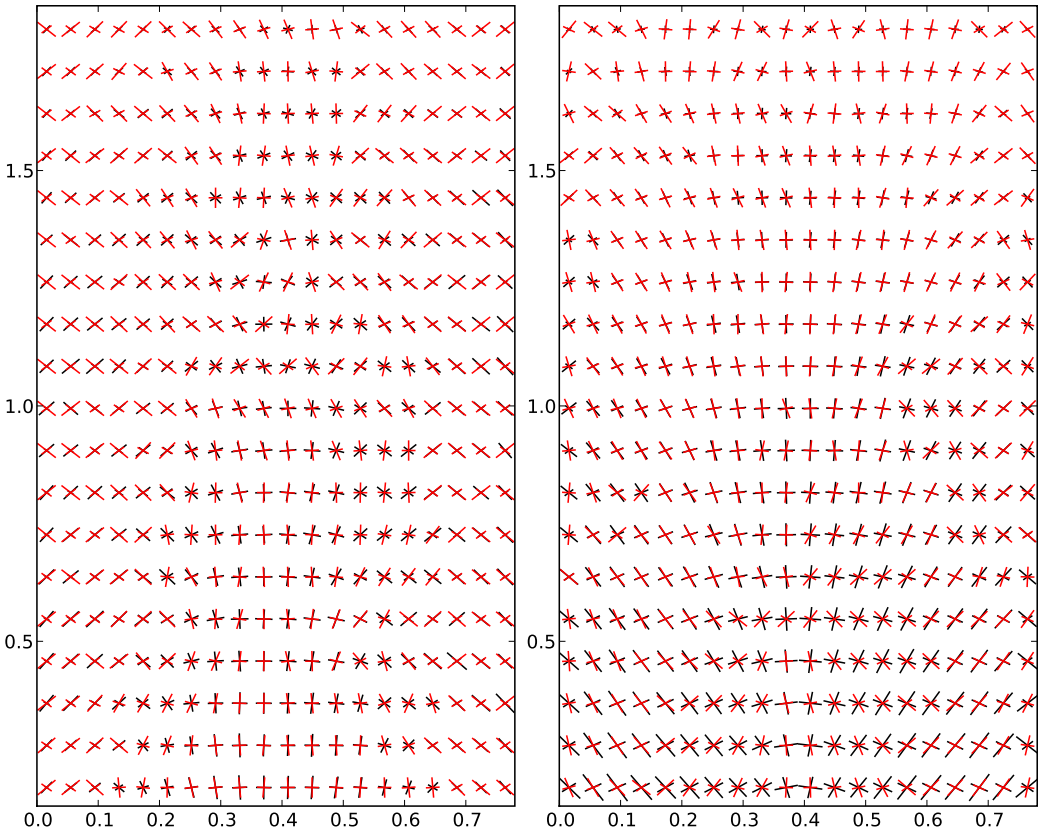

Figure 7.23: *Principal directions of stress (black) and strain (red) for $v = 1.$ m/s and (left) $\mu_{pw} = 1.0$, (right) $\mu_{pw} = 0.4$. Due to the large variations, the principal components of strain are not on scale. Also, the x and y axis are not on scale.*

model proposed by Jop et al. (2006), which extended the $\mu^*(I)$ rheology (G. D. R. Midi, 2004) in three dimensions by means of the law:

$$\sigma_{ij} = -P\delta_{ij} + \tau_{ij} \tag{7.16}$$

$$\tau_{ij} = \frac{\mu^*(I)P}{\dot{\gamma}}\dot{\gamma}_{ij} \tag{7.17}$$

where γ_{ij} is a component of the strain rate tensor and $\dot{\gamma}$ is the shear rate. To test this simple rheology, Figure 7.24 shows the function $\mu^*(I)$ extracted from the data. The typical shape suggested by Jop et al. (2006) for the function is obtained, but the fact that data do not collapse on a single curve seem to suggest that the phenomenology contained in the inertial number is correct but not sufficient to treat the problem of vertical chute flow of granular materials. Figure 7.25 displays solid fraction vs the inertial number. Here,

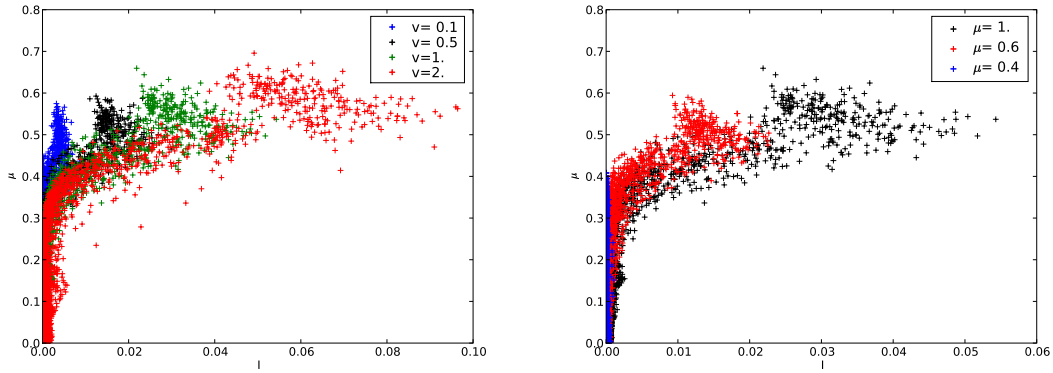

Figure 7.24: *Effective friction coefficient μ^* as a function of the inertial number I for (left) $\mu_{pw} = 1.0$ and different flowrates and (right) $v = 1.0\ m/s$ and different wall friction coefficients.*

the linear dilatancy law proposed by the GDR MiDi (G. D. R. Midi, 2004; da Cruz et al., 2005) seems not to hold, particularly in the shear band, where the shear is higher. Solid fraction appears not to be a function of I alone, as μ^*. It appears that also regarding solid fraction the phenomenology contained in the GDR MiDi's model is correct, but not complete. To complete the framework, probably issues regarding of the normal stress ratio should be addressed(Renouf et al., 2005); however, due to the fact that the assumptions of $\sigma_{xx} = \sigma_{yy}$ and of colinearity of stress and strain rate tensor are not always violated, it is possible that an extension in the direction of the inclusion of fluctuating energy dynamics into the phenomenology as it was done in Chapter 3 is not fully uncorrect. In order to test the validity of the fluctuating energy model, it was looked for a dependence of the shear stress on the remaining variables of the system. Here the scaling of the model extended to treat hysteresis in dense granular flows is adopted,

$$\tau \sim \rho d_p^2 \dot{\gamma}^2. \tag{7.18}$$

To test the validity of the approach, a first step is to look for a function of the granular temperature $f(\theta')$ such that

$$f(\theta') = \frac{\tau}{\rho d_p^2 \dot{\gamma}^2} \tag{7.19}$$

where $\theta' = \frac{\theta}{g d_p}$ is a (tentative) dimensionless granular temperature. Figure 7.26 displays the dependence of $\frac{\tau}{\rho d_p^2 \dot{\gamma}^2}$ on the rescaled temperature, showing that, even if all the simula-

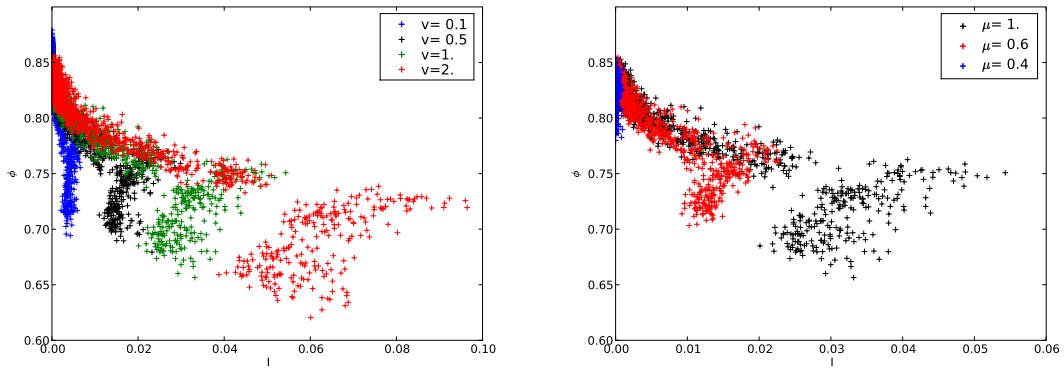

Figure 7.25: *Solid fraction ϕ as a function of the inertial number I for (left) $\mu_{pw} = 1.0$ and different flowrates and (right) $v = 1.0\ m/s$ and different wall friction coefficients.*

tions share a similar power law behavior, curves do not collapse on a master curve. When

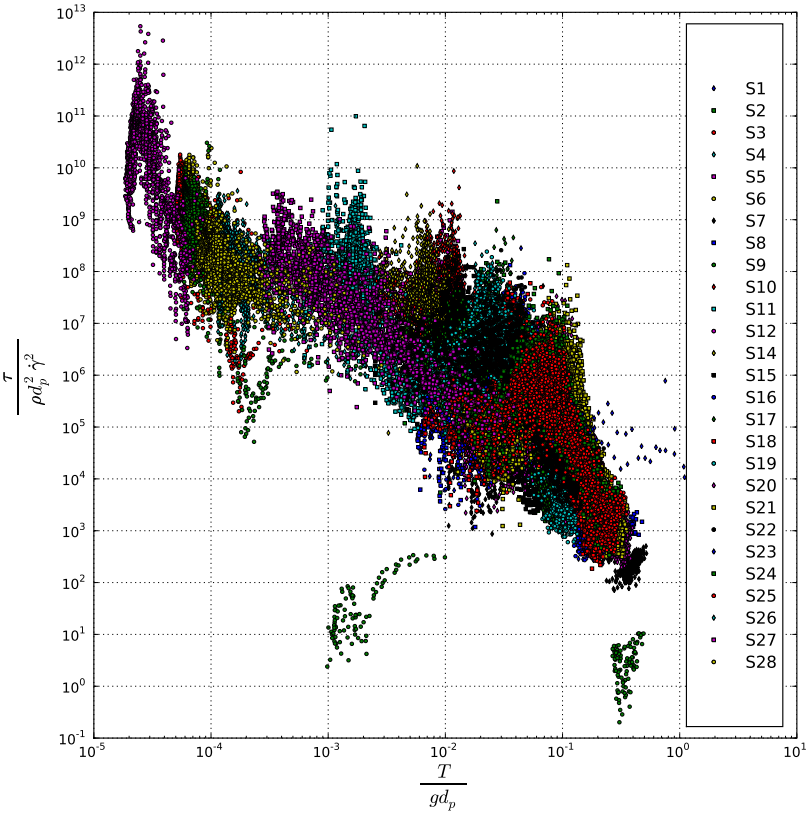

Figure 7.26: *Dependence of dimensionless shear stress on dimensionless granular temperature, extracted from DEM simulations.*

discussing about hysteresis in inclined chute flows, it was supposed that a yield stress exists, dependent on the trace of the stress tensor, $\tau_Y = \mu_Y p$. With this assumption, the

function of the granular temperature to be estimated is given by:

$$f(\theta') = \frac{\tau - \mu_Y p}{\rho d_p^2 \dot{\gamma}^2}, \quad \text{for } \tau > \mu_Y p \tag{7.20}$$

As it is displayed in Figure 7.27, where μ_Y was roughly estimated from figures similar to Figure 7.24 to be nearly 0.37, rescaling the stres subtracting the yield stress allows to obtain a behavior which is not too far from a power-law master curve. The collapse of data on a single curve supports not only the need for rescaling with a yield stress, but also the correctness of scaling on particle diameter (which however would require further simulations being that only one test with a different d_p was performed, test S23) and on gravity (results from tests S14,S15 deviate from the master curve if $\theta' = \theta/gd$ is not choosen as a scaling for temperature). A rough estimate of the function $f(\theta')$, plotted in figure 7.27, can be a simple power law:

$$f(\theta') = 10 \left(\frac{\theta}{g d_p} \right)^{-1.75} \tag{7.21}$$

From the analysis developed it seems also that, being the stress tensor approximately symmetric, a "Cosserat" extension (including the dynamics of angular momentum) should not be correct for the vertical chute configuration. Therefore results from numerical simulations seem to confirm the capability of the fluctuating energy approach in characterizing the rheology of dense granular flows, supporting the assumptions made in the development of constitutive relations for the stress tensor. Checking the validity of the assumptions made on the diffusion and dissipation of fluctuating energy remains a challenge for the future requiring to push forward the averaging methods in order to compute not only velocity, solid fraction, granular temperature and the stress tensor, but also fluxes and generation/dissipation rates of fluctuating energy. Based on the analysis given in this section, constitutive relations suggested in Chapter 3 coud be update with the new findings.

7.7 Comparison with modeling results

It would be interesting to calibrate the parameters of the rheological model on the numerical simulations as for the experiments performed in Chapter 6. At this moment only a qualitative comparison will be given, and a full validation is let for future investigations: due to convergence problems a slightly different law for the stress tensor was adopted,

$$\tau = \rho d_p^2 \dot{\gamma} A \left(\frac{\theta}{g d_p} \right)^{-3} \tag{7.22}$$

where the scaling of viscosity on the shear rate and the presence of a yield stress were dropped out. Such a relationship appeared to be globally as a reasonable approximation

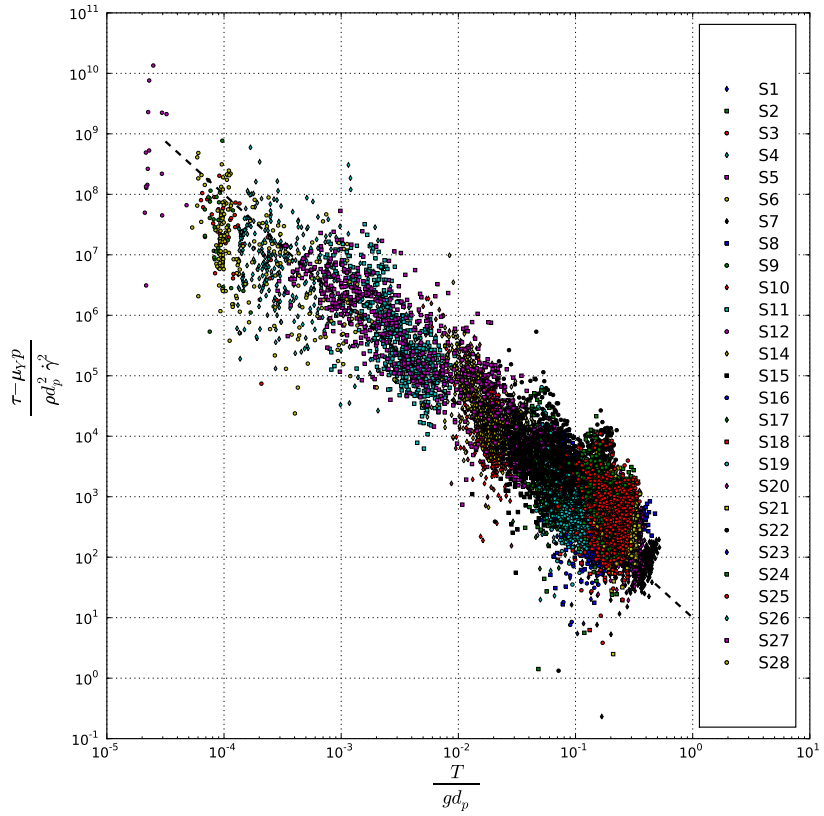

Figure 7.27: *Dependence of dimensionless shear stress distance from yield stress on dimensionless granular temperature, extracted from DEM simulations.*

from DEM simulations. As for the boundary conditions, it was choosen for simplicity to model partial slip with Navier's relation.

In figure 7.28 wall (normal and tangential) stress profiles are shown for a tentative choice of the parameters and for different values of the slip length and compared with the simulation with $\mu_{pw} = 1.$, $v = 0.5$ m/s (in which the slip length was verified from numerical simulations to be around 5 particle diameters). Regarding comparison with DEM, while the shear stress is in good agreement, the normal stress is not. This means that the effective wall friction coefficient is different in the two cases: parameters in the model have to be better tuned in order to recover the profile. Being that profiles share the same shape, it seems not impossible to recover a good quantitative agreement. Apart from the comparison, it is possible to see that the model correctly predicts the effect of reducing wall friction as it was verified in DEM simulations, with stress profiles tending to be linear. The effect of varying the outlet velocity on wall stresses is reported in Figure 7.29. In the range of velocity considered, for high enough velocity, stresses do not depend on flowrate, while for low velocities stresses increase in the whole geometry, keeping the

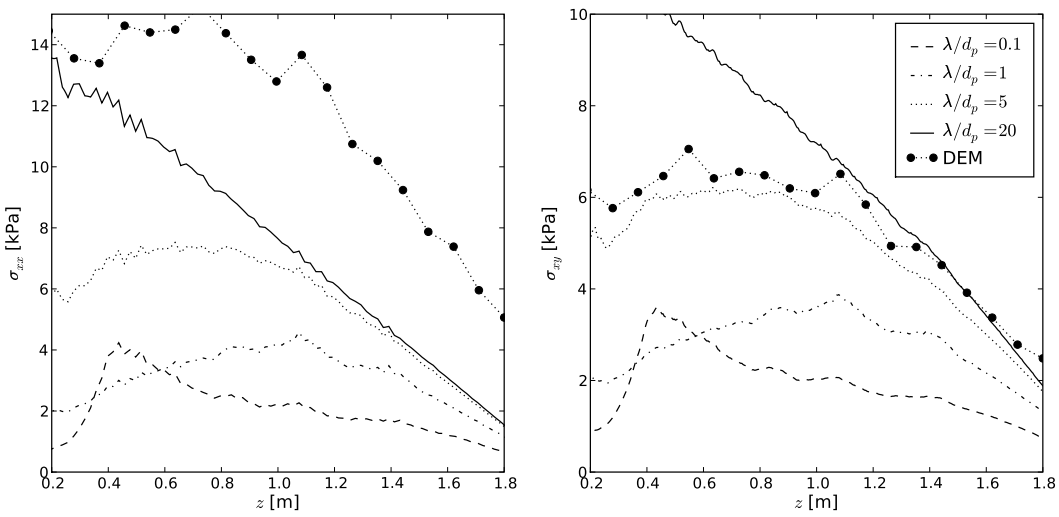

Figure 7.28: *Wall normal stress (left) and wall normal stress (right) obtained from the rheological model for different values of the slip length and* $v = 0.5$ *m/s.*

same qualitative profile. From DEM simulations, it is not possible to extract informations confirming this behavior; on the contrary it seems that stress does not depend on flowrate. Simulations with a smaller flowrate should be carried out in order to verify if the model correctly predicts increasing of stresses at low velocities. However, being that stresses depend strongly on the boundary conditions used, for a full comparison correct boundary conditions should be implemented. As regards velocity profiles, the model predicts

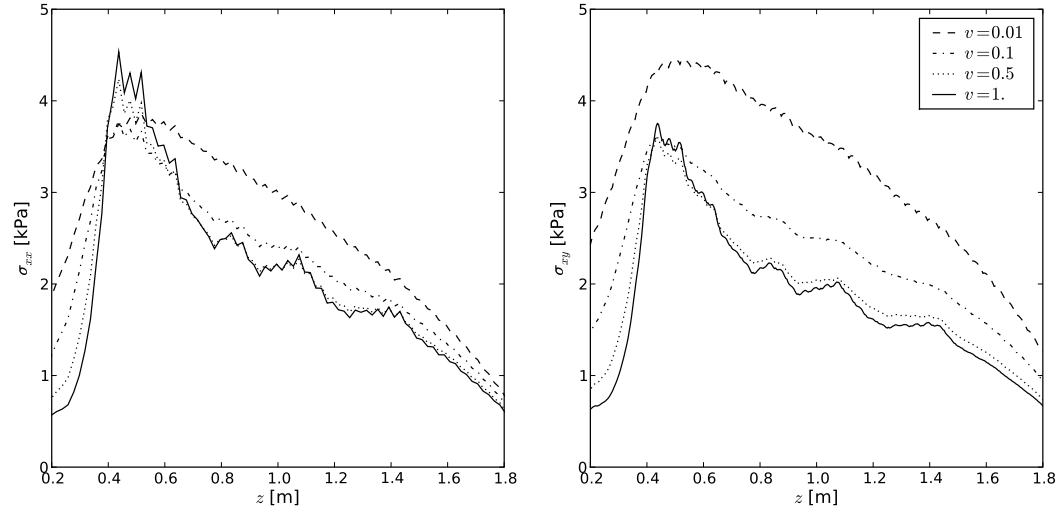

Figure 7.29: *Wall normal stress (left) and wall normal stress (right) obtained from the rheological model for different values of the exit velocity, for* $\lambda/d_p = 0.1$.

a plug flow with shear bands near the wall, whose width is reported in Figure 7.30 as a function of the outlet velocity and for different values of slip length. It is clear that, as for stresses, the limit $v \to 0$ implies a qualitative change in the shear band, which appears to

grow when reducing flowrate. For high velocities the shear band width reaches a plateau. Being that only a qualitative comparison is made at the moment, the velocity at which the plateau is reached and the absolute width of shear bands predicted by the model are not an interesting information: tuning the parameters can surely affect these results. Also this behavior does not correspond to DEM data, which showed shear band independence on flowrate. In fact this independence is commonly reported in Literature; therefore this seems to be a drawback of the model. However recent results (see Chapter 8) seem to cast some doubt on the absoluteness of shear band independence on flowrate. Again, DEM simulations for very low flowrates could be very useful in better understanding this topic. The model correctly predicts, then, the effect of wall friction on the shear band width.

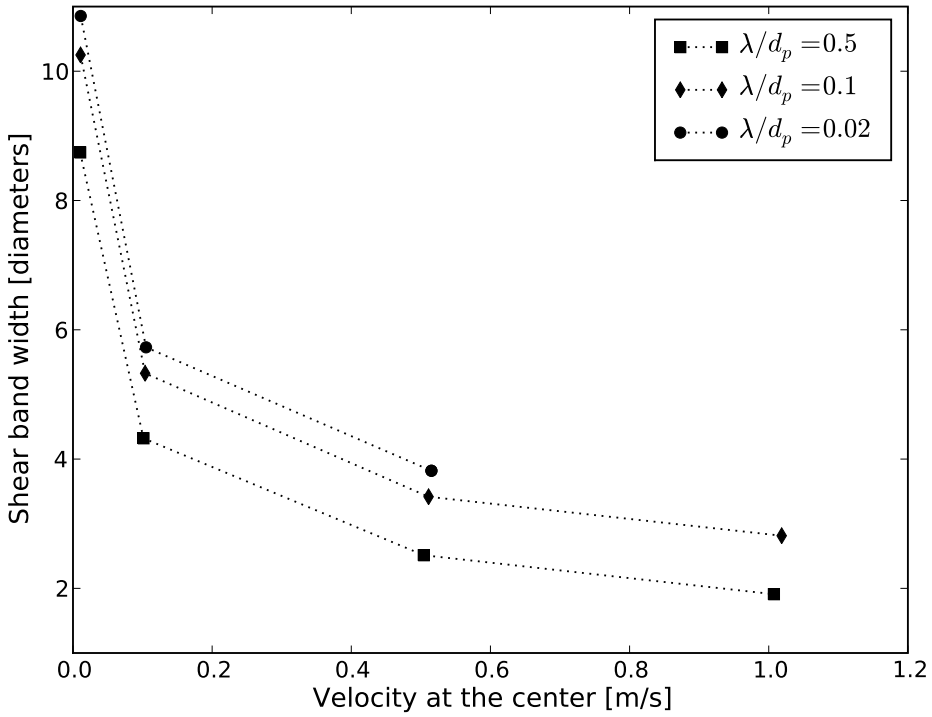

Figure 7.30: *Shear band width obtained for the rheological model as a function of outlet velocity for different values of the slip length.*

7.8 Conclusions

In this chapter, results from DEM simulations of flow of polygons in a vertical chute were presented. An open source discrete element code, LMGC90, was used, with an efficient strategy to control flowrate. First stress and flow profiles for different wall friction coefficient, flowrates, channel widths were obtained, with interesting results consistent with

available data. The effect of particle shape was also evaluated. Then the data were used to provide insights for the rheology and the boundary conditions. It seems that the rheological model developed in Chapter 3 is approximately consistent with the results presented, particularly regarding symmetry and colinearity of the stress tensor, dependence of the constitutive relation on granular temperature, effect of wall friction on wall stress and flow profiles. Regarding the effect of flowrate, the model seems not to behave correctly, but further investigation is needed. Data were also used to extract informations for the boundary conditions, seeming to confirm the extended description involving dimentsional analysis given in Chapter 4.

Chapter 8

Experiments on dense flows in a vertical chute

O nimium coelo et pelago confise sereno,
Nudus in ignota, Palinure, iacebis arena.

Virgilio,*Aen.* VI 870-1

8.1 Introduction

As it was often discussed in previous chapters, though many experiments were performed on the flow of granular materials in vertical channels(Nedderman and Laohakul, 1980; Natarajan et al., 1995; Ananda et al., 2008; Pouliquen and Gutfraind, 1996), it seems that the width of the shear band and the wall slip behavior remain somewhat far from being fully explained. Moreover, the topic of gas-solid flow which was studied in Chapter 5 should be experimentally investigated in simple geometries. For this reason it was choosen to build a vertical chute suitable for granular flow and gas-granular flow experiments. The practical realization of the experimental set-up was done by an undergraduate student (Anzelini, 2009) who gave an important contribution to the research. This chapter briefly describes some research which is currently under development, summarizing the first results. The main features of the set-up are presented, then the analysis technique briefly described, finally first results are summarized. At this moment, only granular flow is studied, and gas-solid coupling will be subject of future research. Even if the research outlined in these pages is mainly preliminar, it seems interesting to describe the first findings in order to oultine perspectives for the future work. In addition, first results of velocity profiles are encouraging and inspiring and, though needing further confirmations, they

seem to be of sufficient interest to put them here.

8.2 Experimental method

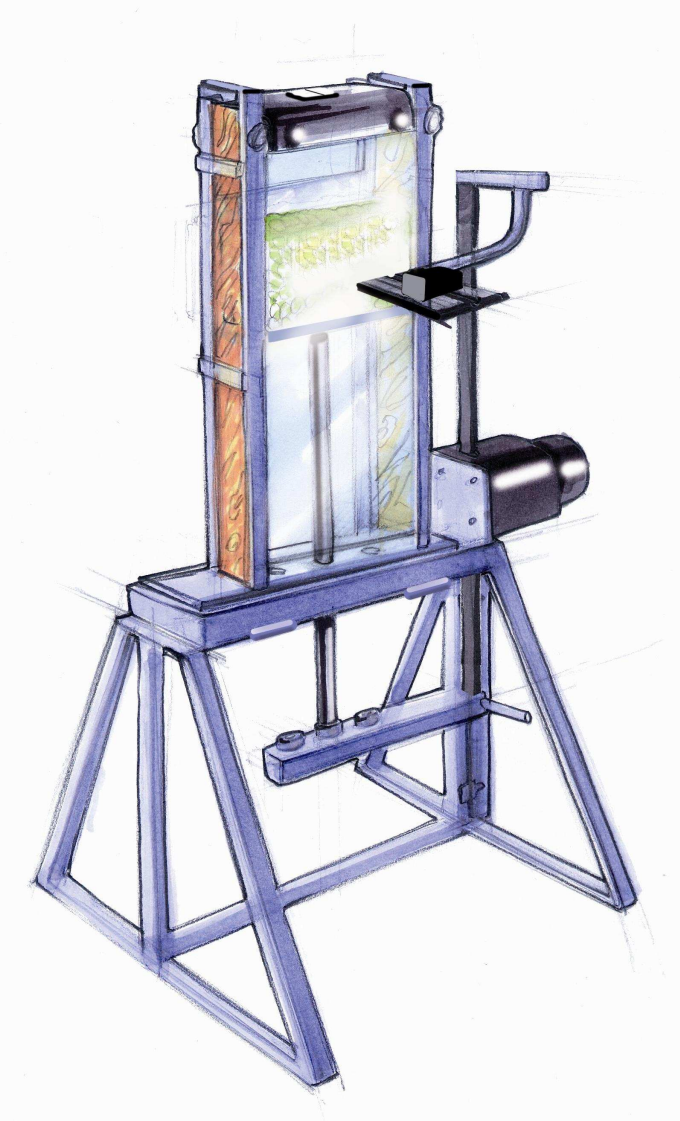

Figure 8.1: *Picture of the experimental set-up(Anzelini, 2009)*

The experimental set-up consists of a vertical chute (shown in Fig. 8.1) where motion of the material was controlled by means of a moving plate. An electric motor equipped with a linear reducer was used to control the velocity of the plate. As shown in the calibration curve, Fig. 8.2, the velocity range spanned nearly on two orders of magnitude, from 0.025 to 2.2 cm/s, being therefore an excellent instrument to test the material behavior in a wide range of flowrates. The channel had a variable width (10-20-30 cm) and a variable thickness (15-30-45 mm). Lateral wooden walls were roughened with 40 and 120 grit sandpaper. A campaign was made with particles of different materi-

als and size; here results from iron beads will be presented, with the characteristics described in Table 8.1. Velocity profiles were computed using Particle Image Velocimetry

diameter [μm]	710
static repose angle [^{o}]	32.27
wall friction angle (wood) [^{o}]	31.5
wall friction angle (g40) [^{o}]	47.7
wall friction angle (g120) [^{o}]	39.0

Table 8.1: *Properties of the material used for experiments.*

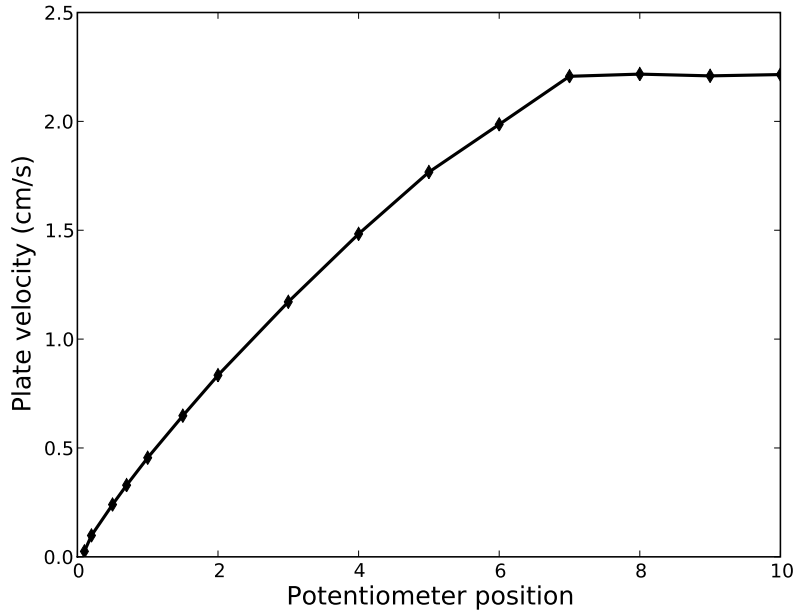

Figure 8.2: *Calibration curve of the velocity control system.*

(PIV); the PIV analysis was performed by means of the freely available code Matpiv (http://www.math.uio.no/ jks/matpiv/), which is a toolbox for Matlab. The CCD camera (mvBlueFox) was set at 25 fps to capture 100 images 1128x532 large, which were acquired with Matrix Vision's software wxPropView and then processed (cropped, resized, subsequently analyzed) in Matlab.

8.3 Results

Results from the first experiments performed on the set-up (december 2009) are reported in the following. It is important to stress that these results are preliminar (refinement of both the experimental procedure and the image analysis is needed), but are reported here because of some nice findings which open new perspectives for the future. Regarding the

experimental set-up, the vertical chute proved to be an efficient facility allowing to gather a lot of data in little time.

Velocity profiles obtained for iron beads varying flowrate are displayed in Figure 8.3. A wide range of velocities was realized, finding the same plug flow + shear bands behavior for all the velocities. The shear band was found to be of order 6-10 particle diameters, and its dependence on flowrate will be discussed in the following.

Regarding shear bands, a wel known issue which was discussed also in previous chapters

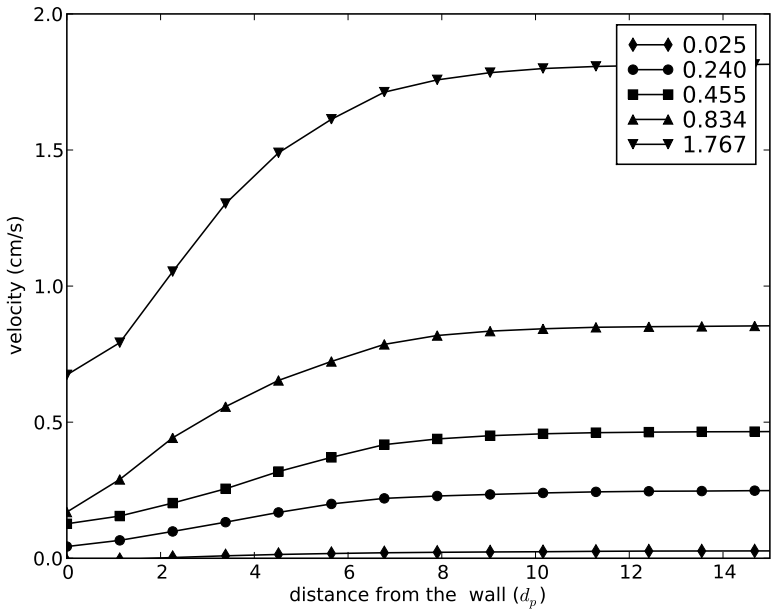

Figure 8.3: *Velocity profiles obtained for iron spheres, for different plate velocities, width of the channel 100 mm, wall roughened with 40 grit sandpaper.*

is their dependence on channel width. Resuming, some researchers(Pouliquen and Gutfraind, 1996) report data showing that the shear band is independent on channel width, while others(Nedderman and Laohakul, 1980) found a slow increase in shear band widh when increasing channel width. Looking at figure 8.4, which shows velocity profiles varying channel width (10-20-30 centimeters corresponding to 140, 280 and 420 particle diameters), it can be noticed that the data suggest a different behavior, with the smallest channel having the largest shear band. Then, due to mass conservation issues, being that the shear band has a limited size, the slip velocity is lower the smaller the channel width. This result appears to be new, and should be further investigated in order to understand its validity. When varying wall roughness, this has obviously a strong effect on both the slip velocity and the shear band width. Figure 8.5 shows that the slip velocity changes by more than a factor 2 passing from wooden to 40 grit sandpaper walls. To well understand the results regarding shear bands, the width of the shear bands is summarized in Figure

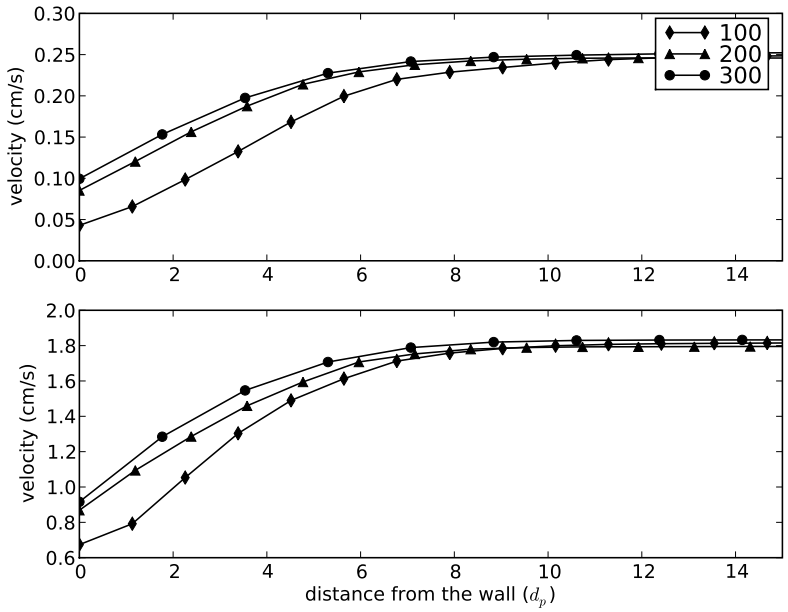

Figure 8.4: *Velocity profiles obtained for iron spheres, varying channel width, with the wall roughened with 40 grit sandpaper.: (top) mean velocity 0.24 cm/s, (bottom) mean velocity 1.77 cm/s.*

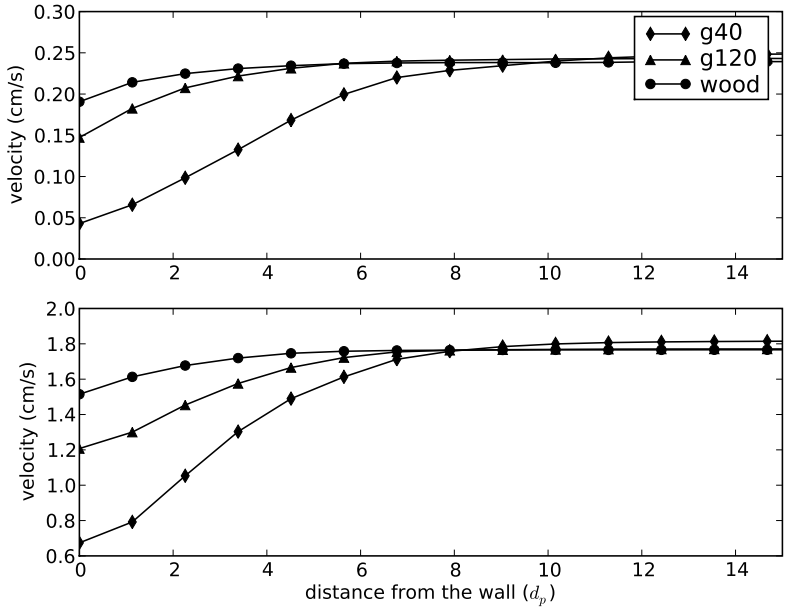

Figure 8.5: *Velocity profiles obtained for iron spheres, varying wall roughness, width of the channel 100 mm: (top) mean velocity 0.24 cm/s, (bottom) mean velocity 1.77 cm/s.*

8.6 for all the tests performed. The shear band width was defined as:

$$x \left| \frac{v(x) - v_{min}}{v_{max} - v_{min}} = 0.95 \right. \tag{8.1}$$

Figure 8.6 suggests as a first important result that the shear band width depends on flowrate, for low enough velocities, while for higher velocities a plateau is found. If these results are confirmed, this would mean that in the quasistatic limit shear bands are larger than in the dense regime; this is important in view of the fact that the shear banding behavior in the quasistatic limit was taken as a benchmark for continuum models, as described in Chapter 2. The constance of shear bands for high velocities supports the idea that a Coulomb-like boundary condition applies there, if the analysis held in Chapter 2 is valid. The change in shear band width with flowrate is not negligible (nearly a factor 1.5), though being shear bands limited around 10 particle diameters. In fig. 8.6 it can be appreciated also the effect of wall roughness and channel width, which was already described. The last step in analyzing results is the study of the boundary condition, which

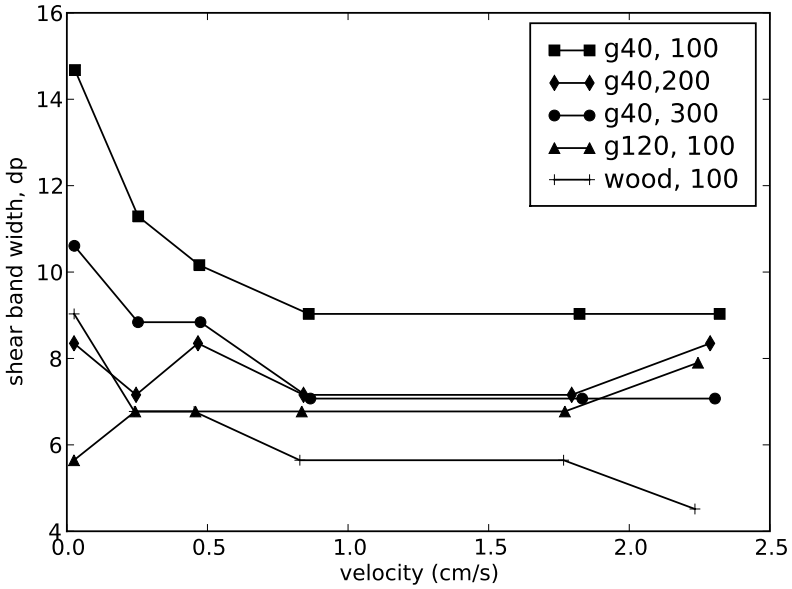

Figure 8.6: *Width of the shear band calculated from velocity profiles, for different channel widths and wall roughness.*

was evident from experiment to correspond to a partial slip boundary condition. Lacking stress measurements for the moment, the only way to characterize the slip behavior is with a Navier relationship. The slip length was calculated from the experiments as

$$\lambda = \frac{v_{slip}}{\partial_x v} \tag{8.2}$$

Figure 8.7 points out that the slip length spans from 5 to 20 particle diameters, increasing slowly with flowrate, depending on wall roughness (wood showing generally a slip length double than sandpaper). The figure suggests also that refinements to the velocity computation strategy are needed: for example a clear dependence on roughness is not found,

probably because of errors induced by the calculation of the derivative. Therefore future investigations, if interested in the computation of the slip length, should somehow take care in obtaining a smooth velocity gradient field. However, experiments like these may be useful to obtain reasonable estimates of the slip length (at least as an order of magnitude) to be used in solving continuum models of dense granular flow. The behavior of the slip length for low velocities (changing abruptly for some tests) could be a signature of the tendence to a no-slip boundary condition in the quasistatic limit, therefore suggesting further refined investigations.

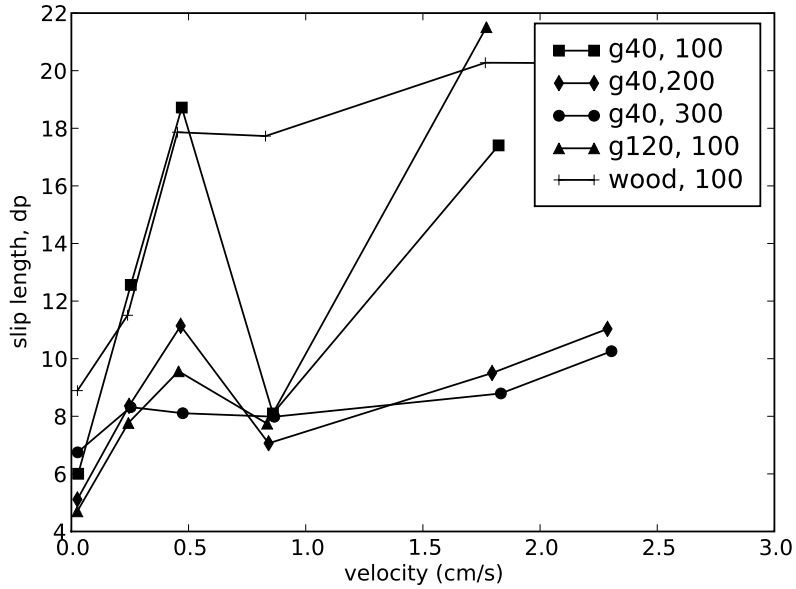

Figure 8.7: *Slip length calculted from velocity profiles, for differentt channel widths and wall roughness.*

8.4 Perspectives

In this chapter, first results from experimental data of flow of iron beads in a vertical channel are presented. Though being preliminar, data seem to show interesting behaviors suggesting to continue refining the analysis. On one side, shear bands were found to take values around 10 particle diameters and to be independent on flowrate only for velocities more than 1 cm/s while in the slow limit an increase was observed, which was not previously reported in Literature. Also the dependence on channel width seemed to be non trivial, with larger shear bands for lower channel widths. The expected dependence on roughness was found. Regarding slip velocities, the slip length was found to be increasing with flowrate, somewhat supporting the idea that a Navier slip relation with constant λ can be a good approximation of slip behavior for a wide range of flowrates, but also that

a different approach, such as the one developed in Chapter 4, would probably give better results.

Chapter 9

Conclusions and Perspectives for future works

Lass' andere auf Trampelpfaden
mit Steinchen hinterher
Wir werden was wir sind, und:
Ende Neu

Einstürzende Neubauten, *Ende Neu*.

9.1 Summary

This thesis was focused on the rheology of dense granular flows, and devoted primarily to the development of a rheological model, which was tested in some configurations against experimental and numerical data. Starting from the analysis of the performance of a simple mixing length rheology proposed in Literature (G. D. R. Midi, 2004) in a vertical chute (a quasi-2D simplification of a silo), it was immediately clear that improvements to the phenomenology were necessary. Refinements were needed not only to the rheology itself, in order to improve the too simple phenomenology contained in the model, but also to the treatment of boundary conditions, in order to allow the models to be applied to realistic flow configurations, and in view of the strong impact of the boundary condition on the global performance of the model which was experienced.

Based on these considerations, the research followed two parallel lines. The first dealt with the development of a new rheological model for the dense flow of granular materials; among the approaches present in Literature, it was choosen to develop a hydrodynamic model of granular flows, i.e. a model in which the equation of balance of *fluctuating energy* is solved for granular temperature, which enters in the constitutive relations defining

the stress tensor. This choice was motivated by analogies with the theory of the viscosity of liquids, and other approaches were discarded due to (supposed) not fully clear physical significance of the parameters of the model or on Literature's criticisms. It was considered that improvements could come from the introduction in the model of the dynamic interplay between mobility induced by shear and jamming induced by pressure's rearranging action. At first, the model was compared with typical flow configurations such as a silo with converging hopper and a silo with flat bottom, showing after a sensitivity analysis on the parameters a quantitative agreement with literature correlations for stresses and experience on the flow pattern. The flat bottomed silo allowed to say that the model predicts also the formation of stagnant zones. After some reworking, the model was also used to study the flow down an inclined chute, showing excellent predictions on qualitative features of that typical configuration of flow, such as the hysteresis of starting and stopping angles, the typical scaling of the velocity field, and the dependence of the cited angles on the flow depth.

The topic of boundary conditions was addressed by means of a simple stochastic model of the behavior of particles at the wall. Already in the application of the fluctuating energy model a simple expression for partial slip was adopted, Navier's boundary condition. By means of the results obtained from the simple stochastic model, it was possible to give a general formulation of the boundary condition to be applied at a smooth frictional wall, in terms of a relationship between a dimensionless slip velocity and an effective wall friction coefficient. The formulation describes the intermediate behavior between no-slip (for no sliding) and Coulomb slip (for steady sliding), when particle motion at a wall is unsteady due to force fluctuations. A thorough investigation based on dimensional analysis was initiated suggesting possible further dependency of the BC on the inertial number, allowing to understand the implications of the previous analysis. It was also shown that the boundary condition developed was consistent with a Navier approach once a mixing length rheology was assumed.

Then, the domain of application of the rheology was extended to situations in which a gas is injected in the material but the material remains below the fluidization threshold (like in drying processes, in moving bed reactors, et cetera), drawing a third research line: a further step was made in considering coupling of the rheology with interstitial gas flow, with a particular focus on gas maldistribution; at first an approach was developed based on a mixing length model for the solids and Ergun correlation for the gas, allowing for the effect of shear-induced solids dilation on preferential paths in the gas. Theoretical results showed that the approach is able to qualitatively capture variations in maldistribution and their dependence on process parameters; it was shown how to derive global (in terms of a

bypass percentage) or specific (using the RTD of the system) measures of the maldistribution.

In order to validate the model on an industrial configuration, an experimental campaign was carried out with an industrial partner on a pilot scale silo. For the scale-up of the silo, original scaling considerations were employed. Then experiments on wall normal stresses and tracer profiles were collected for configurations with and without internal devices, and with and without injection of air. Experimental results gave interesting insights on the effect of air and of the internal devices on both the flow and stress field. Data were used to calibrate the parameters of the fluctuating energy model, which was shown to be in good agreement with them. In order to simulate the effect of air injection, previous considerations were employed, extending them to treat three dimensional gas flow and using the fluctuating energy model as a rheology instead of the mixing length model.

In order to well characterize rheology on a local scale, discrete simulations of flow of slightly polidispersed polygons in a bidimensional vertical chute were also performed, and analysed extensively in order to understand the effect of varying the main parameters on flow and stress patterns, and to extract informations concerning both boundary conditions and rheology. Regarding the effect of process parameters on profiles, typical results were found such as the independence of shear bands on flowrate, and their slight dependence on channel width. Regarding boundary conditions, the extended approach involving a similarity relationship between a dimensionless slip velocity, the effective wall friction coefficient and the inertial number started to be tested, showing from first comparisons that a master curve can be approximately obtained on which all data collapse. Regarding rheology, DEM results proved to be useful in assessing that in the configuration studied the stress tensor is symmetric, and that the fluctuating energy approach can be more correct than a simple mixing length model in studying the type of flow simulated. A new constitutive equation for the stress tensor was thus obtained.

Finally, preliminar experimental results of flow of iron beads in a vertical chute were reported in which velocity profiles were computed, where deviations from behaviors reported in Literature for the shear bands were observed.

9.2 Perspectives

On the basis of this thesis' work, many perspectives appear for the future, which can be structured into the three main directions explored up to this moment: rheology, boundary conditions, gas-solid coupling.

Regarding rheology, being that the model performed well compared with both Literature correlations and experimental data, a deep investigation on the validity of constitutive re-

lations (and particularly on the diffusive flux and the dissipation rate of fluctuating energy) should be carried out by means of discrete element simulations. The model should be also compared with velocity profiles obtained in the experimental facility shown in Chapter 8 to judge its capability of predicting local velocity profiles in real configurations. The need of deepening the knowledge of local phenomena such as shear bands is not only related to modeling issues: in fact, first experiments seem to suggest that a qualitative change in the behavior of the shear bands appears in the quasistatic limit. Confirming this finding would be an important result whether or not the model was able to capture the behavior.
Regarding boundary conditions, while DEM simulations suggested that the expressions developed in the present work are consistent, there is strong need of experiments in order to understand if this applies also to real configurations. In this perspective the facility described in Chapter 8 if equipped with stress measurement devices could be useful to validate globally the framework developed. DEM simulations in another geometry (inclined chute) are currently carried out in order to verify boundary conditions for different configurations of flow. Extensions to the boundary conditions could imply treatment of macroscopic bumpy walls.
As regards gas-solid coupling, while the approach to treat the coupling was somewhat estabilished and compared qualitatively with literature, it was not possible to perform experiments on maldistribution in countercurrent gas-solids flow. This an important issue which should be done in the future, also to understand if the simple assumptions used in Chapter 5 are able to represent the behavior of a real flow. From the modeling point of view, the study of the gas flowing into a moving granular material should be extended with the inclusion of transport and reactive phenomena in order to study more complex configurations involving drying processes, moving bed reactors, and so on.

List of Symbols

Due to different choices for the name of some variables particularly when passing from simple granular flow to gas-solids flow, in the following the main symbols used in this thesis are listed, divided between the two topics.

Granular flow

$\dagger$	transpose
d_p	mean particle diameter
D^{TF}	source of mechanical energy due to the interstitial fluid
$\mathbf{g}$	gravity
$\underline{\underline{K}}$	fluctuating energy diffusivity tensor
k	coefficient of diffusion of fluctuating energy
k'	parameter in the diffusion coefficient of fluctuating energy
p	isotropic part of the stress tensor (pressure)
$\mathbf{q}^T$	(diffusive) energy flux
$\mathbf{t}^F$	drag force exerted by the interstitial fluid
$\bar{\mathbf{v}}$	average velocity field
$\tilde{\mathbf{v}}$	fluctuating velocity field
v_{out}	discharge velocity
z^T	dissipation rate of mechanical energy
$\underline{\underline{\sigma}}$	stress tensor
$\underline{\underline{\tau}}$	deviatoric stress tensor
η	non-newtonian viscosity coefficient
η_0	parameter in the viscosity coefficient
θ	granular temperature
θ^*	granular temperature scale in the viscosity coefficient
λ	slip length
μ	effective friction coefficient (in the dissipation rate of fluctuating energy)

μ_Y yield stress coefficient coefficient
μ_p particle-particle friction coefficient
μ_{pw} particle-wall friction coefficient
μ^* effective bulk friction coefficient
ϕ solid fraction
ρ local density
ρ_p intrinsic particle density
$\rho\epsilon^T$ $= \hat{\rho}(\tilde{\mathbf{v}} \cdot \tilde{\mathbf{v}})/2$ kinetic energy associated with $\tilde{\mathbf{v}}$
ρE^T $= \hat{\rho}(\bar{\mathbf{v}} \cdot \bar{\mathbf{v}})/2$ kinetic energy associated with $\bar{\mathbf{v}}$
δ angle of internal friction
δ_w wall friction angle

Gas-solids flow

ΔP gas phase pressure drop
L column height
b bin half width
$\bar{V}_0$ gas superficial relative velocity
$\vec{v}_g$ gas velocity ($= (u_g,\ v_g,\ w_g)$)
$\vec{v}_s$ solids velocity ($= (u_s,\ v_s,\ -w_s)$)
v_{slip} solid phase wall slip velocity
$\bar{w}_s$ average solid velocity
ϵ bed local porosity
η_g gas viscosity
k local bed pemeability
ρ_g gas density
ρ_s intrinsic particle density
ρ density of the gas solid mixture
g gravitational acceleration
τ solid phase shear stress
p solid phase normal stress
$\dot{\gamma}$ shear rate in the granular material
μ effective friction coefficient
μ_w effective wall friction coefficient
μ_w^∞ steady sliding wall friction coefficient

θ_g	residence time of the gas in the column
θ_s	residence time of the solid in the column
c	tracer concentration
D_{eff}	effective dispersion coefficient
D	molecular diffusion coefficient of the tracer
E	local RTD of the gas in the column
E^*	global RTD of the gas
$\Delta P'$	gas phase dimensionless pressure drop
I	inertial number
Fr_s	average Froude number of the solid
Re_p	Gas (particle) Reynolds number
Re_p^*	average particle Reynolds number
Pe_l	macroscopic Peclet number
Pe_p	particle Peclet number
Sc	Schmidt number of the gas
Ar	Archimedes number

Bibliography

K. S. Ananda, S. Moka, and P. Nott. Kinematics and statistics of dense, slow granular flow through vertical channels. *Journal of Fluid Mechanics*, 610(-1):69–97, 2008. doi: 10.1017/S0022112008002358.

F. Anzelini. Misure di profili di velocità in flussi granulari densi in geometrie confinate. Master's thesis, University of Padova, 2009.

I. S. Aranson and L. S. Tsimring. Continuum description of avalanches in granular media. *Phys. Rev. E*, 64(2):020301, Jul 2001. doi: 10.1103/PhysRevE.64.020301.

I. S. Aranson and L. S. Tsimring. Continuum theory of partially fluidized granular flows. *Phys. Rev. Lett.*, 65:061303, 2002.

I. S. Aranson and L. S. Tsimring. Patterns and collective behavior in granular media: Theoretical concepts. *Reviews of Modern Physics*, 78(2):641, 2006. doi: 10.1103/RevModPhys.78.641.

R. Aris. *Vectors, tensors, and the basic equations of fluid mechanics*. Prentice-Hall, New York, 1962.

R. Artoni, A. Santomaso, and P. Canu. Shear bands in granular flow through a mixing-length model. *EPL (Europhysics Letters)*, 80(3):34004 (6pp), 2007a.

R. Artoni, A. Santomaso, and P. Canu. A pseudo-thermal model for dense granular flows. Poster at PARTEC '07, Nuremberg, 2007b.

R. Artoni, A. Santomaso, and P. Canu. A dissipative coulomb model for dense granular flows. In A. Co, G. L. Leal, R. H. Colby, and A. J. Giacomin, editors, *THE XV INTERNATIONAL CONGRESS ON RHEOLOGY: The Society of Rheology 80th Annual Meeting*, volume 1027, pages 941–943. AIP, 2008. doi: 10.1063/1.2964902.

R. Artoni, A. Santomaso, and P. Canu. A fluctuating energy model for dense granular flows. In C. Appert-Rolland, F. Chevoir, P. Gondret, S. Lassarre, J.-P.Lebacque, and M. Schreckenberg, editors, *Traffic and Granular flow 07*, page 758. Springer, 2009a.

R. Artoni, A. Santomaso, and P. Canu. Effective boundary conditions for dense granular flows. *Physical Review E (Statistical, Nonlinear, and Soft Matter Physics)*, 79(3): 031304, 2009b. doi: 10.1103/PhysRevE.79.031304.

R. Artoni, A. Santomaso, and P. Canu. Simulation of dense granular flows: Dynamics of wall stress in silos. *Chemical Engineering Science*, 64(18):4040 – 4050, 2009c. ISSN 0009-2509. doi: DOI: 10.1016/j.ces.2009.06.008.

E. Azema, F. Radjai, and G. Saussine. Quasistatic rheology, force transmission and fabric properties of a packing of irregular polyhedral particles. *Mechanics of Materials*, 41(6): 729 – 741, 2009. ISSN 0167-6636. Advances in the Dynamics of Granular Materials.

M. Babić. Average balance equations for granular materials. *Int. J. Engng. Sci.*, 35(5): 523–548, 1997.

R. A. Bagnold. Experiments on a gravity-free dispersion of large solid spheres in a Newtonian fluid under shear. *Proc. Royal Soc. London*, 225:49–63, 1954.

R. A. Bagnold. Flow of cohesionless grains in fluids. *Philos. Trans. R. Soc. London, Ser. A*, 249:235, 1956.

A. Baldassarri, F. Dalton, A. Petri, S. Zapperi, G. Pontuale, and L. Pietronero. Brownian forces in sheared granular matter. *Physical Review Letters*, 96(11):118002, 2006. doi: 10.1103/PhysRevLett.96.118002.

P. Basu. *Combustion and Gasification in Fluidized Beds*. CRC, 2006.

E. Ben-Naim, J. B. Knight, and E. R. Nowak. Slow relaxation in granular compaction. *J. Chem. Phys.*, 100:6778, 1996.

R. B. Bird, W. E. Stewart, and E. N. Lightfoot. *Transport Phenomena*. Wiley, New York, second edition, 2002. ISBN 0471364746.

A. A. Boateng and P. V. Barr. Granular flow behaviour in the transverse plane of a partially filled rotating cylinder. *Journal of Fluid Mechanics*, 330(-1):233–249, 1997. doi: 10.1017/S0022112096003680.

L. Bocquet, J. Errami, and T. C. Lubensky. Hydrodynamic model for a dynamical jammed-to-flowing transition in gravity driven granular media. *Phys. Rev. Lett.*, 89 (18):184301, Oct 2002a. doi: 10.1103/PhysRevLett.89.184301.

L. Bocquet, W. Losert, D. Schalk, T. C. Lubensky, and J. P. Gollub. Granular shear flow dynamics and forces: Experiments and continuum theory. *Phys. Rev. E*, 65:011307, 2002b. e-print cond-mat/0012356.

J. U. Böhrnsen, H. Antes, M. Ostendorf, and J. Schwedes. Silo discharge: Measurement and simulation of dynamic behavior in bulk solids. *Chemical Engineering & Technology*, 27(1):71–76, 2004.

R. L. Brown and P. G. W. Hawksley. The internal flow of granular masses. *Fuel*, 27: 159–173, 1947.

S. Chapman and T. G. Cowling. *The mathematical theory of nonuniform gases*. Cambridge University Press, London, 1960.

J. Chen, J. Rotter, J. Ooi, and Z. Zhong. Flow pattern measurement in a full scale silo containing iron ore. *Chemical Engineering Science*, 60:3029 – 3041, 2005.

M. H. Cohen and G. S. Grest. Liquid-glass transition, a free-volume approach. *Phys. Rev. B*, 20(3):1077–1098, Aug 1979. doi: 10.1103/PhysRevB.20.1077.

COMSOL. *COMSOL Multiphysics User's Guide*. COMSOL AB, Stockholm, 2005.

A. Costa and G. Macedonio. Viscous heating in fluids with temperature-dependent viscosity: implications for magma flows. *NONLINEAR PROCESS IN GEOPHYSICS*, 10: 545, 2003.

A. Costa and G. Macedonio. Viscous heating effects in fluids with temperature-dependent viscosity: triggering of secondary flows. *J Fluid Mech.*, 540:21–38, 2005.

C. A. Coulomb. Theorie des Machines Simples. *Academie des Sciences*, 10:166, 1781.

P. A. Cundall and O. D. L. Strack. A discrete numerical model for granular assemblies. *Géotechnique*, 29(1):47–65, 1979.

F. da Cruz, S. Emam, M. Prochnow, J.-J. Roux, and F. Chevoir. Rheophysics of dense granular materials : Discrete simulation of plane shear flows. *Phys. Rev. E*, 72:021309, 2005.

A. Daerr and S. Douady. Two types of avalanche behaviour in granular media. *Letters to Nature*, 399:241–243, 1999.

P.-G. de Gennes. Reflections on the mechanics of granular matter. *Physica A*, 261:267–293, 1998.

A. K. Doolittle. Studies in newtonian flow. i. the dependence of the viscosity of liquids on temperature. *J. Appl. Phys.*, 22:1031–1035, 1951.

F. Dubois and M. Renouf. Méthodes par élements discrets pour la modélisation des milieux divisés, 2009.

T. Dyakowski. Process tomography applied to multi-phase flow measurement. *Meas. Sci.Technol.*, 7:343–353, 1996.

S. F. Edwards and R. B. S. Oakeshott. Theory of powders. *Physica A*, 157:1080–1090, 1989.

D. Einzel, P. Panzer, and M. Liu. Boundary condition for fluid flow: Curved or rough surfaces. *Phys. Rev. Lett.*, 64(19):2269–2272, May 1990. doi: 10.1103/PhysRevLett.64.2269.

S. Ergun. Fluid flow through packed columns. *Chemical Engineering Progress*, 48(2): 89–94, 1952.

D. Ertas and T. C. Halsey. Granular gravitational collapse and chute flow. *EPL (Europhysics Letters)*, 60(6):931–937, 2002.

S. Faderani, U. Tüzün, D. L. O. Smith, and R. B. Thorpe. Discharge and transport of nearly buoyant granular solids in liquids part i: Tomographic study of the interstitial voidage effects governing flow regimes. *Chemical Engineering Science*, 53(3):553 – 574, 1998a. ISSN 0009-2509. doi: DOI: 10.1016/S0009-2509(97)00316-3.

S. Faderani, U. Tüzün, R. B. Thorpe, and D. L. O. Smith. Discharge and transport of nearly buoyant granular solids in liquids : Part ii: An investigation of the effects of particle properties on mixture-discharge rates and pore-pressure profiles. *Chemical Engineering Science*, 53(3):575 – 598, 1998b. ISSN 0009-2509. doi: DOI: 10.1016/S0009-2509(97)00317-5.

M. Faraday. On a peculiar class of acoustical figures; and on certain forms assumed by groups of particles upon vibrating elastic surfaces. *Philos. Trans. R. Soc. London*, 52: 299, 1831.

Y. Forterre and O. Pouliquen. Flows of dense granular media. *Annual Review of Fluid Mechanics*, 40(1):1–24, 2008. doi: 10.1146/annurev.fluid.40.111406.102142.

G. D. R. Midi. On dense granular flows. *Eur. Phys. J. E*, 14(4):341–365, 2004.

D. Gidaspow. *Multiphase flow and Fluidization - Continuum and Kinetic Theory Descriptions*. Academic Press, San Diego, 1994.

V. L. Ginzburg and L. D. Landau. On the Theory of superconductivity. *Zh. Eksp. Teor. Fiz.*, 20:1064–1082, 1950.

S. Glasston, K. G. Laidler, and H. Eyring. *The Theory of Rate Processes*. McGraw Hill, New York, 1941.

J. D. Goddard. From granular matter to generalized continuum. In P. Mariano, G. Capriz, and P. Giovine, editors, *Mathematical models of granular matter, Lecture Notes in Mathematics.*, volume 1937, Berlin, 2008. Springer.

J. D. Goddard. A dissipative anisotropic fluid model for non-colloidal particle dispersions. *Journal of Fluid Mechanics*, 568(-1):1–17, 2006. doi: 10.1017/S0022112006002333.

I. Goldhirsch and C. Goldenberg. On the microscopic foundations of elasticity. *Eur. Phys. J. E*, 9(3):245–251, 2002.

J. S. Goodling, R. I. Vachon, W. S. Stelpflug, S. J. Ying, and M. S. Khader. Radial porosity distribution in cylindrical beds packed with spheres. *Powder Technology*, 35(1):23 – 29, 1983. ISSN 0032-5910. doi: DOI: 10.1016/0032-5910(83)85022-0.

C. Goujon, N. Thomas, and B. Dalloz-Dubrujeaud. Monodisperse dry granular flows on inclined planes: Role of roughness. *Eur. Phys. J. E*, 11:147–157, 2003.

D. S. Grebenkov, M. P. Ciamarra, M. Nicodemi, and A. Coniglio. Flow, ordering, and jamming of sheared granular suspensions. *Physical Review Letters*, 100(7):078001, 2008. doi: 10.1103/PhysRevLett.100.078001.

B. Hage and J. Werther. The guarded capacitance probe a tool for the measurement of solids flow patterns in laboratory and industrial fluidized bed combustors. *Powder Technology*, 93:235–245, 1997.

H. J. Herrmann. Physics of granular media. *Chaos, Solitons & Fractals*, 6:203–212, 1995.

F. Heslot, T. Baumberger, B. Perrin, B. Caroli, and C. Caroli. Creep, stick-slip, and dry-friction dynamics: Experiments and a heuristic model. *Phys. Rev. E*, 49(6):4973, 1994.

W. D. Hibler. A viscous sea ice law as a stochastic average of plasticity. *J. Geophys. Res*, 82:3932–3938, 1977.

A. Ingrama, J. Seville, D. Parker, X. Fan, and R. Forster. Axial and radial dispersion in rolling mode rotating drums. *Powder Technology*, 158:76–91, 2005.

L. Isa, R. Besseling, and W. C. K. Poon. Shear zones and wall slip in the capillary flow of concentrated colloidal suspensions. *Phys. Rev. Lett.*, 98(19):198305, May 2007. doi: 10.1103/PhysRevLett.98.198305.

H. A. Janssen. Versuche über Getreidedruck in Silozellen. *Zeitschr. d. Vereines deutscher Ingenieure*, 39(35):1045–1049, 1895.

M. Jean. The non-smooth contact dynamics method. *Computer Methods in Applied Mechanics and Engineering*, 177(3-4):235 – 257, 1999. ISSN 0045-7825. doi: DOI: 10.1016/S0045-7825(98)00383-1.

J. T. Jenkins. Dense inclined flows of inelastic spheres. *Granular Matter*, 10:47–52, 2007. doi: DOI:10.1007/s10035-007-0057-z.

J. T. Jenkins and M. Y. Louge. On the flux of fluctuation energy in a collisional grain flow at a flat, frictional wall. *Physics of Fluids*, 9(10):2835–2840, 1997.

J. T. Jenkins and M. W. Richman. Kinetic theory for plane shear flows of a dense gas of identical, rough, inelastic, circular disks. *Phys. of Fluids*, 28:3485–3494, 1985.

J. T. Jenkins and S. B. Savage. A theory for the rapid flow of identical, smooth, nearly elastic, spherical particles. *J. Fluid Mech.*, 130:187–202, 1983.

J. Johanson. Stress and velocity fields in the gravity flow of bulk solids. *Journal of Applied Mechanics*, 31:499–506, 1964.

J. Johanson. The placement of inserts to correct flow in bins. *Powder Technology*, 1(6): 328 – 333, 1968. ISSN 0032-5910. doi: DOI: 10.1016/0032-5910(68)80015-4.

J. Johanson. Modeling flow of bulk solids. *Powder Technology*, 5(2):93 – 99, 1972. ISSN 0032-5910. doi: DOI: 10.1016/0032-5910(72)80006-8.

P. Jop, Y. Forterre, and O. Pouliquen. Crucial role of side walls for granular surface flows: consequences for the rheology. *Journal of Fluid Mechanics*, 541:167–192, 2005.

P. Jop, Y. Forterre, and O. Pouliquen. A constitutive law for dense granular flows. *Nature*, 441:727–730, 2006.

C. Josserand, P.-Y. Lagree, and D. Lhuillier. Granular pressure and the thickness of a layer jamming on a rough incline. *EPL (Europhysics Letters)*, 73(3):363–369, 2006.

K. Kamrin and M. Z. Bazant. Stochastic flow rule for granular materials. *Physical Review E (Statistical, Nonlinear, and Soft Matter Physics)*, 75(4):041301, 2007. doi: 10.1103/PhysRevE.75.041301.

H. Kishida and M. Uesugi. Tests of the interface between sand and steel in the simple shear apparatus. *Géotechnique*, 37(1):45–52, 1987.

D. Kolymbas. *Constitutive modelling of granular materials*, volume 61. Springer, 2000.

T. S. Komatsu, S. Inagaki, N. Nakagawa, and S. Nasuno. Creep motion in a granular pile exhibiting steady surface flow. *Phys. Rev. Lett.*, 86(9):1757–1760, Feb 2001. doi: 10.1103/PhysRevLett.86.1757.

D. Kunii and O. Levenspiel. *Fluidization engineering*. Wiley, New York, 1969. ISBN 0471510807.

A. F. Lacerda, M. H. Lisboa, and M. A. S. Barrozo. Heat and mass transfer in a countercurrent moving bed dryer. *Applied Thermal Engineering,*, 25(16):2641–2652, 11 2005.

P. A. Langston, M. S. Nikitidis, U. Tüzün, D. M. Heyes, and N. M. Spyrou. Microstructural simulation and imaging of granular flows in two and three-dimensional hoppers. *Powder Technology*, 94:59–72, 1997.

O. Levenspiel and W. Smith. Notes on the diffusion-type model for the longitudinal mixing of fluids in flow. *Chemical Engineering Science*, 50:3891–3896(6), December 1995. doi: doi:10.1016/0009-2509(96)81817-3.

T. S. Lira, V. V. Murata, M. A. S. Barrozo, and A. J. Assis. Effect of radial air profiles on a countercurrent moving bed drying. *Food and Bioproducts Processing,*, 85(3):241–246, 9 2007.

W. Losert, L. Bocquet, T. C. Lubensky, and J. P. Gollub. Particle dynamics in sheared granular matter. *Phys. Rev. Lett.*, 85(7):1428–1431, 2000.

S. Luding, M. Latzel, W. Volk, S. Diebels, and H. J. Herrmann. From discrete element simulations to a continuum model. *Computer Methods in Applied Mechanics and Engineering*, 191(1-2):21 – 28, 2001. ISSN 0045-7825. doi: DOI: 10.1016/S0045-7825(01)00242-0.

M. Machin, A. Santomaso, M. Mazzucato, M. Cozzi, M. Battiston, L. De Marco, and P. Canu. Single particle tracking across sequences of microscopical images: application to platelet adhesion under flow. *Annals of Biomedical Engineering*, 34:833–846, 2006.

H. C. Marques Fernandes, J. J. Arenzon, Y. Levin, and M. Sellitto. A nonlinear diffusion model for granular segregation. *Physica A: Statistical Mechanics and its Applications*, 327(1-2):94 – 98, 2003. ISSN 0378-4371. doi: DOI: 10.1016/S0378-4371(03)00457-6. Proceedings of the XIIIth Conference on Nonequilibrium Statistical Mechanics and Nonlinear Physics.

S. McNamara, E. G. Flekkøy, and K. J. Måløy. Grains and gas flow: Molecular dynamics with hydrodynamic interactions. *Phys. Rev. E*, 61(4):4054–4059, Apr 2000. doi: 10.1103/PhysRevE.61.4054.

A. Mehta and S. F. Edwards. Statistical mechanics of powder mixtures. *Physica A*, 157: 1091, 1989.

L. S. Mohan, K. K. Rao, and P. R. Nott. A frictional Cosserat model for the slow shearing of granular materials. *J. Fluid Mech.*, 457:377–409, 2002.

G. E. Mueller. Radial void fraction distributions in randomly packed fixed beds of uniformly sized spheres in cylindrical containers. *Powder Technology*, 72(3):269 – 275, 1992. ISSN 0032-5910. doi: DOI: 10.1016/0032-5910(92)80045-X.

D. M. Mueth, G. F. Debregeas, G. S. Karczmar, P. J. Eng, S. R. Nagel, and H. M. Jaeger. Signatures of granular microstructure in dense shear flows. *Nature*, 406:385–389, 2000. e-print cond-mat/0003433.

M. Nakagawa, S. Altobelli, A. Caprhian, and E. Fukushima. Nmri study: axial migration of radially segregated core of granular mixtures in a horizontal rotating cylinder. *Chemical Engineering Science*, 52:4423–4428, 1997.

S. Nasuno, A. Kudrolli, A. Bank, and J. P. Gollub. Time-resolved studies of stick-slip friction in sheared granular layers. *Phys. Rev. E*, 58(2):2161–2171, 1998.

V. V. R. Natarajan, M. L. Hunt, and E. D. Taylor. Local measurements of velocity fluctuations and diffusion coefficients for a granular material flow. *J. Fluid Mech.*, 304:1, 1995.

C. Navier. Memoire sur les lois de comportement de fluides. *Mem. Acad. Roy. Inst. Sci.*, 1823.

R. M. Nedderman. *Statics and kinematics of granular materials*. Cambr. Univ. Press, Cambridge, 1992.

R. M. Nedderman and C. Laohakul. The thickness of the shear zone of flowing granular material. *Powder Technol.*, 25:91, 1980.

J. Nielsen. Pressures from flowing granular solids in silos. *Philosophical Transactions: Mathematical, Physical and Engineering Sciences*, 356(1747):2667–2684, 1998. ISSN 1364503X.

M. S. Nikitidis, U. Tüzün, and N. M. Spyrou. Measurement of size segregation by self diffusion in slow-shearing binary mixture flows using dual photon gamma ray tomography. *Chemical Engineering Science*, 53:2335–2351, 1998.

R. B. S. Oakeshott and S. F. Edwards. Local theory of the statistics of sphere packings. *Physica A*, 189:188, 1992.

M. Oda and K. Iwashita, editors. *Mechanics of Granular Materials: An Introduction*. A.A. Balkema, Rotterdam, 1999.

J. Ooi, J. Chen, and J. Rotter. Measurement of solids flow patterns in a gypsum silo. *Powder Technology*, 99:272–284, 1998.

D. R. Parisi and M. A. Laborde. Modeling of counter current moving bed gas-solid reactor used in direct reduction of iron ore. *Chemical Engineering Journal*, 104(1-3):35 – 43, 2004. ISSN 1385-8947. doi: DOI: 10.1016/j.cej.2004.08.001.

W. Paterson, E. Berresford, D. Moppett, D. Scott, V. Simmons, and R. Thorpe. Gas flow maldistribution in moving beds of monosized particles. *Chemical Engineering Science*, 55:3515–3527(13), September 2000. doi: doi:10.1016/S0009-2509(99)00598-9.

O. Pouliquen. On the shape of granular fronts down rough inclined planes. *Physics of Fluids*, 11(7):1956–1958, 1999. doi: 10.1063/1.870057.

O. Pouliquen and F. Chevoir. Dense flows of dry granular material. *Comptes Rendus Physique*, 3:163–175, 2002.

O. Pouliquen and Y. Forterre. A non-local rheology for dense granular flows. *Philosophical Transactions of the Royal Society A: Mathematical, Physical and Engineering Sciences*, 367(1909):5091–5107, 2009. doi: 10.1098/rsta.2009.0171.

O. Pouliquen and R. Gutfraind. Stress fluctuations and shear zones in quasi-static granular chute flows. *Phys. Rev. E*, 53(1):552, 1996.

O. Pouliquen, C. Cassar, Y. Forterre, P. Jop, and M. Nicolas. How do grains flow: towards a simple rheology for dense granular flows. In *Proc. Powders & Grains 2005*. A. A. Balkema, Rotterdam, 2006.

F. Y. Pouliquen O. Friction law for dense granular flows: application to the motion of a mass down a rough inclined plane. *J.Fluid Mech.*, 453:133–151, 2002.

M. Prochnow. *Dense flows of dry grains*. PhD thesis, Ecole Nationale des Ponts et Chaussées, Paris, 2002.

M. Renouf, F. Dubois, and P. Alart. A parallel version of the non smooth contact dynamics algorithm applied to the simulation of granular media. *Journal of Computational and Applied Mathematics*, 168(1-2):375 – 382, 2004. ISSN 0377-0427. doi: DOI: 10.1016/j.cam.2003.05.019. Selected Papers from the Second International Conference on Advanced Computational Methods in Engineering (ACOMEN 2002).

M. Renouf, D. Bonamy, F. Dubois, and P. Alart. Numerical simulation of two-dimensional steady granular flows in rotating drum: On surface flow rheology. *Physics of Fluids*, 17(10):103303, 2005. doi: 10.1063/1.2063347.

O. Reynolds. On the dilatancy of media composed of rigid particles in contact. *Philos. Mag. Ser. 5*, 50-20:469, 1885.

J. Richardson and W. Zaki. Sedimentation and fluidisation: Part i. *Trans. IChemE*, 32: 35–53, 1954.

J. F. Richardson, J. M. Coulson, J. H. Harker, and J. R. Backhurst. *Coulson and Richardson's chemical engineering vol.2: Particle technology and separation processes*. Butterworth-Heinemann, 2002.

M. W. Richman and C. S. Chou. Boundary effects on granular shear flows of smooth disks. *J. Appl. Math. Phys. (ZAMP)*, 39:885, 1988.

C. H. Rycroft, G. S. Grest, J. W. Landry, and M. Z. Bazant. Analysis of granular flow in a pebble-bed nuclear reactor. *Phys. Rev. E*, 74(2):021306, Aug 2006. doi: 10.1103/PhysRevE.74.021306.

C. H. Rycroft, A. V. Orpe, and A. Kudrolli. Physical test of a particle simulation model in a sheared granular system. *Phys. Rev. E*, 80(3):031305, Sep 2009. doi: 10.1103/PhysRevE.80.031305.

A. C. Santomaso and P. Canu. Transition to movement in granular chute flows. *Chemical Engineering Science*, 56(11):3563 – 3573, 2001. ISSN 0009-2509. doi: DOI: 10.1016/S0009-2509(01)00026-4.

A. C. Santomaso, L. Peteno, and P. Canu. Radial segregation driven by axial convection. *EPL (Europhysics Letters)*, 75(4):576–582, 2006.

S. B. Savage. Analyses of slow high-concentration flows of granular materials. *J. Fluid Mech.*, 377:1–26, 1998.

A. N. Schofield and C. P. Wroth. *Critical State Soil Mechanics*. McGraw-Hill, 1968.

D. Schulze. *Powders and Bulk Solids. Behavior, Characterization, Storage and Flow*. Springer, 2008.

J. Schwedes and H. Feise. Modelling of pressures and flow in silos. *Chemical Engineering & Technology*, 18:96–109, 1995.

J. Seville and R. Clift. Granular bed filter. In J. Seville, editor, *Gas Cleaning Demanding Applications*, pages 170–192. Blackie Academic, London, 1997.

C. Slominski, M. Niedostatkiewicz, and J. Tejchman. Application of particle image velocimetry (piv) for deformation measurement during granular silo flow. *Powder Technology*, 173:1–18, 2007.

D. A. Steingart and J. Evans. Measurements of granular flows in two-dimensional hoppers by particle image velocimetry. part i: experimental method and results. *Chemical Engineering Science*, 60:1043–1051, 2005.

M. Strumendo and P. Canu. Method of moments for the dilute granular flow of inelastic spheres. *Phys. Rev. E*, 66(4):041304, Oct 2002. doi: 10.1103/PhysRevE.66.041304.

M. Tarzia, A. de Candia, A. Fierro, M. Nicodemi, and A. Coniglio. Glass transition in granular media. *EPL (Europhysics Letters)*, 66(4):531–537, 2004.

U. Tüzün and R. Nedderman. Gravity flow of granular materials round obstacles–i: Investigation of the effects of inserts on flow patterns inside a silo. *Chemical Engineering Science*, 40(3):325 – 336, 1985a. ISSN 0009-2509. doi: DOI: 10.1016/0009-2509(85)85095-8.

U. Tüzün and R. Nedderman. Gravity flow of granular materials round obstacles–ii: Investigation of the stress profiles at the wall of a silo with inserts. *Chemical Engineering Science*, 40(3):337 – 351, 1985b. ISSN 0009-2509. doi: DOI: 10.1016/0009-2509(85)85096-X.

U. Tüzün, M. Adams, and B. Briscoe. An interface dilation model for the prediction of wall friction in a particulate bed. *Chemical Engineering Science,* 43(5):1083 – 1098, 1988. ISSN 0009-2509. doi: DOI: 10.1016/0009-2509(88)85069-3.

D. Volfson, L. S. Tsimring, and I. S. Aranson. Order parameter description of stationary partially fluidized shear granular flows. *Phys. Rev. Lett.*, 90:254301, 2003.

D. Vortmeyer and J. Schuster. Evaluation of steady flow profiles in rectangular and circular packed beds by a variational method. *Chemical engineering science,* 38(10): 1691–1699, 1983.

G. B. Wallis. *One-dimensional Two-Phase Flow*. McGraw-Hill, New York, 1969.

R. H. Wilhelm and M. Kwaku. Fluidization of solid particles. *Chem. Eng. Prog.*, 44:201, 1948.

Y.-H. Wu, J. M. Hill, and A. Yu. A finite element method for granular flow through a frictional boundary. *Communications in Nonlinear Science and Numerical Simulation*, 12(4):486 – 495, 2007. ISSN 1007-5704. doi: DOI: 10.1016/j.cnsns.2005.04.005.

N. Xu and C. S. O'Hern. Effective temperature in athermal systems sheared at fixed normal load. *Phys. Rev. Lett.*, 94(5):055701, Feb 2005. doi: 10.1103/PhysRevLett.94.055701.

Z. Yang, P. Fryer, S. Bakalis, X. Fan, D. Parker, and J. Seville. An improved algorithm for tracking multiple, freely moving particles in a positron emission particle tracking system. *Nuclear Instruments and Methods in Physics Research A*, 577:585–594, 2007.

F. A. Zenz. Fluidization phenomena and fluidized bed technology. In M. E. Fayed and L. Otten, editors, *Handbook of powder science and technology*. Chapman & Hall, 1997.

H. P. Zhu and A. B. Yu. Averaging method of granular materials. *Phys. Rev. E,* 66(2): 021302, Aug 2002. doi: 10.1103/PhysRevE.66.021302.

K. Zhu, S. M. Rao, C.-H. Wang, and S. Sundaresan. Electrical capacitance tomography measurements on vertical and inclined pneumatic conveying of granular solids. *Chemical Engineering Science,* 58:4225–4245, 2003.

K. Zhu, S. M. Rao, Q. H. Huang, C.-H. Wang, S. Matsusaka, and H. Masuda. On the electrostatics of pneumatic conveying of granular materials using electrical capacitance tomography. *Chemical Engineering Science*, 59:3201–3213, 2004.

List of Figures